Non-invasive Quantum dot based Sensors for the Detection of Glucose and Cholesterol in Saliva

Thesis submitted in accordance with the requirements of the University of Liverpool

for the degree of Doctor in Philosophy

by

Imtiaz Ahmad, BSc, B.Ed, MSc, MS

July 2017

Abstract

This project was aimed to develop highly sensitive Quantum dots (QDs) based sensors for the detection of glucose and cholesterol. Glutathione (GHS) and Mercaptopropionic acid (MPA) capped Cadmium-Tellurium (CdTe) QDs were used for the development of optical H_2O_2 glucose and cholesterol sensors. The whole process involves the synthesis of fluorescent QDs, selection of QD via experimental analysis, the sensor measurements via solution phase by equilibrium and kinetic methods, and the fabrication, characterization, and calibrations of a solid state sensor based on encapsulation of QDs in polymer matrix. Initially, thiol-capped CdTe quantum dots were synthesized and characterized.

The pH responses of QDs were investigated and it was found that QDs were highly sensitive to pH change. A reversible linear range of pH change was 6.5 to 12. The sensitivity of selected thiols capped QDs to H_2O_2 were measured, and GHS capped QDs found to be the most sensitive (4243.9 CPS/µM of linear range) with the linear range of 100 to 1200 µM. The sensitivity of MPA QDs was 2624.2 CPS with linear range of 100 to 750. Therefore GHS and MPA QDs were used for further analysis.

The initial measurement was done in solution phase. The measuring procedure and conditions were optimized for H_2O_2 sensing and further applied to measure glucose. The linear range of detection for glucose and cholesterol was 33 to 300 and 1 to 45 µM with the detection limit of 8.2 and 1.5 respectively for glucose and cholesterol.

The pseudo-first order kinetic model for H_2O_2, glucose, and cholesterol analysis was established and verified. The pseudo first order rates constant were found to be a function of H_2O_2, glucose, or cholesterol concentrations. The linear range of detection for H2O2 measurement was 0.37 to 396 µM with detection limit of 0.2 µM. The linear range of detection of glucose and cholesterol was 8 to 200, and 17 to 136 µM with a detection limit of 2.0 and 3.46 µM respectively. The kinetic analysis was fast (2 - 5 Sec) and sensitive enough to measure glucose at a low level. The methods were validated and verified via bio kinetic stopped flow and the linear range of measurement for H_2O_2 a glucose was 32 to 2048 and 80 to 2560 µM with detection limit of 14.9 and 75.6 µM respectively.

QDs were encapsulated in nafion and polyvinyl alcohol (PVA) polymer membrane to develop a solid-state sensor. The formulation ratio of nafion, polyvinyl alcohol (PVA), quantum QDs, and enzymes were optimized to improve the performance of the sensor. The developed sensor was with improved sensitivity and selectivity and hence the linear range of H_2O_2 and glucose measurement was 4 to 360 and 6 to 400 µM respectively. The detection limit for H_2O_2 was 1 µM and 2.5 µM for glucose. The sensor was further used to detect glucose in artificial and human saliva for normal (stimulated and non-stimulated) and diabetic individuals. The results of saliva measurement by proposed solid-solid state sensor and liquid phase sensor were validated, using Gas chromatography (GC). The developed glucose sensor was with high stability and resist to interference and could be applicable for clinics. The glucose oxidase (GOx) was replaced with cholesterol oxidase (ChOx) and hence the glucose sensor was modified to detect cholesterol. The linear range was 9.9 to 150 µM with detection limit of 4.5 µM.

ACKNOWLEDGEMENTS

In the name of Allah, the Most Gracious and the Most Merciful, all praises to Allah for the strengths and His blessing in completing this thesis.

The first and the most important person that I would like to express my gratitude is my PhD supervisor Professor Kim King Tong Lau, his consistent supervision and invaluable help, suggestions, and advises, enhance my expertise and skills in this area. I am stating that this thesis would be not have been finished without his suggestions, guidance. A very special and sincerely thanks to you Professor Kim Lau for giving me this opportunity to take this journey of science. I would also like to thanks to Dr. Heife Zhang my UoL supervisor for giving me the opportunity to work under his supervision.

I would like to express my gratitude to Dr. Eric Amigues, Dr. Graham Dowson, Dr. Li Yang, Dr. Yi Li for suggestion guidance. Thank you all for consistent support during my PhD.

I would also like to say thanks to all the staff member of chemistry department for the constructive and valuable research environment, that I was able to peruse my thesis and lab work.

Thanks to the lab manager of chemistry Jianfeng Wu and all other technical staff of the chemistry department for supporting and help during my laboratory work.

I would especially thanks to all my friends, Dr. Qasim Khan, and Dr. Femi Eghbari, in Suzhou University and Dr. Zaka Ullah in SINANO for helping and supporting me with TEM analysis of quantum dots.

I will also like to thanks to Dr. Wang chang group in Suzhou university medical school for providing me an opportunity to work in Suzhou university test center for nanomaterials analysis.

Thanks to my PhD colleagues and lab fellows Miss. Shirika Jothi, Mr. Xiao Qi, Mr. Tianhao, Mr. Chen Zhang and Mr Vijaykummar.

XJTLU and UoL made my PhD possible by providing opportunity and financial support during my PhD, I am very thankful of financial support.

The last but the most precious is my life is my family members, my parents Muhammad hadees, and Haseena bigam, brothers and sisters for their love, support, care for the whole duration of my PhD. I did not see them during my PhD but their care, love, and support was always with me.

Table of Contents

List of Figures

List of Tables

List of Appendix

1. Ahmad I, Zhang H, and Lau K. The Reaction Kinetics of Glutathione-Capped Quantum Dots for the Detection of Hydrogen Peroxide. Austin J Biosens & Bioelectron. 2015; 1(2): 1010.
2. Ahmad I, Zhang H, and Lau K. Ultrasensitive quantum dot based biosensor using kinetic model for analysis. 4th Nano Today Conference 6-9 December 2015 Dubai.

List of Abbreviation

AusDiab	Australian Diabetes, Obesity, and Lifestyle study
AHA	American Heart association
ChOx	Cholesterol Oxidase
QDs	Quantum Dots
FDA	Food and Drug administration
FADH	Flavin adenine dinucleotide
GHS	Glutathione
GOx	Glucose Oxidase
IDF	International diabetes federation
LOD	Limit of Detection
LOQ	Limit of Quantification
MS	Metabolic Syndrome
MPA	Mercaptopropionic acid
MSA	Mercaptosuccinic acid
NHLBI	National Heart, Lung, and Blood Institute Scientific Statement
NADH	Nicotinamide adenine dinucleotide
NCEP: ATP III	National Cholesterol Education Programs, Adult Treatment Panel III
PVA	Polyvinyl alcohol
TGA	Thioglycolic acid

WHO	World health organization
GC	Gas Chromatography
GC-MS	Gas Chromatography Mass Spectroscopy
S	Stimulated Saliva
N	Non-stimulated Saliva

Chapter 1. Introduction and Literature review

1.1. Metabolic syndrome

Metabolic syndrome (MS) is a constellation of metabolic diseases that caused by the increases in the glucose, cholesterol, and triglyceride level in the body. Alterations in metabolic pathways of these bio-molecules result in energy imbalances and disturb all normal body functions; often lead to obesity and hypertension[1]. International Diabetes Federation (IDF) and American Heart Association/National Heart, Lung, and Blood Institute (AHA/NHLBI) all has provided criteria for the detection of MS. All the definitions mainly describing the core components of MS; high fasting glucose level, abdominal obesity, dyslipidemia, and hypertension. A definition of MS is agreed by IDF and AHA, according to them; any three of components, mentioning below the cause of MS in an individual [2].

- Central obesity or waist circumference; population dependent component.
- Elevated triglyceride; ≥ 150 mg/DL (1.69 mmol/L), insulin resistance leads to developed triglycridemia.
- Reduced high-density lipoprotein (HDL) cholesterol; < 40 mg/dL (1.04 mmol/L) in men and < 50 mg/dL (1.29 mmol/L) in women.
- Hypertension: ≥130 mmHg systolic blood pressure or ≥ 85mmHg diastolic blood pressure.
- Raised fasting glucose level; leads to Hyperglycemia, High fasting glucose: ≥110 mg/DL (≥ 6. 1 mmol/L) leads to acidosis and ketoacidosis, development insulin resistance.

Consequences of MS are cardiovascular disease, including myocardial infarction, heart failure, peripheral artery disease, heart stroke, insulin resistance which leads to diabetes mellitus, kidney disease [3-7], and also associated with lipotoxicity [8]. The recent approach on epidemiological data for MS and individuals with cardiovascular disease (SVDs) suggest that; the mortality rate in MS individual is greater twice than the individuals suffering from heart stroke [9].

Increase of MS in human population is an emerging risk to public health overall the world. Miccoli, Bianchi, Odoguardi, Penno, Caricato, Giovannitti, Pucci and Del Prato [10]

reported the epidemiological data for an Italian adult population, which shows that; the prevalence of MS was 21% in man and 18% in women. According to the National Health and Nutrition Examination Survey in 2003–2006 the prevalence of MS is 34.3% in US adults [1]. In China occurrences of MS increases by 12 % at the age range of 32 to 45 and exponentially increases to 45.4 % at the age of 75 [11]. According to AusDiab (Australian Diabetes, Obesity and Lifestyle Study) survey of 11,247 Australians in 2005, the prevalence of MS in adults Australian was 30.7 %, using IDF criteria of MS detection [12]. Metabolic syndrome frequency was 32 % for a woman and 35.1 % for men. The metabolic syndrome prevalence among the world population is high, hence it is important to diagnose and control at an early stage of development.

Utmost population-based epidemiological studies for the detection of MS pursued the guidelines of world health authorities AHA, IDF, and ATP, all of them use the serum as a medium for the diagnosis and detection of MS. The biomarkers used for the detection and diagnosis of MS are serum glucose, triglyceride, and cholesterol. According to the criteria set by health authorities exceeding the optimal concentration of these markers identifies MS in an individual[13].

Neuroleptic drugs had adverse effects and liabilities on the human body; they potentially cause obesity, disrupt the normal metabolic process, particularly involving to disrupt glucose and lipid metabolism. [14,15]. Dopamine antagonistic shows a variety of side effects on psychotic patients and eventually develops MS. The comprehensive studies show the initiation of metabolic syndrome in patients under antipsychotic drugs management [16,17]. Lithium is the first line of therapy for psychotic patients, which is sufficiently a risk for the development of MS in Psychotic Patients [18]. Psychotic drugs are a threat for psychotic patients; they are risky and propagate MS during antipsychotic managements. Psychotic patients under antipsychotic managements are at high risk of MS as compare to the normal subject so it is important to monitor these risk factors for these group of population. The routine laboratory methods for the glucose, cholesterol, and triglyceride are time-consuming. Non-invasive sensor

will provide a close look for practitioners to predict the progression of MS and also will help to switch on or off antipsychotic drugs.

1.2 Saliva is an indicator for the detection of MS

Blood is an important medium that can give useful information that is indicative of human health status[19]. World health authority established the cutoff level of glucose, cholesterol, and triglyceride in blood [20-30] and blood has been using in clinical practices for diagnosis metabolic syndrome and another disease. Routine blood sampling methods for the diagnosis of metabolic markers are painful for psychotic patients, and infants, especially the infants born with low body weight have a complication with blood sampling. The patient and especially patient with psychotic disorders resist for painful blood sampling. There is an intense need to pursue painless sampling methods and to develop a non-invasive sensor for the detection of glucose, cholesterol, and triglyceride. An alternative body fluid for example tears, saliva, urine should be considered that could be easy to collect multiple time. Among them, saliva body fluid is easy to collect and could be used for continuous glucose monitoring.

Saliva was selected as a medium to detect the risk factors especially glucose to detect MS in psychotic patients. The saliva sampling will replace the painful blood sampling in psychotic patients and other individuals suffering from diabetes and MS. Saliva is easy to collect compared to tears, blood, and urine and saliva-based glucose sensor can potentially improve the diagnoses process and will help practitioners to real time monitor glucose in diabetes and patient suffering from MS.

Saliva is a hypotonic colorless and odorless mixture consisting of secretion from salivary acini from salivary glands, oral mucosal exudates and gingival crevicular fluid from gums. The saliva is approximately 90 % secreted by salivary glands (salivary acini). Salivary glands consist of parotid glands which are the largest salivary gland located near the angle of the jaw. The second type is sublingual glands, which is the smallest of gall salivary glands. It is located on the floor of the mouth below mucosa. Submandibular glans is a type which is located under mandible[31].

Salivary acini are berry-shaped secretary cell of salivary glands connected to salivary glands ducts[32]. The basic unit of salivary gland salivon, consist of ducts and acinus is shown in the figure 1.1 below. The salivary glands are surrounded by abundant capillaries, hence the exchange of molecules between blood capillaries and salivary gland acini lead to the production of saliva. The molecules in the blood can infiltrate acini and secrete to saliva. [33,34].

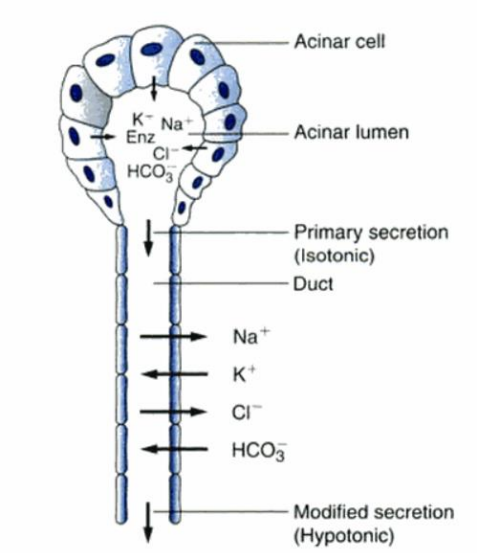

Figure 1.1 The production of saliva in salivary acinus and salivary ducts [35] (copyrights Elsevier).

The mechanism of saliva secretion involved two phases, the primary absorption of fluid by acinar cells from blood capillaries, which is secreted to salivary ducts. Initially, the saliva is isotonic and the concentration of I^-, F^-, $H_2PO_4^-$, HCO_3^-, Mg^{2+}, Na^+, Ca^{+2}, Cl^-, and K^+ is similar to blood plasma. The salivary ducts contain various receptors and modified the electrolytes concentrations in final secretion to the oral cavity. The salivary ducts re-absorb of Na^+ and Cl^- and hence the concentration of Na^+ and Cl^- decreases in saliva. HCO^-_3 and K^- concentration increase because of the secretion of salivary ducts. After secretion of saliva from ducts to oral cavity the nature of saliva change from isotonic to hypotonic[35]

1.2.1 Saliva Composition

Saliva has variety of constituents but almost 99 % of saliva is composed of water and the remaining are inorganic electrolytes; I^-, F^-, $H_2PO_4^-$, HCO_3^-, Mg^{2+}, Na^+, Ca^{2+}, Cl^-, K^+ and

thiocyanate ions, organic molecules; glucose, cholesterol, fatty acid, ammonia, urea, uric acid, glycol lipid, amino acid, steroid hormones, triglycerides, mucin. The salivary proteins are glycoproteins, albumin from plasma, immunoglobins, and variety of peptides including slathering, proline and cysteine [36,37].

Salivary and blood electrolytes;

- Sodium 139.4 mM in blood[38] while 6 mM in saliva[39], Saliva Na^+ is lower than blood Na^+ level.
- Chlorine; 103 mM in blood[38] while 16 mM in saliva[39], Saliva Cl^- is lower than blood Cl^- level.
- Potassium; 4 mM in blood[38] and 10 to 36 mM in saliva[40], Saliva K^+ is higher than blood K^+ level.
- Calcium; 5 mM in blood while 1.3 to 1.7 mM in saliva[41], Saliva Ca^{2+} in most cases similar but sometimes slightly lower than blood.
- Magnesium; 0.081 mM[38] in blood and 0.08 to 0.5 mM in saliva[42].
- Bicarbonate; 27 mM in blood[38] and 37 mM in saliva[43], The HCO^-_3 level is higher than blood.
- Phosphate; 11.2 mM in blood [38] 1.4 to 20 mM in saliva [43]

Salivary enzymes and other constitutes

- α-amylase catalyzed the hydrolysis of starch; is secreted by the salivary glands acinar cells[44].
- Lingual lipase is secreted by sublingual acinar cells and its help to hydrolyzed triglycerides[44].
- Proline help with enamel formations [45]
- Lysozymes, lactoferrin is also produced by salivary glands, which is an antimicrobial[44].
- Salivary mucus present in human saliva, it is composed of glycoprotein and mucopolysaccharides[46].
- A number of orals bacterial are present in saliva and the up to 8 million cells are present in saliva.
- The epidermal growth factors, opiorphin[47], and haptocorrin are also present in human saliva.

Saliva and blood are biological fluid and blood have the same constituents as present in saliva. Human blood consists blood cells, blood plasma. The blood plasma is the liquid medium of blood which is 55 % of the blood. Blood plasma consists of 92 % of water, 8 percent

of blood proteins and other organic and inorganic materials. The plasma consists of glucose, amino acid, fatty acid, urea, lactic acid, serum albumin, immunoglobin, lipoprotein, and electrolytes Mg^{2+}, Na^{+}, Ca^{2+}, Cl^{-}, K^{+}, $H_2PO_4^{-}$, and HCO_3^{-}.

1.2.2 Saliva flow rate

The saliva flow rates vary, it is 500 to 2500 mL/day in adults which is corresponding to the average of 0.32 mL/min in un-stimulated and 1.7 mL/min stimulated. The salivary constituent's concentration changes with the salivary flow. Sodium bicarbonates ions concentration increases on increasing the flow rate of saliva the other concentrations like potassium and $H_2PO_4^{-}$ unchanged at different flow rates. The salivary pH is dependent on the composition of saliva which is ranging from 6.5 to 7.8 for healthy individuals. The sodium and chloride concentrations increases with the increased in salivary rate flow. The pH of the saliva is also dependant on the salivary flow rate, increasing the flow rate enhancing the pH [37].

1.2.3 Correlation of saliva and blood glucose and cholesterol

We reviewed the recent study on saliva and blood glucose. The level of saliva glucose is higher in diabetic patients than that of normal subjects [48-52]. Arati et al. estimated a positive correlation between saliva glucose and fasting blood glucose in patients with uncontrolled diabetes [53].

Sashikumar and Kannan [54] reported the concentration of saliva glucose for the normal subject which was 132-96 μM. Abikshyeet, Ramesh and Oza [55] report the range of glucose concentration in saliva 28 to 130 μM. The mean is 69 μM and standard deviation of 22 μM, for normal subjects. Jurysta, Bulur, Oguzhan, Satman, Yilmaz, Malaisse and Sener [48] report 76.4 ± 3.8 μM for normal subjects, while Maria et al. estimated the saliva glucose concentration 328±111 μM among males and 332±87 μM for women [56]. Ye, Liang, Li, Luo, Zhang, Chen and Kong [57] group recently reported saliva glucose concentration range 30 to 80 μM.

According to a review, tear glucose concentration is directly correlated with blood glucose in diabetes and normal subjects [58-60]. Baca, Taormina, Feingold, Finegold, Grabowski

and Asher [61] estimated that; tear glucose concentrations is 350 ± 40 μM and 160 ± 30 μM, respectively for diabetic and non-diabetic patients. The glucose concentration in tear is higher than saliva glucose level but the production rate of tear is also slow. Ohashi, Dogru and Tsubota [62] estimated 0.5–2.2 μL/min tear production rate from lacrimal gland and other accessory glands.

The comparative relation of the concentration of glucose, cholesterol, and triglyceride in saliva and blood is presented in the table below [63-66].

Medium	**Blood Glucose mM**	**Saliva Glucose μM**	**Tear Glucose μM**	**Blood Cholesterol mM**	**Saliva Cholesterol μM**	**Blood Triglyceride mM**	**Saliva Triglyceride μM**
Normal	4.0 - 5.9	76.4 ± 3.8	160 ± 20	4.89 - 5.18	1.36 - 1.06	1.7	21.4
Diabetes	> 6.0	187.3 ± 20	350 ± 20	> 6.2	> 7.5	2.06 – 4.44	25 – 89

Table 1.1 Comparison of glucose, cholesterol, and triglyceride concentrations in saliva and blood.

1.2.4 Factor affecting the biomarker concentration in saliva

Saliva biomarkers concentrations may be affected by many factors. Including the selection of appropriate marker (metabolized or non-metabolized), the representative sampling techniques, the factors influencing the biomolecules concentrations are categorized into three groups. The first is physiochemical properties of the molecules and fraction bounded to proteins in blood plasma; which predicts the infiltration of analyte from the bloodstream to saliva. The second factors in the individual status including age, gender, health, nutrition, and medication. The third factors involved the sampling techniques storage conditions, processing for the analytical measurement[67].

The health status of an individual also influence the composition of saliva biomarkers, saliva has been used as a marker for the diagnosis of dental caries, periodontal diseases, oral cancer-Sjögren's syndrome, diabetes mellitus, pancreatic cancer, cardiovascular disease, breast cancer, lungs cancer, prostate cancer, and gastric ulcer [68]. Saliva is pronounced indicator for the diagnosis of chronic liver disease because patients have significant high level of salivary

caffeine[69], Saliva of a patient with chronic renal failure are with the high level of nitric oxide [70].

1.2.5 Saliva sampling methods

The accuracy of saliva biomarkers measurements is essential for the diagnosis, hence it is important to use an appropriate method for saliva collection. The composition of saliva is dependent on appropriate sampling method and experimental methods. A common protocol in saliva collections regardless of the method used is, the individual should rinse the mouth with deionized water prior to saliva collection, the individual should seat in the upright position comfortably with eyes opened to collected non-stimulated saliva. The subject should abstain from eating, smoking 1 to 2 hours prior to saliva collection. Herein we summarizing the most common techniques for saliva collection [71,72]

1. Absorbent method; the saliva is collected by cotton, absorbent pad, swab or gauze. The absorbent is placed in the mouth prior to saliva collection, after absorption, the saliva is extracted by centrifugation.
2. Suction method; Saliva has to be sucked out from the mouth continuously into saliva collecting tube.
3. Spitting method; the subject has to accumulate saliva in the mouth and have to expectorate in saliva collecting tube.
4. Draining method; the saliva is drip out of the lower lips into saliva collector. The subject has to expectorate into the collector at the end.
5. Chewing method; Chewing rubber band or chewing gum or paraffin wax.

A normal person produces approximately 600 mL of saliva per day. The health status and medication also affect the salivary composition and flow rate. The time of the day also affect the flow rate of saliva hence the saliva collection time should be standardized for each individual.

The sampling method influences the concentration of the analyte. In a recent study, the influence of sampling procedures on the salivary urate and lactate concentration was determined and it was confirmed that sampling method significantly influences the salivary

composition[73] because of different flow rates during saliva collection. Hence the standard sampling method should be used minimalized the era in analytical measurements.

A number of saliva collecting kits are available in the market, below is the example of one of the procedures of the collection.

SALIMETRICS SalivaBio; collection method is based on passive drool with saliva collection aid, below are the method used in the protocol of saliva collection of SalivaBio passive drool method[74].

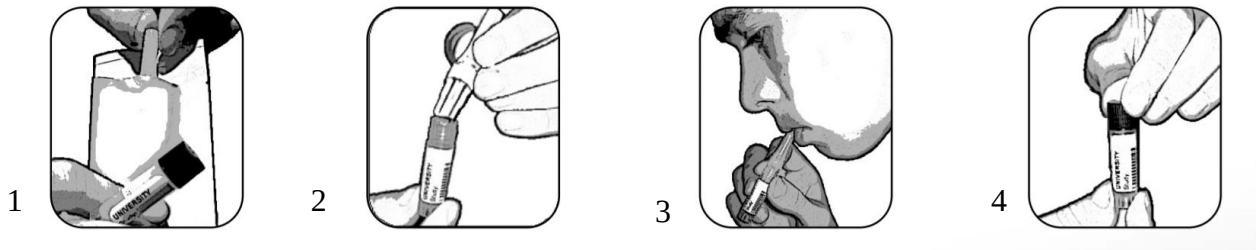

Figure 1.2 Diagram representing the saliva collection method of SalivaBio passive drool method[74].

Step 1: Open a sterile foil pouch and remove the saliva collecting Aid.

Step 2: connect the saliva collecting aid to the saliva collecting vial.

Step 3: Saliva should be pooled in the mouth followed gentle forcing of saliva through saliva collecting aid into the vial.

Step 4: Remove the saliva collecting aid and cap the vial.

Step 4: The saliva collected should be immediately stored at -20 ^{o}C, sample stored for more than four-month should be stored at -80 ^{o}C.

The important precautions before saliva collection are the contamination of species that highly interfere the results. The most important are the food with high sugar, caffeine, or acid contents should be not taken before the collections. The species might lower the pH level or increase the amount of peroxidase as these items enhancing the oral bacterial growth. Alcohol, nicotine,

caffeine, and any over-the-counter medication of prescription should be avoided 12 hours before the saliva collections[75].

1.3 Glucose measurement methods

1.3.1 Enzymatic glucose sensor

There is diversity in glucose sensing techniques. The glucose biosensors are evolved and developed over many years. The first blood glucose sensors did not contain enzymes. One was based on reflectometry[76] and the other colorimetric [77]. A number of methods developed were based on aggressive reagents, which needed a high temperature for reaction and the reaction was slow [78].

The advancement and development in glucose sensor come with the introduction of enzymes. The glucose is colorless, non-fluorescent and the electrochemical properties are not enough to be detected. The glucose oxidase and glucose dehydrogenase methods have been developed based on different detection techniques. The use of enzymes the glucose was converted to a colour species which could be detectable. Enzymes made glucose much easier to be measured [79,80].

Enzymatic glucose sensors are dominant in the sensing industry. Glucose oxidase is the ideal enzyme for the catalytic oxidation of glucose with high selectivity, stability, and sensitivity compared to other enzymes. Glucose oxidase consists of a large mass of protein and Flavin adenine dinucleotide (FAD) working as a redox complex. FAD is deeply embedded in the protein mass. The redox center of Flavin oxidized glucose. Flavin is oxidized by three ways; by natural oxygen, mediator, or using electrode for direct oxidation (Figure 1.2 and 1.3) (Reaction scheme 1.1) [81]. Hexokinase and glucose dehydrogenase also react with glucose and are used for a glucose sensing[82].

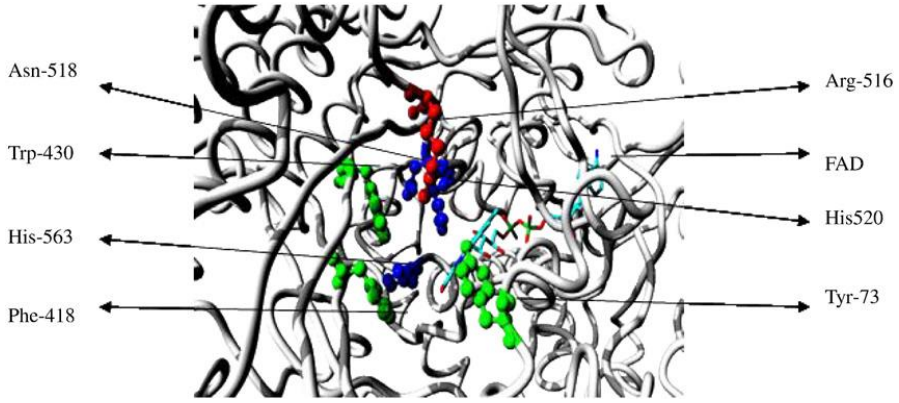

Figure 1.3 Glucose oxidase from P. amagasakiense showing the FAD moiety in protein mass (copyright from Acta Crystallogr.,Sect.D)[81] PDB [83].

(a) (b)

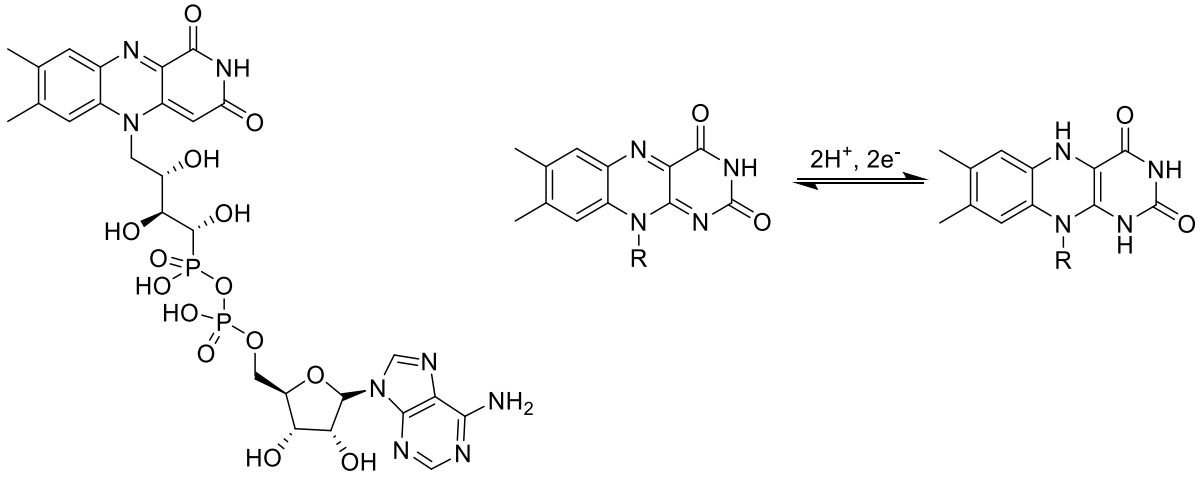

Figure 1.4 (a) The structure of Flavin Adenine Dinucleotide and redox state of FAD (b) FAD reduced to $FADH_2$ by taking up two electrons.

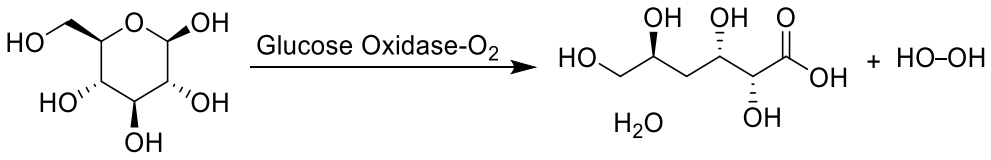

Reaction scheme 1.1 The oxidations of glucose by glucose oxidase produce gluconic acid and H_2O_2

The first method for glucose enzymatic sensor was based on the consumption of oxygen during the enzymatic reaction, both optical and electrochemical methods were used to detect oxygen. Enzyme electrode was introduced in early stage of enzymatic sensor based on the measurement of oxygen consumptions. Oxygen electrode was used to measure the diffusion of oxygen across the plastic membrane. The current output of oxygen electrode was linearly related to the amount of oxygen diffused. Figure 1.4 shows the dual membrane electrode. The enzymes electrode was made by immobilization of enzymes in acrylamide gel over oxygen electrode membrane. When the biological solution containing glucose was diffused into the membrane, the oxygen diffusion decreased, which shows that oxygen is consumed by enzymes catalyzed reaction which oxidized glucose [84].

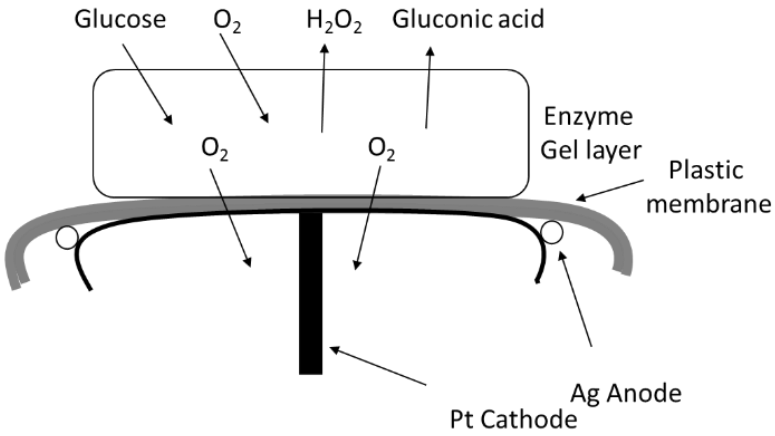

Figure 1.5 The illustration of a glucose sensor, based on the oxygen electrode, which changes the current on oxygen flow across the oxygen electrode membrane.

In another sensing system the H_2O_2 (reaction scheme 1.1) produced was measured by optical or electrochemical methods. The europium (III) Eu^{3+} and antibiotic tetracycline bind to H_2O_2 and the fluorescence intensity increased [85]. The drawback of this method was the high pH dependency, below pH 6.6 and above pH 7.2 the fluorescence emission of europium (III) tetracycline and H_2O_2 complex decreases. This method was not sensitive to be used glucose detection (Figure 1.5) in micro molar range and later was extended to image glucose [86]

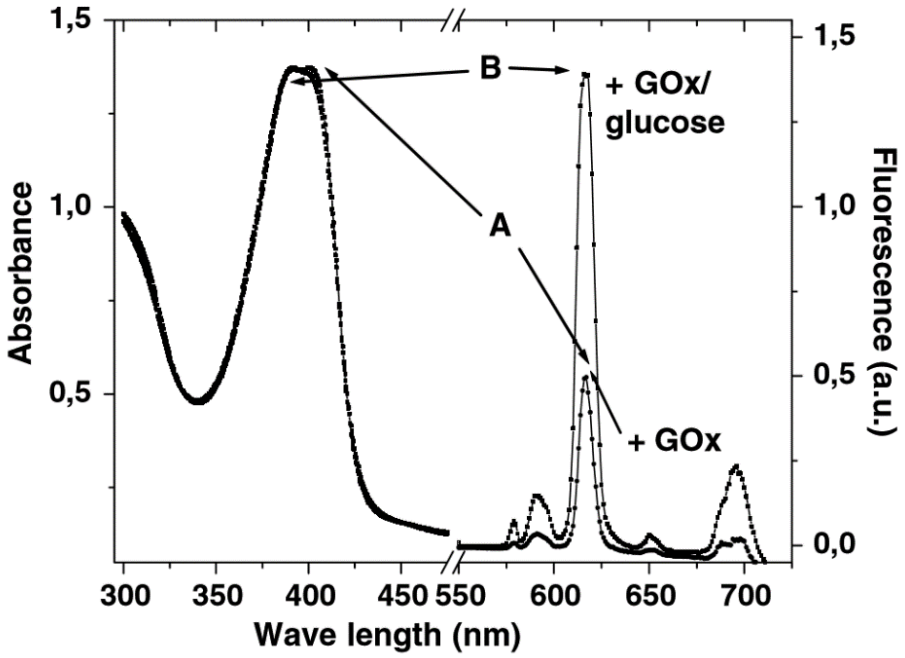

Figure 1.6 The absorbance (left) and the fluorescence emission spectra of Eu/GOx in the absence (A) and the presence (B) of glucose [85] (copyrights from Springer Science).

Prussian blue is a well-known pigment, having spectral and electrochemical properties. It has been widely used for the measurement of H_2O_2 and glucose. The solid film of Prussian blue has an optical properties. Which were used for the detection of redox species. Before the detection of glucose, the Prussian blue was reduced to Prussian white by applying a strong reductant ascorbic acid. The Prussian white or transparent film was re-oxidized to Prussian blue by H_2O_2 produced from the enzymatic oxidation of glucose. The reversible Prussian B/W redox reaction was a monitor at 720 nm absorbance wavelength [87].

The glucose is also measured via pH change during the enzymatic reaction of glucose oxidase with glucose to produce gluconic acid along with H_2O_2. Gluconic acid reduces the pH

of the system. Thus pH has been also used as an analytical signal. However, this method is limited because of the initial pH of the system and the sample is unknown. The example of pH based glucose sensor is polyaniline spectra, which is highly pH sensitive. The absorbance of polyanilines at 840 nm enhance with increasing the pH while the absorption decreased at 600 nm [88].

Other enzymes are also used in enzymatic glucose sensing system. Glucose dehydrogenase catalyzed the production of gluconolactone from glucose. The concentration of NADH produced is measured at 455 nm from its fluorescence emission but the reaction is not easily reversible and ends at once [89].

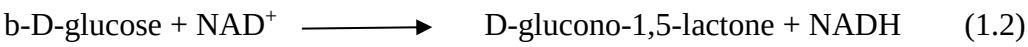

The limited oxygen supply for the sensor and its rate of consumption was a problem for the first generation of sensors so the synthetic, electron-accepting mediators e.g. ferro/ferricyanide, hydroquinone, ferrocene, and various redox organic dyes were introduced to facilitate the electron transfer, third generation of glucose sensor is free of natural or synthetic mediator and involved in the direct transfer of electron between flavin complex and electrode [90-935].

Ferrocene dye was used as a mediator for electron transfer between immobilized glucose oxidase and electrode. However, this reaction is slower. A Linear current response was measured for different glucose concentration. The linear range of detection was 1-30 mM. The potential difference of 60 mV was used with the scan rate of 1 to 100 mV^{-S}.

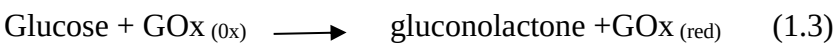

1.3.2 Non-Enzymatic Glucose Sensors

Nonenzymatic glucose sensor has advantages over enzymatic glucose sensors; they do not need enzymes, stability against temperature change and high humidity, working at a wide range of pH, and free from oxygen limitations [94]. The non- Enzymatic glucose sensor is based on metal-

catalyzed oxidation of glucose. The number of transition metals is used to catalytic the oxidation of glucose are, Nickel, Platinum, Cerium, Gold, Copper, Indium, Tin, Silicon, and Aluminum (reaction scheme 1.2). The process of electrocatalysis is explained through the adsorption of the glucose to the surface of the electrode, the d-orbital electrons of the metal are involved in binding with the analyte. Electro-oxidation on platinum electrode was reported by many research groups. The glucose is oxidized to gluco-lactone, and then hydrolysis to gluconic acid (Reaction scheme 1.3).

Nanomaterials have a large surface area, surface to volume ratio (allowed large signals, and better catalysis) and analyte can move more rapidly through the sensor. These features can make the non-enzymatic sensor more accurate and reliable [95]. They are in the form of nanostructured metal oxide, semiconductor, alloy, and complexes. Carbon bases nanostructures (Carbon nanotube, graphene, and boron doped diamond) are designed and fabricated. The combination of carbon nanotube with metals enhances sensing ability. In non-enzymatic sensors the deposition and absorption process of the organic moiety in the metal center increase the sensitivity. Overall, in non-enzymatic glucose sensing the oxidation of glucose by metal hydroxide is ambiguous and unexplained [91].

Metal oxides (Titanium oxide, zinc oxide and silicon oxide nanoparticles) are widely used for glucose sensing applications they were fabricated combined with polymer or embedded in composite with carbon nanotube. Cerium oxide is widely used for non-enzymatic sensors glucose sensing. The uniqueness of cerium oxide nanostructure is the electrochemical redox coupling property, which produced a mediator-less glucose sensing system. Among metals, sensor cerium oxide and cerium oxide have high ionization potential (IEP) might be suitable for electrochemical measurements. Nanomaterials make a remarkable development in the improvement of glucose sensors (Table 1.2) but still need of non-invasive portable continuous glucose sensor for practical implementation in hospitals[96].

Electrode	Method	Sensitivity/Detection Limit (µM)	RS /Applied potential (V)	Ref
ZnO nanorod	Amperometric	23.µA mM-1 $cm^{-2/10}$	<5/+0.8	97
ZnO nanotube	Amperometric	21.7 µA mM-1 $cm^{-2/1}$	3/+0.8	98
MWNTs/ZnO nanoparticle	Amperometric	50.2mA cm−2 M-1/0.25	6/-0.1	99
RhO_2 modified carbon Ink 64	Amperometric	µA mM-1 $cm^{-2/1.11}$	28/-0.2	100

Table 1.2 Metal oxide nanostructure based glucose sensor, the limit of detection with sensitivity.

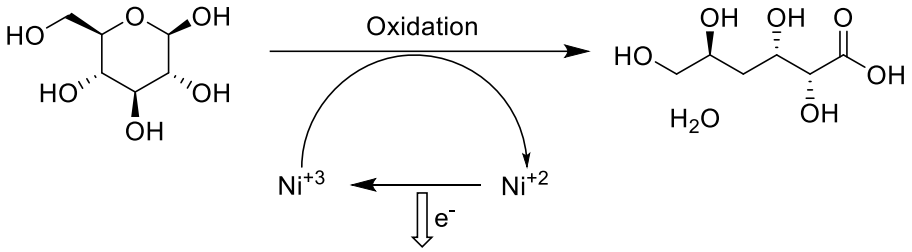

Reaction scheme 1.2 of Electro-oxidation of glucose at a nickel oxide/hydroxide surface.

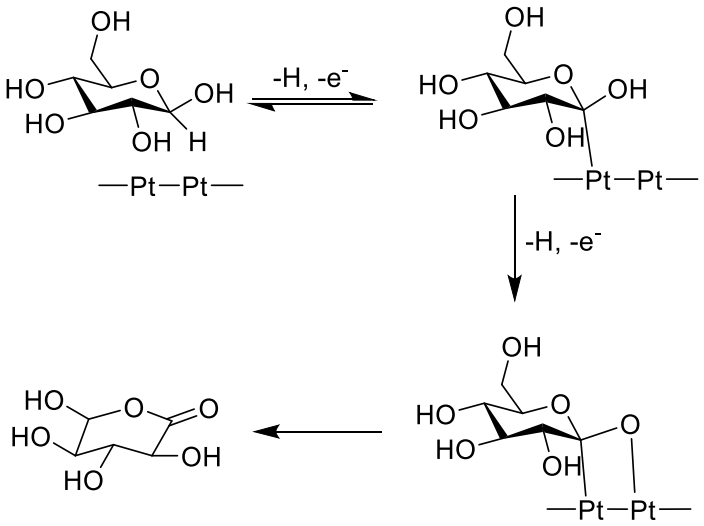

Reaction Scheme 1.3 Mechanism of electrochemical Oxidation of glucose on the platinum surface in Phosphate buffer[101].

The non-enzymatic glucose sensors were modified to achieve the maximum sensitivity and low detection range within minimum time by a carbon nanotube. It is considered to be the new area of carbon nanotube-metal nanoparticles research. Some examples based on carben nanotube with metal oxide nanoparticals are cupric oxide (CuO) nanoparticles onto multi-walled carbon nanotube arrays with linear range up to 3 mM and sensitivity of 2190 $\mu A\ mM^{-1}\ cm^{-2}$ [102]. Palladium nanoparticles were supported on functional carbon nanotubes, the linear range of detection was 1 to 46 mM with sensitivity of 11.4 $\mu A\ cm^{-2}\ mL\ mol^{-1}$ [103]. Copper nanotubes were electrically deposited on vertically well-aligned multi-walled carbon nanotube arrays , the electrochemical response was <1s sensitivity of 1096 $\mu A\ mM^{-1}\ cm^{-2}$, and the linear range was up to 7.5 mM[104]. Carbon nanotube/chitosan/gold nanoparticles layer-by-layer assembly were made the linear range of glucose measurement was 0.1 to 6 mM with detection limit of 30 µM [105]. Bimetallic PtM ((M = Ru, Pd and Au)) nanoparticles were deposit on on carbon nanotubes by electrical method, the linear response was up to 15 mM with detection limit of 50 µM and the sensitivity of 10.7 $\mu A\ cm^{-2}\ mM^{-1}$ was achieved [106]. Gold nanoparticles and carbon nanotubes nanocomposite have sensitive response to with the detection range of 50 to 150 µM [107].

Non-enzymatic copper oxide nanosheets were grown on a gold coated glass substrate. The sensitivity of $5.20 \times 10^2\ \mu A mM^{-1} \cdot cm^{-2}$ was achieved [108]. A three-dimensional (3D) nanostructured nickel oxide (NiO) electrode was fabricated by an electrode deposition method employing nickel foam as a scaffold and used for glucose detection nonenzymatically [109].

Recently a variety of methods has been developed. Nanoscale metal oxide, noble metal doped oxide metal oxide-CNTs nanocomposites and metal oxide, polymer composites i.e. ZnO nanorod formed on an ITO electrode, Cu (I)(II) Oxides Nanosphere's, MnO2, TiO2, CeO2, ZrO2 [90]. Nanoparticles composed of silver, Nickel, gold and nickel/palladium, gold nanowire, nickel hydroxide nanocomposites, boron-doped diamond Nano-rod and platinum nanomaterial are developed for the sensing of glucose [95].

1.3.3 Electrochemical sensor

The first generation of glucose sensor was based on measurement of Oxygen and hydrogen peroxide production during the enzymatic oxidation of glucose. The reduction of Flavin (FAD) in enzyme by the biocatalyst reaction of glucose formed reduced Flavin ($FADH_2$). The reduced flavin is reoxidized by oxygen and regenerates the oxidized form of flavin [110]

The recently electrochemical sensor was developed by Mitchell from carbon nanotube with functionalized with pyrene-1-boronic acid, have a response to glucose range 1 to 100 mM (1-2 V de pending on the concentration of glucose) with a minimum detection limit of 300 nM, the sensor is highly selective and sensitive to glucose[111].

The amperometric glucose enzymatic sensor made by was immobilizing glucose oxidase with polypyrrole for constructing a multi-walled carbon nanotube film (integrated with micro electro mechanical system electrode) the linear range was obtained from 5 to 80 mM with sensitivity of 97.3 mA M^{-1} cm^{-2} [112].

GOx was immobilized on poly (2,6-diaminopyridine)/multi-walled carbon nanotube/glassy carbon electrode (poly(2,6-DP)/MWNT/GCE) linear plot was obtained to glucose in the concentration ranged from 0.42 μM to 8.0 mM had a good correlation coefficient of 0.95, sensitivity the sensor had remarkable sensitivity, reproducibility and stability[113].

Graphene with QDs and gold nanomaterials enhance the charge transfer in the solid film and increase the sensitivity and performance of glucose sensors. Unique electrochemical sensor compose on the gold electrode was fabricated Graphene–gold nanocomposites with CdTe–CdS core–shell QDs had a good sensitivity and for H_2O_2 with linearity range of 1×10^{-10} M to 1.2×10^{-8} M and detections limit 3.2×10^{-11} M[114].

Similarly, Graphene QD immobilized with GOx and modified electrode, which sensing oxygen were constructed. Graphene QD increases the absorption ability of glucose oxidase on the electrode surface. The amount glucose was the function of reduced current peak, which is due to the decrease of oxygen on the electrode surface. The detection limit for glucose was 1.73 μM. The sensor had a high affinity to glucose[115].

InN QDs were immobilization or conjugation with enzymes glucose oxidase for the direct oxidation of glucose [116]. Mn-Doped ZnS Quantum Dots conjugation with glucose oxidase for the direct sensing of glucose [117].

1.3.4 Colorimetric glucose sensor

The colorimetric sensing techniques are simple, real time, widely used in analytical chemistry. In the colorimetric method, the concentration of color chemical species is determined is by a change in its color. The methods do not need so sophisticated instruments and can be applied for analysis and diagnosis in a single point measurement. It is used in common laboratory practices and varieties of glucose colorimetric assay kits are commercially available. The key challenges in the colorimetric glucose sensor are the chemical species use to change its color by glucose. A variety of species is used. Nano-materials also get attention for colorimetric analysis of glucose; they are in conjugation with sensitive probes contain polyoxometalates, metal oxide, metal sulfide and bimetallic alloy[118,119].

Prussian blue (PB), is reported for electron transfer mediator in electrochemical biosensors. Prussian blue has Fe^{3+}/Fe^{2+} redox couples, hence it exhibits intrinsic peroxidase-like activity. Zhang et al. 2013 developed Prussian blue based colorimetric method for the detection of glucose with a detection limit of 0.031 µM and linear range of 0.05 to 50 µM. The mechanism of the sensor was to oxidize ABTS (2, 20-azino-bis (3-ethyl- benzothiazoline-6-sulfonic acid) diammonium salt) by H_2O_2 using the catalytic Prussian blue nanoparticles. The color is produced by ABTS, which colorimetrically detected. The sensor was highly sensitive however the developed sensors performance was limited to pH 4[120].

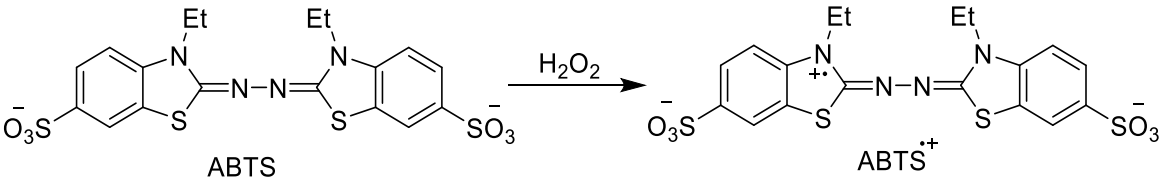

Reaction Scheme 1.4. The oxidation of ABTS by hydrogen peroxide.

CdTe/CdS quantum dots were introduced for the colorimetric-based assay. A sensing strip was constructed of three layers of thin films; green emitting wavelength CdTe/CDs QDs layer was set as a background color and platinum- porphyrin red color was used as oxygen sensor. The GOx was immobilized in sol-gel and PVA matrix and deposit on the oxygen sensitive layer. The glucose oxidases react with glucose and consume oxygen. The concentration of oxygen change was calorimetrically detected. The sensor determined glucose concentration of 0.2 to 3 mM [119].

1.3.5 Quantum dot based glucose sensors

Fluorescent QDs contribute in analytical recognition of varieties of markers, it is not only used for quantitative analysis but been used extensively for qualitative analysis, which significantly improving the methods and techniques in scientific areas. The QDs improved the sensing technology by their tremendous optical properties. The unique properties of fluorescent quantum dot (QDs) are size-dependent fluorescence emission and narrow emission peak, they resist to photobleaching and stable than organic dye[121]. The QDs morphology could be controlled and designed by surface to volume ratio that can potentially improve mechanical, optical, electronic, and magnetic properties and quantum confinement effect[122]. All these properties of QDs have been proved for biological and chemical sensing[123,124].

QDs have been used for glucose sensing application due to the unique optical characteristics. Quantum dot fluorescence quenching or fluorescence enhancing principle, Fluorescence resonance energy transfer (FRET) was used for glucose sensing by different groups. Quantum dots used for glucose detection were synthesized from group II–VI, III–V, or group IV–VI atoms e.g. CdTe, ZnSe, CdS [125], CdSe, CdSe/ZnS [126], InP[127].

Cd, Te, S, Se, and Zn metals based nanocrystals QDs have remarkable optical and electronic properties, with large surface volume ratio and nano size. The QDs are made of cadmium, selenium, cadmium sulfur, and zinc sulfate quantum dots or they may be individually coated with a compatible capping agent that could recognize the glucose sensing event. Fluorescence resonance energy transfer (FRET) method among two CdTe quantum dots of

different color was also been developed. The electron transfer between these two quantum dots causes fluorescence quenching and glucose molecules inhibit the pathway of electron transfer between quantum dots. Increasing the concentration of glucose cause enhancing in fluorescence intensity, the developed sensor had a linear range of 100 to 2000 μM with a detection limit of 30 μM.

A new approach has been developed by Zhibei and its coworkers; they linked Graphene quantum dots with boronic acid and developed a fluorescence base non-enzymatic sensor. The fluorescence of quantum dot are quenched by glucose, quenching mechanism involves the binding of glucose with boronic acid. The increase in glucose concentration indicated that more of the boronic hydroxyl groups are occupied by glucose molecules[128]. Similar work is done on CdSe QDs coated by 3-Aminobenzeneboronic acid. The glucose concentration directly correlates with the fluorescence intensity of quantum dots, as the level of glucose increasing the quenching effect is so fast[129]. Wu group incorporation 3-aminophenylboronic acid with CdTe/ZnTe/ZnS QDs was subjected to different glucose concentration. The fluorescence intensity is responsive to glucose concentrations. The quenching effect occurs when glucose bind to the hydroxyl groups of boronic acids[130]. Comparative study of glucose sensing using quantum dots with their sensitivity, selectivity, and limit of detection ranges are tabulated (Table 1.3).

Quantum dots Description	**Enzymatic/ Non-enzymatic**	**LOD**	**Linearity**	**Ref.**
CdTe nanocomposites film	Glucose oxidase	3 mM	2-12 mM	[131]
CdTe QDs on a screen-printed carbon electrode surface	Glucose oxidase Immobilization	0.3 μM	0.8 to 100 μM	[132]
TGA-caped CdTe Quantum dots	Glucose oxidase	7 μM		[133]
Phenylboronic Acid Modified CdTe/ZnTe/ZnS QDs	Non-enzymatic	0.4–20.0 mM	Sensitive	[130]
Conjugation of concanavalin and CdTe QDs	Non-enzymatic	0.01 mM	0.04–0.2	[134]
Glutathione-capped CdTe QDs	Glucose oxidase	0.1 μM	-------	[135]

CdTe/CdS QDs	Glucose oxidase	1 mM	2 mM to 30 mM	[136]
Bifunctional Nanocomposites of CdTe and Fe3O4	Glucose oxidase			[137]
CdTe-CdS core-shell quantum dot	Glucose oxidase	3×10^{-12} M	1×10^{-11} M to 1×10^{-8} M	[138]
CdTe QDs and glucose oxidase GOx assembly	Glucose oxidase	0.10 microM	----------	[139]
CdTe/CdS QDs	glucose oxidase	1.8 µM	2–30 mM	[140]
CdSe/ZnS D,L-MPA capped QDs	Glucose oxidase	Not estimated	0.2–10mM or 2–30 mM	[141]
Nine legends QDs systems; CdSe-CdS, CdSe-ZnS and CdS-ZnS	Glucose oxidase	Not estimated	K_m is 0.28 mM	[142]

Table 1.3 The table shows the detail of CdTe base quantum dots with different coating used for Sensing.

1.3.6 Commercial glucose meter

To know the glucose level within the body is important for diabetic management. These are a variety of blood glucose meter available on the market. In the last 10 year the efficiency and efficacy of the meters are increased.

Commercially four companies are prominent in glucose sensing devices; LifeScan, Bayer, Abbott, and Roche.

- FreeStyle is electrochemical or colorimetric based glucose meter, by abbot laboratories. The range of glucose measurement is 50 to 500 mg/dL. The meter can work in 5 to 90% non-condensing humidity. Temperature range is 4 to 40 °C and the sample size is 0.3 µL (Figure 1.6) [143]. The freeStyle blood glucose meter was approved by the FDA in 2000, in 2009 the meter was developed to array system and was used in the United States since 2009. The sensing strip of freeStyle comprised of printed parallel plate coulometer, with the gap of 20 µm between the electrodes. The working electrode is carbon and the other is Ag/AgCl electrode. The mediator $Os_2^{2+/3+}$ (Os complex) electro-oxidized on the printed carbon electrode[144].

(a) (b)

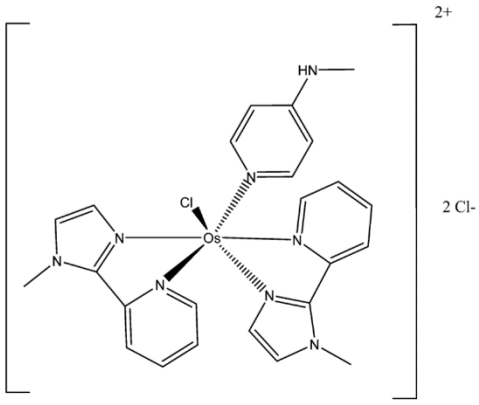

Figure 1.7 (a) FreeStyle Glucose meter of Abbott Laboratories. (b) The redox mediater of FreeStyle sensing strip.

- Bayer Counter Glucose meter. The range of glucose measurement is 10 to 600 mg/dL. The meter can work in 10 to 93% humidity with temperature range is 5 to 56 ºC. The sample size is 0.6 µL (Figure 1.7) [145]. Bayer has used ferricyanide as a mediator with Flavin adenine dinucleotide (FAD) with glucose dehydrogenase (GDH) system for the measurement [146]. Ferricyanide has been widely used in commercial glucose sensors because it is a fast mediator for enzymatic reactions [147,148].

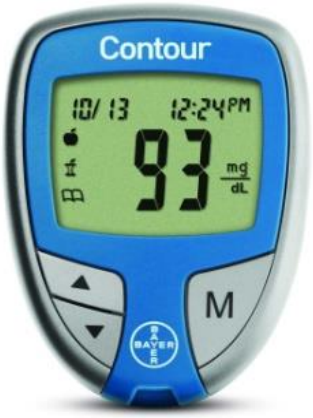

Figure 1.8 Bayer Counter Glucose meter by Bayer

- OneTouch UltraMini is provided by LifeScan. The sensor is based on glucose oxidase. The reported range for the meter is 20-600 mg/dL, the response time of 5 sec, 6–43°C temperature and relative humidity ranged from 10 to 90% (Figure 1.8)[149]. LifeScan

OneTouch® Ultra® sensing system also used hexacyanoferrate III/hexacyanoferrate II as a mediator, this reaction is simple[144].

Figure 1.9 OneTouch UltraLink Glucose meter of LifeScan

1.3.6 Glucose measurements in clinical laboratories

A significant research has been performed to improve the clinical techniques and performance of laboratory methods. The market for glucose sensors is the biggest in diagnostic devices which is been reported to 30 billion € per year (2011) [78]. The clinical laboratory testing has the advantage of reproducibility and high accuracy in comparison to point care devices. Clinical multi-parametric instrumentation is widely used for the measurement of glucose along with pH, Na^+, K^+, pO_2 and Cl^- lactate or urea. The benefit of clinical measurement is that the sensor has been reused by washing the surface of the sensor and calibrated before and after the measurement.

A Variety of methods has been used for the measurements of glucose in the clinical laboratory, among them the electrochemical methods are mostly established in commercial glucose sensors, although the spectrometric method has been also used in the clinical analysis. The common principle of glucose assay is based glucose oxidase or glucose dehydrogenase enzymes[150].

Commercially biochemistry analyzers are available for the diagnostic labs, the analyzers are designed for a large number of samples. The competitive manufacturers of chemistry analyzers are GE Healthcare, Shimadzu, Abbott, Siemens, and Roche. The commonly used biochemistry analyzers are Beckman Coulter DxC800, Roche Cobas 6000, and ADVIA chemistry analyzer XPT system of Siemens [151].

Abbott laboratories introduced a variety of biochemistry analyzers that can analyze electrolytes, along with blood glucose and cholesterol. ARCHITECT ci4100 is capable of performing 400 test per hour. It has 115 refrigerated reagent positions. The Abbot Biochemistry analyzer ARCHITECT (model c4000, c8000, c16000, i1000sr) is based on photometric, turbidimetric methods. The analyzer is designed to measured glucose level in serum, plasma, whole blood and urine [152]. According to the FDA (www.accessdata.fda.gov) assessment of Abbot ARCHITECT, the linear rang of glucose in serum was 0.5 to 500 mM and the limit of detection was 0.28 mM. ARCHITECT ci4100 is capable of performing 900 test per hour and with a feature to load 180 samples.

The Abbot analyzers measure glucose and cholesterol, creatinine and bilirubin by enzyme selective method. The enzymes convert these substrates to a product that can be photometrically monitored. Glucose is measured by the hexokinase method. Glucose reacts with hexokinase that produced glucose-6-phosphate, which turned to nicotinamide adenine dinucleotide phosphate and measured at the ultraviolet absorption of 340 nm. The glucose detection is carried out by endpoint method. The cholesterol is also measured via enzymatic and photometry, the cholesterol is reacted with ChOx and oxidized all the cholesterol (non-bonded cholesterol). In a second step, the lipoprotein bounded cholesterol react with cholesterol esterase, and the resultant product monitor by photometry [153].

Figure 1.9 Architect c4000 biochemistry analyzer for the blood chemistry including glucose and cholesterol by abbot [152].

Figure 1.10 ADVIA chemistry analyzer XPT system from siemens Healthineers [154]

Siemens Healthineers is a medical technology company in competition with Abbott, Siemens produces medical diagnostic systems. The glucose and cholesterol analyzer is ADVIA Chemistry XPT System from Siemens healthineers was introduced which is capable of multiple assays. The system is capable to performed 1800 tests/hour by photometric method. The method of analysis used in this system is Potentiometric, photometric, and turbidimetric. The microvolume technology has been used. The glucose is measured by enzymatic method both via hexokinase and glucose oxidase [154]. According to the FDA (www.accessdata.fda.gov) the linear range of glucose assay using ADVIA system was 0.277 to 40 mM with detection limit of 0.111 mM and the system is capable to performed 2400 tests per hour.

Roche is a Swiss multinational healthcare company that produces pharmaceutical and diagnostic healthcare devices. Roche has introduced a number of chemistry analyzers, the 5th generation Roche chemistry analyzer is cobas c4000. Cobas is fully automatic analyzer for clinical chemistry and homogeneous immunology. The serum, plasma, urine sample can be analyzed. This instrument is based on photometric and kinetic photometric method and used

the sample in microliter amount. Cobas c4000 is used to determined glucose in serum, plasma, cerebrospinal fluid. The measuring mode is based on the increase in absorbance at wavelength 340/652 nm using hexokinase enzymes to catalyze the reaction. The method used to measure the endpoint of a reaction. The cholesterol is also measured via an increase in absorbance at 700/505 nm of the byproduct of enzymatic reaction of cholesterol and cholesterol oxidase. According to the FDA (www.accessdata.fda.gov) the linear range of glucose assay using Cobas 800 is 0.277 to 27.2 mM with detection limit of 0.270 mM, the analyzer is capable to performed 600 samples per hours.

Figure 1.11 Cobas c6000 series chemistry analyzer from Roche.

The cost of glucose testing varies with the use of different methods and analyzers, vary from region to region. Herein we describing an exemplary few diagnostic laboratories cost for the glucose and cholesterol.

Health Testing Center; is a diagnostic center at Florida USA, providing a complete health profile of patients. The cost of fasting or non-fasting glucose testing is $ 11, while the case for cholesterol with complete blood lipid cholesterol is $ 29. [155] The prevalence of diabetes and metabolic disorders is increasing in world population and hence the total cost for the diabetic diagnosis and management is increasing with high proportion. According to the National Diabetes statistic United state report, 30.3 million people have diabetes which 9.4 % of the total United State population. The cost for the diabetes diagnosis in the united states in 2012 was estimated $245 billion [156].

1.4 Cholesterol sensing

Cholesterol is a type of sterol; a subgroup of steroids, at position 3 hydroxyl groups is polar and the side chain consists of 8-9 carbons are non-polar, dissolved in organic fatty solvents (Figure 1.12). It is the major components of all cell and cell organelle membranes found abundantly in the brain, nervous, adrenals and skins, mainly it is synthesized in the liver. Cholesterol is involved in the synthesis of hormones. Cholesterol is an important component involved in the various physicochemical process of the body, especially directly correlated with heart diseases, and metabolic syndromes [157].

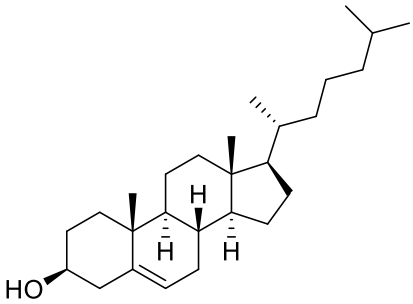

Figure 1.13 Chemical structure of cholesterol

In 2001 US National heart, lungs, and blood institutes provides a guideline for the evaluation, testing and normal cholesterol level in the body of adults and cholesterol managements. The panel classified the LDL as Optimal, near optimal, or above optimal, borderline, high and very high (Table 1.4)[158].

CHL	**Optimal/Low (mg/dL)**	**Near optimal/above optimal (mg/dL)**	**Borderline high (mg/dL)**	**High (mg/dL)**	**Very high (mg/dL)**
LDL	<100	100-129	130-159	160-189	190
HDL	<40	------	------	>60	----

Table 1.4 LDL Cholesterol level Classifications by US NHLBI.

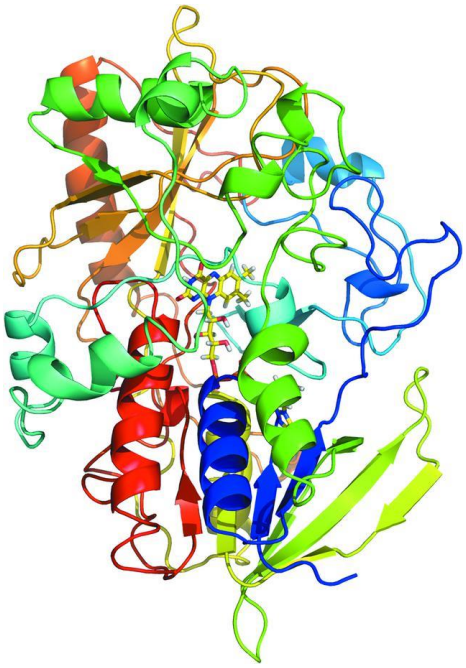

Figure 1.14 Three-dimensional structure of Cholesterol oxidase from Streptomyces sp. The cofactor FAD is labeled yellow-red and shows in-between (copyright from Acta Cryst.) [159] PDB[160].

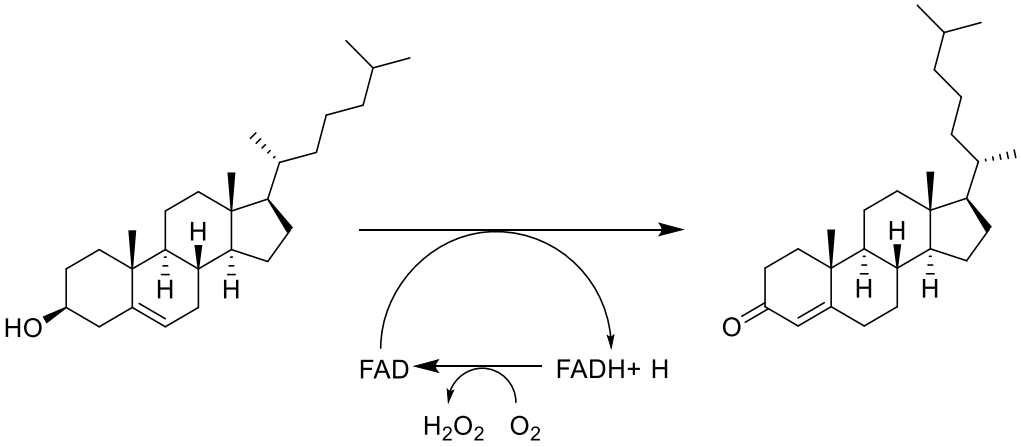

Reaction scheme 1.5 The reaction scheme of cholesterol oxidase catalyzed the reaction, oxidized cholesterol to cholest-4-en-3one.

1.4.1 Cholesterol measurement in clinics

In routine laboratory practices, cholesterol is quantified by colorimetric and fluorometric assays, both assays are enzyme based. Cholesterol dehydrogenase and cholesterol oxide (Figure 1.13) are used in the enzymatic quantification of cholesterol. Cholesterol

dehydrogenase catalyzed the generation of Cholest-4-ene-3-one which further reduce NAD+ to NADH. NADH is a strong reducing agent react with probe molecule and its absorbance measured spectrophotometrically.

Cholesterol oxidase oxidized the cholesterol forming ketone; cholest-4-en-3-one plus hydrogen peroxide. Hydrogen peroxide was estimated by the highly sensitive probe. The spectrophotometric absorbance in both assays is directly proportional to the quantity of cholesterol, the mechanism is explained in a reaction scheme 1.5 [161,162] [163].

Variety of electrochemical methods has been developed for the estimation of body cholesterol. All the methods are enzyme based including cholesterol esterase, cholesterol dehydrogenase, and Cholesterol peroxidase and cholesterol oxidase.

1.4.2 Nanomaterials for cholesterol sensing

Electrochemical sensors for cholesterol were fabricated by a carbon nanotube, nanowire, and nanostructures. They help as a mediator for electron transport between enzymes and electrode in electrochemical sensing. The carbon nanotube has a special structure dependent metallic properties that facilitate the electron transfer reaction between enzymes and nanotube. Carbon nanotube sensors are summarized for its comparative study and evaluation on the base of sensitivity, Linearity range, limit of detection in Table 1.5.

Description	**Linear range**	**Response time**	**LOD**	**Ref.**
MWNTs	6.0 mM		0.2 mM	[164]
Sol-gel chitosan/silica and MWCNTs hybrid composite	8.0×10^{-6} to 4.5×10^{-4} M	25s	0.41 mM	[165]
Polyaniline–carbon nanotube onto ITO-coated glass plate	1.29 to 12.93 mM	10S	1mM	[166]
Flow injection microfluidic device with functionalized carbon nanotubes	50 and 400 mg/dl	------	2.8mM	[167]
Poly(diallyldimethylammonium chloride)–carbon nanotubes composites	0.02–1.2 mM	------	4.4 μM	[168]
carbon nanotubes–gold nanoparticles composite covered with chitosan	0.5–5 mM	7S	0.5 mM	[169]

Table 1.5 Electrochemical Cholesterol Sensor using carbon nanotube.

The emergence of nanomaterials has extended research on cholesterol sensing the various nanostructures are fabricated to modulate the cholesterol sensor. The fluorescence base sensors are based on quantum dots. Extensive research had been reported on electrochemical sensor utilizing Graphene quantum dots, carbon nanotube, carbon nanorod and a multi-wall carbon nanotube with deposition of metal nanomaterials or metal oxide nanomaterial for the reliable result of carbon electrode base sensors. Graphene oxide is also utilized as cholesterol sensing materials for cholesterol estimation. Graphene oxide based sensor activity had been improved by the deposition, nanocomposite, or decoration of metal or metal oxide nanoparticles. Zinc oxide nanoparticles, nanorod, crystalline flower, and hybrid with other nanoparticles were fabricated for cholesterol sensing. Nonenzymatic glucose sensors are based on gold, silver, and platinum nanoparticles.

Graphene, have a two-dimensional architecture, high quality of electronic transportation characteristics, unique physio-chemicals properties and high surface to volume ratio. Graphene has an excellent conductivity six times more than that of SWCNTs. The electrode fabricated with Graphene had a better electrolytic performance than that of the carbon nanotube [170,171]. Graphene base sensors are developed by Cao S, et al and Park O, et al. The sensor developed by Cao S, et al has very Low detection of 0.017 μM for cholesterol estimation, this sensor is composed of TiO_2–graphene–Pt–Pd hybrid nanocomposite. Park had developed a sensor base on graphene and bi-enzymes assembly had the detection limit of 0.05 μM. We summarized the current research work on the Graphene-based sensor in table 1.6 [172].

Graphene	**Linear range**	**LOD**	**Ref**
TiO_2–graphene–Pt–Pd hybrid nanocomposites had a wide surface area enhancing the electronic transmission rate	5.0×10^{-8}–5.9×10^{-4} M	0.017 μM	[173]
functionalized Graphene (FG) modified graphite electrode	50 to 300 μM	15 μM	[170]
platinum–palladium–chitosan–graphene hybrid nanocomposites functionalized glassy carbon electrode	2.2×10^{-6} to 5.2×10^{-4} M	0.75 μM	[174]

Graphene nanocomposites with, polyvinylpyrrolidone and polyaniline	50 µM to 10 mM	1 µM	[175]
Graphene–enzyme–nanoparticle bioelectrode	0.05 to 0.35 mM,	0.05 µM	[172]
Gold nanoparticles decorated Graphene nanoplatelets	up to 135 µM	135 µM	[176]

Table 1.6 Graphene-b ased cholesterol electrochemical sensors.

Zinc oxide nanoparticles have unique properties and a high surface area. The non-toxicity feature of Zinc oxide nanoparticles makes it compatible with the biological environment and optical transparency. The ZnO has also chemical and photochemical stability. One of the important characteristics is that; they have high efficiency of electron transport. These entire features made Zinc oxide nanoparticles suitable and effective for biosensors [177]. Contrast to carbon nanotube a few works had been done on ZnO nanoparticles for the sensing of cholesterol a wide work had been done on carbon nanotube due to their tremendous ability of electron transfer, they improve the linearity of the sensor and make it more sensitive. The drawback of the CNT is the solubility, in most solvent chitosan is used to overcome this problem, but overall the stability of the sensor is minimized, but Zoo is highly suitable and can be applied in biological media[178]. The reported methods for ZnO nanoparticles for cholesterol sensing are listed in Tab 7, the linearity range, and limit of detection, sensitivity is compared (Table 1.7).

Zinc Oxide Nano Practical Description	**Linearity**	**RT**	**LOD**	**Sensitivity**	**Ref**
Zinc oxide Nano particles	1.0 to500.0 nM	5 S	0.37± 0.02 nM	23.7 $\mu AmM^{-1}\ cm^{-2}$	[179]
Platinum–gold hybrid functionalized ZnO nanorods	0.1–759.3 µM		0.03 µM	26.8 $\mu A\ mM^{-1}$	[178]
well-crystallized flower-shaped ZnO	0–15.0 µM	5S	0.012µM	61.7 $\mu A\mu M^{-1}\ cm^{-2}$	[177]
Zinc Oxide Film	0.277–22.2 mM/L	10 s	27µM	0.059 $\mu A/mgdl^{-1}cm^{-2}$	[180]
ZnO nanorods were chemically grown on Ag wire	1µM to 2000 µM	10 s	1µM	35.2 mV per decade	[181]
Zinc oxide nanoparticles-chitosan composite film	0.227 to 16.6 mM		0.227	$1.41x10^{-4}$ A mg dl^{-1}	[180]

Table 1.7 Enzymatic Zinc oxide based cholesterol sensors.

Parra et al developed a sensor base on gold nanoparticles, immobilized with cholesterol oxidase by direct absorption on gold electrode. It had detection limits and sensitivity of 60 μM and 0.13 μA mM^{-1} respectively [182]. Gomathi, P et al, immobilized of ChOx on the chitosan nanofibers and gold nanoparticles composite. The linear range of the sensor was recorded as 1 to 45 M, with sensitivity of 1.02 A/M and response time of 5s[183]. Cholesterol oxidase was immobilized covalently with gold nanoparticles the linearity recorded was 0.04 to 0.22 mM with the detection limit of 36 μM.

Bansi D. M et al immobilize cholesterol Oxidase in cerium oxide–Chitosan nanocomposite film onto indium-tin oxide coated glass plate. The linear range of the developed sensor was 10–400 mg/dL with a detection limit of 5 mg/DL. The response time was 10 S [184]. A chitosan-tin oxide nanobiocomposite film has been deposited onto an indium-tin-oxide glass plate to immobilize cholesterol oxidase (ChOx) for cholesterol detection. Anees design a sensor base on immobilizing of cholesterol oxidase onto chitosan-tin oxide nanocomposite film fabricated on indium-tin-oxide glass plate. The detection limit was 5 mg/dL with sensetivity of 34.7 μA/mg dL[1184].

1.5 Fluorescent based measurement methods

Photo luminescence is the emission of light of longer wavelength from materials or single molecules after absorbing lower wavelength light. The electron of the valence band is excited to the conduction band, after some time the electron loss energy in the form of photons (fluorescence emission) and back to valence band. The fluorescence emission depends on photo- luminescence materials, it varies with the materials. The fluorescent materials chemical or physically interact with the species to be detected, thus the change in the fluorescent signal is proportional to the amount of interacted chemical species [185].

Fluorescence recognition event is the most dominant transduction mechanisms[186] to report the chemical or biological trace. A number of fluorometric detection techniques based on the lifetime, emission intensity, emission wavelength shifting, and anisotropy have been developed recentrly[187-190]. The fluorescence detection is enormously sensitive and allows even

the recognition of single molecules[187,191-193]. The fluorometric is selective enough to perform remote analysis, they are used to measured simultaneously concentrations of the target analytes in a different part of a living cell [194]. Fluorescence measurement techniques are anticipated as the future analytical methods and will replace other analytical techniques[195]. The feature of fluorescence-based detection methods is enlisted below.

1. A specific fluorophore can be designed for the analyte detection.
2. A wide range of parameters can be used to measure a signal, the fluorescence emission signal, fluorescence anisotropy, time-resolved lifetime response, Wavelength-Shift Sensing, and Förster Resonance Energy Transfer (FRET).
3. High-speed response; the fluorescence measurement response is very fast, 10^{-8}–10^{-10} s.
4. The high resolution that can be used to detect a single molecule.
5. The fluorescence methods are not harmful to a biological system and can be used for the biomedical applications.

The success of fluorescence detection technique depends on the fluorescent probe that provides useful information to investigate the molecular interactions [196]. The fluorescence probes consist of binding site which recognizes the respective chemicals or biological species and the detection is quantified by changing in optical signaling [197-202].

Fluorescent polymers are highly bright with very large emission in contrast to organic dyes and they resist to self-quenching because of exciton delocalization in the polymer repeated units. The quantum efficiency of the fluorescent polymer is 80 %, which is higher than organic dye[203], rhodamine, fluorescein, coumarin, stilbene, umbelliferone, tetracene, and others laser dye [204]. All fluorescent polymers are insoluble in water, which is modified by incorporation of pendant polar moieties. The typical water soluble fluorescent polymers comprise of two parts; p-conjugated backbone, responsible for excellent optical properties and the second part are the charge functionalities, makes it soluble in water. The charge moieties of the fluorescent polymer interact with an analyte which changes the chromophore dimension[205-207]. The optical properties and performance of fluorescent polymer depend on the molecular structure and the uniform distribution in solution or solid film. The conjugated polymers easily aggregate in water by hydrophilic functionalities and the change the confirmation of optically active unit.

The aggregations lower the quantum yields, which can be used for the sensitive and selective biosensor developments.

1.6 Quantum dots

Quantum dots (QDs) are semiconductor nanocrystal, smaller than the size of its exciton Bohr radius, their size range from 2 to 10 nanometers [208]. The conduction electrons in bulk semiconductor are freely moving as a resultant the energy continues. The small size of the quantum dot leads to the quantum confinement effect; the excitons (electron-hole pair) are confined in three spatial dimensions, the energy spectrum is discreet and the bandgap energy is high. QD have size-dependent optical and electronic properties which could be understood through confined the motion of conduction band electron and excitons in three spatial dimensions (Figure. 1.14). [209]. The addition or removal of electrons from quantum dots can change its electrical and optical properties which are widely used recently in sensor research.

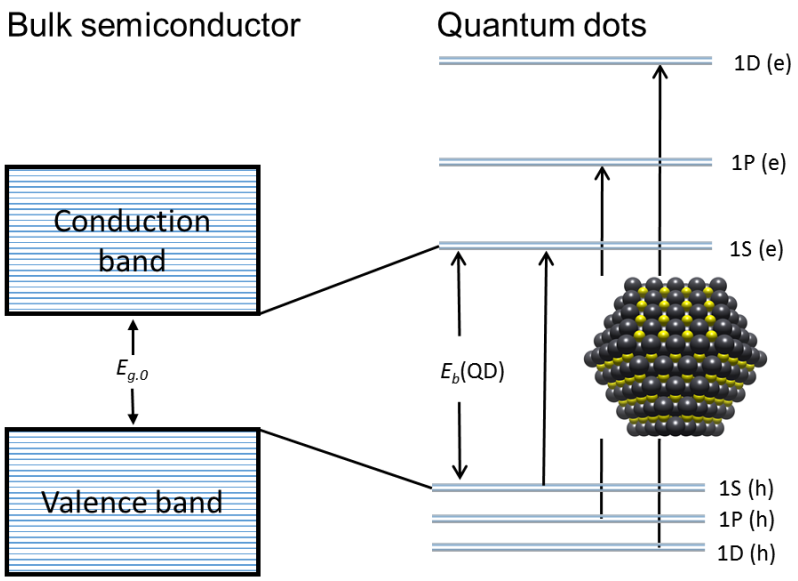

Figure 1.15 Energy level diagram of bulk semiconductors had continuous conduction and valence energy bands, while semiconductor QDs are with discrete energy level due to the quantum confinement effect [210].

The fluorescent semiconductor QDs has a wide range of applications. The unique light-absorbing quality and energy transferring make QDs as suitable materials for solar cells,

optoelectronic devices such as light-emitting diodes, water splitting, Photodetectors, biomedical and sensing applications.

1.6.1 The Origin of fluorescence in QDs

Quantum dots consist of a core or have a core-shell structure. The core is made of groups II-VI, IV-VI, or III-V. Cadmium selenide CdSe, Cadmium telluride CdTe, indium arsenide InAs, zinc sulfide ZnS cadmium supplied CdS, and indium phosphide InP is the commonly used materials. The shell of QDs consist of higher bandgap energy elements such as cadmium sulfide CdS, ZnS, ZnTe, CdS, ZnSe[211-225]. Recently a hybrid organic (CH_3NH_3Pb-X_3) and inorganic ($CsPb$-X_3) perovskite quantum dots (QDs) with X = Cl, Br, I, is reported in several kinds of literature [226-230] Graphene, graphene Oxide, and carbon dots is also reported [231,232]. The emission wavelength of QDs is tunable from blue to near infrared by growing the nanocrystal size during synthesis.

The size of the QD approaches to the size of electron-hole distance (Bohr radius). The strong confinement in QDs gives high bandgap i.e. the difference in energy between the conduction band and valence band that controls the emission of the nanoparticles. The fluorescence occurs when the photon of sufficient energy is absorbed to excite an electron from the valence to conduction band. Controlling the size of QDs allowed us to engineer the optoelectronic properties of QDs [233] (Figure 1.15).

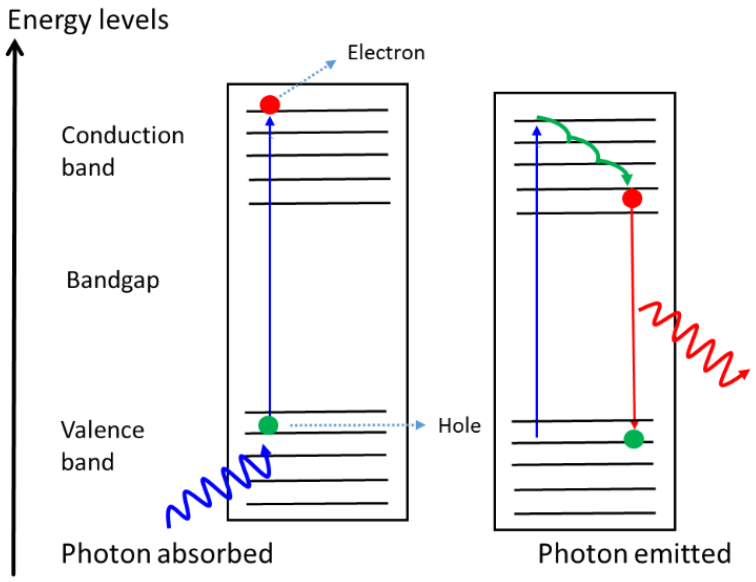

Figure 1.16 Mechanism of absorption and emission of a photon in a semiconductor.

The electron is excited by short wavelength (350 to 450 nm) light, the excited electron stays in the conduction band and then relaxed to the valance band, the back relaxation of electron occurs in two phases. he first relaxation is falling down to the lower level of conduction band, in the second phase the excited electron in conduction band; recombines to the hole in valence band by emitting the photon energy equaling to the bandgap energy [234,235]. The size and materials compositions affect the bandgap energy and bring variation in the fluorescence emission of QDs. The confinement of an exciton in quantum dots also associates with the tunable bandgap energy. The strong quantum confinements in QDs lead to increase in the bandgap energy density state [236], which potentially increase the nonradioactive recombination [237,238].

The quantum confinement effect is explained in Figure 1.13. When in bulk semiconductor the size of the particle is squeezed into the electron-hole distance (Bohr radius) quantum confinement occurs. This effect occurs when the size of particles becomes smaller than the electron-hole distance in an exciton (Bohr's radius) that might be formed in a bulk semiconductor. The confined electron change the nature of the semiconductor and their energy spectrum is discrete which have significant effects on the bandgap energy, addition of single atom or removal of a single atom has a deeper impact on bandgap[239]. QDs size is varying from

1 to 10 nm, the smaller nanocrystal has a higher bandgap, with blue or violet shift, while the large nanocrystals i.e. 6 to nm have narrow bandgap with red or infrared shift [240,241].

QDs core and shell have strong quantum confinement, the shell of QDs increase the stability of optoelectronic feature and will increase the stability toward chemical reactivity. The electrical, as well as an optical feature of QDs, could be designed by selecting appropriate core-shell structure[242].

QDs core-shell structure reduces the blinking behavior of photo-luminescence, the blinking of QDs strongly dependent on the core-shell structure as well on the thickness of QDs. The design of QDs structure with core-shell predicting strong optical properties and non-blinking QDs can be obtained from the core-shell structure. The Core-shell QDs thick crystalline structure also prevents the photobleaching and leaching of a toxic element from the core. Blinking of QDs and other fluorophore has been extensively studied which is the strong obstacle for the development of QDs based optical devices. The use of QDs core-shell system could be extended to other application along with biological detection and optoelectronic devices. The nature of capping agent is important, it stabilizes the QDs core-shell nanostructure and prevents the aggregation of nanocrystal. Various surface capping agent had been used for the QDs including Tri-n-octylphosphine oxide (TOPO), Trioctylphosphine, Amines, Thiols, and Carboxylic acids [243-246]. Among these capping agents thiol caps are bifunctional, it works as a caps and also the part of QDs shell structure, CdTe structure with thiol caps are of wide bandgap. It seems that the Sulphur of thiol is making an additional shell layer on the surface of CdTe [247]. The thiol capping agent could replace the core-shell structure and the synthetic process of core-thiol QDs is easy in comparison with core-shell QDs.

Quantum dots have outstanding fluorescence properties over traditional organic chromospheres [248,249] and potentially a better material for the designing of optical sensors. The QDs are small nanostructures the surface volume or the surface legend ratio could be controlled by synthetic procedures. Below is the possible methodology for the designing of optical sensors [250].

1. Chemiluminescence enhancing or quenching of QDs with analyte [251-257].

2. Fluorescence resonance energy transfer (FRET): is the non-radiative transition of electrons from a donor to an acceptor over the distance of 10 nm[258-264].

3. Fluorescence intensity quenching or enhancing [265].

4. Chemiluminescence resonance energy transfer (CRET): the non-radiative transfer chemiluminescent donor and fluorescent acceptor[254,266,267].

5. Annihilation or co-reactant electroluminescence[185]: an electroluminescent device is fabricated with a co-reactant species that react to analyte decrease of increase or shift the electroluminescent signal. The system is been used for the sensitive detection of lead (II) ion and dopamine[268,269].

6. Colorimetric QDs sensors: QDs are used as a background color to differentiate the color change of a fluorescent probe or another organic dye sensitive for an analyte [270,271].

7. Surface-plasmon-resonance of QDs is extremely sensitive. This technique could provide an alternative detection scheme for biological species detection [272,121].

The above mentioned techniques have made nanocrystals QDs potentially useful for the development of highly sensitive biological and chemical sensor. Along with these techniques the optoelectronic feature of QDs are outstanding for designing of analyte-specific detector to with high accuracy[273,274]. These magnificent properties of quantum dots have attracted extensive work had been done on its implementation in biological and medical sciences [275,276].

1.6.2 Quantum dots versus Organic fluorophores

Various fluorescence probes have been used for the development of optical sensors. The accuracy, sensitivity, selectivity, signal-to-noise ratio, is totally depend on the optical feature of the fluorophore. QDs characteristics distinguish it from typical organic fluorophore or fluorescent proteins [277]. Herein we are comparing the organic fluorophore versus the quantum

dots, in term of optical and electronic status. Below we enlist the important feature of fluorescent material for the designing of optical sensors [278-281]

1. A wide absorption range to facilitate the electron-hole recombination process.
2. Molar absorbance coefficient; absorbance divided by the absorption at given wavelength and given a concentration of the analyte.
3. Fluorescence quantum yield; is the ratio of emitted and absorb a photon.
4. Lifetime or decay: it's the time of fluorophores stayed in the excited state before its decay.
5. Brightness; depend on the molar absorption coefficient at an excited wavelength and quantum yield; it is the intensity of fluorescence.
6. Stokes shift; is the difference between excitation and emission wavelength.

QD's features versus organic dye are described here in detail [282 (Resch-Genger, 2008 #159].

1. The Absorption spectra of QDs is wide The (FWHM) of absorption spectra gradually increase toward UV regions [277], while organic dye has discrete [283] bands. QDs are excellent to be excited at a wide range of spectra.
2. The emission spectra of the QDs are symmetrical with no tailing factor [284] but the contrast to organic dye, FWHM profile range from 30 to 90 [285,286].
3. Molar absorption coefficient of QD's is higher than organic dye, small QD's have an extinction coefficient of similarity to R6G 200,000 $M^{-1}cm^{-1}$, larger QD's have an extinction coefficient greater than 2×10^{6} $M^{-1}cm^{-1}$ [282]
4. QD's solubility is controlled by a surface capping agent while in Organic dye is controlled by substitution pattern [280,287].
5. QD's are highly stable to photobleaching versus organic dye which or less stable.
6. Fluorescence lifetimes of QD's are 100 times stable than organic dye.
7. QD have greater quantum yield than organic fluorophores[279].

A quantum dot is a novel fluorophores and with an advance feature for a wide range of sensing devices, we select QD's for our sensing device. Red QD's have a larger wavelength with intense emission wavelength and narrow FHMW was selected for the sensor.

1.7 Aim and approach

Metabolic syndrome (MS) is the cluster of serious diseases, including diabetes and cardiovascular diseases. In routine clinical practices, serum blood is used to quantify the MS markers. The blood sampling is painful and it is a hinder to use it for continuous and real-time monitoring of glucose. Hence we selected saliva as a medium for the detection of MS components glucose and cholesterol. Measuring glucose in saliva is challenging because of its very low concentration i.e. 75-100 µM.

This project was design and aim to develop a non-invasive Quantum dots-based optical sensor for cholesterol and glucose detection at very concentrations ranges. For the purpose a review was done on the available sensor, techniques and materials and extremely sensitive fluorescence detection methods were used and the glucose recognition specie QDs was selected as a fluorescence probe.

Thiol-capped QDs are highly biocompatible and fluorescent. They have been used for the detection of biomolecules and they were stable in a living cell for weeks. Initially QDs with selected biocompatible thiol capps were synthesized and characterized. It was resolved that MPA and GHS QDs are easy and fast in synthesis than MSA and CYS capped QDs. The GHS capped QDs are with a wide range of fluorescence emission (GHS emission was 514 to 612 nm) and with smaller size than CYS, MPA, and MSA capped QDs.

The QDs based optical detection techniques were used for the analysis of H_2O_2, glucose, and cholesterol. Initially, the pH sensitivity of QDs was investigated, it was found that QDs are very sensitive to hence buffer was used for all analysis. The basic model was established for H_2O_2 measurement and was further extended to glucose and cholesterol measurements. The cholesterol and glucose sensors are based on enzymes, thus the measurement methods for cholesterol and glucose was investigated using an adequate amount of oxidases. We concluded with that GHS-capped QDs can be used for the highly sensitive measurement of saliva, tear, blood, and urine glucose.

The sensors responses were studied in solution phase kinetic rate constant methods. Kinetic methods of analysis were feasible for the detection of H_2O_2, glucose and cholesterol by QDs as an optical transducer. The methods have high accuracy, repeatability, reproducibility as well the analysis results are comparable with the results obtained from the equilibrium method. The kinetic methods of analysis is fast, easy, simple and cheap, the analysis need low amount of sample usually in microliter.

QDs were embedded in a polymeric matrix that stabilized QDs environment interference and increasing the performance optical signal. The encapsulated QDs had a high optical response to H_2O_2, glucose, and cholesterol. The polymers composition was optimized for all the species to be measured. The developed sensors based on QD encapsulation in polymers provide a new platform for optical analysis with greater sensitivity and selectivity. The sensor was used to detect glucose in human saliva, which was 94.2, 72.2, 62.2 for normal subject, and 141.04 for diabetes. The developed sensors are with high stability and resist to interference and could be applicable for hospital applications.

1.8 References

(1) Ford, E. S.; Li, C.; Zhao, G. Prevalence and correlates of metabolic syndrome based on a harmonious definition among adults in the US*. *Journal of Diabetes* **2010,** *2* (3), 180.

(2) Sadikot, S.; Hermans, M. Here we go again… The metabolic syndrome revisited! *Diabetes & Metabolic Syndrome: Clinical Research & Reviews* **2010,** *4* (2), 111.

(3) Lappalainen, R.; Sairanen, E.; Järvelä, E.; Rantala, S.; Korpela, R.; Puttonen, S.; Kujala, U. M.; Myllymäki, T.; Peuhkuri, K.; Mattila, E. The effectiveness and applicability of different lifestyle interventions for enhancing wellbeing: the study design for a randomized controlled trial for persons with metabolic syndrome risk factors and psychological distress. *BMC public health* **2014,** *14* (1), 310.

(4) Cabrera, M. A. S.; Gebara, O. C. E.; Diament, J.; Nussbacher, A.; Rosano, G.; Wajngarten, M. Metabolic syndrome, abdominal obesity, and cardiovascular risk in elderly women. *International Journal of Cardiology* **2007,** *114* (2), 224.

(5) Mitka, M. Metabolic syndrome recasts old cardiac, diabetes risk factors as a new entity. *Jama* **2004,** *291* (17), 2062.

(6) Ritz, E. Metabolic syndrome and kidney disease. *Blood purification* **2008,** *26* (1), 59.

(7) Ritz, E. Metabolic syndrome: an emerging threat to renal function. *Clinical Journal of the American Society of Nephrology* **2007,** *2* (5), 869.

(8) Dominguez, J.; Wu, P.; Packer, C. S.; Temm, C.; Kelly, K. J. Lipotoxic and inflammatory phenotypes in rats with uncontrolled metabolic syndrome and nephropathy. *American Journal of Physiology-Renal Physiology* **2007,** *293* (3), F670.

(9) Ford, E. S. Prevalence of the metabolic syndrome defined by the International Diabetes Federation among adults in the US. *Diabetes care* **2005,** *28* (11), 2745.

(10) Miccoli, R.; Bianchi, C.; Odoguardi, L.; Penno, G.; Caricato, F.; Giovannitti, M. G.; Pucci, L.; Del Prato, S. Prevalence of the metabolic syndrome among Italian adults according to ATP III definition. *Nutrition, metabolism and cardiovascular diseases* **2005,** *15* (4), 250.

(11) Wang, G.-R.; Li, L.; Pan, Y.-H.; Tian, G.-D.; Lin, W.-L.; Li, Z.; Chen, Z.-Y.; Gong, Y.-L.; Kikano, G. E.; Stange, K. C.et al. Prevalence of metabolic syndrome among urban community residents in China. *BMC Public Health* **2013,** *13* (1), 599.

(12) Cameron, A. J.; Magliano, D. J.; Zimmet, P. Z.; Welborn, T.; Shaw, J. E. The metabolic syndrome in Australia: prevalence using four definitions. *Diabetes research and clinical practice* **2007,** *77* (3), 471.

(13) Helvaci, M. R.; Ozcura, F.; Inci, M. Metabolic syndrome and cataract. *Middle East Journal of Internal Medicine* **2012,** *5* (1), 29.

(14) Riordan, H. J.; Antonini, P.; Murphy, M. F. Atypical antipsychotics and metabolic syndrome in patients with schizophrenia: risk factors, monitoring, and healthcare implications. *American health & drug benefits* **2011,** *4* (5), 292.

(15) Lieberman III, J. A. Metabolic changes associated with antipsychotic use. *Primary care companion to the Journal of clinical psychiatry* **2004,** *6* (suppl 2), 8.

(16) Cai, J.; Yi, Z.; Lu, W.; Fang, Y.; Zhang, C. Crosstalk between 5-HT2cR and PTEN signaling pathway in atypical antipsychotic-induced metabolic syndrome and cognitive dysfunction. *Medical hypotheses* **2013,** *80* (4), 486.

(17) Yogaratnam, J.; Biswas, N.; Vadivel, R.; Jacob, R. Metabolic complications of schizophrenia and antipsychotic medications-an updated review. **2013**.

(18) COOKSON, J. Use of antipsychotic drugs and lithium in mania. *The British Journal of Psychiatry* **2001,** *178* (41), s148.

(19) Lew, K. In *Comprehensive Sampling and Sample Preparation*; Academic Press: Oxford, 2012, DOI:http://dx.doi.org/10.1016/B978-0-12-381373-2.00068-5 http://dx.doi.org/10.1016/B978-0-12-381373-2.00068-5.

(20) Alberti, K. G.; Eckel, R. H.; Grundy, S. M.; Zimmet, P. Z.; Cleeman, J. I.; Donato, K. A.; Fruchart, J. C.; James, W. P.; Loria, C. M.; Smith, S. C., Jr.et al. Harmonizing the metabolic syndrome: a joint interim statement of the International Diabetes Federation Task Force on Epidemiology and Prevention; National Heart, Lung, and Blood Institute; American Heart Association; World Heart Federation; International Atherosclerosis Society; and International Association for the Study of Obesity. *Circulation* **2009,** *120* (16), 1640.

(21) Alberti, K. G. M. M.; Zimmet, P.; Shaw, J. The metabolic syndrome—a new worldwide definition. *The Lancet* **2005,** *366* (9491), 1059.

(22) Cameron, A. J.; Magliano, D. J.; Zimmet, P. Z.; Welborn, T.; Shaw, J. E. The metabolic syndrome in Australia: prevalence using four definitions. *Diabetes Res Clin Pract* **2007,** *77* (3), 471.

(23) Ford, E. S. Risks for all-cause mortality, cardiovascular disease, and diabetes associated with the metabolic syndrome: a summary of the evidence. *Diabetes Care* **2005,** *28*.

(24) Grundy, S. M. Pre-diabetes, metabolic syndrome, and cardiovascular risk. *J Am Coll Cardiol* **2012,** *59* (7), 635.

(25) Gu, D.; Reynolds, K.; Wu, X.; Chen, J.; Duan, X.; Reynolds, R. F.; Whelton, P. K.; He, J. Prevalence of the metabolic syndrome and overweight among adults in China. *The Lancet* **2005,** *365* (9468), 1398.

(26) Guize, L.; Pannier, B.; Thomas, F.; Bean, K.; Jego, B.; Benetos, A. Recent advances in metabolic syndrome and cardiovascular disease. *Arch Cardiovasc Dis* **2008,** *101* (9), 577.

(27) Haffner, S. M. The metabolic syndrome: inflammation, diabetes mellitus, and cardiovascular disease. *Am J Cardiol* **2006,** *97* (2A), 3A.

(28) Hossain, S.; Fatema, K.; Ahmed, K. R.; Akter, J.; Chowdhury, H. A.; Shahjahan, M.; Acharyya, A.; Rahim, M. A.; Ali, L. Prevalence and determinants of metabolic syndrome among newly diagnosed type 2 diabetic subjects according to different criteria. *Diabetes Metab Syndr* **2015,** *9* (2), 120.

(29) Ritz, E. Metabolic syndrome: an emerging threat to renal function. *Clin J Am Soc Nephrol* **2007,** *2* (5), 869.

(30) Zimmet, P.; Alberti, K. G. M. M.; Serrano Ríos, M. A New International Diabetes Federation (IDF) Worldwide Definition of the Metabolic Syndrome: the Rationale and the Results. *Revista Española de Cardiología (English Edition)* **2005,** *58* (12), 1371.

(31) Rhoades, R. A.; Bell, D. R. *Medical phisiology: Principles for clinical medicine*; Lippincott Williams & Wilkins, 2012.

(32) Bradley, P. J. In *Otorhinolaryngology, Head and Neck Surgery*; Anniko, M.;Bernal-Sprekelsen, M.;Bonkowsky, V.;Bradley, P. J.;Iurato, S., Eds.; Springer Berlin Heidelberg: Berlin, Heidelberg, 2010, DOI:10.1007/978-3-540-68940-9_36 10.1007/978-3-540-68940-9_36.

(33) Nieuw Amerongen, A. v.; Ligtenberg, A. J. M.; Veerman, E. C. I. Implications for Diagnostics in the Biochemistry and Physiology of Saliva. *Annals of the New York Academy of Sciences* **2007,** *1098* (1), 1.

(34) Van der Bilt, A.; Engelen, L.; Pereira, L.; Van der Glas, H.; Abbink, J. Oral physiology and mastication. *Physiology & behavior* **2006,** *89* (1), 22.

(35) Khurana, I. *Textbook of human physiology for dental students*; Elsevier Health Sciences, 2014.

(36) Edgar, W. Saliva: its secretion, composition and functions. *British dental journal* **1992,** *172* (8), 305.

(37) Humphrey, S. P.; Williamson, R. T. A review of saliva: normal composition, flow, and function. *The Journal of prosthetic dentistry* **2001,** *85* (2), 162.

(38) Cotlove, E.; Harris, E. K.; Williams, G. Z. Biological and analytic components of variation in long-term studies of serum constituents in normal subjects. *Clinical Chemistry* **1970,** *16* (12), 1028.

(39) Dawes, C.; Pedersen, A. M. L.; Villa, A.; Ekström, J.; Proctor, G.; Vissink, A.; Aframian, D.; McGowan, R.; Aliko, A.; Narayana, N. The functions of human saliva: A review sponsored by the World Workshop on Oral Medicine VI. *Archives of oral biology* **2015,** *60* (6), 863.

(40) Roberts, K. B. Essentials of human physiology. *Canadian Medical Association Journal* **1979,** *121* (3), 335.

(41) Dreisbach, R. H. Calcium Binding by Normal Human Saliva. *Journal of Dental Research* **1960,** *39* (6), 1133.

(42) Bales, C. W.; Freeland-Graves, J. H.; Askey, S.; Behmardi, F.; Pobocik, R. S.; Fickel, J. J.; Greenlee, P. Zinc, magnesium, copper, and protein concentrations in human saliva: age-and sex-related differences. *The American journal of clinical nutrition* **1990,** *51* (3), 462.

(43) Bardow, A.; Madsen, J.; Nauntofte, B. The bicarbonate concentration in human saliva does not exceed the plasma level under normal physiological conditions. *Clinical Oral Investigations* **2000,** *4* (4), 245.

(44) Hay, D.; Moreno, E.; Tenovuo, J.; Boca Raton, FL: CRC Press, 1989.

(45) Oppenheim, F. G.; Hay, D. I.; Franzblau, C. Proline-rich proteins from human parotid saliva. I. Isolation and partial characterization. *Biochemistry* **1971,** *10* (23), 4233.

(46) Mandel, I. D. The functions of saliva. *Journal of dental research* **1987,** *66* (1_suppl), 623.

(47) Wisner, A.; Dufour, E.; Messaoudi, M.; Nejdi, A.; Marcel, A.; Ungeheuer, M.-N.; Rougeot, C. Human Opiorphin, a natural antinociceptive modulator of opioid-dependent pathways. *Proceedings of the National Academy of Sciences* **2006,** *103* (47), 17979.

(48) Jurysta, C.; Bulur, N.; Oguzhan, B.; Satman, I.; Yilmaz, T. M.; Malaisse, W. J.; Sener, A. Salivary glucose concentration and excretion in normal and diabetic subjects. *BioMed Research International* **2009,** *2009*.

(49) Aydin, S. A comparison of ghrelin, glucose, alpha-amylase and protein levels in saliva from diabetics. *BMB Reports* **2007,** *40* (1), 29.

(50) López, M. E.; Colloca, M. E.; Páez, R. G.; Schallmach, J. N.; Koss, M. A.; Chervonagura, A. Salivary characteristics of diabetic children. *Brazilian dental journal* **2003,** *14* (1), 26.

(51) Chávez, E. M.; Borrell, L. N.; Taylor, G. W.; Ship, J. A. A longitudinal analysis of salivary flow in control subjects and older adults with type 2 diabetes. *Oral Surgery, Oral Medicine, Oral Pathology, Oral Radiology, and Endodontology* **2001,** *91* (2), 166.

(52) Sashikumar, R.; Kannan, R. Salivary glucose levels and oral candidal carriage in type II diabetics. *Oral Surgery, Oral Medicine, Oral Pathology, Oral Radiology, and Endodontology* **2010,** *109* (5), 706.

(53) Panchbhai, A. S. Correlation of salivary glucose level with blood glucose level in diabetes mellitus. *Journal of oral & maxillofacial research* **2012,** *3* (3).

(54) Sashikumar, R.; Kannan, R. Salivary glucose levels and oral candidal carriage in type II diabetics. *Oral surgery, oral medicine, oral pathology, oral radiology, and endodontics* **2010,** *109* (5), 706.

(55) Abikshyeet, P.; Ramesh, V.; Oza, N. Glucose estimation in the salivary secretion of diabetes mellitus patients. *Diabetes, metabolic syndrome and obesity: targets and therapy* **2012,** *5*, 149.

(56) Soares, M. S.; Batista Filho, M. M.; Pimentel, M. J.; Passos, I. A.; Chimenos Küstner, E. Determination of salivary glucose in healthy adults. *Medicina Oral, Patología Oral y Cirugia Bucal, 2009, vol. 14, num. 10, p. 510-513* **2009**.

(57) Ye, D.; Liang, G.; Li, H.; Luo, J.; Zhang, S.; Chen, H.; Kong, J. A novel nonenzymatic sensor based on CuO nanoneedle/graphene/carbon nanofiber modified electrode for probing glucose in saliva. *Talanta* **2013,** *116*, 223.

(58) Chen, R.; Jin, Z.; Colon, L. Analysis of tear fluid by CE/LIF: a noninvasive approach for glucose monitoring. *Journal of capillary electrophoresis* **1995,** *3* (5), 243.

(59) Sen, D.; Sarin, G. Tear glucose levels in normal people and in diabetic patients. *British journal of ophthalmology* **1980,** *64* (9), 693.

(60) Romano, A.; Rolant, F. A non-invasive method of blood glucose evaluation by tear glucose measurement, for the detection and control of diabetic states. *Metabolic, pediatric, and systemic ophthalmology (New York, NY: 1985)* **1987,** *11* (1-2), 78.

(61) Baca, J. T.; Taormina, C. R.; Feingold, E.; Finegold, D. N.; Grabowski, J. J.; Asher, S. A. Mass spectral determination of fasting tear glucose concentrations in nondiabetic volunteers. *Clinical chemistry* **2007,** *53* (7), 1370.

(62) Ohashi, Y.; Dogru, M.; Tsubota, K. Laboratory findings in tear fluid analysis. *Clinica Chimica Acta* **2006,** *369* (1), 17.

(63) Karjalainen, S.; Sewon, L.; Soderling, E.; Larsson, B.; Johansson, I.; Simell, O.; Lapinleimu, H.; Seppänen, R. Salivary cholesterol of healthy adults in relation to serum cholesterol concentration and oral health. *Journal of dental research* **1997,** *76* (10), 1637.

(64) Al-Rawi, N. H. Oxidative stress, antioxidant status and lipid profile in the saliva of type 2 diabetics. *Diabetes and Vascular Disease Research* **2011,** *8* (1), 22.

(65) Vasconcelos, A. C. U.; Soares, M. S. M.; Almeida, P. C.; Soares, T. C. Comparative study of the concentration of salivary and blood glucose in type 2 diabetic patients. *Journal of oral science* **2010,** *52* (2), 293.

(66) Larsson, B.; Olivecrona, G.; Ericson, T. Lipids in human saliva. *Archives of Oral Biology* **1996,** *41* (1), 105.

(67) Michalke, B.; Rossbach, B.; Göen, T.; Schäferhenrich, A.; Scherer, G. Saliva as a matrix for human biomonitoring in occupational and environmental medicine. *International archives of occupational and environmental health* **2015,** *88* (1), 1.

(68) Zhang, C.-Z.; Cheng, X.-Q.; Li, J.-Y.; Zhang, P.; Yi, P.; Xu, X.; Zhou, X.-D. Saliva in the diagnosis of diseases. *International journal of oral science* **2016,** *8* (3), 133.

(69) Tripathi, A.; Tiwari, B.; Patil, R.; Khanna, V.; Singh, V. The role of salivary caffeine clearance in the diagnosis of chronic liver disease. *Journal of oral biology and craniofacial research* **2015,** *5* (1), 28.

(70) Pallos, D.; Leão, M. V.; Togeiro, F. C.; Alegre, L.; Ricardo, L. H.; Perozini, C.; Ruivo, G. F. Salivary markers in patients with chronic renal failure. *Archives of oral biology* **2015,** *60* (12), 1784.

(71) Holm-Hansen, C.; Tong, G.; Davis, C.; Abrams, W. R.; Malamud, D. Comparison of oral fluid collectors for use in a rapid point-of-care diagnostic device. *Clinical and diagnostic laboratory immunology* **2004,** *11* (5), 909.

(72) Navazesh, M. Methods for collecting saliva. *Annals of the New York Academy of Sciences* **1993,** *694* (1), 72.

(73) Lomonaco, T.; Ghimenti, S.; Biagini, D.; Bramanti, E.; Onor, M.; Bellagambi, F.; Fuoco, R.; Di Francesco, F. The effect of sampling procedures on the urate and lactate concentration in oral fluid. *Microchemical Journal* **2017**.

(74) Salimetrics; Salimetrics, 2017; Vol. 2017.

(75) Elmongy, H.; Abdel-Rehim, M. Saliva as an alternative specimen to plasma for drug bioanalysis: A review. *TrAC Trends in Analytical Chemistry* **2016,** *83* (Part B), 70.

(76) Hubert, C. A.; Google Patents, 1971.

(77) Drury, M. I.; Timoney, F. J.; Delaney, P. DEXTROSTIX--A RAPID METHOD OF ESTIMATING BLOOD GLUCOSE LEVELS. *Journal of the Irish Medical Association* **1965,** *56*, 52.

(78) Steiner, M.-S.; Duerkop, A.; Wolfbeis, O. S. Optical methods for sensing glucose. *Chemical Society Reviews* **2011,** *40* (9), 4805.

(79) Gochman, N.; Schmitz, J. M. Application of a new peroxide indicator reaction to the specific, automated determination of glucose with glucose oxidase. *Clinical Chemistry* **1972,** *18* (9), 943.

(80) Duine, J.; Jzn, J. F.; Van Zeeland, J. Glucose dehydrogenase from Acinetobacter calcoaceticus: a 'quinoprotein'. *FEBS letters* **1979,** *108* (2), 443.

(81) Wohlfahrt, G.; Witt, S.; Hendle, J.; Schomburg, D.; Kalisz, H. M.; Hecht, H.-J. 1.8 and 1.9 Å resolution structures of the Penicillium amagasakiense and Aspergillus niger glucose oxidases as a basis for modelling substrate complexes. *Acta Crystallographica Section D: Biological Crystallography* **1999,** *55* (5), 969.

(82) Wu, G.; Fang, Y.-Z.; Yang, S.; Lupton, J. R.; Turner, N. D. Glutathione metabolism and its implications for health. *The Journal of nutrition* **2004,** *134* (3), 489.

(83) Wohlfahrt, G.; Witt, S.; Hendle, J.; Schomburg, D.; Kalisz, H. M.; Hecht, H. J. 1.8 and 1.9 A resolution structures of the Penicillium amagasakiense and Aspergillus niger glucose oxidases as a basis for modelling substrate complexes. *Acta crystallographica. Section D, Biological crystallography* **1999,** *55* (Pt 5), 969.

(84) Updike, S. J.; Hicks, G. P. The Enzyme Electrode. *Nature* **1967,** *214* (5092), 986.

(85) Wu, M.; Lin, Z.; Dürkop, A.; Wolfbeis, O. S. Time-resolved enzymatic determination of glucose using a fluorescent europium probe for hydrogen peroxide. *Analytical and Bioanalytical Chemistry* **2004,** *380* (4), 619.

(86) Schäferling, M.; Wu, M.; Wolfbeis, O. S. Time-Resolved Fluorescent Imaging of Glucose. *Journal of Fluorescence* **2004,** *14* (5), 561.

(87) Lenarczuk, T.; Wencel, D.; Głb, S.; Koncki, R. Prussian blue-based optical glucose biosensor in flow-injection analysis. *Analytica Chimica Acta* **2001,** *447* (1–2), 23.

(88) Piletsky, S. A.; Panasyuk, T. L.; Piletskaya, E. V.; Sergeeva, T. A.; El'skaya, A. V.; Pringsheim, E.; Wolfbeis, O. S. Polyaniline-coated microtiter plates for use in longwave optical bioassays. *Fresenius' journal of analytical chemistry* **2000,** *366* (8), 807.

(89) D'Auria, S.; Di Cesare, N.; Gryczynski, Z.; Gryczynski, I.; Rossi, M.; Lakowicz, J. R. A thermophilic apoglucose dehydrogenase as nonconsuming glucose sensor. *Biochemical and biophysical research communications* **2000,** *274* (3), 727.

(90) Yoo, E.-H.; Lee, S.-Y. Glucose biosensors: an overview of use in clinical practice. *Sensors* **2010,** *10* (5), 4558.

(91) Toghill, K. E.; Compton, R. G. Electrochemical non-enzymatic glucose sensors: a perspective and an evaluation. *Int. J. Electrochem. Sci* **2010,** *5* (9), 1246.

(92) Palleschi, G.; Faridnia, M. H.; Lubrano, G. J.; Guilbault, G. G. Ideal hydrogen peroxide-based glucose sensor. *Applied Biochemistry and Biotechnology* **1991,** *31* (1), 21.

(93) Okuda, J.; Wakai, J.; Yuhashi, N.; Sode, K. Glucose enzyme electrode using cytochrome b 562 as an electron mediator. *Biosensors and Bioelectronics* **2003,** *18* (5), 699.

(94) Park, S.; Boo, H.; Chung, T. D. Electrochemical non-enzymatic glucose sensors. *Analytica Chimica Acta* **2006,** *556* (1), 46.

(95) Cash, K. J.; Clark, H. A. Nanosensors and nanomaterials for monitoring glucose in diabetes. *Trends in molecular medicine* **2010,** *16* (12), 584.

(96) Rahman, M. M.; Ahammad, A.; Jin, J.-H.; Ahn, S. J.; Lee, J.-J. A comprehensive review of glucose biosensors based on nanostructured metal-oxides. *Sensors* **2010,** *10* (5), 4855.

(97) Wei, A.; Sun, X. W.; Wang, J. X.; Lei, Y.; Cai, X. P.; Li, C. M.; Dong, Z. L.; Huang, W. Enzymatic glucose biosensor based on ZnO nanorod array grown by hydrothermal decomposition. *Applied Physics Letters* **2006,** *89* (12).

(98) Kong, T.; Chen, Y.; Ye, Y.; Zhang, K.; Wang, Z.; Wang, X. An amperometric glucose biosensor based on the immobilization of glucose oxidase on the ZnO nanotubes. *Sensors and Actuators B: Chemical* **2009,** *138* (1), 344.

(99) Wang, Y.-T.; Yu, L.; Zhu, Z.-Q.; Zhang, J.; Zhu, J.-Z.; Fan, C.-h. Improved enzyme immobilization for enhanced bioelectrocatalytic activity of glucose sensor. *Sensors and Actuators B: Chemical* **2009,** *136* (2), 332.

(100) Kotzian, P.; Brázdilová, P.; Řezková, S.; Kalcher, K.; Vytřas, K. Amperometric Glucose Biosensor Based on Rhodium Dioxide-Modified Carbon Ink. *Electroanalysis* **2006,** *18* (15), 1499.

(101) Ernst, S.; Heitbaum, J.; Hamann, C. The electrooxidation of glucose in phosphate buffer solutions: kinetics and reaction mechanism. *Berichte der Bunsengesellschaft für physikalische Chemie* **1980,** *84* (1), 50.

(102) Yang, J.; Jiang, L.-C.; Zhang, W.-D.; Gunasekaran, S. A highly sensitive non-enzymatic glucose sensor based on a simple two-step electrodeposition of cupric oxide (CuO) nanoparticles onto multi-walled carbon nanotube arrays. *Talanta* **2010,** *82* (1), 25.

(103) Chen, X.-m.; Lin, Z.-j.; Chen, D.-J.; Jia, T.-t.; Cai, Z.-m.; Wang, X.-r.; Chen, X.; Chen, G.-n.; Oyama, M. Nonenzymatic amperometric sensing of glucose by using palladium nanoparticles supported on functional carbon nanotubes. *Biosensors and Bioelectronics* **2010,** *25* (7), 1803.

(104) Yang, J.; Zhang, W.-D.; Gunasekaran, S. An amperometric non-enzymatic glucose sensor by electrodepositing copper nanocubes onto vertically well-aligned multi-walled carbon nanotube arrays. *Biosensors and Bioelectronics* **2010,** *26* (1), 279.

(105) Wang, Y.; Wei, W.; Liu, X.; Zeng, X. Carbon nanotube/chitosan/gold nanoparticles-based glucose biosensor prepared by a layer-by-layer technique. *Materials Science and Engineering: C* **2009,** *29* (1), 50.

(106) Xiao, F.; Zhao, F.; Mei, D.; Mo, Z.; Zeng, B. Nonenzymatic glucose sensor based on ultrasonic-electrodeposition of bimetallic PtM (M = Ru, Pd and Au) nanoparticles on carbon nanotubes–ionic liquid composite film. *Biosensors and Bioelectronics* **2009,** *24* (12), 3481.

(107) Zhu, H.; Lu, X.; Li, M.; Shao, Y.; Zhu, Z. Nonenzymatic glucose voltammetric sensor based on gold nanoparticles/carbon nanotubes/ionic liquid nanocomposite. *Talanta* **2009,** *79* (5), 1446.

(108) Ibupoto, Z. H.; Khun, K.; Beni, V.; Liu, X.; Willander, M. Synthesis of novel CuO nanosheets and their non-enzymatic glucose sensing applications. *Sensors* **2013,** *13* (6), 7926.

(109) Guo, C.; Wang, Y.; Zhao, Y.; Xu, C. Non-enzymatic glucose sensor based on three dimensional nickel oxide for enhanced sensitivity. *Analytical Methods* **2013,** *5* (7), 1644.

(110) Wang, J. Electrochemical glucose biosensors. *Chemical reviews* **2008,** *108* (2), 814.

(111) Lerner, M. B.; Kybert, N.; Mendoza, R.; Villechenon, R.; Lopez, M. A. B.; Johnson, A. C. Scalable, non-invasive glucose sensor based on boronic acid functionalized carbon nanotube transistors. *Applied Physics Letters* **2013,** *102* (18), 183113.

(112) Xi, S.; Shi, T.; Liu, D.; Xu, L.; Long, H.; Lai, W.; Tang, Z. Integration of carbon nanotubes to three-dimensional C-MEMS for glucose sensors. *Sensors and Actuators A: Physical* **2013,** *198*, 15.

(113) Kamyabi, M. A.; Hajari, N.; Turner, A. P.; Tiwari, A. A high-performance glucose biosensor using covalently immobilised glucose oxidase on a poly (2, 6-diaminopyridine)/carbon nanotube electrode. *Talanta* **2013,** *116*, 801.

(114) Zhiguo, G.; Shuping, Y.; Zaijun, L.; Xiulan, S.; Guangli, W.; Yinjun, F.; Junkang, L. An ultrasensitive hydrogen peroxide biosensor based on electrocatalytic synergy of graphene–gold nanocomposite, CdTe–CdS core–shell quantum dots and gold nanoparticles. *Analytica chimica acta* **2011,** *701* (1), 75.

(115) Razmi, H.; Mohammad-Rezaei, R. Graphene quantum dots as a new substrate for immobilization and direct electrochemistry of glucose oxidase: Application to sensitive glucose determination. *Biosensors and Bioelectronics* **2013,** *41*, 498.

(116) Alvi, N.; Rodriguez, P. S.; Gómez, V.; Kumar, P.; Amin, G.; Nur, O.; Willander, M.; Nötzel, R. Highly efficient potentiometric glucose biosensor based on functionalized InN quantum dots. *Applied Physics Letters* **2012,** *101* (15), 153110.

(117) Wu, P.; He, Y.; Wang, H.-F.; Yan, X.-P. Conjugation of glucose oxidase onto Mn-doped ZnS quantum dots for phosphorescent sensing of glucose in biological fluids. *Analytical chemistry* **2010,** *82* (4), 1427.

(118) Li, R.; Zhen, M.; Guan, M.; Chen, D.; Zhang, G.; Ge, J.; Gong, P.; Wang, C.; Shu, C. A novel glucose colorimetric sensor based on intrinsic peroxidase-like activity of C 60-carboxyfullerenes. *Biosensors and Bioelectronics* **2013,** *47*, 502.

(119) Wang, X.-d.; Chen, H.-x.; Zhou, T.-y.; Lin, Z.-j.; Zeng, J.-b.; Xie, Z.-x.; Chen, X.; Wong, K.-y.; Chen, G.-n.; Wang, X.-r. Optical colorimetric sensor strip for direct readout glucose measurement. *Biosensors and Bioelectronics* **2009,** *24* (12), 3702.

(120) Zhang, W.; Ma, D.; Du, J. Prussian blue nanoparticles as peroxidase mimetics for sensitive colorimetric detection of hydrogen peroxide and glucose. *Talanta* **2014,** *120*, 362.

(121) Murphy, C. J. Peer reviewed: optical sensing with quantum dots. *Analytical Chemistry* **2002,** *74* (19), 520 A.

(122) Green, M. The nature of quantum dot capping ligands. *Journal of Materials Chemistry* **2010,** *20* (28), 5797.

(123) Zheng, X. T.; Ananthanarayanan, A.; Luo, K. Q.; Chen, P. Glowing graphene quantum dots and carbon dots: properties, syntheses, and biological applications. *Small* **2015,** *11* (14), 1620.

(124) Karakoti, A. S.; Shukla, R.; Shanker, R.; Singh, S. Surface functionalization of quantum dots for biological applications. *Advances in colloid and interface science* **2015,** *215*, 28.

(125) Murray, C. B.; Norris, D. J.; Bawendi, M. G. Synthesis and characterization of nearly monodisperse CdE (E = sulfur, selenium, tellurium) semiconductor nanocrystallites. *Journal of the American Chemical Society* **1993,** *115* (19), 8706.

(126) Hines, M. A.; Guyot-Sionnest, P. Synthesis and Characterization of Strongly Luminescing ZnS-Capped CdSe Nanocrystals. *The Journal of Physical Chemistry* **1996,** *100* (2), 468.

(127) Micic, O. I.; Curtis, C. J.; Jones, K. M.; Sprague, J. R.; Nozik, A. J. Synthesis and Characterization of InP Quantum Dots. *The Journal of Physical Chemistry* **1994,** *98* (19), 4966.

(128) Qu, Z.-b.; Zhou, X.; Gu, L.; Lan, R.; Sun, D.; Yu, D.; Shi, G. Boronic acid functionalized graphene quantum dots as a fluorescent probe for selective and sensitive glucose determination in microdialysate. *Chemical Communications* **2013,** *49* (84), 9830.

(129) Wang, S. W.; Zhang, X. O.; Yu, J. H. Advanced Materials Research, 2011; p 1338.

(130) Wu, W.; Zhou, T.; Berliner, A.; Banerjee, P.; Zhou, S. Glucose-Mediated Assembly of Phenylboronic Acid Modified CdTe/ZnTe/ZnS Quantum Dots for Intracellular Glucose Probing. *Angewandte Chemie International Edition* **2010,** *49* (37), 6554.

(131) Li, X.; Zhou, Y.; Zheng, Z.; Yue, X.; Dai, Z.; Liu, S.; Tang, Z. Glucose Biosensor Based on Nanocomposite Films of CdTe Quantum Dots and Glucose Oxidase. *Langmuir* **2009,** *25* (11), 6580.

(132) Cheng, L.; Deng, S.; Lei, J.; Ju, H. Disposable electrochemiluminescent biosensor using bidentate-chelated CdTe quantum dots as emitters for sensitive detection of glucose. *Analyst* **2012,** *137* (1), 140.

(133) Li, Y.; Li, B.; Zhang, J. H2O2-and pH-sensitive CdTe quantum dots as fluorescence probes for the detection of glucose. *Luminescence* **2013,** *28* (5), 667.

(134) Wang, J.-H.; Li, Y.-Q.; Zhang, H.-L.; Wang, H.-Q.; Lin, S.; Chen, J.; Zhao, Y.-D.; Luo, Q.-M. Bioconjugation of concanavalin and CdTe quantum dots and the detection of glucose. *Colloids and Surfaces A: Physicochemical and Engineering Aspects* **2010,** *364* (1), 82.

(135) Yuan, J.; Guo, W.; Yin, J.; Wang, E. Glutathione-capped CdTe quantum dots for the sensitive detection of glucose. *Talanta* **2009,** *77* (5), 1858.

(136) Hu, M.; Lu, H.; Yuwen, L.; Wang, L. 2010 3rd International Nanoelectronics Conference (INEC), 2010; p 868.

(137) WANG, X.; ZHONG, J.; Liu, Y.; WEN, A.; Shan, Z.; YANG, W. Preparation of Magnetic and Fluorescent Bifunctional Nanocomposites and Its Application to Separation and Detection of Glucose. *Acta Chim. Sinica* **2010,** *20*, 2063.

(138) Zhiguo, G.; Shuping, Y.; Zaijun, L.; Xiulan, S.; Guangli, W.; Yinjun, F.; Junkang, L. An ultrasensitive electrochemical biosensor for glucose using CdTe-CdS core–shell quantum dot as ultrafast electron transfer relay between graphene-gold nanocomposite and gold nanoparticle. *Electrochimica Acta* **2011,** *56* (25), 9162.

(139) Cao, L.; Ye, J.; Tong, L.; Tang, B. A new route to the considerable enhancement of glucose oxidase (GOx) activity: the simple assembly of a complex from CdTe quantum dots and GOx, and its glucose sensing. *Chemistry–A European Journal* **2008,** *14* (31), 9633.

(140) Hu, M.; Tian, J.; Lu, H.-T.; Weng, L.-X.; Wang, L.-H. H 2 O 2-sensitive quantum dots for the label-free detection of glucose. *Talanta* **2010,** *82* (3), 997.

(141) Huang, C.-P.; Liu, S.-W.; Chen, T.-M.; Li, Y.-K. A new approach for quantitative determination of glucose by using CdSe/ZnS quantum dots. *Sensors and Actuators B: Chemical* **2008,** *130* (1), 338.

(142) Saran, A. D.; Sadawana, M. M.; Srivastava, R.; Bellare, J. R. An optimized quantum dot-ligand system for biosensing applications: Evaluation as a glucose biosensor. *Colloids and Surfaces A: Physicochemical and Engineering Aspects* **2011,** *384* (1), 393.

(143) Abbott In *Abbott Free style Glucose Monitoring system manual*; Abbott; Vol. 5-15.

(144) Vashist, S. K.; Zheng, D.; Al-Rubeaan, K.; Luong, J. H. T.; Sheu, F.-S. Technology behind commercial devices for blood glucose monitoring in diabetes management: A review. *Analytica Chimica Acta* **2011,** *703* (2), 124.

(145) Bayer, 2016.

(146) Witkowska Nery, E.; Kundys, M.; Jeleń, P. S.; Jönsson-Niedziółka, M. Electrochemical Glucose Sensing: Is There Still Room for Improvement? *Analytical Chemistry* **2016,** *88* (23), 11271.

(147) Taylor, C.; Kenausis, G.; Katakis, I.; Heller, A. "Wiring" of glucose oxidase within a hydrogel made with polyvinyl imidazole complexed with [(Os-4,4′-dimethoxy-2,2′-bipyridine)Cl] + 2+1. *Journal of Electroanalytical Chemistry* **1995,** *396* (1-2), 511.

(148) Xiang, L.; Zhang, Z.; Yu, P.; Zhang, J.; Su, L.; Ohsaka, T.; Mao, L. In situ cationic ring-opening polymerization and quaternization reactions to confine ferricyanide onto carbon nanotubes: A general approach to development of integrative nanostructured electrochemical biosensors. *Analytical Chemistry* **2008,** *80* (17), 6587.

(149) meter, O. U. OneTouch UltraMini Blood glucose monitering system. **2016**.

(150) Yoo, E.-H.; Lee, S.-Y. Glucose Biosensors: An Overview of Use in Clinical Practice. *Sensors* **2010,** *10* (5), 4558.

(151) Estey, M. P.; Cohen, A. H.; Colantonio, D. A.; Chan, M. K.; Marvasti, T. B.; Randell, E.; Delvin, E.; Cousineau, J.; Grey, V.; Greenway, D.et al. CLSI-based transference of the CALIPER database of pediatric reference intervals from Abbott to Beckman, Ortho, Roche and Siemens Clinical Chemistry Assays: Direct validation using reference samples from the CALIPER cohort. *Clinical Biochemistry* **2013,** *46* (13), 1197.

(152) Abbott Abbott Park, Illinois, U.S.A., 2017; Vol. 2017.

(153) Abbott; Abbot, 20; Vol. 2017.

(154) Siemens UK, 2017; Vol. 2017.

(155) Centers, H. T., 2017; Vol. 2017.

(156) USA, C. o. D. C. a. P. C.; CDC, 2017; Vol. 2017.

(157) Cook, R. P. *Cholesterol: chemistry, biochemistry, and pathology*; Elsevier, 2015.

(158) NCEP, 2001.

(159) Zarychta, B.; Lyubimov, A.; Ahmed, M.; Munshi, P.; Guillot, B.; Vrielink, A.; Jelsch, C. Cholesterol oxidase: ultrahigh-resolution crystal structure and multipolar atom model-based analysis. *Acta Crystallographica Section D* **2015,** *71* (4), 954.

(160) Zarychta, B.; Lyubimov, A.; Ahmed, M.; Munshi, P.; Guillot, B.; Vrielink, A.; Jelsch, C. Cholesterol oxidase: ultrahigh-resolution crystal structure and multipolar atom model-based analysis. *Acta crystallographica. Section D, Biological crystallography* **2015,** *71* (Pt 4), 954.

(161) Khan, M. A.; Gallo, R. M.; Renukaradhya, G. J.; Du, W.; Gervay-Hague, J.; Brutkiewicz, R. R. Statins impair CD1d-mediated antigen presentation through the inhibition of prenylation. *The Journal of Immunology* **2009,** *182* (8), 4744.

(162) Mellado, M.; Garcia, J. E.; Pittroff, W. Rough agave flowers as a potential feed resource for growing goats. *Rangeland ecology & management* **2008,** *61* (6), 640.

(163) CellBioLab, I., 2012; Vol. 2013.

(164) Guo, M.; Chen, J.; Li, J.; Nie, L.; Yao, S. Carbon Nanotubes-Based Amperometric Cholesterol Biosensor Fabricated Through Layer-by-Layer Technique. *Electroanalysis* **2004,** *16* (23), 1992.

(165) Tan, X.; Li, M.; Cai, P.; Luo, L.; Zou, X. An amperometric cholesterol biosensor based on multiwalled carbon nanotubes and organically modified sol-gel/chitosan hybrid composite film. *Analytical Biochemistry* **2005,** *337* (1), 111.

(166) Dhand, C.; Arya, S. K.; Datta, M.; Malhotra, B. Polyaniline–carbon nanotube composite film for cholesterol biosensor. *Analytical biochemistry* **2008,** *383* (2), 194.

(167) Wisitsoraat, A.; Sritongkham, P.; Karuwan, C.; Phokharatkul, D.; Maturos, T.; Tuantranont, A. Fast cholesterol detection using flow injection microfluidic device with functionalized carbon nanotubes based electrochemical sensor. *Biosensors and Bioelectronics* **2010,** *26* (4), 1514.

(168) Eguílaz, M.; Villalonga, R.; Agüí, L.; Yáñez-Sedeño, P.; Pingarrón, J. Gold nanoparticles: Poly (diallyldimethylammonium chloride)–carbon nanotubes composites as platforms for the preparation of electrochemical enzyme biosensors: Application to the determination of cholesterol. *Journal of electroanalytical chemistry* **2011,** *661* (1), 171.

(169) Gopalan, A. I.; Lee, K.-P.; Ragupathy, D. Development of a stable cholesterol biosensor based on multi-walled carbon nanotubes–gold nanoparticles composite covered with a layer of chitosan–room-temperature ionic liquid network. *Biosensors and Bioelectronics* **2009,** *24* (7), 2211.

(170) Kumar, S. P.; Manjunatha, R.; Nethravathi, C.; Suresh, G. S.; Rajamathi, M.; Venkatesha, T. V. Electrocatalytic oxidation of NADH on functionalized graphene modified graphite electrode. *Electroanalysis* **2011,** *23* (4), 842.

(171) Manjunatha, R.; Suresh, G. S.; Melo, J. S.; D'Souza, S. F.; Venkatesha, T. V. An amperometric bienzymatic cholesterol biosensor based on functionalized graphene modified electrode and its electrocatalytic activity towards total cholesterol determination. *Talanta* **2012,** *99*, 302.

(172) Parlak, O.; Tiwari, A.; Turner, A. P.; Tiwari, A. Template-directed hierarchical self-assembly of graphene based hybrid structure for electrochemical biosensing. *Biosensors and Bioelectronics* **2013,** *49*, 53.

(173) Cao, S.; Zhang, L.; Chai, Y.; Yuan, R. An integrated sensing system for detection of cholesterol based on TiO 2–graphene–Pt–Pd hybridnanocomposites. *Biosensors and Bioelectronics* **2013,** *42*, 532.

(174) Cao, S.; Zhang, L.; Chai, Y.; Yuan, R. Electrochemistry of cholesterol biosensor based on a novel Pt–Pd bimetallic nanoparticle decorated graphene catalyst. *Talanta* **2013,** *109*, 167.

(175) Ruecha, N.; Rangkupan, R.; Rodthongkum, N.; Chailapakul, O. Novel paper-based cholesterol biosensor using graphene/polyvinylpyrrolidone/polyaniline nanocomposite. *Biosensors and Bioelectronics* **2014,** *52*, 13.

(176) Aravind, S. S. J.; Baby, T. T.; Arockiadoss, T.; Rakhi, R. B.; Ramaprabhu, S. A cholesterol biosensor based on gold nanoparticles decorated functionalized graphene nanoplatelets. *Thin Solid Films* **2011,** *519* (16), 5667.

(177) Umar, A.; Rahman, M.; Al-Hajry, A.; Hahn, Y.-B. Highly-sensitive cholesterol biosensor based on well-crystallized flower-shaped ZnO nanostructures. *Talanta* **2009,** *78* (1), 284.

(178) Wang, C.; Tan, X.; Chen, S.; Yuan, R.; Hu, F.; Yuan, D.; Xiang, Y. Highly-sensitive cholesterol biosensor based on platinum–gold hybrid functionalized ZnO nanorods. *Talanta* **2012,** *94*, 263.

(179) Umar, A.; Rahman, M.; Vaseem, M.; Hahn, Y.-B. Ultra-sensitive cholesterol biosensor based on low-temperature grown ZnO nanoparticles. *Electrochemistry Communications* **2009,** *11* (1), 118.

(180) Khan, R.; Kaushik, A.; Solanki, P. R.; Ansari, A. A.; Pandey, M. K.; Malhotra, B. Zinc oxide nanoparticles-chitosan composite film for cholesterol biosensor. *Analytica chimica acta* **2008,** *616* (2), 207.

(181) Israr, M. Q.; Sadaf, J. R.; Asif, M.; Nur, O.; Willander, M.; Danielsson, B. Potentiometric cholesterol biosensor based on ZnO nanorods chemically grown on Ag wire. *Thin Solid Films* **2010,** *519* (3), 1106.

(182) Saxena, U.; Chakraborty, M.; Goswami, P. Covalent immobilization of cholesterol oxidase on self-assembled gold nanoparticles for highly sensitive amperometric detection of cholesterol in real samples. *Biosensors and Bioelectronics* **2011,** *26* (6), 3037.

(183) Gomathi, P.; Ragupathy, D.; Choi, J. H.; Yeum, J. H.; Lee, S. C.; Kim, J. C.; Lee, S. H.; Do Ghim, H. Fabrication of novel chitosan nanofiber/gold nanoparticles composite towards improved performance for a cholesterol sensor. *Sensors and Actuators B: Chemical* **2011,** *153* (1), 44.

(184) Ansari, A. A.; Kaushik, A.; Solanki, P. R.; Malhotra, B. e. D. Electrochemical Cholesterol Sensor Based on Tin Oxide-Chitosan Nanobiocomposite Film. *Electroanalysis* **2009,** *21* (8), 965.

(185) Lakowicz, J. R.; Nature Publishing Group, 2006.

(186) Eftink, M.; Lakowicz, J.; Plenum: New York, 1991; Vol. 2.

(187) Meixner, A. J. In *Advances in Photochemistry*; John Wiley & Sons, Inc., 2007, DOI:10.1002/9780470133552.ch1 10.1002/9780470133552.ch1.

(188) Poole, R. A.; Hawe, A.; Jiskoot, W.; Braeckmans, K. In *Analysis of Aggregates and Particles in Protein Pharmaceuticals*; John Wiley & Sons, Inc., 2012, DOI:10.1002/9781118150573.ch9 10.1002/9781118150573.ch9.

(189) Valeur, B. In *Molecular Fluorescence*; Wiley-VCH Verlag GmbH, 2001, DOI:10.1002/3527600248.ch11 10.1002/3527600248.ch11.

(190) Valeur, B.; Berberan-Santos, M. N. In *Molecular Fluorescence*; Wiley-VCH Verlag GmbH & Co. KGaA, 2012, DOI:10.1002/9783527650002.ch14 10.1002/9783527650002.ch14.

(191) Lupton, J. M. Single-Molecule Spectroscopy for Plastic Electronics: Materials Analysis from the Bottom-Up. *Advanced Materials* **2010,** *22* (15), 1689.

(192) Orte, A.; Clarke, R. W.; Klenerman, D. Single-Molecule Fluorescence Coincidence Spectroscopy and its Application to Resonance Energy Transfer. *ChemPhysChem* **2011,** *12* (3), 491.

(193) Schleifenbaum, F.; Blum, C.; Brecht, M.; Meixner, A. J. In *Handbook of Spectroscopy*; Wiley-VCH Verlag GmbH & Co. KGaA, 2014, DOI:10.1002/9783527654703.ch21 10.1002/9783527654703.ch21.

(194) Irvine, D. J.; Purbhoo, M. A.; Krogsgaard, M.; Davis, M. M. Direct observation of ligand recognition by T cells. *Nature* **2002,** *419* (6909), 845.

(195) Pope, A. J.; Haupts, U. M.; Moore, K. J. Homogeneous fluorescence readouts for miniaturized high-throughput screening: theory and practice. *Drug Discovery Today* **1999,** *4* (8), 350.

(196) Eun Jun, M.; Roy, B.; Han Ahn, K. "Turn-on" fluorescent sensing with "reactive" probes. *Chemical Communications* **2011,** *47* (27), 7583.

(197) Heagy, M. D. Book Review of Advanced Fluorescence Reporters in Chemistry and Biology I: Fundamentals and Molecular Design. *Journal of the American Chemical Society* **2011,** *133* (19), 7619.

(198) Hess, S. T.; Huang, S.; Heikal, A. A.; Webb, W. W. Biological and Chemical Applications of Fluorescence Correlation Spectroscopy: A Review. *Biochemistry* **2002,** *41* (3), 697.

(199) Jaffé, R.; Cawley, K. M.; Yamashita, Y. In *Advances in the Physicochemical Characterization of Dissolved Organic Matter: Impact on Natural and Engineered Systems*; American Chemical Society, 2014; Vol. 1160.

(200) Newman, A. Product Review: X-Ray Fluorescence Makes It Elementary. *Analytical Chemistry* **1997,** *69* (15), 493A.

(201) Petty, J. T. Book Review of Advanced Fluorescence Reporters in Chemistry and Biology II: Molecular Constructions, Polymers and Nanoparticles. *Journal of the American Chemical Society* **2011,** *133* (26), 10323.

(202) Sarder, P.; Maji, D.; Achilefu, S. Molecular Probes for Fluorescence Lifetime Imaging. *Bioconjugate Chemistry* **2014,** *26* (6), 963.

(203) Gather, M. C.; Meerholz, K.; Danz, N.; Leosson, K. Net optical gain in a plasmonic waveguide embedded in a fluorescent polymer. *Nature Photonics* **2010,** *4* (7), 457.

(204) Yariv, A.; Yeh, P. *Photonics: optical electronics in modern communications (the oxford series in electrical and computer engineering)*; Oxford University Press, Inc., 2006.

(205) Pinto, M. R.; Schanze, K. S. Conjugated polyelectrolytes: Synthesis and applications. *Synthesis* **2002,** *2002* (09), 1293.

(206) Feng, X.; Liu, L.; Wang, S.; Zhu, D. Water-soluble fluorescent conjugated polymers and their interactions with biomacromolecules for sensitive biosensors. *Chemical Society Reviews* **2010,** *39* (7), 2411.

(207) Liu, B.; Wang, S.; Bazan, G. C.; Mikhailovsky, A. Shape-adaptable water-soluble conjugated polymers. *Journal of the American Chemical Society* **2003,** *125* (44), 13306.

(208) Rogach, A. L. Semiconductor nanocrystal quantum dots. *Wien-New York: Springer* **2008**.

(209) Trindade, T.; O'Brien, P.; Pickett, N. L. Nanocrystalline semiconductors: synthesis, properties, and perspectives. *Chemistry of Materials* **2001,** *13* (11), 3843.

(210) Klimov, V. I. *Nanocrystal quantum dots*; CRC Press, 2010.

(211) Ando, M.; Kamimura, T.; Uegaki, K.; Biju, V.; Shigeri, Y. Sensing of ozone based on its quenching effect on the photoluminescence of CdSe-based core-shell quantum dots. *Microchimica Acta* **2016,** *183* (11), 3019.

(212) El Haouari, M.; Talbi, A.; Feddi, E.; El Ghazi, H.; Oukerroum, A.; Dujardin, F. Linear and nonlinear optical properties of a single dopant in strained AlAs/GaAs spherical core/shell quantum dots. *Optics Communications* **2017,** *383*, 231.

(213) Hung, L. X.; Thang, P. N.; Van Nong, H.; Yen, N. H.; Chinh, V. Đ.; Van Vu, L.; Hien, N. T. T.; de Marcillac, W. D.; Hong, P. N.; Loan, N. T.et al. Synthesis, Structural and Optical Characterization of CdTeSe/ZnSe and CdTeSe/ZnTe Core/Shell Ternary Quantum Dots for Potential Application in Solar Cells. *Journal of Electronic Materials* **2016,** *45* (8), 4425.

(214) Jie, G.; Lu, Z.; Zhao, Y.; Wang, X. Quantum dots bilayers/Au@Ag-based electrochemiluminescence resonance energy transfer for detection of thrombin by autocatalytic multiple amplification strategy. *Sensors and Actuators, B: Chemical* **2017,** *240*, 857.

(215) Jing, L.; Kershaw, S. V.; Li, Y.; Huang, X.; Li, Y.; Rogach, A. L.; Gao, M. Aqueous Based Semiconductor Nanocrystals. *Chemical Reviews* **2016,** *116* (18), 10623.

(216) Kuang, W. J.; Li, Q.; Sun, Y.; Chen, J.; Tolner, H. Near-band-edge emission characteristics of ZnO-MgO core-shell quantum-dots. *Materials Letters* **2016,** *178*, 27.

(217) Ling, L.; Wang, W.; Wang, C. F.; Chen, S. Fast access to core/shell/shell CdTe/CdSe/ZnO quantum dots via magnetic hyperthermia method. *AIChE Journal* **2016,** *62* (8), 2614.

(218) Sagar, L. K.; Walravens, W.; Zhao, Q.; Vantomme, A.; Geiregat, P.; Hens, Z. PbS/CdS core/shell quantum dots by additive, layer-by-layer shell growth. *Chemistry of Materials* **2016,** *28* (19), 6953.

(219) Savchenko, S. S.; Vokhmintsev, A. S.; Weinstein, I. A. Optical properties of InP/ZnS quantum dots deposited into nanoporous anodic alumina. *Journal of Physics: Conference Series* **2016,** *741* (1).

(220) Shcherbinin, D. P.; Konshina, E. A. Ionic impurities in nematic liquid crystal doped with quantum dots CdSe/ZnS. *Liquid Crystals* **2016**, DOI:10.1080/02678292.2016.1227483 10.1080/02678292.2016.1227483, 1.

(221) Talbi, A.; Feddi, E.; Zouitine, A.; Haouari, M. E.; Zazoui, M.; Oukerroum, A.; Dujardin, F.; Assaid, E.; Addou, M. Control of the binding energy by tuning the single

dopant position, magnetic field strength and shell thickness in ZnS/CdSe core/shell quantum dot. *Physica E: Low-Dimensional Systems and Nanostructures* **2016,** *84*, 303.

(222) Vatansever, F.; Hamblin, M. R. Surface-initiated ring-opening metathesis polymerization (SI-ROMP) to attach a tethered organic corona onto CdSe/ZnS core/shell quantum dots. *Journal of Nanoparticle Research* **2016,** *18* (10).

(223) Xiao, X.; Tang, H.; Zhang, T.; Chen, W.; Chen, W.; Wu, D.; Wang, R.; Wang, K. Improving the modulation bandwidth of LED by CdSe/ZnS quantum dots for visible light communication. *Optics Express* **2016,** *24* (19), 21577.

(224) Zhao, M. Y.; Zhao, R. M.; Li, W.; Ma, Y. Q.; Wang, T. X.; Dai, X. Q. Magnetic properties of the 2D Fe<inf>n</inf> core X<inf>m</inf> (X = C, N, O, Cl, S and F) shell clusters embedded in graphene. *Applied Surface Science* **2017,** *392*, 277.

(225) Zhou, R.; Wan, L.; Niu, H.; Yang, L.; Mao, X.; Zhang, Q.; Miao, S.; Xu, J.; Cao, G. Tailoring band structure of ternary CdS<inf>x</inf>Se<inf>1-x</inf> quantum dots for highly efficient sensitized solar cells. *Solar Energy Materials and Solar Cells* **2016,** *155*, 20.

(226) Castañeda, J. A.; Nagamine, G.; Yassitepe, E.; Bonato, L. G.; Voznyy, O.; Hoogland, S.; Nogueira, A. F.; Sargent, E. H.; Cruz, C. H. B.; Padilha, L. A. Efficient Biexciton Interaction in Perovskite Quantum Dots under Weak and Strong Confinement. *ACS Nano* **2016,** *10* (9), 8603.

(227) Maity, P.; Dana, J.; Ghosh, H. N. Multiple Charge Transfer Dynamics in Colloidal CsPbBr<inf>3</inf> Perovskite Quantum Dots Sensitized Molecular Adsorbate. *Journal of Physical Chemistry C* **2016,** *120* (32), 18348.

(228) Peng, L.; Tang, A.; Yang, C.; Teng, F. Size-controlled synthesis of highly luminescent organometal halide perovskite quantum dots. *Journal of Alloys and Compounds* **2016,** *687*, 506.

(229) Tang, X.; Hu, Z.; Chen, W.; Xing, X.; Zang, Z.; Hu, W.; Qiu, J.; Du, J.; Leng, Y.; Jiang, X.et al. Room temperature single-photon emission and lasing for all-inorganic colloidal perovskite quantum dots. *Nano Energy* **2016,** *28*, 462.

(230) Yang, G. L.; Zhong, H. Z. Organometal halide perovskite quantum dots: synthesis, optical properties, and display applications. *Chinese Chemical Letters* **2016,** *27* (8), 1124.

(231) Liu, F.; Jang, M. H.; Ha, H. D.; Kim, J. H.; Cho, Y. H.; Seo, T. S. Facile synthetic method for pristine graphene quantum dots and graphene oxide quantum dots: origin of blue and green luminescence. *Advanced materials* **2013,** *25* (27), 3657.

(232) Sun, Y.-P.; Zhou, B.; Lin, Y.; Wang, W.; Fernando, K. S.; Pathak, P.; Meziani, M. J.; Harruff, B. A.; Wang, X.; Wang, H. Quantum-sized carbon dots for bright and colorful photoluminescence. *Journal of the American Chemical Society* **2006,** *128* (24), 7756.

(233) Klimov, V. I.; Mikhailovsky, A.; Xu, S.; Malko, A.; Hollingsworth, J.; Leatherdale, C.; Eisler, H.-J.; Bawendi, M. Optical gain and stimulated emission in nanocrystal quantum dots. *Science* **2000,** *290* (5490), 314.

(234) Alivisatos, A. P. Semiconductor clusters, nanocrystals, and quantum dots. *Science* **1996,** *271* (5251), 933.

(235) Takagahara, T.; Takeda, K. Theory of the quantum confinement effect on excitons in quantum dots of indirect-gap materials. *Physical Review B* **1992,** *46* (23), 15578.

(236) Nirmal, M.; Norris, D. J.; Kuno, M.; Bawendi, M. G.; Efros, A. L.; Rosen, M. Observation of the" dark exciton" in CdSe quantum dots. *Physical review letters* **1995,** *75* (20), 3728.

(237) Klimov, V. I.; Mikhailovsky, A. A.; McBranch, D. W.; Leatherdale, C. A.; Bawendi, M. G. Quantization of Multiparticle Auger Rates in Semiconductor Quantum Dots. *Science* **2000,** *287* (5455), 1011.

(238) Klimov, V. I.; Mikhailovsky, A. A.; Xu, S.; Malko, A.; Hollingsworth, J. A.; Leatherdale, C. A.; Eisler, H.-J.; Bawendi, M. G. Optical Gain and Stimulated Emission in Nanocrystal Quantum Dots. *Science* **2000,** *290* (5490), 314.

(239) Wise, F. W. Lead Salt Quantum Dots: the Limit of Strong Quantum Confinement. *Accounts of Chemical Research* **2000,** *33* (11), 773.

(240) Rowan, B.; Mc Cormack, S.; Doran, J.; Norton, B. Proceedings of SPIE - The International Society for Optical Engineering, 2007.

(241) Sengupta, S.; Acharya, S. AIP Conference Proceedings, 2011; p 75.

(242) Fricke, M.; Lorke, A.; Kotthaus, J. P.; Medeiros-Ribeiro, G.; Petroff, P. M. Shell structure and electron-electron interaction in self-assembled InAs quantum dots. *EPL (Europhysics Letters)* **1996,** *36* (3), 197.

(243) Ebrahim, S.; Labeb, M.; Abdel-Fattah, T.; Soliman, M. CdTe Quantum Dots Capped with Different Stabilizing Agents for Sensing of Ochratoxin A. *Journal of Luminescence 182*, 154.

(244) Hepburn, W. G.; Batchelor-McAuley, C.; Tschulik, K.; Kachoosangi, R. T.; Ness, D.; Compton, R. G. Use of the capping agent for the electrochemical detection and quantification of nanoparticles: CdSe quantum dots. *Sensors and Actuators B: Chemical* **2014,** *204*, 445.

(245) Khan, Z. M. S. H.; Khan, S. A.; Zulfequar, M. Study of thiol capped CdSe quantum dots using SeO2 precursor for selenium source. *Materials Science in Semiconductor Processing* **2017,** *57*, 190.

(246) Rajabi, H. R.; Farsi, M. Study of capping agent effect on the structural, optical and photocatalytic properties of zinc sulfide quantum dots. *Materials Science in Semiconductor Processing* **2016,** *48*, 14.

(247) Green, M. The nature of quantum dot capping ligands. *Journal of Materials Chemistry* **2010,** *20* (28), 5797.

(248) Martinić, I.; Eliseeva, S. V.; Petoud, S. Near-infrared emitting probes for biological imaging: Organic fluorophores, quantum dots, fluorescent proteins, lanthanide(III) complexes and nanomaterials. *Journal of Luminescence*.

(249) Costa-Fernández, J. M.; Pereiro, R.; Sanz-Medel, A. The use of luminescent quantum dots for optical sensing. *TrAC Trends in Analytical Chemistry* **2006,** *25* (3), 207.

(250) Frigerio, C.; Ribeiro, D. S. M.; Rodrigues, S. S. M.; Abreu, V. L. R. G.; Barbosa, J. A. C.; Prior, J. A. V.; Marques, K. L.; Santos, J. L. M. Application of quantum dots as analytical tools in automated chemical analysis: A review. *Analytica Chimica Acta* **2012,** *735*, 9.

(251) Bao, L.; Sun, L.; Zhang, Z.-L.; Jiang, P.; Wise, F. W.; Abruña, H. D.; Pang, D.-W. Energy-Level-Related Response of Cathodic Electrogenerated-Chemiluminescence of Self-Assembled CdSe/ZnS Quantum Dot Films. *The Journal of Physical Chemistry C* **2011,** *115* (38), 18822.

(252) Dong, S.; Liu, F.; Lu, C. Organo-Modified Hydrotalcite-Quantum Dot Nanocomposites as a Novel Chemiluminescence Resonance Energy Transfer Probe. *Analytical Chemistry* **2013,** *85* (6), 3363.

(253) Dong, Y.-P.; Gao, T.-T.; Zhou, Y.; Zhu, J.-J. Electrogenerated Chemiluminescence Resonance Energy Transfer between Luminol and CdSe@ZnS Quantum Dots and Its Sensing Application in the Determination of Thrombin. *Analytical Chemistry* **2014,** *86* (22), 11373.

(254) Freeman, R.; Liu, X.; Willner, I. Chemiluminescent and Chemiluminescence Resonance Energy Transfer (CRET) Detection of DNA, Metal Ions, and Aptamer–Substrate Complexes Using Hemin/G-Quadruplexes and CdSe/ZnS Quantum Dots. *Journal of the American Chemical Society* **2011,** *133* (30), 11597.

(255) Liu, J.; Chen, H.; Lin, Z.; Lin, J.-M. Preparation of Surface Imprinting Polymer Capped Mn-Doped ZnS Quantum Dots and Their Application for Chemiluminescence Detection of 4-Nitrophenol in Tap Water. *Analytical Chemistry* **2010,** *82* (17), 7380.

(256) Tang, Y.; Su, Y.; Yang, N.; Zhang, L.; Lv, Y. Carbon Nitride Quantum Dots: A Novel Chemiluminescence System for Selective Detection of Free Chlorine in Water. *Analytical Chemistry* **2014,** *86* (9), 4528.

(257) Xu, S.; Li, X.; Li, C.; Li, J.; Zhang, X.; Wu, P.; Hou, X. In Situ Generation and Consumption of H2O2 by Bienzyme–Quantum Dots Bioconjugates for Improved Chemiluminescence Resonance Energy Transfer. *Analytical Chemistry* **2016,** *88* (12), 6418.

(258) Bhatnagar, D.; Kumar, V.; Kumar, A.; Kaur, I. Graphene quantum dots FRET based sensor for early detection of heart attack in human. *Biosensors and Bioelectronics* **2016,** *79*, 495.

(259) Kurabayashi, T.; Funaki, N.; Fukuda, T.; Akiyama, S.; Suzuki, M. CdSe/ZnS quantum dots conjugated with a fluorescein derivative: A FRET-based pH sensor for physiological alkaline conditions. *Analytical Sciences* **2014,** *30* (5), 545.

(260) Li, C.; Wang, X.; Ye, C.; Wang, Y.; Hu, Y.; Yan, Z. Synthesis and characterization of fluorescence resonance energy transfer-based nanoprobes by coating CdTe QDs with rhodamine B in gelatin nanoparticles. *Journal of Nanoscience and Nanotechnology* **2013,** *13* (6), 4330.

(261) Stanisavljevic, M.; Krizkova, S.; Vaculovicova, M.; Kizek, R.; Adam, V. Quantum dots-fluorescence resonance energy transfer-based nanosensors and their application. *Biosensors and Bioelectronics* **2015,** *74*, 562.

(262) Zamaleeva, A. I.; Despras, G.; Luccardini, C.; Collot, M.; De Waard, M.; Oheim, M.; Mallet, J. M.; Feltz, A. FRET-based nanobiosensors for imaging intracellular Ca2+ and H+ microdomains. *Sensors (Switzerland)* **2015,** *15* (9), 24662.

(263) Zeng, Q.; Li, Q.; Ji, W.; Bin, X.; Song, J. Highly Sensitive Homogeneous Immunoassays Based on Construction of Silver Triangular Nanoplates-Quantum Dots FRET System. *Scientific Reports* **2016,** *6*.

(264) Zhang, Y.; Zhou, D.; He, J. FRET studies between CdTe capped by small-molecule ligands and fluorescent protein. *International Journal of Nanoscience* **2015,** *13* (5-6).

(265) Rene-Boisneuf, L.; Scaiano, J. C. Sensitivity versus Stability: Making Quantum Dots More Luminescent by Sulfur Photocuring without Compromising Sensor Response. *Chemistry of Materials* **2008,** *20* (21), 6638.

(266) Golub, E.; Niazov, A.; Freeman, R.; Zatsepin, M.; Willner, I. Photoelectrochemical Biosensors Without External Irradiation: Probing Enzyme Activities and DNA Sensing Using Hemin/G-Quadruplex-Stimulated Chemiluminescence Resonance Energy Transfer (CRET) Generation of Photocurrents. *The Journal of Physical Chemistry C* **2012,** *116* (25), 13827.

(267) Hu, L.; Liu, X.; Cecconello, A.; Willner, I. Dual Switchable CRET-Induced Luminescence of CdSe/ZnS Quantum Dots (QDs) by the Hemin/G-Quadruplex-Bridged Aggregation and Deaggregation of Two-Sized QDs. *Nano Letters* **2014,** *14* (10), 6030.

(268) Deng, S.; Ju, H. Electrogenerated chemiluminescence of nanomaterials for bioanalysis. *Analyst* **2013,** *138* (1), 43.

(269) Fu, X.; Tan, X.; Yuan, R.; Chen, S. A dual-potential electrochemiluminescence ratiometric sensor for sensitive detection of dopamine based on graphene-CdTe quantum dots and self-enhanced Ru(II) complex. *Biosensors and Bioelectronics*, DOI:http://dx.doi.org/10.1016/j.bios.2016.11.025 http://dx.doi.org/10.1016/j.bios.2016.11.025.

(270) Gas sensors: Colorful oxygen. *NPG Asia Mater* **2008**.

(271) Tang, S.; Wang, M.; Li, Z.; Tong, P.; Chen, Q.; Li, G.; Chen, J.; Zhang, L. A novel sensitive colorimetric sensor for Cu2+ based on in situ formation of fluorescent quantum dots with photocatalytic activity. *Biosensors and Bioelectronics*, DOI:http://dx.doi.org/10.1016/j.bios.2016.09.105 http://dx.doi.org/10.1016/j.bios.2016.09.105.

(272) Zayats, M.; Kharitonov, A. B.; Pogorelova, S. P.; Lioubashevski, O.; Katz, E.; Willner, I. Probing Photoelectrochemical Processes in Au−CdS Nanoparticle Arrays by Surface Plasmon Resonance: Application for the Detection of Acetylcholine Esterase Inhibitors. *Journal of the American Chemical Society* **2003,** *125* (51), 16006.

(273) Pal, D.; Stoleru, V.; Towe, E.; Firsov, D. Quantum dot-size variation and its impact on emission and absorption characteristics: An experimental and theoretical modeling investigation. *Japanese journal of applied physics* **2002,** *41* (2R), 482.

(274) Elward, J. M.; Chakraborty, A. Effect of Dot Size on Exciton Binding Energy and Electron–Hole Recombination Probability in CdSe Quantum Dots. *Journal of chemical theory and computation* **2013,** *9* (10), 4351.

(275) Jamieson, T.; Bakhshi, R.; Petrova, D.; Pocock, R.; Imani, M.; Seifalian, A. M. Biological applications of quantum dots. *Biomaterials* **2007,** *28* (31), 4717.

(276) Aich, U. Materials Science Forum, 2013; p 1.

(277) Alivisatos, A. P. Semiconductor Clusters, Nanocrystals, and Quantum Dots. *Science* **1996,** *271* (5251), 933.

(278) Lakowicz, J. R. *Principles of fluorescence spectroscopy*; Springer Science & Business Media, 2013.

(279) Resch-Genger, U.; Grabolle, M.; Cavaliere-Jaricot, S.; Nitschke, R.; Nann, T. Quantum dots versus organic dyes as fluorescent labels. *Nat Meth* **2008,** *5* (9), 763.

(280) Pinaud, F.; Clarke, S.; Sittner, A.; Dahan, M. Probing cellular events, one quantum dot at a time. *Nat Meth* **2010,** *7* (4), 275.

(281) Valeur, B.; Berberan-Santos, M. N. *Molecular fluorescence: principles and applications*; John Wiley & Sons, 2012.

(282) Schmelz, O.; Mews, A.; Basché, T.; Herrmann, A.; Müllen, K. Supramolecular complexes from CdSe nanocrystals and organic fluorophors. *Langmuir* **2001,** *17* (9), 2861.

(283) Pockrand, I.; Swalen, J.; Santo, R.; Brillante, A.; Philpott, M. Optical properties of organic dye monolayers by surface plasmon spectroscopy. *The Journal of Chemical Physics* **1978,** *69* (9), 4001.

(284) Scholes, G. D. Book Review of Semiconductor Nanocrystal Quantum Dots: Synthesis, Assembly, Spectroscopy and Applications. *Journal of the American Chemical Society* **2008,** *130* (52), 18028.

(285) Cheng, Z.; Lin, J. Synthesis and application of nanohybrids based on upconverting nanoparticles and polymers. *Macromolecular Rapid Communications* **2015,** *36* (9), 790.

(286) Carbonaro, C. M.; Chiriu, D.; Ricci, P. C. Are organic compounds good candidates to substitute rare earth materials in fluorescent applications? *Physica Status Solidi (C) Current Topics in Solid State Physics* **2016**, DOI:10.1002/pssc.201600130 10.1002/pssc.201600130.

(287) Fernandez-Suarez, M.; Ting, A. Y. Fluorescent probes for super-resolution imaging in living cells. *Nat Rev Mol Cell Biol* **2008,** *9* (12), 929.

Chapter 2. Synthesis and Characterization of Quantum dots (QDs)

2.1 Introduction

QDs can be synthesized from various metals and semiconducting materials, especially from group III-V, II-VI, IV-VI and VI-I. The selection of materials depends on the application and uses. Among metals CdSe, CdTe, PbSe, ZnSe, PbSe, CdSe, CdTeSe, GeSi are promising semiconducting metals for the synthesis and preparation of highly fluorescence QDs[1,2]. Recently carbon materials were also used for the preparation of QDs; Graphene QDs, carbon dots [3], graphene oxide QDs [4]. The colloidal QDs are highly stable, with high quantum yield, controllable, cost-effective, and scalable [5]. To date variety of QDs has been synthesized with a different structure, morphology, and metal compositions with surface capping agents [6]. The colloidal QDs synthesis route is further categorized into water aqueous method and organic route. The organic phase synthesized QDs are non-soluble in an aqueous medium, which cannot be used for the application of biological study or the prepared QDs can be subjected to surface modification to make it compatible with biological applications, while aqueous phase synthesized QDs do not need any further surface modifications [7]. The advantages of aqueous phase synthesis methods are that the reaction can proceed relative low temperature which simplifying the synthetic procedure and that there is the availability of wide range of water soluble materials that could be used for a variety of QDs preparations.

The capping agent of QDs is important for preparation of QDs with inorganic procuress. The capping agents have multiple functions; they stabilizing the nanocrystals, by providing solubility and colloidal stability. The surface caps precisely controlling the growth rate, particle morphology, particle uniformity and size distribution, reaction pathway and also prevents the aggregation of nanocrystals [8]. We can assume that electronic and chemical properties of the surface ligand contribute to the chemical, physical, and optoelectronic nature of the dot. The ligand completely blocking the surface and controlling the fluorescence quantum yield and the spectral position [9,10]. Among the different surface capping agent, thiols are the best surfactant

to control the nucleation and growth of QDs nanocrystals composed of group II-VI elements. Thiols are highly reactive and react with metals in nanocrystals yielding the sulphur-metal linkage in an aqueous. Thiol-capped quantum dots synthesized in an aqueous medium are cost effective, less toxic and highly biocompatible as compared to the synthesis in organo-metallic pathway [11].

Cadmium telluride (CdTe) QDs with biocompatible ligand are one of the potential candidates that can be synthesized via aqueous phase and could be used in biological media[12]. QDs are nano-size crystals and thermodynamically unstable, they are stabilized and the size is controlled by capping agents during the crystal growth. The capping agent arrests the nanocrystals and prevents them from aggregating and precipitate [13]. Thiol appears to be an excellent capping agent for most CdTe quantum dots. Micic et al, for the first time, explore the use of thiol to stabilized CdTe nanoparticles, which is the most used surface ligand of QDs [14]. The thiol-stabilized QDs are used in the biological system and are stables for many days[15]. Computational modeling of thiols on quantum dot surfaces[16] and nuclear magnetic resonance[17] study of thiol-stabilized QDs suggest that thiol is connected to the metal through sulfur-bound hydrogen or only sulfur. Thiol-capping agent make an additional buffer layer that could stabilize QDs and increase the bandgap, that is the reason that thiol-capped CdTe QDs are highly luminescent[18], but this explanation failed in CdSe QDs although core-shell CdSe and ZnS QDs are high luminescent, one reason is the electronic structure and the position of energy level of thiol interaction with core CdSe suppress the optical properties of CdSe-thiol-capped QDs[13]. The popular capping agent used for the quantum dots are thioglycolic acid [19], mercaptopropionic acid (MPA), glutathione (GHS), and cysteine (CYS). Among these glutathione and cysteine are highly biocompatible and have a vital role in the human body. The highest growth rate was reported for GHS capped QD and the GHS QDs are highly photostable as compared to thioglycolic acid and mercaptopropionic acid capped quantum dots [20]. In this study, we synthesized cysteine, mercaptopropionic acid, dimercaptosuccinic acid and glutathione (Figure 2.1) stabilized cadmium tellurium quantum dots. The QDs are characterized and the optical was investigated.

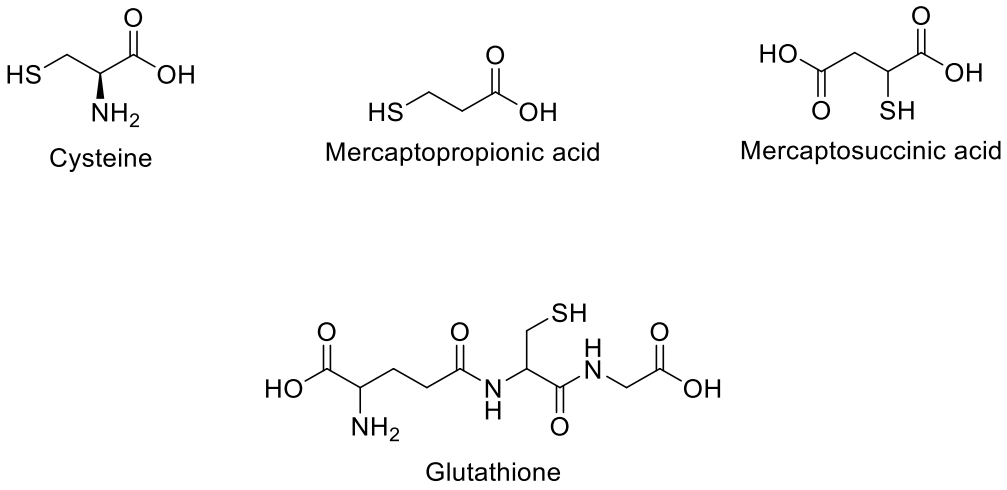

Figure 2.1. The structure of cysteine, mercaptopropionic acid, mercaptosuccinic acid, and glutathione capping agents of CdTe QDs.

2.2 Experimental

2.2.1 Materials

Analytical grade chemicals were used. Tellurium (V) Oxide 99%, cadmium chloride 99% sodium borohydride 98% Hydrogen peroxide, L-Cysteine, glutathione, mercaptopropionic acid, and mercaptosuccinic acid were obtained from Acros Organic USA. Sodium hydroxide and sodium citrate dihydrate were purchased from Enox® Changshu, China. Milli-Q water (Millipore Co., Billerica, MA, USA) were used for all synthesis.

2.2.2 Instruments for characterization

Spectrofluorometer consist of Xenon lamp of 150-W ozone free xenon arc lamp (FluoroMax-4 spectrophotometer Horiba scientific USA) was used for recording fluorescence spectra; Cary 300 UV-VIS spectrophotometer (Agilent Technology USA) was used for recording UV-Visible spectra. IR spectra of MPA and GHS were recorded by FTIR spectrometer carry 600 series (Agilent Technology USA). STEM images were obtained from transmission electron microscope Tecnal G2 F20, (FEI USA).The x-ray powder diffraction was carried out by diffractometer (Bruker, Karlsruhe, Germany) With radiation source (40 kV, 40 mA) of Cu *K*

α, spanning a 2θ ranging from 20° to 50° at 1°/s scan rate. The pH meter (Mettler Toledo, model SevenMulti from USA, Washington) was use for adjusting the pH of reaction mixture.

2.2.3 Synthesis of cysteine-capped (CYS) CdTe QDs

L-Cysteine capped CdTe quantum dots were prepared accordingly to the previously reported methods [21,22] with modifications. Cadmium chloride 0.970 g (0.0052 M) and 0.733 g (0.006 M) of L-cysteine were dissolved in 200 mL water. The initial pH of the mixture was 2.7, which was adjusted to 10.6 by dropwise addition of 1 M NaOH with continuous stirring. While adjusting the pH dropwise the mixture was precipitates with white colour at pH 3.23 to 6.5. A clear solution of reactants was obtained at pH 7.1 by a further increase by the dropwise addition of 1 M NaOH solution. Tellurium oxide 0.032 g (0.0003 M) and sodium borohydride 0.2 g (0.005 M) of was added to the reaction mixture. The solution was transferred to 1000 mL conical flask and degassed with argon for 5 minutes. The L-Cysteine capped CdTe nanocrystals were grown at 100 Cº in the absence of oxygen. 2 mL aliquots of reaction mixture were withdrawn at an interval of 20, 40, 80, 120, 160, and 220 minutes for further characterization.

The obtained QDs after 220 minutes of reaction were precipitated in an equal volume of 1-propanol and water. QDs solution 50 mL (first fraction) was added dropwise in an equal amount of 1-propanol in a beaker with constant stirring. The first fraction QDs obtained was collected by centrifugation (15 minutes) at the rate of 2000 rpm per minute. The QDs first fraction was re-dispersed in 30 mL water and re-precipitated from 1-propanol. The precipitations followed by centrifugation of QDs were repeated thrice. The clean CYS QDs were redispersed in 10 ml of water and was stored in a fridge at 4 ºC.

2.2.4 Synthesis of GHS-capped CdTe QDs

Glutathione (GHS) capped CdTe quantum dots were synthesized according to Sheng, Han, Hu and Chi [23,24] method with modifications. 0.2 g (0.001 M) of cadmium chloride, 0.5 g (0.002 mM) of citric acid trisodium dihydrate, 0.4 g (0.0012 M) of glutathione, 0.1 g (0.003 M) of sodium borohydride, and 0.05 g (0.0002 M) of sodium tellurium (IV) oxide were dissolved into 100 mL water in 250 mL conical flask. The pH was adjusted to 10.5 with 1 molar

solution of sodium hydroxide. The molar ratio of $Cd^{+,}$ $TeO_3^{-,}$ and GHS used was 5:1:6 respectively. The color of the solution changed to dark brown after the addition of all chemicals. The reaction mixture was kept stirring for 5 minute. Once all the chemicals are completely dissolved the solution was heated at 100 °C under stirring. The colour of the reaction mixture was changed to light yellow in 5 minutes and then to orange and red. Aliquots of 2 mL QDs were collected at the different interval (15, 35, 90, 105, and 115 minutes) and was observed under UV lamp (365 nm).

The obtained QDs from the reaction mixture were purified by precipitation followed by centrifugation described above. Initially, the synthesized GHS QDs solution of 80 mL was added dropwise in an equal amount of 1-propanol in 100 ml beaker with continuous gentle stirring. The precipitations followed by centrifugation of GHS QDs were repeated thrice. The obtained QDs were re-dispersed in 10 mL of water and stored.

2.2.5 Synthesis of MPA-capped QDs

MPA-capped CdTe QDs were synthesized by direct oxidation of tellurium oxide. 0.37 g (0.002 M) of $CdCl_2$ was dissolved in 100 mL of water in a conical flask, and MPA (0.0054 M) was added while stirring. The initial pH of the solution observed was the 2, which were adjusted to 10.0 by spiking of 1.0 molar NaOH solution gradually. TeO_2 0.08 g (0.0005 M) was added to the solution. The molar ratios of cadmium, tellurium and MPA in a reaction mixture were 1.2, 0.4, and 5.4 mM. The color of the reaction mixture was changed to light yellow after the addition of TeO_2. The solution was kept under stirring for 40 minutes until the color disappeared and the solution was reacted at 100 C° for 1 hour and aliquots were collected at the equal interval (23, 30, 40, 50 60, and 70 minutes) for optical characterization. The cleaning process of the prepared QDs consists of precipitation with an equal amount of 1-propanol and water followed by centrifugation. The first fractions of QDs were res-dispersed in water and were precipitated again with 1-propanol followed by centrifugation. This process was repeated three times. The cleaned QDs were stored.

2.2.6 Synthesis of MSA quantum dots

0.256 g (0.002 M) of $CdCl_2$, was dissolved into 100 mL of water in a two-necked flask. 0.825 g (0.0008 M) of trisodium citrate dehydrates, 0.019 g (0.0003 M) of Na_2TeO_3, 0.875 g (0.0007 M) of MSA, and sodium borohydride ($NaBH_4$, 0.435 g) were then added. The reaction mixture was stirred at room temperature for 30 mins. The reaction mixture was colorless. The reaction mixture was reacted at 100 °C for two hours. Green and orange quantum dots aliquots were collected at an interval of 40, 85, 120 and 150 minutes and were characterized. The obtained quantum dots were precipitated by an equal volume of ethanol and water followed by centrifugation for 15 minutes at the rate of 2000 RPM per minute. The first fraction of QDs precipitate was re-dissolved in 20 mL of water and re-precipitate with an equal amount of 1-propanol followed by centrifugation for 25 minutes at 2000 RPM per minute. The QDs precipitate was re-dissolved in 35 mL water and was kept in the fridge at 4 ^oC.

2.3 Results and discussion

2.3.1 CYS-capped CdTe QDs

The synthesis of nanocrystals following Ostwald ripening principles; the nanocrystals precursors are dissolved and then crystals of different size grow. The precursor chemicals used in the synthesis were $CdCl_2.5H_2O$ and TeO_2, and cysteine was chosen as a capping agent. The reaction involved two steps; first nucleation and second is growth. Thiol has a tendency toward metals, in this reaction cadmium-cysteine complex was formed (Eq. 2.1). TeO_2 is reduced by sodium $NaBH_2$ to Te^{2-} (Eq. 2.2) which reacts to cadmium-cysteine complex and form nanocrystals capped with cysteine (Eq. 2.3). In the second phase is the growth of the CdTe quantum dots (Eq. 2.4) [21].

$$Cd^{2+} + \text{Cysteine} \longrightarrow Cd^{2+}\text{Cysteine} \quad (2.1)$$

$$5TeO_2^- + BH_4^- \longrightarrow 5Te^{2-} + 4BO_2 + 2H_2O \quad (2.2)$$

$$Cd^{2+}\text{Cysteine} + Te^{2-} \longrightarrow \text{CdTe-cysteine} \quad (2.3)$$

$$n\text{CdTe-cysteine} \longrightarrow (\text{CdTe-cysteine})_n \quad (2.4)$$

After the reaction, the excess of cysteine stabilizer and Cd^{+} were removed by precipitating thrice from 1-propanol. The removal of unreacted chemical is essential before using QDs for biological assays. It is proven that post purified have better optical properties than unpurified QDs [21].

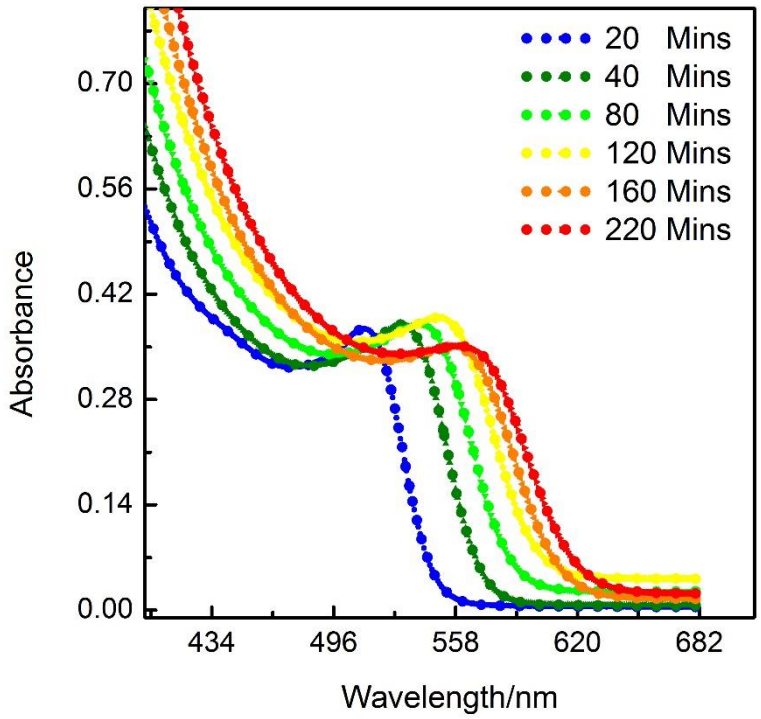

Figure 2.2 Uv-visible absorbance spectra of CYS-capped QDs obtained from reaction mixture at different reaction time.

The UV-visible absorption spectra of CYS QDs in Figure 2.2 are of broad absorption. The lambda maximum was 551, 531, 542, 550, 560, and 565 nm. The red shifting of absorption spectrum also confirming the growth of QDs.

The sizes of QDs of different absorption spectra were calculated according to the method developed by Peng X *et al*. They give an empirical relationship between the first excitonic peak and size of the quantum dots [25]. The Empirical relation of first excitonic peak versus the size of CdTe QDs is

$$D = (9.8127 \times 10^{-7})\,\lambda^{3} - (1.7147 \times 10^{-3})\,\lambda^{2} + (1.0064)\,\lambda - (194.84).$$

Where D is the size of CYS capped CdTe QDs and λ is the first excitonic peak. The calculated size for samples with different reaction time was 3.3, 3.5, 3.7, 3.9, 4.0, and 4.1 nm (Table 2.1).

The emission of CYS-QDs was performed and shown in Figure 2.3. The fluorescence of CYS-QDs was measured at room temperature. The fluorescence emission wavelength is red-shifted from 536 to 603 nm with gradual increase in reaction time, which indicates the size increase of the nanocrystals. The narrow emission spectra and high fluorescence intensity suggest that CdTe crystals were uniformly capped by cysteine. The full width at half maxima (FWHM) was calculated from Gaussian distribution varied from 38 to 57 nm, which are lower than organic dyes.

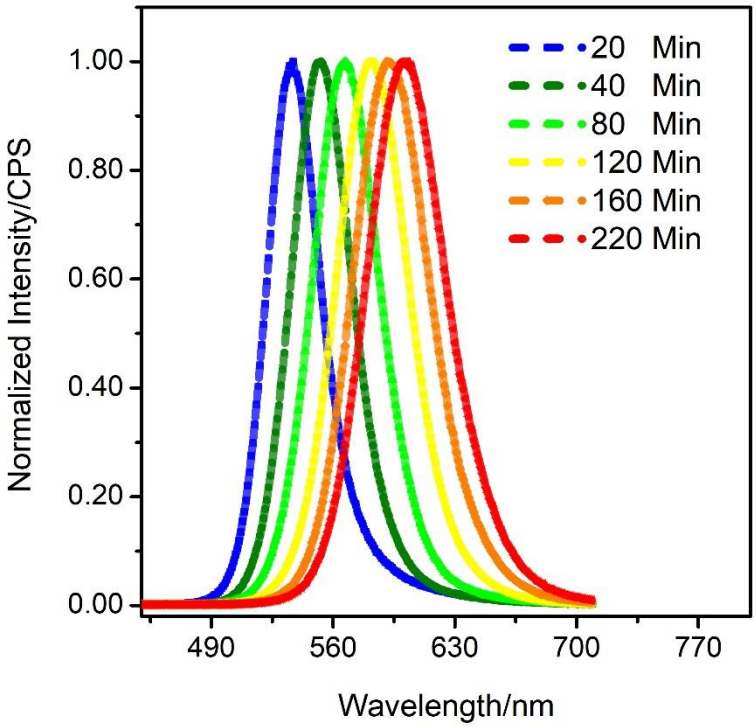

Figure 2.3 Fluorescence spectra of CYS-capped QDs obtained from reaction mixture at different reaction time.

Reaction time (min)	**λ_{max} of Absorption**	**Calculated size (nm)**	**λ_{max} of Emission**	**FWHM (nm)**
20	511	3.3	536	38
40	531	3.5	552	42
80	542	3.7	567	46
120	550	3.9	587	50

160	560	4.0	591	53
220	565	4.1	603	55.9

Table 2.1 The table shows the emission, the lambda max absorption, calculated size, and full width half maximum (FWHM) of CYS-capped QDs obtained from the reaction mixture at different interval.

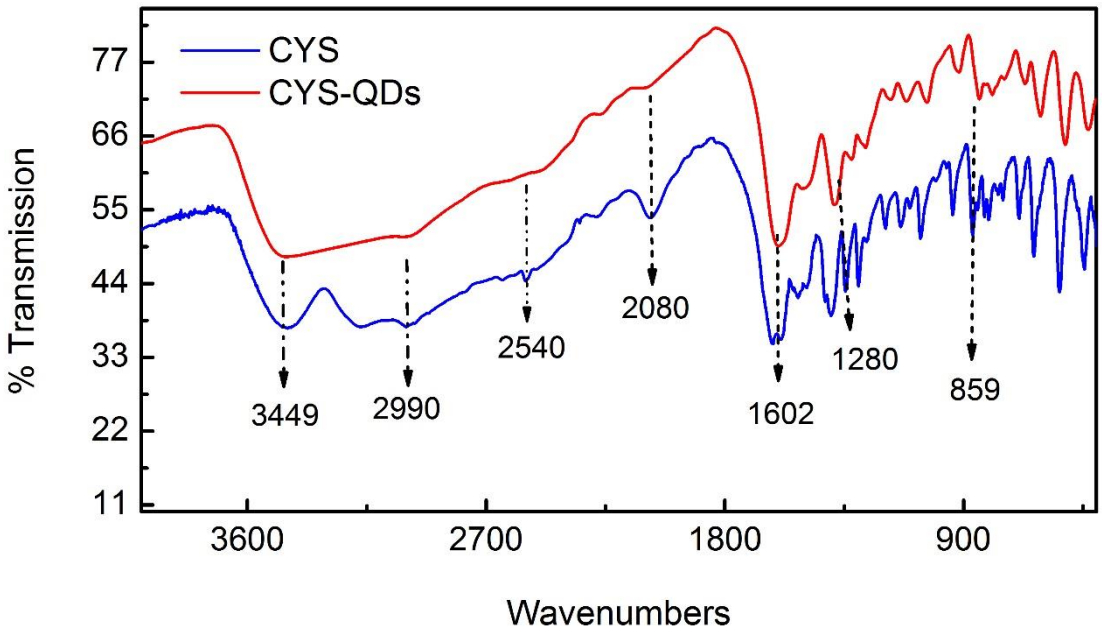

Figure 2.4 The FTIR spectra of cysteine and cysteine-capped quantum dots.

The FTIR spectra of cysteine and CYS QDs and cysteine are presented in Figure 2.4. The peak observed for CdTe CYS QDs 1602 cm^{-1} correspond to a carbonyl group. Another band located at 2900 cm^{-1} corresponds to C-H stretching. The peak 3300 cm^{-1} to 3449 cm^{-1} of the cysteine and CYS QDs can be assigned to N-H stretching[57]. The absence of the peak for S-H at 2540 cm^{-1} in CYS capped CdTe QDs confirmed the formation of thiol bond between cysteine and CdTe. It has been reported [21, 27] before that thiol and carboxyls groups are covalently linked to Cd^{+2} ions on QDs surface, thus the –SH stretching on the surface of QDs disappeared.

The cysteine-capped CdTe quantum dot synthesized at 100 ^{o}C was analyzed by high-resolution transmission electron microscopy and powder x-ray diffraction (PXRD). The HR-TEM image is shown in Figure 2.5 shows the QDs size distribution and the particle sized is

shown in TEM image. ImageJ was used to analyze the TEM image. The calculated average size of the QDs (fluorescence emission at 603 nm) from the TEM image was 4.3 nm with standard deviation of 0.6 nm. The size calculated from the UV-visible absorbance spectra was 4.1. The size calculated from TEM image and VU-visible spectra are comparable.

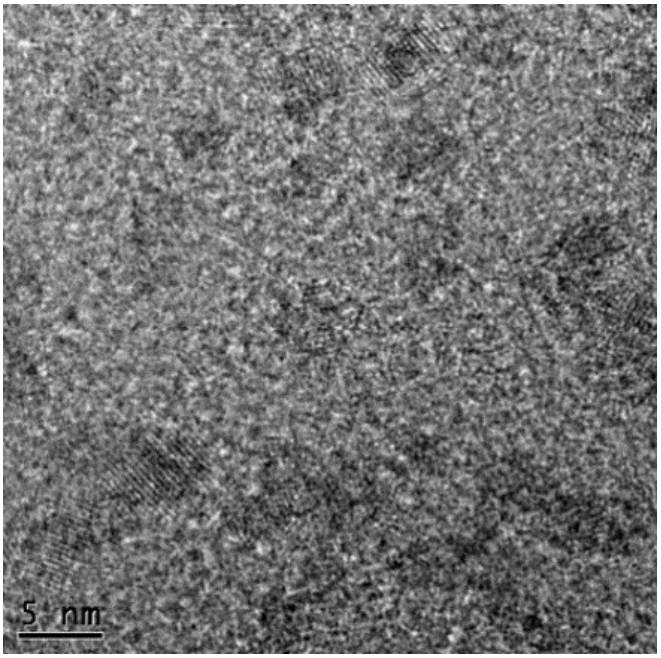

Figure 2.5 TEM image showing quantum dot size and distribution of cysteine-capped CdTe QDs.

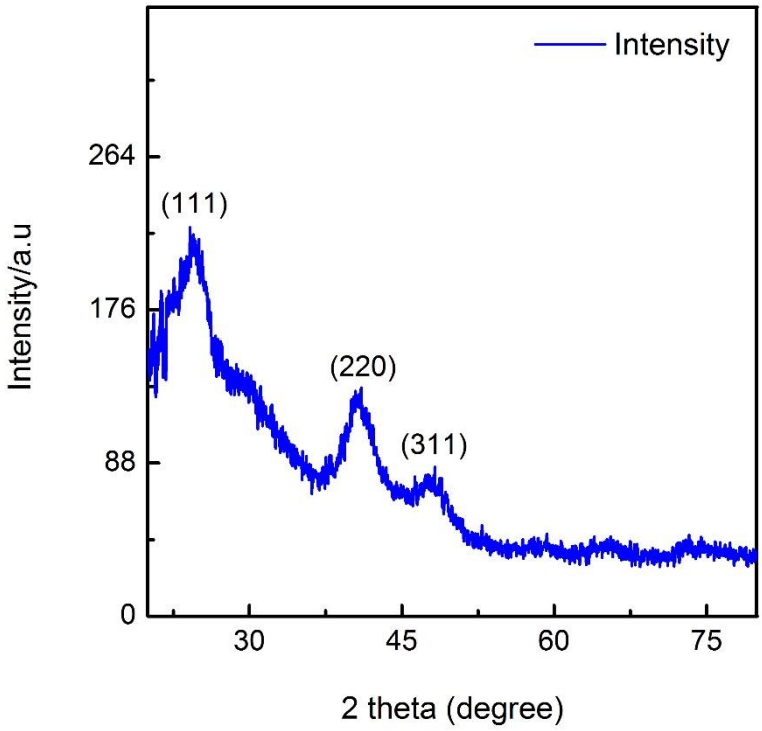

Figure 2.6 X-ray diffraction spectra of Cysteine capped CdTe nanocrystals. The positions XRD peaks (111), (220), and (311) represent cubic (zinc-blende) phase of CdTe nanocrystals.

The XRD pattern cysteine-capped CdTe QDs (emission at 624 nm) shown in Figure 2.6. The three XRD peaks at around 25°, 41°, and 47°, are of (111), (220) and (311) planes of the cubic zinc-blende phase structure of nanocrystals of CdTe, respectively. The PXRD peaks positions of CdTe were located between the values of the cubic CdTe in figure 2.6. There is as slit shifting the peak position which shows the hydrolysis of thiol group and the formation of CdS. This XRD pattern is reported before in thiol capped CdTe QDs. The peaks are at 59° and 65° are too weak to observe. The XRD pattern is reported by many research group for CdTe nanocrystals.

2.3.2 Characterization of GHS-capped quantum dots

GHS capped QDs have been prepared by many groups [28,29]. In this work water soluble GHS-capped QDs were synthesized according to the methods previously reported [30]. We used $CdCl_2$ $2.H_2O$ and TeO_2 as precursors and glutathione as a capping agent. The synthesis of GHS QDs

consists of nucleation and growth. The growth was achieved at 100 ^{o}C in the ambient environment.

Uv-visible spectra of GHS-capped CdTe QDs were shown in Figure 2.7. The shifting to longer wavelength was confirming the synthesis of QDs of different size. In Figure 2.7 it is shown that the reaction time increases from 15 to 115 minutes the lambda maximum shift to longer wavelength (431 to 550). The size of the QDs were calculated and shown in Table 2.2 according to Peng *et al* empirical relationship between QDs size and the first excitonic peak of the UV-visible spectra ($D = (9.8127 \times 10^{-7})\lambda^3 - (1.7147 \times 10^{-3})\lambda^2 + (1.0064)\lambda - (194.84)$[25]. The calculated size was 3.3, 3.5, 3.7, 3.9, 4.0, and 4.1 nm respectively for QDs with an emission peak of 514, 537, 561, 594, and 612 nm.

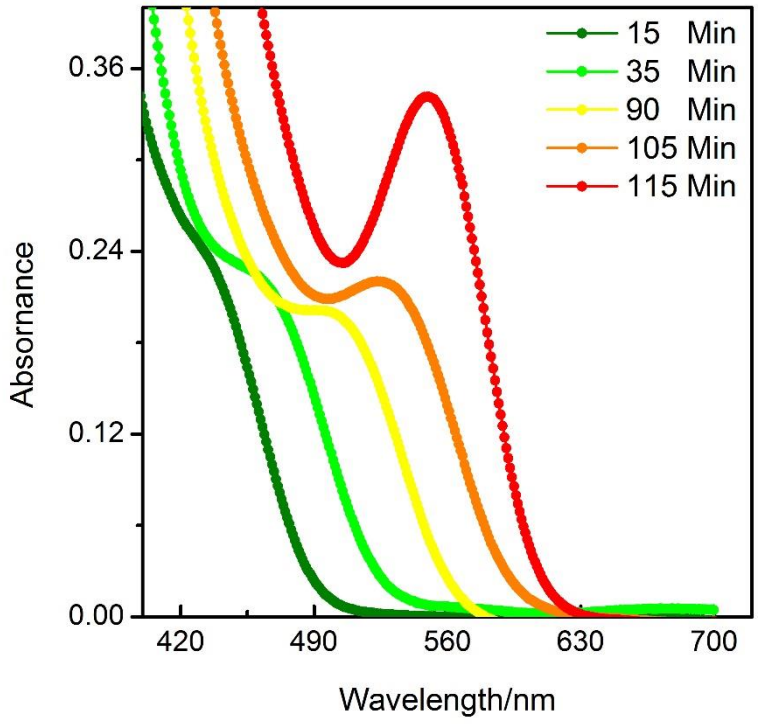

Figure 2.7. UV-visible absorbance spectra of GHS-capped CdTe QDs obtained from reaction mixture at different reaction times.

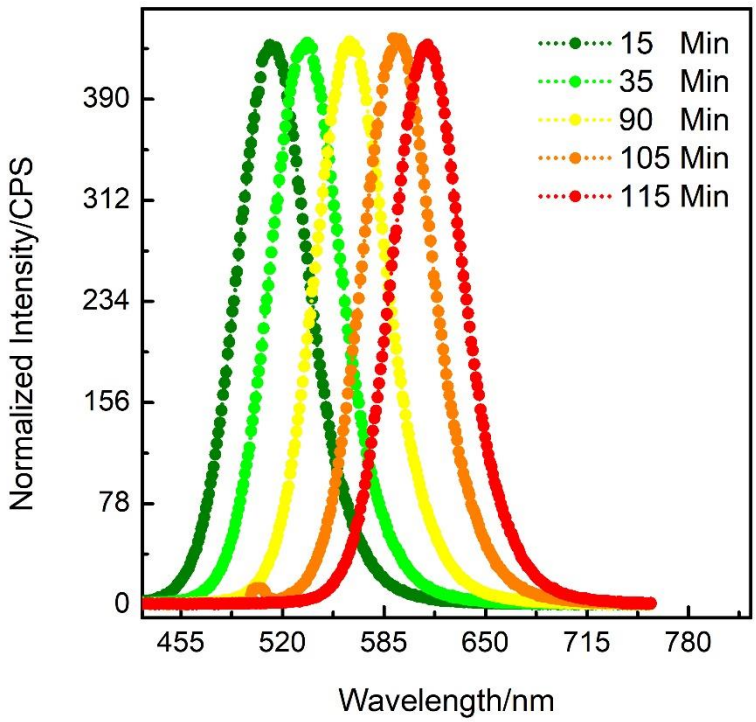

Figure 2.8 the fluorescence emission spectra of GHS-capped CdTe QDs obtained from reaction mixture at different reaction time.

Reaction time (min)	**λ_{max} of absorption**	**Calculated size (nm)**	**λ_{max} of Emission**	**FWHM(nm)**
15	439	2.3	513	53
35	464	3.0	537	58
90	505	3.6	567	54
105	526	3.7	595	57
115	550	4.0	614	55

Table 2.2 Emission, lambda maximum of UV-visible spectra, Size, and full width at half maximum (FWHM) versus reaction time of GHS capped CdTe QDs.

The fluorescence emission spectrum gradually increased from 514 to 612 nm, which indicating a red shift. The full width at half maximum (FWHM) of the emission spectra predicting the particle size distribution and the purity of QDs. The FWHM of GHS QDs emission spectra were uniform overall. The data shows that the rate of formation of GHS-capped QDs was faster than CYS-capped QDs and it also faster than the mercaptoacetic acid MAA-capped CdTe QDs previously reported in literature [31].

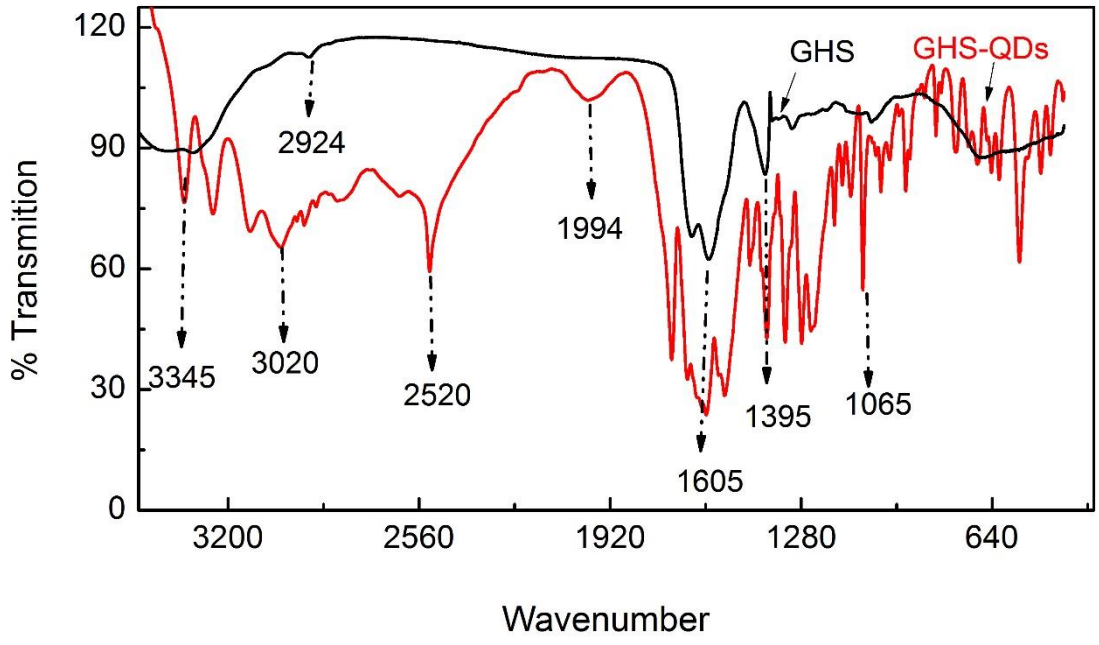

Figure 2.9 FTIR spectra of glutathione and glutathione-capped CdTe QDs.

The FTIR spectrum of glutathione and glutathione-capped CdTe quantum dots are presented in figure 2.9. The spectrum comparison of glutathione and GHS-capped QD shows that there are significant changes in the IR spectrum of GHS-capped QDs. The thiol group stretching vibration is at 2520 cm^{-1} is absent. The carboxylic group shifting was also observed, this pattern is reported by Li before [21].

The morphology of the GHS-QDs of 594 nm fluorescence emitting wavelength was studied by TEM as shown in Figure 2.10. The QDs are in spherical in shape and the distribution of QDs is uniformed. The average diameter calculated from the TEM image using ImageJ software was 3.7 nm standard deviation of 0.53 nm. The size of quantum dots was calculated

from the UV-visible absorption spectra using the empirical relationship between the size and first excitonic peak of QDs obtained at different reaction times. The calculated sized was 2.3, 3.0, 3.6, 3.7, 4.0 nm for an emission wavelength of 514, 537, 561, 594, and 611 nm respectively. The size determination by empirical relationship and TEM is matching [25].

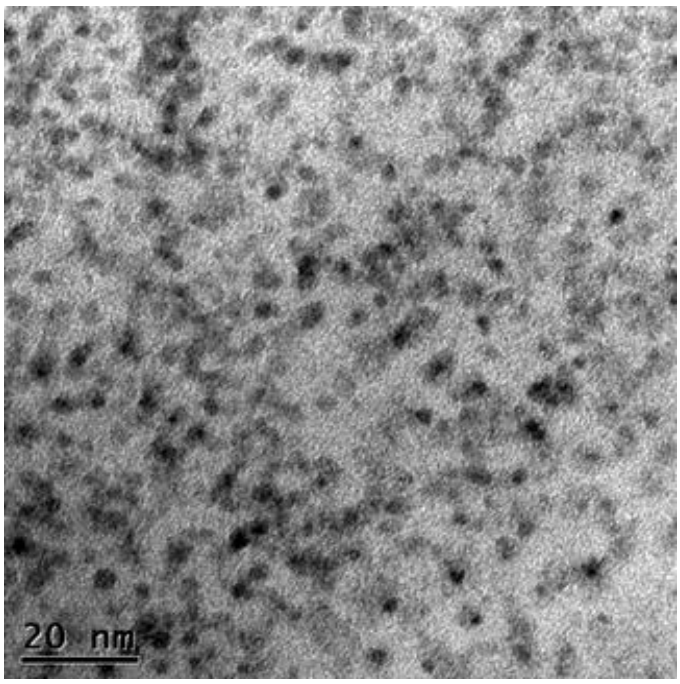

Figure 2.10 Transmission electron microscopic (TEM) image of glutathione-capped CdTe QDs (594 nm emission wavelength).

The CdTe lattice for cysteine-capped was already determined in Figure 2.6. The diffraction pattern for GHS capped CdTe QDs was determined which are comparable. The powder x-ray diffraction pattern of GHS QDs (figure 2.11) is a cubic blend lattice of CdTe, but the peaks are slightly shifted CdS as reported before [32].

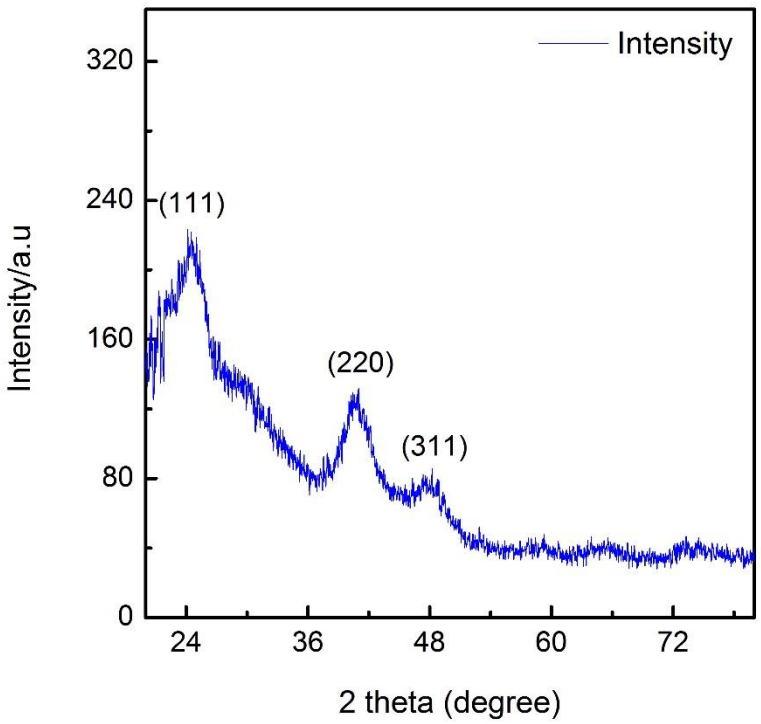

Figure 2.11 X-ray diffraction (XRD) pattern of CdTe lattices (GHS capped CdTe QDs). The positions XRD peaks (111), (220), and (311) represent cubic (zinc-blende) phase of CdTe nanocrystals.

2.3.3 Characterization of MPA-capped QDs

Uv-visible spectra and the emission spectra of GHS-capped CdTe QDs were shown in Figure 2.12 and 2.13. As the reaction proceeding, the absorption and emission peak gradually shift to longer a wavelength, which confirming the growth of CdTe crystals. The PL emission spectrum gradually increased from 542 to 601 nm red shifted. The size of QDs with different emission wavelength was calculated from absorption spectrum [26]. The size for emission 542, 559, 575, 587, 594, and 601 were 3.3, 3.5, 3.6, 3.7, 3.8, and 3.9 respectively (Table 2.3).

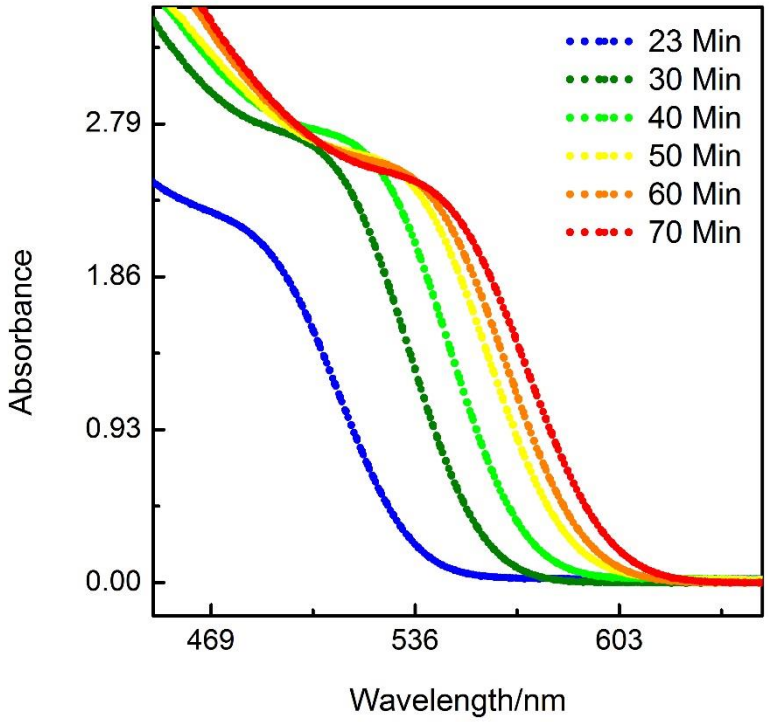

Figure 2.12 UV-visible absorbance spectra of MPA-capped QDs obtained from a reaction mixture at different time.

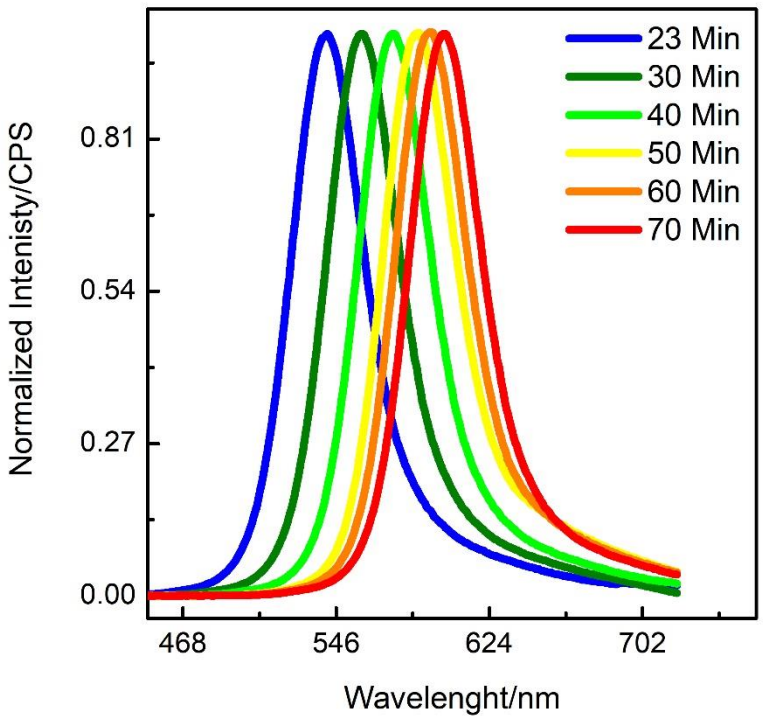

Figure 2.13 Size-dependent fluorescence emission spectra of MPA QDs obtained Obtain with different reaction time (Excitation 400 nm).

Reflux time (min)	λ_{max} of absorption	Calculated size (nm)	λ_{max} of Emission	FWHM (nm)
23	480	3.3	542	55.2
30	502	3.5	559	54.1
40	511	3.6	575	54.5
50	519	3.7	587	52.1
60	529	3.8	594	52.5
70	540	3.9	601	51.1

Table 2.3 Emission, first excitonic peak of UV-visible spectrum, Size, and full width half maximum versus reaction time of MPA-capped CdTe QDs

The FTIR spectra of mercaptopropionic acid (MPA) and MPA-capped CdTe QDs is presented in Figure 2.14.The surface capping agent MPA has absorption around 2500 cm^{-1} due to the thiol (S-H) functional group. The S-H stretching is found in mercaptopropionic acid (MPA) at 2550 cm^{-1} while the stretching at 2500 cm^{-1} range in MPA-capped QDs was absent. The absence of S-H absorbance in MPA QDs represented that the Sulphur is covalently bound to the surface of nanocrystal via Cd-S bond. This observation has been reported before [33].

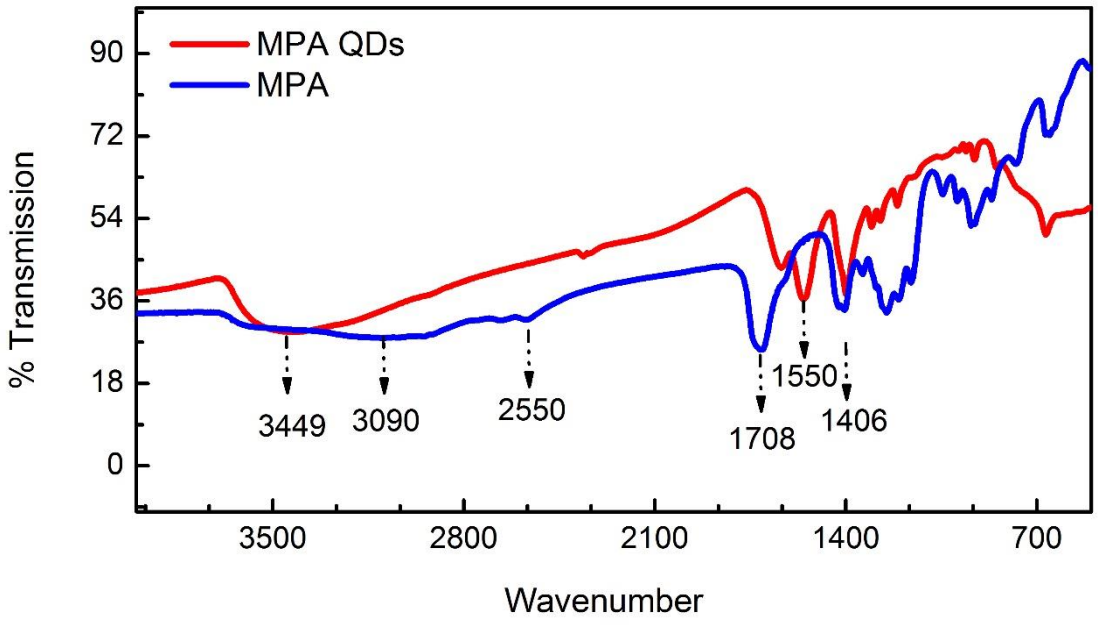

Figure 2.14 FTIR spectra of mercaptopropionic acid (MPA) and MPA-capped CdTe QDs.

The morphology and size of MPA-capped CdTe QDs with emission wavelength of 594 nm was analyzed by high-resolution transmission electron microscope (TEM), the obtained images are presented in Figure 4 (d), shows, the particle size distribution, and the average size calculated was 4.3 nm with standard deviation of 0.63 nm.

As observed in Figure 2.16 the powder X-ray diffraction, (XRD) spectrum peaks can be indexed to the (1 1 1), (2 2 0) and (3 1 1) planes of the cubic zinc blende lattice of CdTe (JCPDS 15-0770). The corresponding peaks (111), (220), and (311) are close to the peaks of CdS (JCPDS 89-0440) which indicate the formation of CdS on the surface of CdTe. The formation of CdS layer on the top of CdTe QDs with thiol stabilizer is confirms.

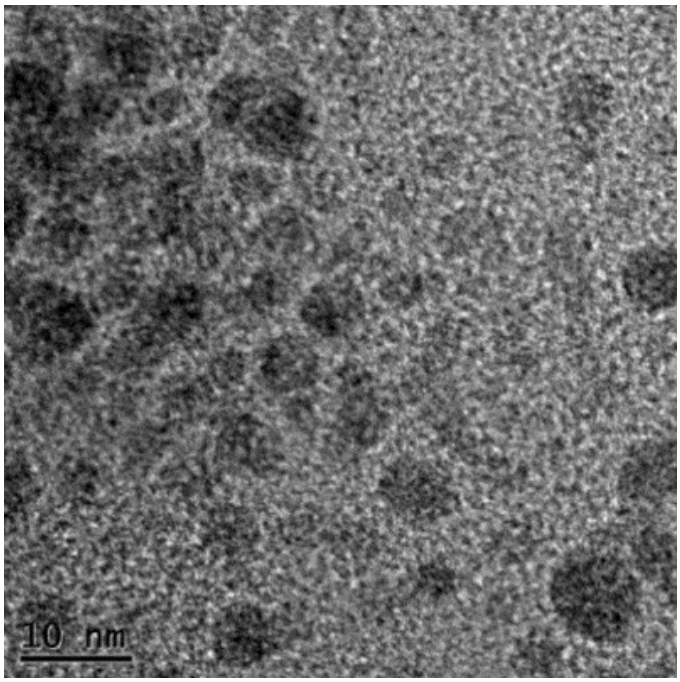

Figure 2.15 TEM Image of mercaptopropionic acid capped CdTe QDs

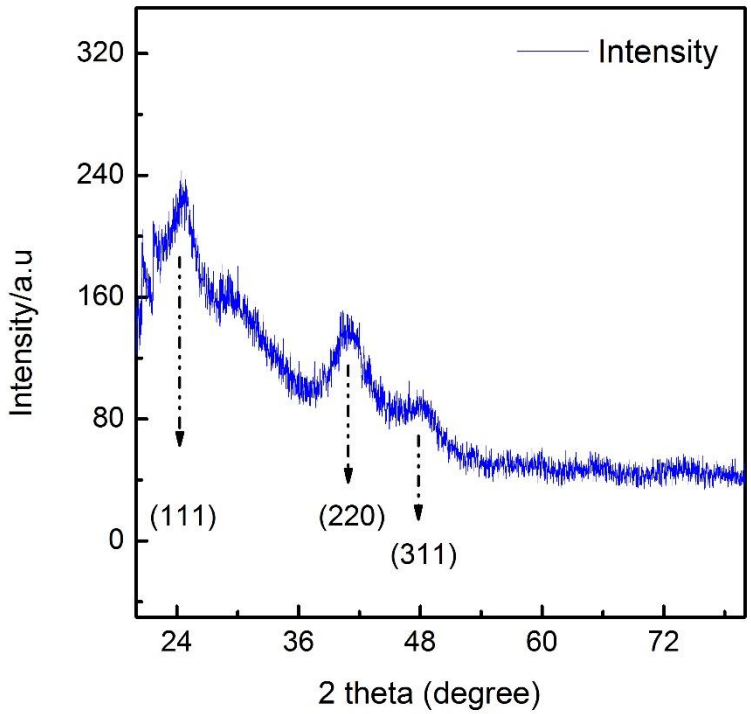

Figure 2.16 Powder X-ray diffraction of MPA-capped CdTe quantum dots. The positions XRD peaks (111), (220), and (311) represent cubic (zinc-blende) phase of CdTe nanocrystals.

2.3.4 Characterization of MSA quantum dots

The fluorescence and absorption spectra were recorded of the aliquots take from the reacting solution with a different time period to monitor the growth and another optical parameter of MSA QDs (Figure 2.17 and 2.18). As in Figure 2.18 shows that shifting of emission wavelength, the initial wavelength was 510 nm and after 125 mints it shifted to 586 nm that confirming the growth of nanocrystals. The lambda maximum of absorption spectra was also shifted from 508 to 552. The size of QDs was calculated with respective absorption spectra obtained from the reaction mixture at different time interval [26]. The calculated size from the absorption spectra is shown in Table 2.4. The size of MSA QDs was growing from 2.7 to 3.7 nm. These feature confirming the sized dependent emission of MSA QDs.

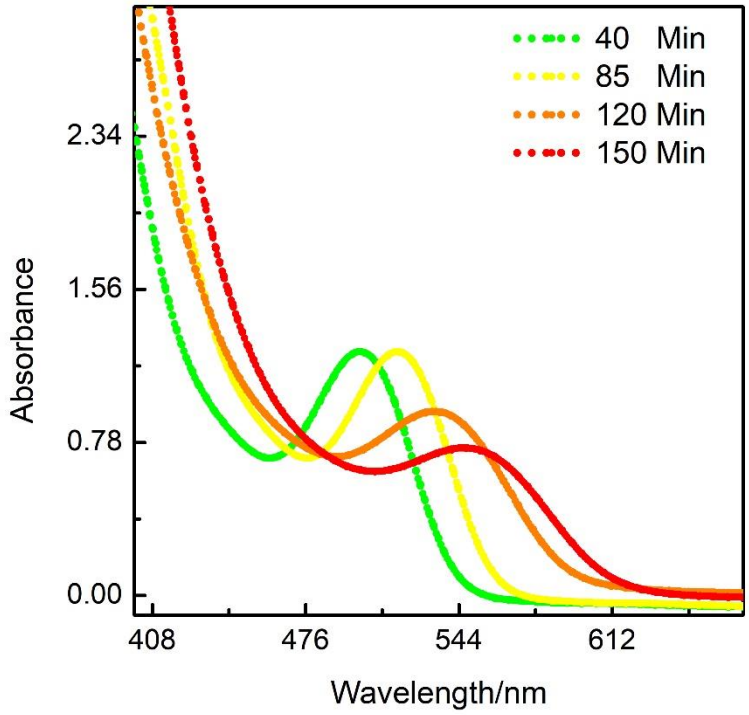

Figure 2.17 The UV-visible absorbance spectra of MSA capped CdTe QDs obtained from reaction mixture at different times.

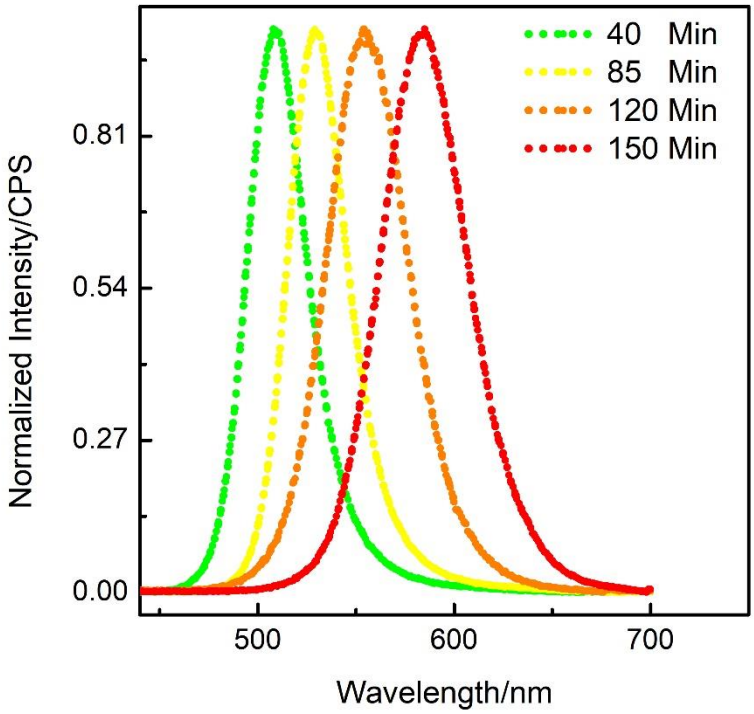

Figure 2.18 Size-dependent fluorescence emission spectra obtained Obtain from a reaction mixture at different reaction time (Excitation 400 nm).

Reaction time (min)	λ_{max} of absorption	Size (nm)	λ_{max} of Emission	FWHM (nm)
40	499	2.7	511	36
85	517	3.1	532	35
120	537	3.5	556	46
150	555	3.7	584	49

Table 2.4 Emission, first excitonic peak of UV-visible spectrum, Size, and full width half maximum versus reaction time of MSA capped CdTe QDs.

FT-IR spectra of pure MSA and MSA-capped QDs are shown in Figure 2.19. The most pronounced IR absorption bands occurred at 3046 cm^{-1} (vOH, COOH), 2550 cm^{-1} (vS–H), 1696 cm^{-1} (vC=O), 1413 cm^{-1} (sCOOH), 1319 cm^{-1}(vC–O), 940 cm^{-1} (δOH) for MSA and 1696 cm^{-1} (vC=O), 1413 cm^{-1} (vC=O) (sCOOH), 1319 cm^{-1} (vC–O),and 923 cm^{-1} (δOH) for MSA capped QDs. Absorption bands from carboxyl and carbonyl groups occurred in QDs spectra, indicating their coexistence on the QDs surface. S–H vibration of MSA (2556-2654 cm^{-1}) was not detectable as assumed for covalently bound thiols to the QDs surface.

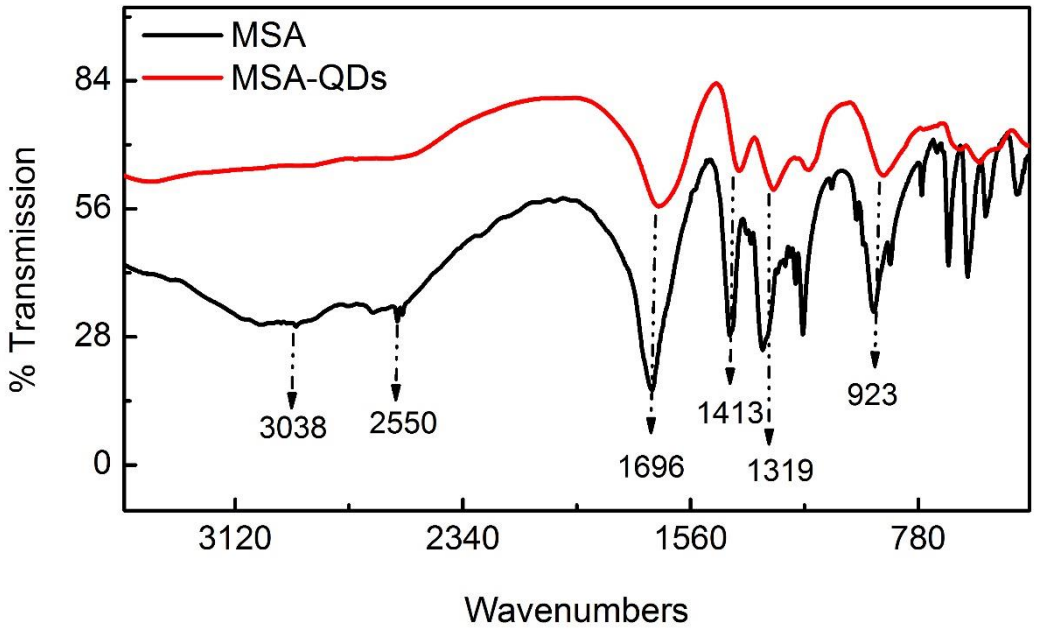

Figure 2.19 The FTIR spectra of mercaptosuccinic acid (MSA) and MSA capped CdTe QDs.

The further demonstration of the size and morphology of MSA capped QDs was obtained from the TEM image as shown in Figure 2.20. The TEM image of MSA QDs (586

nm emission) appeared as a spherical dots with the size of 3.9 nm, which is compared with size determination by UV-visible spectra.

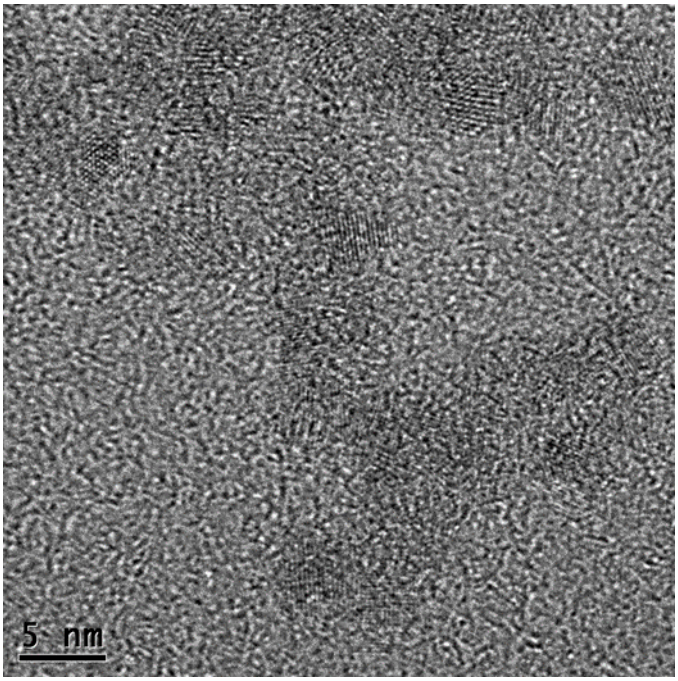

Figure 2.20 TEM Image and size distribution of MSA QDs (emission of 586 nm).

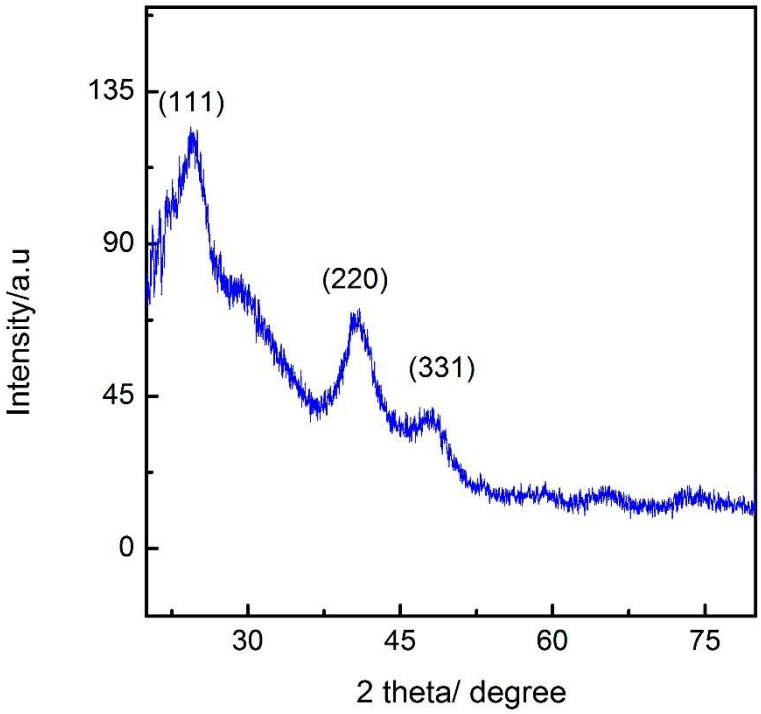

Figure 2.21 X-ray powder diffraction pattern of MSA-capped CdTe quantum dots. The positions XRD peaks (111), (220), and (311) represent cubic (zinc-blende) phase of CdTe nanocrystals.

The lattice parameter derived identified it as a cubic zinc blend structure. Which is reported previously for CdTe nanocrystals. The XRD peak positions (Figure 2.21) was the same as for pure cubic CdTe crystals and clearly, shows the presence of cadmium and tellurium.

Stabilizers	Emission (nm)	Lifetime/ns	Size/nm	FWHM/nm
MPA	601	42.1	4.1	51.1
CYS	603	30.3	3.5	56
GHS	596	45.2	3.4	55
MSA	585	45.2	3.7	49

Table 2.5 The lifetime, size, FWHM of emission spectra, of MPA, CYS, and GHS capped QDs.

2.4 Conclusion

CdTe QDs with CYS, GHS, MPA, and MSA water soluble and biocompatible stabilizers were synthesized and characterized. The optical properties of QDs were compared. We resolved that MPA and GHS QDs are easy and fast in synthesis than MSA and CYS capped QDs. The GHS capped QDs are with a wide range of fluorescence emission (GHS emission was 514 to 612 nm) than CYS, MPA, and MSA capped QDs. The size MPA QDs is the bigger than other QDs while GHS QDs size is smaller than MSA and CYS QDs. In conclusive thiol-capped QDs are highly bright and soluble in aqueous solution, although the solubility in water decreases on longer storage time.

2.5 References

(1) Kumar, S.; Nehra, M.; Deep, A.; Kedia, D.; Dilbaghi, N.; Kim, K. H. Quantum-sized nanomaterials for solar cell applications. *Renewable and Sustainable Energy Reviews* **2017,** *73*, 821.

(2) Rauf, I. A.; Rezai, P. A review of materials selection for optimized efficiency in quantum dot sensitized solar cells: A simplified approach to reviewing literature data. *Renewable and Sustainable Energy Reviews* **2017,** *73*, 408.

(3) Namdari, P.; Negahdari, B.; Eatemadi, A. Synthesis, properties and biomedical applications of carbon-based quantum dots: An updated review. *Biomedicine and Pharmacotherapy* **2017,** *87*, 209.

(4) Peng, J.; Gao, W.; Gupta, B. K.; Liu, Z.; Romero-Aburto, R.; Ge, L.; Song, L.; Alemany, L. B.; Zhan, X.; Gao, G.et al. Graphene Quantum Dots Derived from Carbon Fibers. *Nano Letters* **2012,** *12* (2), 844.

(5) The rise of colloidal quantum dots. *Nat Photon* **2009,** *3* (6), 305.

(6) Guyot-Sionnest, P. Colloidal quantum dots. *Comptes Rendus Physique* **2008,** *9* (8), 777.

(7) Sturzenbaum, S. R.; HocknerM; PanneerselvamA; LevittJ; Bouillard, J. S.; TaniguchiS; Dailey, L. A.; Khanbeigi, R. A.; Rosca, E. V.; ThanouMet al. Biosynthesis of luminescent quantum dots in an earthworm. *Nat Nano* **2013,** *8* (1), 57.

(8) de Silva, R. M.; Palshin, V.; de Silva, K. M. N.; Henry, L. L.; Kumar, C. S. S. R. A new role for surfactants in the formation of cobalt nanoparticles. *Journal of Materials Chemistry* **2008,** *18* (7), 738.

(9) Milliron, D. J. Quantum dot solar cells: The surface plays a core role. *Nat Mater* **2014,** *13* (8), 772.

(10) Hines, D. A.; Kamat, P. V. Quantum Dot Surface Chemistry: Ligand Effects and Electron Transfer Reactions. *The Journal of Physical Chemistry C* **2013,** *117* (27), 14418.

(11) Wang, J.-H.; Li, Y.-Q.; Zhang, H.-L.; Wang, H.-Q.; Lin, S.; Chen, J.; Zhao, Y.-D.; Luo, Q.-M. Bioconjugation of concanavalin and CdTe quantum dots and the detection of glucose. *Colloids and Surfaces A: Physicochemical and Engineering Aspects* **2010,** *364* (1), 82.

(12) Han, B.; Yuan, J.; Wang, E. Sensitive and selective sensor for biothiols in the cell based on the recovered fluorescence of the CdTe quantum dots− Hg (II) system. *Analytical chemistry* **2009,** *81* (13), 5569.

(13) Green, M. The nature of quantum dot capping ligands. *Journal of Materials Chemistry* **2010,** *20* (28), 5797.

(14) Rajh, T.; Micic, O. I.; Nozik, A. J. Synthesis and characterization of surface-modified colloidal cadmium telluride quantum dots. *The Journal of Physical Chemistry* **1993,** *97* (46), 11999.

(15) Medintz, I. L.; Uyeda, H. T.; Goldman, E. R.; Mattoussi, H. Quantum dot bioconjugates for imaging, labelling and sensing. *Nature materials* **2005,** *4* (6), 435.

(16) Pong, B.-K.; Trout, B. L.; Lee, J.-Y. Modified ligand-exchange for efficient solubilization of CdSe/ZnS quantum dots in water: A procedure guided by computational studies. *Langmuir* **2008,** *24* (10), 5270.

(17) Hasan, M.; Bethell, D.; Brust, M. The fate of sulfur-bound hydrogen on formation of self-assembled thiol monolayers on gold: 1H NMR spectroscopic evidence from solutions of gold clusters. *Journal of the American Chemical Society* **2002,** *124* (7), 1132.

(18) Rogach, A. L.; Kornowski, A.; Gao, M.; Eychmüller, A.; Weller, H. Synthesis and characterization of a size series of extremely small thiol-stabilized CdSe nanocrystals. *The Journal of Physical Chemistry B* **1999,** *103* (16), 3065.

(19) Rizvi, S. B.; Yildirimer, L.; Ghaderi, S.; Ramesh, B.; Seifalian, A. M.; Keshtgar, M. A novel POSS-coated quantum dot for biological application. *Int J Nanomedicine* **2012,** *7*, 3915.

(20) Silva, F. O.; Carvalho, M. S.; Mendonça, R.; Macedo, W. A.; Balzuweit, K.; Reiss, P.; Schiavon, M. A. Effect of surface ligands on the optical properties of aqueous soluble CdTe quantum dots. *Nanoscale research letters* **2012,** *7* (1), 1.

(21) Li, M.; Zhou, H.; Zhang, H.; Sun, P.; Yi, K.; Wang, M.; Dong, Z.; Xu, S. Preparation and purification of L-cysteine capped CdTe quantum dots and its self-recovery of degenerate fluorescence. *Journal of luminescence* **2010,** *130* (10), 1935.

(22) Saez, L.; Molina, J.; Florea, D. I.; Planells, E. M.; Cabeza, M. C.; Quintero, B. Characterization of L-cysteine capped CdTe quantum dots and application to test Cu(II) deficiency in biological samples from critically ill patients. *Anal Chim Acta* **2013,** *785*, 111.

(23) Sheng, Z.; Han, H.; Hu, X.; Chi, C. One-step growth of high luminescence CdTe quantum dots with low cytotoxicity in ambient atmospheric conditions. *Dalton Transactions* **2010,** *39* (30), 7017.

(24) Sheng, Z.; Han, H.; Hu, X.; Chi, C. One-step growth of high luminescence CdTe quantum dots with low cytotoxicity in ambient atmospheric conditions. *Dalton Trans.* **2010,** *39* (30), 7017.

(25) Yu, W. W.; Qu, L.; Guo, W.; Peng, X. Experimental determination of the extinction coefficient of CdTe, CdSe, and CdS nanocrystals. *Chemistry of Materials* **2003,** *15* (14), 2854.

(26) Kim, J.; Huy, B. T.; Sakthivel, K.; Choi, H. J.; Joo, W. H.; Shin, S. K.; Lee, M. J.; Lee, Y.-I. Highly fluorescent CdTe quantum dots with reduced cytotoxicity-A Robust biomarker. *Sensing and Bio-Sensing Research* **2015,** *3* (Supplement C), 46.

(27) Ribeiro, D. S. M.; de Souza, G. C. S.; Melo, A.; Soares, J. X.; Rodrigues, S. S. M.; Araújo, A. N.; Montenegro, M. C. B. S. M.; Santos, J. L. M. Synthesis of distinctly thiol-capped CdTe quantum dots under microwave heating: multivariate optimization and characterization. *Journal of Materials Science* **2017,** *52* (6), 3208.

(28) Qian, H.; Dong, C.; Weng, J.; Ren, J. Facile One-Pot Synthesis of Luminescent, Water-Soluble, and Biocompatible Glutathione-Coated CdTe Nanocrystals. *Small* **2006,** *2* (6), 747.

(29) Zheng, Y.; Gao, S.; Ying, J. Y. Synthesis and cell-imaging applications of glutathione-capped CdTe quantum dots. *Advanced Materials* **2007,** *19* (3), 376.

(30) Bao, H.; Wang, E.; Dong, S. One-pot synthesis of CdTe nanocrystals and shape control of luminescent CdTe-cystine nanocomposites. *Small* **2006,** *2* (4), 476.

(31) Zhang, X.; Wang, G.; Zhang, W.; Wei, Y.; Fang, B. Fixure-reduce method for the synthesis of Cu2O/MWCNTs nanocomposites and its application as enzyme-free glucose sensor. *Biosens Bioelectron* **2009,** *24* (11), 3395.

(32) Lin, X.; Xu, S.; Wang, C.; Wang, Z.; Cui, Y. Synthesis of thiosalicylic acid-capped CdTe quantum dots. *RSC Advances* **2014,** *4* (10), 4993.

(33) Jai Kumar, B.; Sumanth Kumar, D.; Mahesh, H. M. A facile single injection Hydrothermal method for the synthesis of thiol capped CdTe Quantum dots as light harvesters. *Journal of Luminescence* **2016,** *178*, 362.

Chapter 3 H_2O_2, glucose, and cholesterol measurements in aqueous phase

3.1 Introduction

The aim of the project is to develop non-invasive, and sensitive sensors that can detect saliva glucose and cholesterol level in humans. Thus an ideal QDs system with thiols capps was used to screen pH sensitivity, H_2O_2, glucose, and cholesterol response. Colloidal QDs are easily dispersible in solution phase, which decreases the possibility of QDs aggregations in comparison with the solid phase. The aggregation of QDs induces fluorescence quenching which reported before [1]. Thiol-capped QDs are highly dispersible, stable, and highly fluorescent in an aqueous medium [2,3]. Hence we selected an aqueous medium to determine and calibrate the response of QDs to H_2O_2, glucose, and cholesterol. The pH change of a system could also alter the results thus it is important to investigate the response of QDs toward pH change. Glucose oxidase and cholesterol oxidase oxidized glucose and cholesterol to H_2O_2 [4] (reaction scheme 3.1) hence sensing of H_2O_2 could be used to measure glucose and cholesterol concentration.

Glucose and cholesterol are MS markers involved in serious metabolic complications but they are in low concentration in saliva and tears[5]. Additionally, H_2O_2 is an important indicator of the biological system involved in various physiochemical processes, regulates signaling transduction and generated by the response to various stimuli i.e. cytokinesis and growth factors. H_2O_2 is produced in the body by multiple ways and regulated by antioxidant enzymes. Antioxidant enzymes are the key regulator for the tracking and respond to H_2O_2 in the body [6].

The potential H_2O_2 sensing capabilities of four QDs capped with different capping agents was evaluated. GHS QDs were found to be more sensitive to H_2O_2. Therefore GHS-capped CdTe quantum dots were chosen for the sensitive detection of H_2O_2, glucose, and cholesterol.

All the enzymatic catalyzed reactions are pH sensitive, our sensing system is based on GOx and ChOx, and hence the pH sensitivity of the GHS QDs was investigated prior to its application in sensing system.

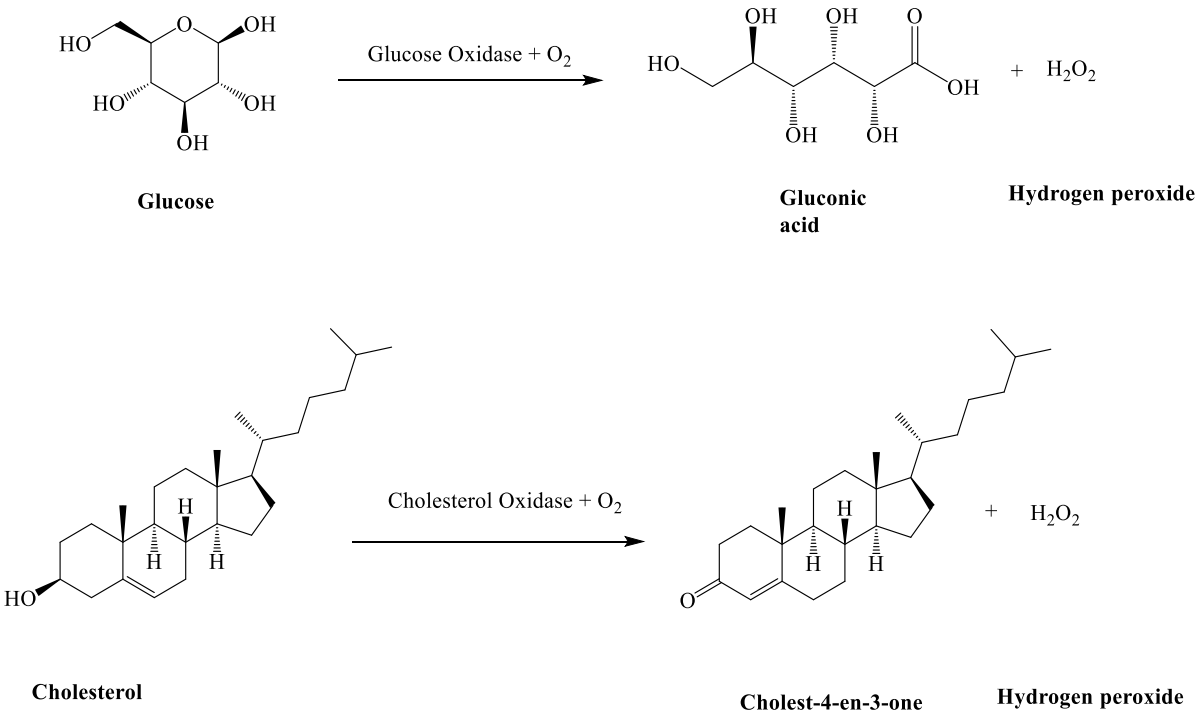

Reaction scheme 3.1 Enzymatic oxidation reactions of glucose and cholesterol by glucose oxidase and cholesterol oxidase, which produce H_2O_2.

3.2 Experimental

3.2.1 Materials

GHS quantum dots were synthesized in-house, (refer to chapter 2). D-glucose was purchased from Aladdin China. Hydrochloric acid 37%, Cholesterol, Cholesterol oxidase and glucose oxidase (GOx) (17300 Units/G) were from Sigma-Aldrich USA. Sodium hydroxide, dipotassium hydrogen phosphate, dihydrogen potassium phosphate, citric acid trisodium salt dihydrate 99 %, sodium chloride 99.5 %, H_2O_2 35 % in water, glutathione (GHS) and 1-prohanol were obtained from Across Organic USA. All the chemicals were of analytical grade and ultra-purified water of Milli-Q system (Millipore Co., Billerica, MA, USA) were used in all analysis.

3.2.2 Instruments for analysis

FluoroMax-4 spectrophotometer (Horiba scientific USA) was used for recording fluorescence spectra. The pH meter (Mettler Toledo, model SevenMulti from USA, Washington) was use for the pH sensitivity measurement of QDs.

3.2.3 Measuring the response of QDs to H_2O_2

The analysis was performed at constant conditions for all QDs. QDs standard solution was made of 0.791 mg/L in 5 mM potassium phosphate buffer of pH 7.5 and was subjected to stirring for 30 minutes. The hydrogen peroxide standards of 5 to 50 mM were made in water and were used for the whole analysis. Aliquots of the hydrogen peroxide standard were spiked into 20 ml QDs solution with stirring and the fluorescence spectra were recorded after each addition. The final concentration of hydrogen peroxide was 100 to 30 00 µM. the excitation used were: GHS-QDs 390 nm, MPA-QDs 400 nm, MSA-QDs 420 nm, and CYS-QDs 400 nm respectively. A slit width of 2 for excitation and emission were used for all experiments.

3.2.4 pH sensitivity of QDs

The pH sensitivity of GHS QDs was investigated. GHS QDs (596 nm emission wavelength) stock solution of 0.26 mg/L, 3 M hydrochloric acid, and 3 M sodium hydroxide solution made in milli-Q water. 50 mL of GHS QDs was subjected to continuous stirring in a conical flask and the pH was monitored by pH meter. The pH of QDs solution was adjusted by dropwise addition of a 3 molar hydrochloric acids solution or a 3 molar sodium hydroxide solution to a desire value and the fluorescence spectrium was measured three time. Four calibrations were preformed using hydrochloric acid or sodium hydroxide. The fluorescence spectra were recorded at 596 nm with an excitation wavelength of 420 nm and a slit width of 2 nm was used for both emission and excitation.

3.2.5 H_2O_2 analysis with GHS QDs

The methods of H_2O_2 analysis was optimized by successive experimentation. 25 ml QDs solution (in 5mM potassium phosphate buffer of pH 7.4) in a conical flask was subjected to

continuous stirring and 5, 10, 15, 20, 30, 40, 50, 60 µL of 0.1M freshly prepared H_2O_2 stock solutions (in 5mM potassium phosphate buffer of pH 7.4) were added gradually to the QDs solution. The final concentration of H_2O_2 was 20, 39.9, 59.9, 79.8, 119.6, 159.2, 198.6, and 237 µM respectively. The fluorescence emission spectra were recorded each time after the addition of H_2O_2. The emission spectra were recorded exciting by 420 nm wavelength.

3.2.6 Glucose analysis by GHS QDs

2 mL of QDs stock solution was diluted to 30 mL potassium phosphate buffer of 5 mM at pH 7 in 50 ml conical flasks. 70 µL of GOx (1.7 mg/mL) was spiked to the QDs solution (0.165 mg/L) with continuous stirring for 3 min. 10, 20, 30, 40, 50, 60, 70, 80 and 100 µL of 0.1M glucose solution was titrated to the reaction mixture and the fluorescence spectra were recorded respectively 5 mins after the addition of glucose. The final concentration of glucose measured was 33.2, 66.4, 99.6, 132.8, 166.0, 199.1, 232.2, 265.3, 331.4, 397.4, 529.2, 595, 660.7, 791.8 µM. The emission intensity was recorded at 596 nm excited by 390 nm wavelength, slit width 2 was used for both excitation and emission. All measurements were recorded thrice.

3.2.7 Saliva glucose analysis

A 0.87 mg/mL QDs stock solution was made in 25 mL of 10 mM pH 7.5 sodium phosphate buffer solution by the addition of 500 µL of 18.3 mg/mL QDs solution in 25 mL. Glucose oxidase solution was made by the addition of 5 mg GOx in 2 mL of 10 mM sodium phosphate buffer pH 7.5. 500 µL of prepared GOx solution was spiked into 5 mL QDs stock solution was stirred for two minutes. The pH of the QDs-GOx solution was checked and readjusted to 7.5 by the addition of 1 mM sodium hydroxide. Glucose standard of 2.3, 3.6, and 7.2 mM was made in phosphate buffer from 5 mM glucose solution in phosphate buffer pH 7.5.

125 µL of QDs-GOx solution was spiked into 96 well microplate followed by the addition of 25 µL of saliva. The pH of the saliva was checked and was adjusted to 7.5 prior to the addition of QD-GOx solution. 3, 2, and 2 µL of 2.3, 3.6, and 7.2 mM respectively of glucose standard was added into the QD-GOx solution. The final concentration of glucose standard was 45, 91, and 183 µM. Stimulated and non-stimulated saliva glucose of individual A1 and A2

was measured. Each measurement was repeated three times. All the measurement was performed 5 minutes after the addition of saliva or glucose standard. All the measurements were recorded at 605 nm of emission wavelength with excitation of 396 nm. The data were collected for 5 minutes and the averages of 10 points were used to calibrate glucose standard.

3.2.8 Cholesterol analysis by GHS QDs

50 mg of Cholesterol was added into 1 mL triton-100 (density 1.067) in a 50 mL volumetric flask followed by sonication and heating at 70 ºC for one hour. The cholesterol triton mixture was then diluted to 50 mL with 100 mM potassium phosphate buffer of pH 7.2. The obtained concentration of cholesterol used for analysis was 1.29 mM in 1% triton. QDs stock solution (0.115 mg/L) was made by diluting 0.5 ml of 2.3 mg/L of QDs solution 10 mL of 5 mM potassium phosphate buffer at pH 7.2 in a 25 ml conical flasks. 70 µL cholesterol oxidase (1.7mg/mL) solutions were spiked to the QDs solution in a conical flask. The QDs-ChOx solution was stirred for 5 mins. The baseline fluorescence intensity of QDs-ChOx was measured and the gradual addition of 50, 100, 150, 200, 300, 400, and 600 µL of cholesterol solution (1.29 mM) was spiked to measure the change in the signal. The final concentration of cholesterol was 0, 2.6, 5.1, 7.7, 10.2, 15.3, 20.3, 30.2, and 40 µM in a reaction mixture. The emission spectra were recorded at 596 nm excited by 390 nm wavelength, slit width 2 was used for both excitation and emission. All measurements were recorded three times.

3.3 Results and discussions

3.3.1 Measurement of H_2O_2

H_2O_2 is an important indicator of the biological system involved in various physiochemical processes regulate signaling transduction and generated by the response to various stimuli i.e. cytokinesis and growth factors. H_2O_2 is produced in the body by multiple ways and regulated by antioxidant enzymes. Antioxidant enzymes are the key regulator for the tracking and respond to hydrogen peroxide in the body [12]. It is important to measure H_2O_2 because it is also produced by various oxidase catalyzed reactions, the measurement of H_2O_2 directly related to the oxidized species.

Among the diverse glucose and cholesterol sensing techniques we have chosen the methods based on H_2O_2 measurement. Glucose and cholesterol can be measured through H_2O_2 produced during the oxidation of glucose and cholesterol caused by GOx and ChOx respectively. The concentration of H_2O_2 produced can be directly related to the concentration of glucose and cholesterol. The enzymatic oxidation of glucose produced H_2O_2, gluconic acid and consumes oxygen. The QDs are sensitive to pH change hence the phosphate buffer of pH 7.4 was used for all analysis.

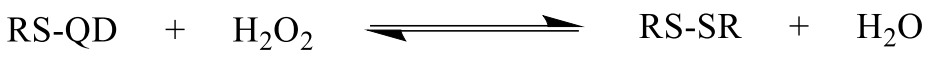

Reaction Scheme 3.3 The reaction between QDs and hydrogen peroxide.

H_2O_2 is an oxidant. It reacts with QDs and diminished the fluorescence of QDs. H_2O_2 break the Cd-S linkage between the thiol and CdTe nanocrystals hence the QDs became unstable which cause aggregations of nan ocrystals to big partials (reaction scheme 3.3). The oxidative damage of Cd-S linkage has been confirmed by many authors [13]. It has been also assumed in many reports that H_2O_2 can make an intermediate complex with the surface stabilizer of QDs (H_2O_2 + QDs-GHS → QDs-GHS-H_2O_2) which affects the electron-hole recombination during the fluorescence emission [14] but this phenomenon has not been confirmed. The denaturing of QDs during the oxidative reaction can be confirmed from the formation of a non-fluorescent precipitate.

The glucose and cholesterol sensing performance of QDs is based on the ability to respond to H_2O_2. Therefore the range of thiol caps including CYS, GHS, MPA, and MSA capped were studied.

In Figure 3.1 (a-b) GHS capped QDs were calibrated to measure the response to H_2O_2. The fluorescence spectra were quenched by 100, 200, 400, 600, 800, 1200, 1600, 2400, and 3200 µM of H_2O_2. 95 % of the QDs fluorescence was quenched.

The data was plotted in Figure 3.1 b. The data shows that the fluorescence quenched was linearly related to H_2O_2 concentrations. The linear range of H_2O_2 measurement was from

100 to 1000 µM. The slope of the linear range was 4243 CPS/µM and the correlation coefficient calculated was 0.9986. The limit of detection calculated from the calibration curve was 58.7 µM. The standard error of the blank was used to calculate detection limit. (LOD = [(Blank + 3* STD of Blank) - C/ m). The presented data shows that GHS QDs are highly sensitive to H_2O_2 with wide linear range and good sensitivity.

(a)

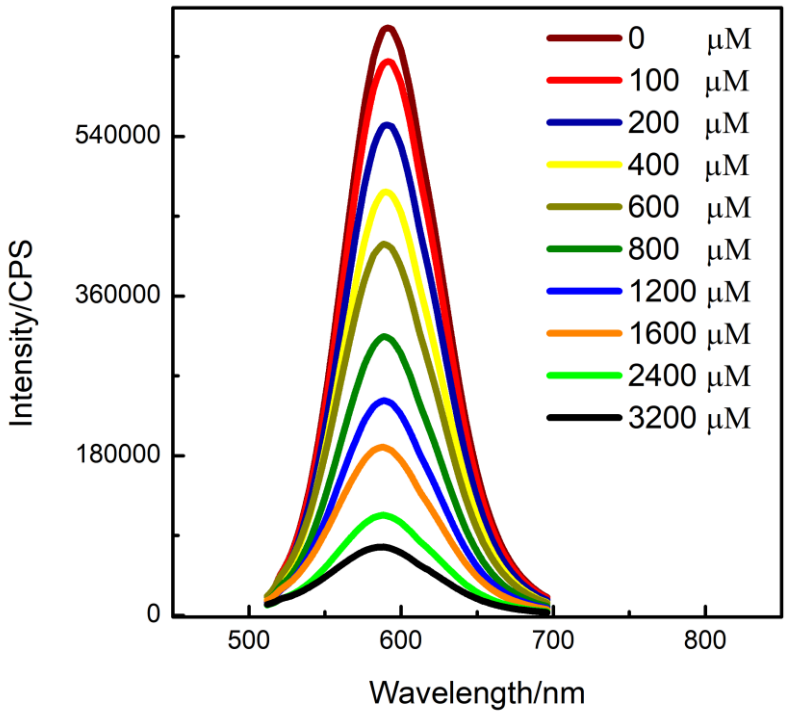

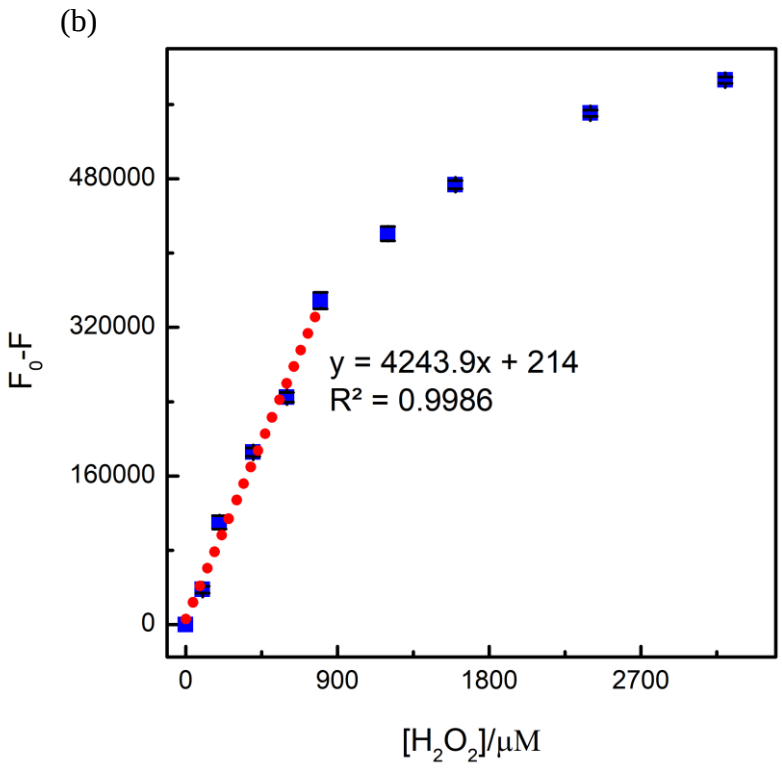

Figure 3.1 (a) Fluorescence emission spectra of GHS capped QDs, quenched with the addition of H_2O_2 and (a) corresponding calibration plot, where error bar N = 3.

MPA-capped CdTe QDs have been reported for many sensing applications. In this report we studied the MPA-capped QDs sensitivity to H_2O_2. In Figure 3.2 (a) the fluorescence spectra of MPA-capped QDs was quenched on the addition of 100, 200, 600, 800, 1200, 1600, and 2400 µM H_2O_2. It shows that MPA QDs are sensitive to H_2O_2.

The quenched fluorescence of QDs at the emission wavelength of 592 nm was plotted against H_2O_2 concentrations. The data is presented in Figure 3.2 (b) and shows that the linear range of H_2O_2 measurement was from 100 to 750 µM with a sensitivity of 2624 CPS/µM. The correlation coefficient of the linear range was 0.991. The limit of detection calculated from the calibration curve was 55.07 µM. MPA-capped QDs are sensitive enough to be used for H_2O_2 determinations but the sensitivity is 38 % lower than GHS-capped QDs.

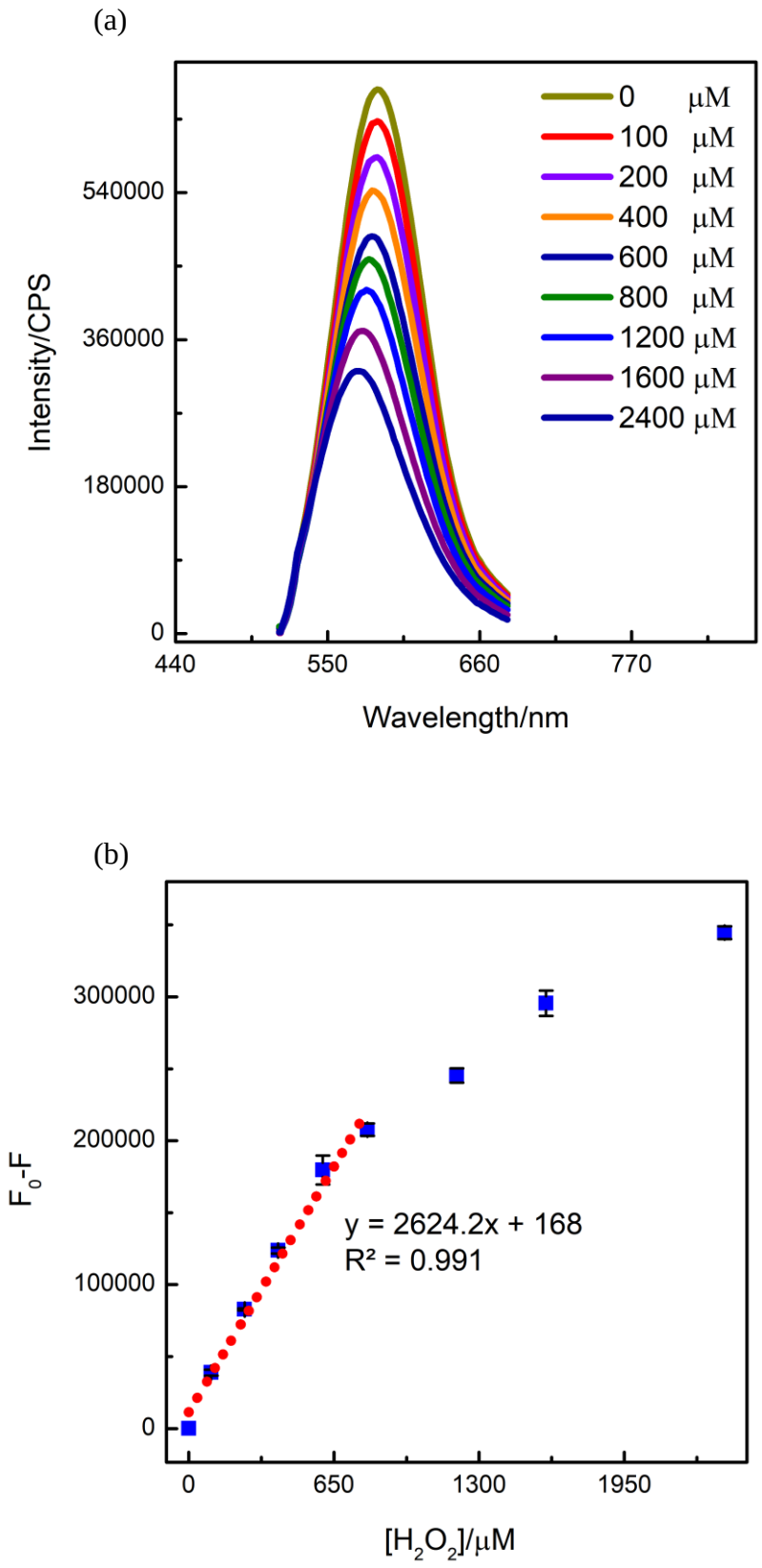

Figure 3.2 (a) Fluorescence emission spectra of MPA capped QDs, quenched with the addition of H_2O_2 and (a) corresponding calibration plot, where error bar N = 3.

Cysteine is an important amino acid and plays an important role in the body. CYS capped QDs are highly biocompatible and reported for many bios and chemical detections [15]. CYS capped QDs were also studied. The data is presented in Figure 3.3 (a). The graph shows that QDs fluorescence is gradually decreased by 100 to 3200 µM of H_2O_2.

The fluorescence response of CYS capped QDs was plotted against H_2O_2 concentrations in Figure 3.3 (b). The calibrations plot shows that the fluorescence quenched is linearly related to the H_2O_2 concentration. The linear range of detection was 100 to 750 µM with a sensitivity of 2272 CPS/µM of H_2O_2. The detection limit was 43.8 µM. The correlation coefficient for the linear range was 0.989. The sensitivity of CYS capped QDs is relatively lowered than MPA and GHS capped QDs.

(a)

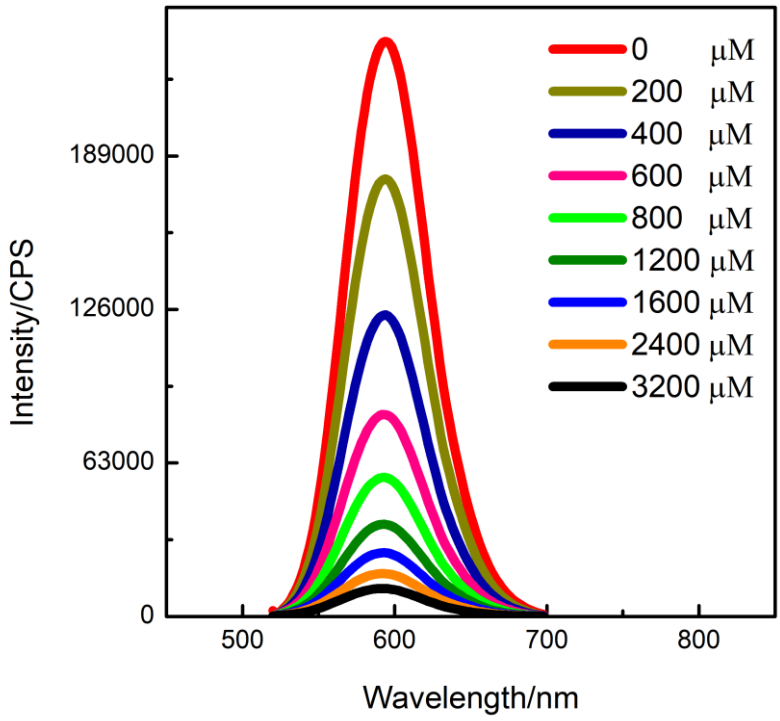

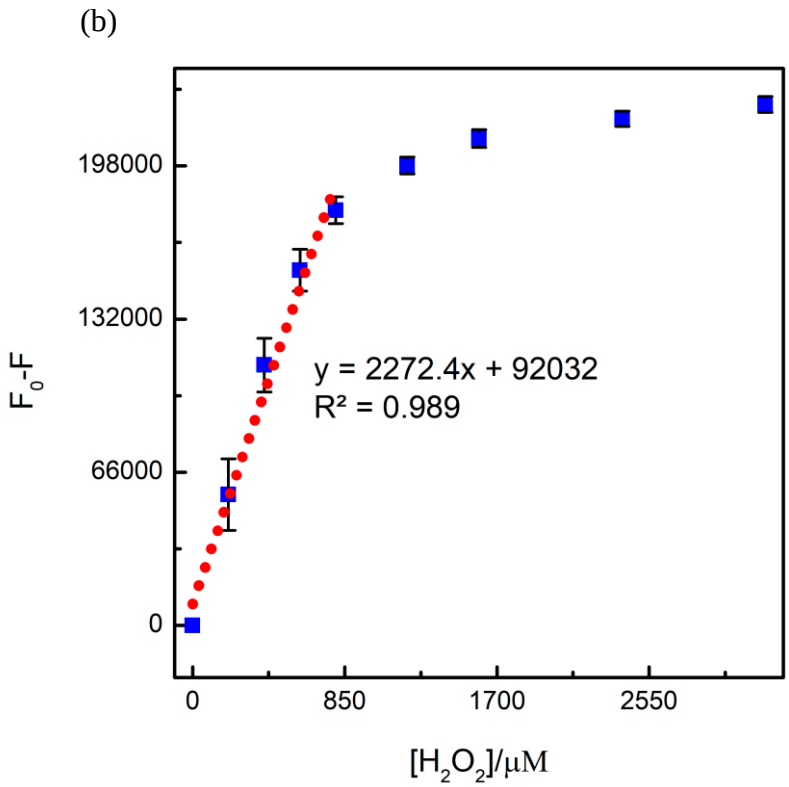

Figure 3.3 (a) Fluorescence emission spectra of CYS capped QDs, quenched with the addition of H_2O_2 and (a) corresponding calibration plot, where error bar N = 3.

MSA QDs are with high fluorescent quantum yield (70 %) [16]. The response of MSA QDs to H_2O_2 was investigated and the data is shown in Figure 3.4 (a-b). The Figure shows that fluorescence of MSA capped QDs were quenched by 100, 200, 600, 800, 1200, 1600, 2400, and 3200 µM of H_2O_2. The fluorescence gradually decreased by the H_2O_2 but the response was not enough sensitive as GHS and MPA capped QDs mention above.

The fluorescence response of MSA QDs was plotted in Figure 3.4 (b). The calibration plot shows fluorescence response is with the wide standard deviation (error bars represent standard deviation of the response in Figure 3.4 (b)). The sensitivity of MSA QDs for H_2O_2 was 20 47 CPS/µM, which is lower than GHS, MPA, and CYS capped QDs. The correlation coefficient of the linear range was 0.965. The detection limit evaluated from the calibration curve was 110.2 µM.

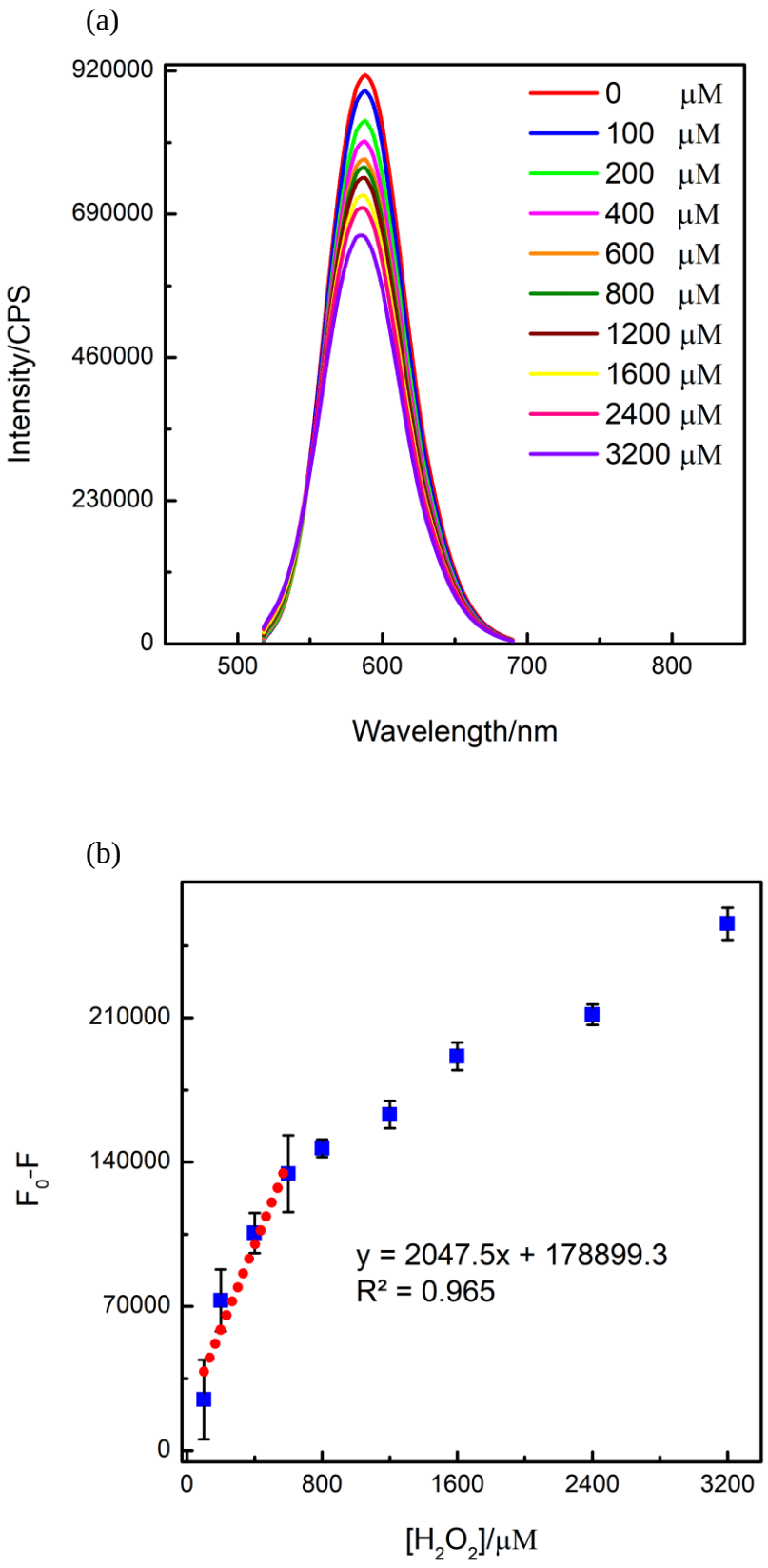

Figure 3.4 (a) Fluorescence emission spectra of MSA capped QDs quenched with the addition of H_2O_2 and (a) corresponding calibration plot, where error bar N = 3.

The procedure for all QDs was kept identical. The concentration of all QDs used was 0.791 ± 0.006 g/L. The linear response, sensitivity, and detection limit for all QDs are tabulated (Table 3.1). GHS capped QDs are highly sensitive to H_2O_2 the slope obtained from the calibration curve of GHS QDs fluorescence response to H_2O_2 was 4243.9 CPS/µM of H_2O_2. The linear range of H_2O_2 measurement was 100 to 1200 µM for GHS capped QDs. The second most sensitive QDs were MPA-capped, the slope obtained from the calibration of fluorescence of MPA QDs quenched versus the concentration of H_2O_2 was 2624.2 CPS/µM. The linear range of response for MPA QDs was 100 to 750 µM of H_2O_2. The sensitivity of MPA QDs was 38 % lower the GHS capped QDs. The sensitivity of CYS QDs was 2272 CPS/µM with the linear range of 250 to 1000 µM. The least sensitivity of CYS capped QDs was 47 % lower than GHS QDs. The less sensitive QDs for H_2O_2 was MSA capped QDs with a sensitivity of 2047 CPS/µM. The linear range of H_2O_2 detection for MSA capped QDs was 250 to 750 µM. We concluded that GHS and MPA QDs are highly sensitive to H_2O_2 with a wide linear range of detection. The additional benefit of GHS capping agent is the biocompatible [7] and can be used in biological systems.

Capping agent	**Linear range/µM**	**Sensitivity (CPS/µM)**	**Detection limit/µM**
GHS	100 - 1000	4243.9	49.9
MPA	100 - 750	2624.2	55.07
CYS	250 - 1000	2272	43.8
MSA	250 - 750	2047	110.2

Table 3.1 The linear response, sensitivity, and detection limit of GHS, MPA, CYS, and MSA capped QDs to H_2O_2.

3.3.2 pH sensitivity of QDs

The effect of pH to the emission of QDs was studied. The pH study is vital for the development of sensitive, selective, and reliable sensors. Herein we were focusing on GHS capped QDs. The pH sensitivity of GHS-QDs was investigated between 4-12 pH units. In this study, HCl and NaOH were used to adjust the pH..

The original pH of QDs was 9.6. In Figure 3.5 the gradual addition of 3 M HCl decreased the fluorescence emission intensity. The data shows that at pH 9.6 the GHS-QDs are highly fluorescent and pH 4 the fluorescence intensity completely diminished. The fluorescence quenched is plotted against the pH. Figure 3.6 shows the relationship of GHS QDs fluorescence emission and pH change. The plot shows that within the pH range of 9.6 to 8.5 the QDs fluorescence emission is stable and that fluorescence quenching starts at pH 8 to 4. The linear range of fluorescence-quenched versus pH was found from 8 to 6.5. The slope of the linear range was 221743 CPS/pH with a correlation coefficient of 0.968. A negligible change in fluorescence was observed by changing pH 5 to 3.5, the QDs were precipitated which caused the aggregation QDs.

99 % of the fluorescence QDs was quenched at pH 3.2. This low pH of QDs (precipitated solutions of QDs with null fluorescence) was readjusted by the addition of NaOH. The data is represented in Figure 3.7 and 3.8. At the pH range of 4 to 8 there is no increase in the fluorescence but above pH 8 3.5 % of the initial fluorescence was regenerated.

Below pH 3.5 the fluorescence was not recoverable by increasing the pH on the addition of NaOH. It is well known that GHS covalently linked to QDs CdTe nanocrystals, which contribute to the fluorescence emission and stability of QDs. When a significant amount of HCl was added. The GHS-H formed dissociated from the surface of the nanocrystals hence destabilizing the QDs structure and precipitation was seen to form. The GHS QDs were aggregated at pH below 3 hence the fluorescence was not recoverable due to the degenerated structure of QDs.

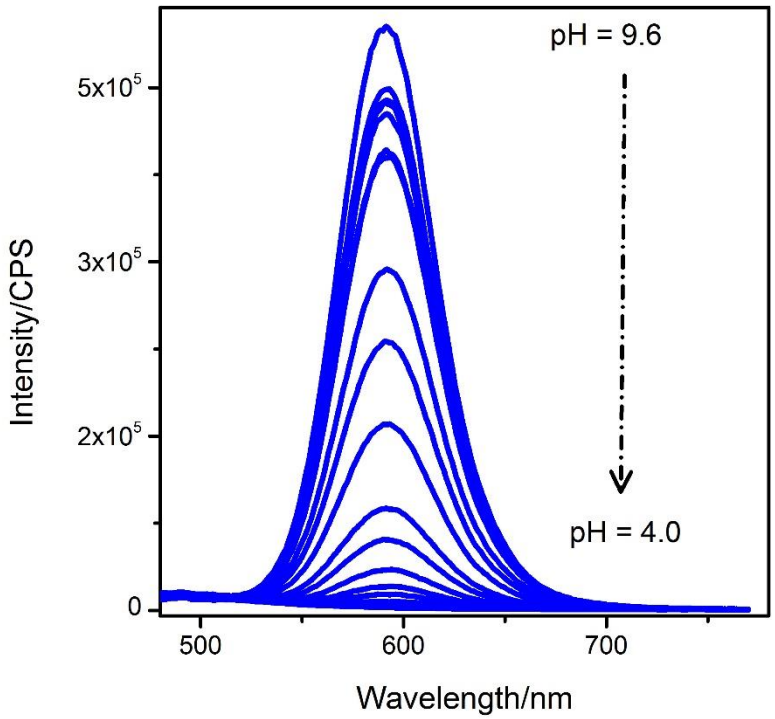

Figure 3.5 The quenching of QDs fluorescence induced by the titration 3 M HCl (pH change from 9.6 to 4).

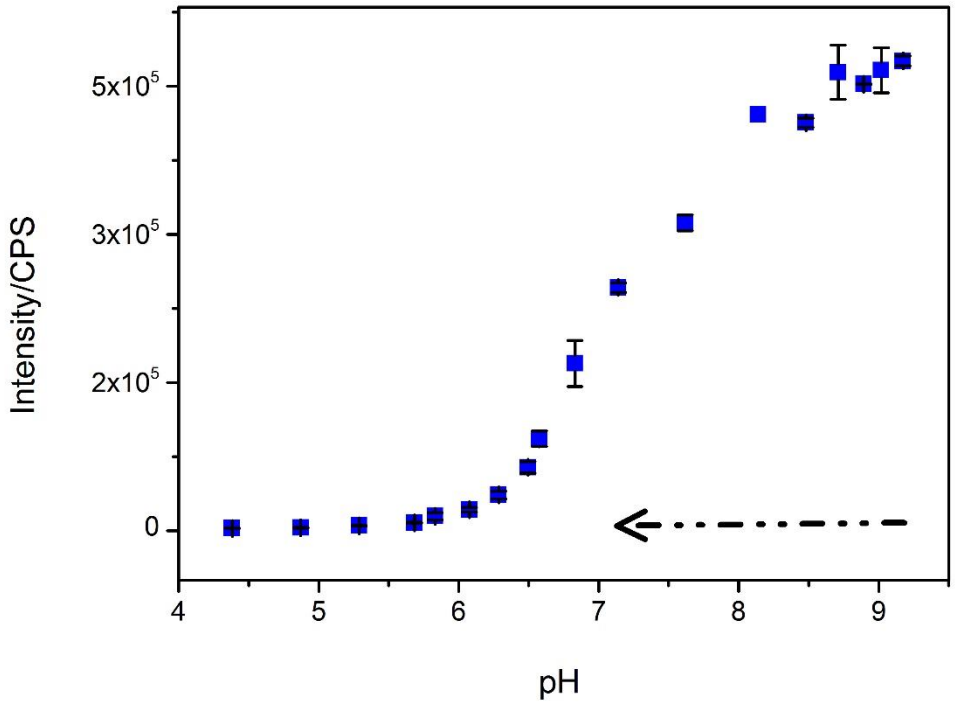

Figure 3.6 Calibration plot of pH-induced fluorescence decay of GHS QDs at pH range of 9.6 to 4. The error bars represent the standard deviation of three repeats.

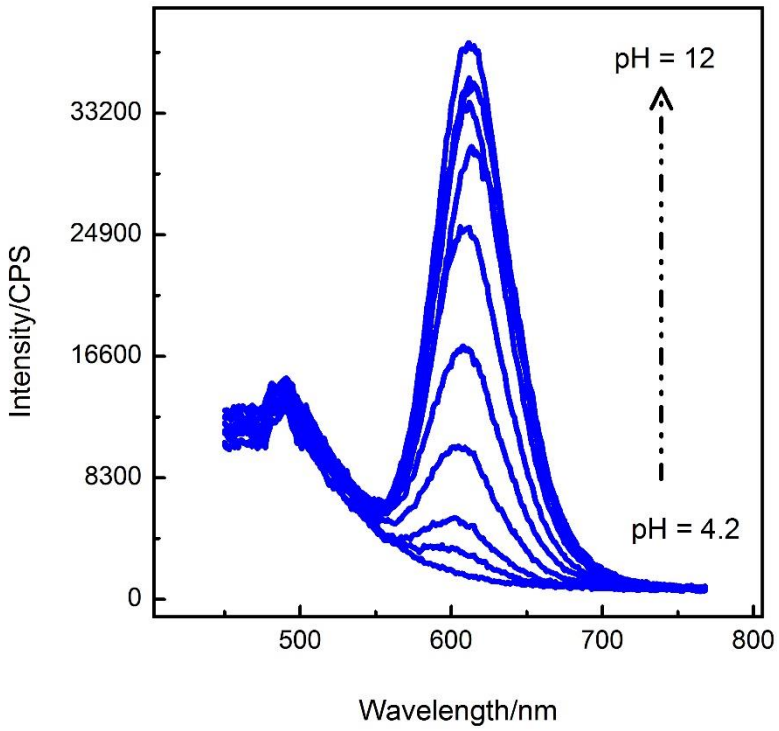

Figure 3.7 Regeneration of fluorescence spectra by adjusting the pH by the addition of NaOH.

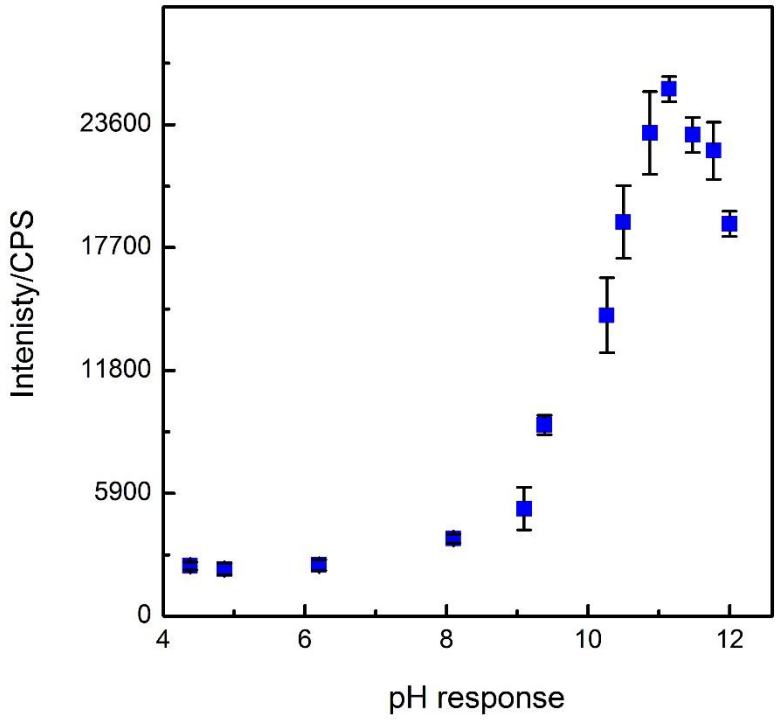

Figure 3.8 Calibration plot of fluorescence response by adjusting pH from 4.2 to 12 (Error bar N = 3).

The acid induced fluorescence change can be partially regenerated by the addition of NaOH. The data in Figure 3.7 showed the fluorescence increased on the addition of NaOH. The fluorescence was enhanced, which was linearly related to the pH change at the range of 6 to 12. The slope of the linear range was 27648 CPS/pH and the correlation coefficient was 0.992. We assumed that at pH 6 the surface capping agent was protonated, which depressed the fluorescence intensity. At pH 6 the surface capping agent of QDs was stable hence on deprotonation the fluorescence was regenerated.

Figure 3.5 shows that by changing the pH of the QD solution from 12 down to 4, there was a 99.5% loss of emission intensity. Interestingly, in another experiment to vary the pH from 12 to down to 6 and then change it back to pH 12 approximately 33.8% of the emission was recovered when the pH was raised to 12. It is evidenced that most of the loss emission was not regenerated by reversing the pH of the solution. We therefore can propose a simplified reaction mechanisms, shown in scheme 3.2 to describe the observation. The glutathione attached to the original QD (A) was first protonated on the addition of HCl to form an intermediate (B), which had the electronic structure disturbed and became non-fluorescent. The intermediate could either go back to the original QD or the reaction could move to the right to prouce a molecule of glutathione and QD^* (C). At the higher pH range of 9-12, the kinetic of reforming RS-QD is faster than the formation of free RSH, i.e $-k_1 >> k_2$, it is possible to almost fully recover the original RS-QD as shown by the recovery of emission intensity. The degree is pH dependent and decreases with pH. At low pH range (below pH 6) k_2 *becomes* important and significant permanent loss of fluorescence was observed. Below pH 3, $k_2 >> -k_1$ a total loss of emission and precipitation of solid resulted, which would not be able to regenerate (B) due to the higher energy barrier and slow kinetics i.e. $k_2 >> k_2$. At this stage, the fluorescence could be regenerated by reversing the pH as the k_1 is k_2.

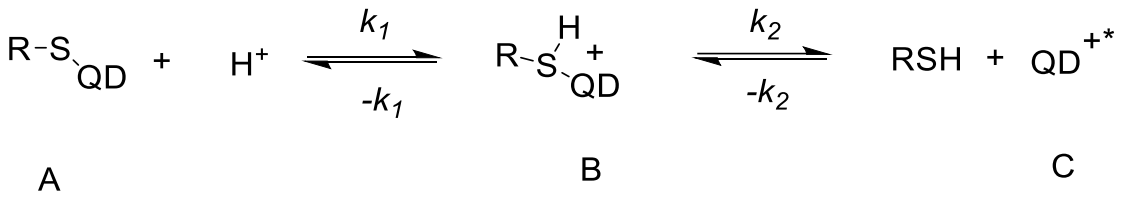

Reaction Scheme 3.2 The mechanism of QDs denaturing and the intermediated formation.

Figures 3.9 to 3.12 shows the pH and fluorescence relationship at the range of pH 12 to 6. The original pH of QDs stock solution was 9.6. The pH was raised to 12 by the addition of NaOH and then was decreased to pH 6 by the addition of HCl. The fluorescence response and the pH relationship are shown in Figures 3.9 and 3.7. The linear range was from 9 to 6 with the slope of 90513 CPS/pH with a correlation coefficient of 0.986.

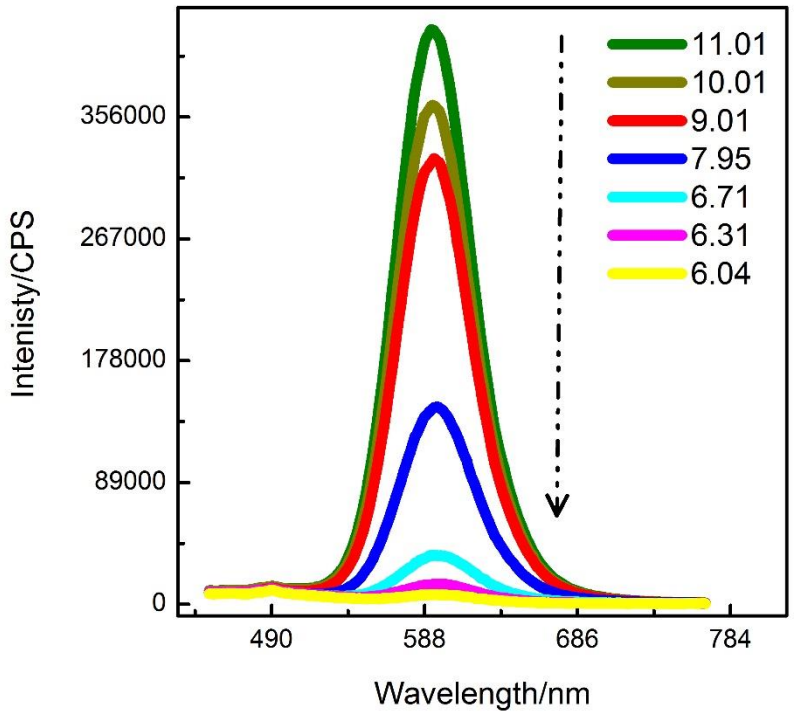

Figure 3.9 The fluorescence spectra quenched by the adjusting pH down to 6.04.

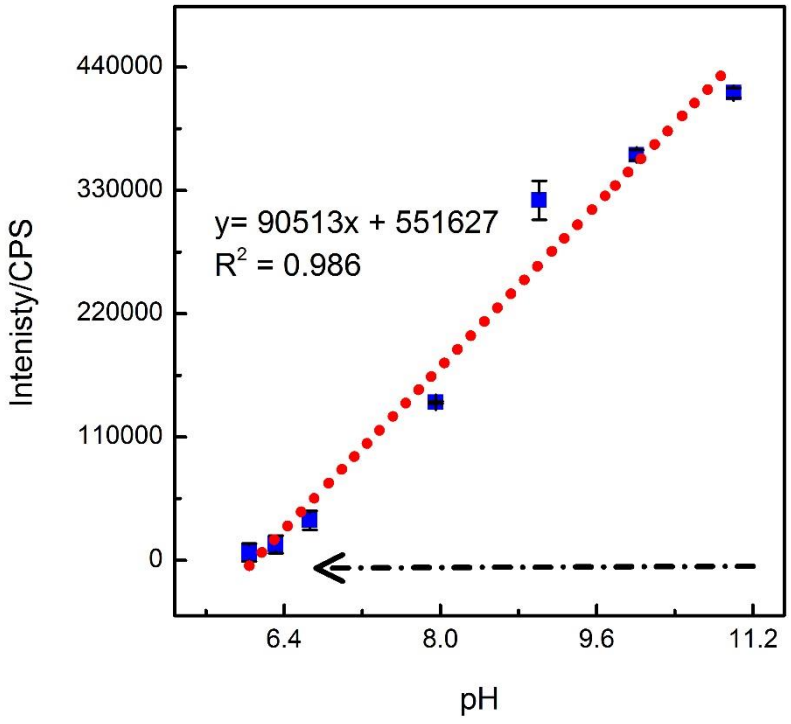

Figure 3.10 The quenching of QDs fluorescence by the addition of HCl (pH range of 12 to 6), Error bar N = 3.

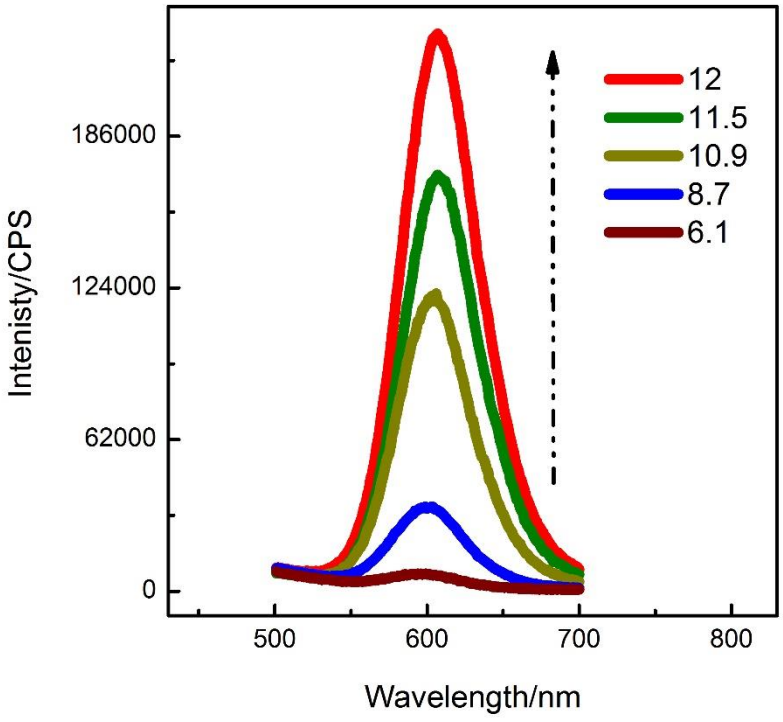

Figure 3.11 The enhancement in QDs fluorescence spectra by increasing the pH to 12 using 3 M HCl.

.

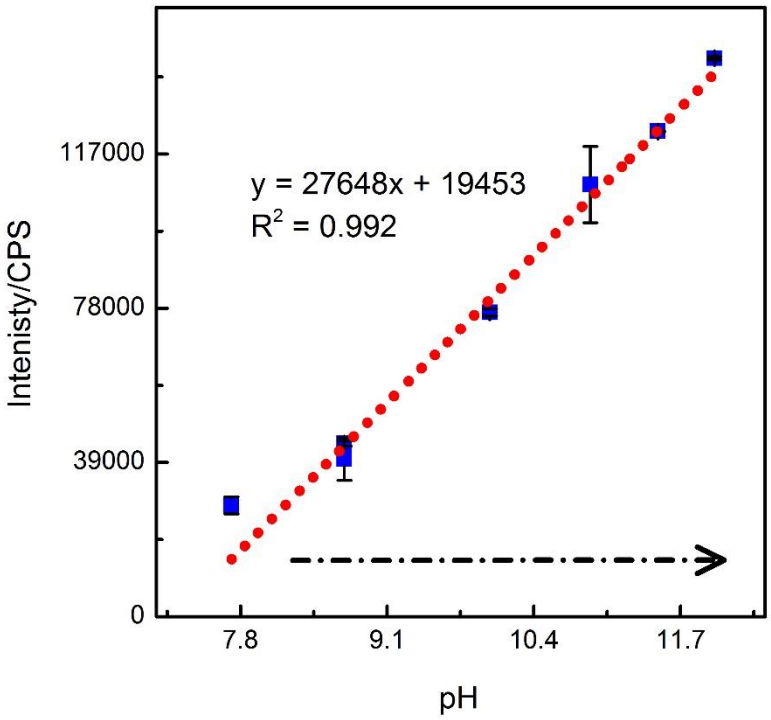

Figure 3.12 The regeneration of the depressed fluorescence by NaOH addition (error bar N = 3).

It is clear from the data that QDs are more stable in high pH environment above pH 9 and is very sensitive to pH change below.

Therefore it is very important to control the pH of a system for glucose and cholesterol sensing. All the sensing analysis was carried out in phosphate buffer. Hence the pH was controlled and the fluorescence change was brought by H_2O_2, produced from the enzymatic oxidation of glucose and cholesterol.

3.3.3 Optimization of H_2O_2 sensing by GHS-capped QDs

H_2O_2 induced fluorescence quenching of GHS-capped QDs was further investigated. The response and sensitivity were higher than other thiol-capped (QDs Figure 3.3 a-b). Herein we focused on the sensing capability in the micromolar region, which could givr information on whether it can be used to detect saliva glucose concentration.

Initially, high concentration of H_2O_2 was used. Figure 3.13 (the data obtained from single point measurement at 591 nm emission) illustrate that the QDs (0.110 mg/L)

fluorescence was quenched by of 0.4 to 22 mM of H_2O_2. The linear range was from 0.39 to 7 mM of H_2O_2, a nonlinear range of 7 to 23 mM of H_2O_2 is due to the unavailability of QDs as 75 % of QDs is already consumed by 7 mM of H_2O_2. It is important to increase the concentration of QDs to avoid the dilution effect and saturation effect. The detection limit for this calibration was 0.16 mM and the correlation coefficient was 0.995.

The calibration shows that QDs are a highly sensitive to high concentration of H_2O_2. In the calibration fluorescence quenched by 0.399 and 0.799 mM is 5617 and 14245 CPS with a standard deviation of 3121 and 8950 CPS respectively. It is important to reduce the standard deviation and improve accuracy of the sensor while measuring the low H_2O_2 concentration.

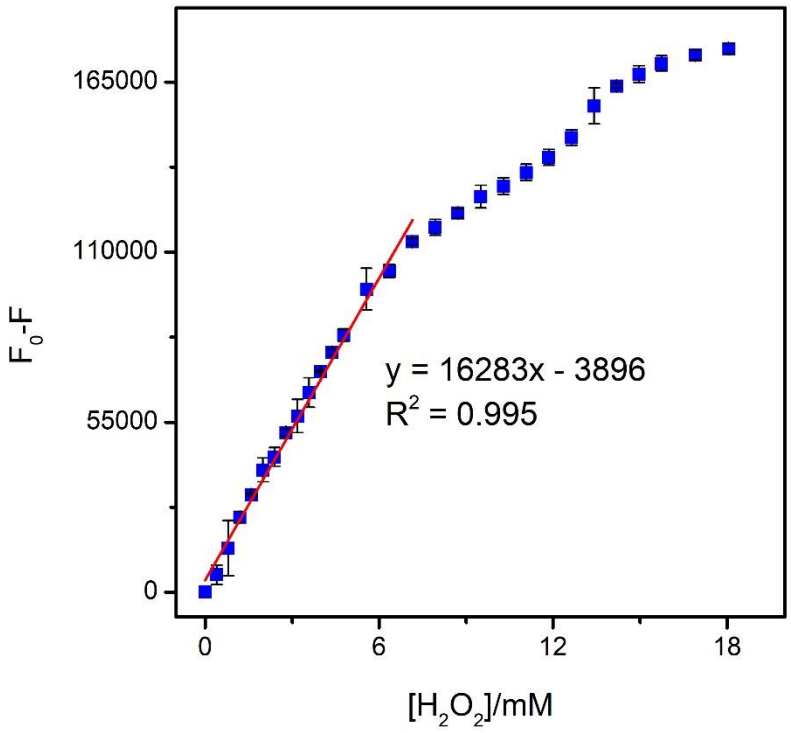

Figure 3.13 The fluorescence response of GHS capped QDs (0.11 mg/L) on the addition of 0.4 to 23 mM H_2O_2. The error bars N = 4, represent the standard deviation of four repeats.

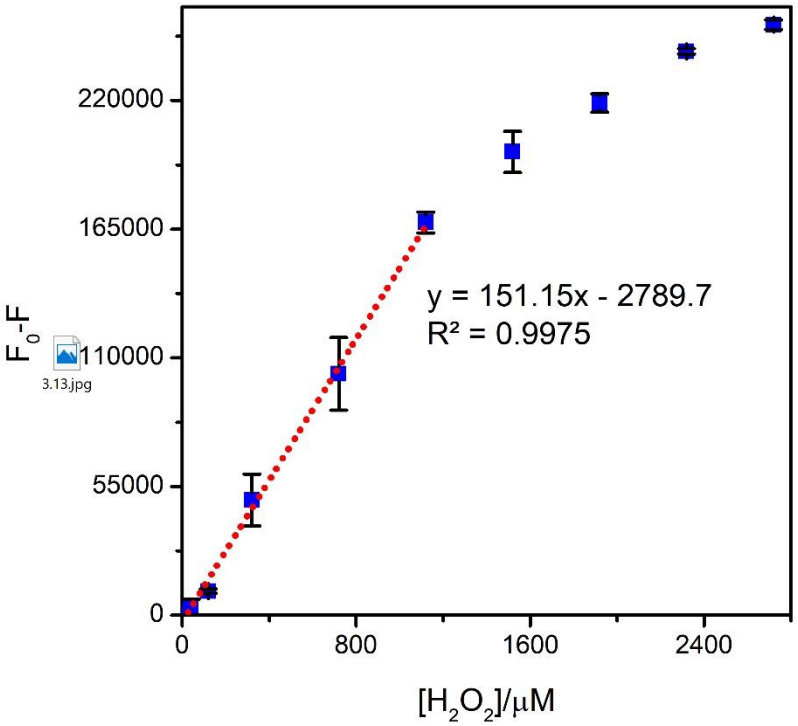

Figure 3.14 The fluorescence response of GHS capped QDs (0.128 mg/L) on the addition of 40 to 2500 µM H_2O_2. The error bars N = 3, represent the standard deviation of three repeats.

The concentration of QDs was increased to 0.128 mg/L and range of 39.9 to 2720 µM H_2O_2 was used. A linear relationship of H_2O_2 was 39.9 to 1107 µ M with a correlation coefficient of 0.9905. The detection limit calculated was 11.8 µM. Although the low concentration of 46 µM can be measured using this system but the sensitivity and standard deviation of the response is high. The standard deviation of the response (quenched fluorescence 10300 CPS) calculated for the 39.9 µM was 875 CPS.

In another investigation, a low QD concentration 0.086 mg/L was used to measure low concnetration of H_2O_2 (4 to 16 µM). The obtained results were shown in Figure 3.15 (a-b). The Figure 3.15 (a) shows the fluorescence spectra on addition of 4 to 16 µM of H_2O_2. The results indicate that 4 to 8 µM of H_2O_2 can be measured but the fluorescence signal is not consistant and was with high error. The linear range was 4 to 16 µM with a detection limit of 0.58 µM achieved for this calibrations. The correlation coefficient of the linear range was 0.982. In this investegation, we found that low QDs concentration can be used for low concentration of H_2O_2 measurement but with unstable fluorescence. The use of low QDs concentration gives a narrow

linear range which is not required. To achieved a stable fluorescence spectra and with a broad linear range of measurement it is important to used adequate QDs concentration.

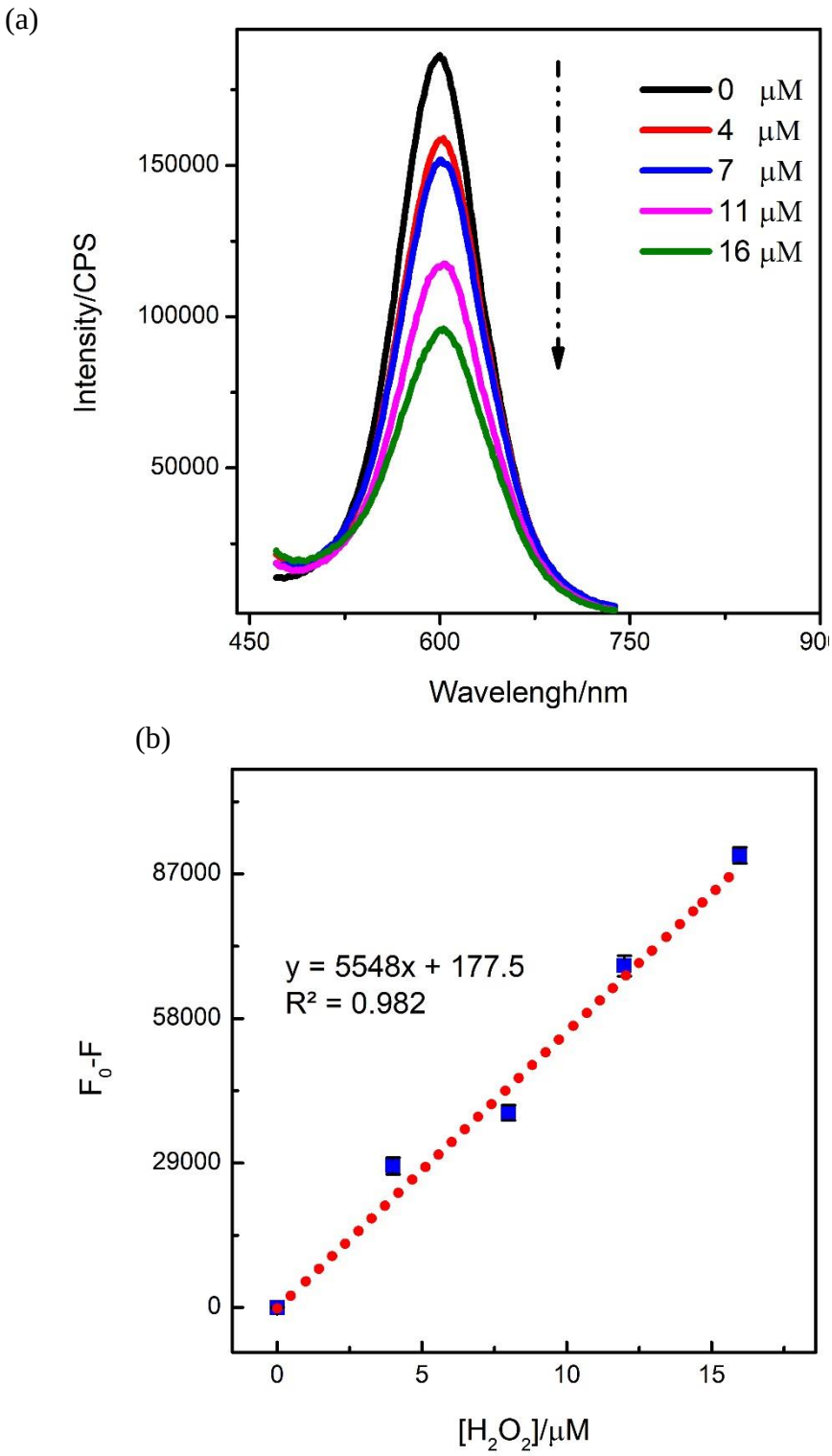

Figure 3.15 (a) The Fluorescence spectra of GHS capped QDs (0.086 mg/L) quenched with the addition of 4 to 16 µM H_2O_2 and (b) the corresponding calibration plot. Where the error bar N = 3.

The QDs concentration was further increased to acquire a stable fluorescence signal, for the analysis of low H_2O_2 concentration with broad linear range (saliva glucose range 75 µM). The QDs concentration of 0.238 mg/L was used to measure the H_2O_2 over the range of 20 to 237 µM. The fluorescence spectra of QDs solution (0.238 mg/L) and QDs with H_2O_2 are shown in Figure 3.16 (a). The QDs spectrum is quenched by the addition of 40, 60, 80, 120, 159, 198, 237, and 300 µM H_2O_2. The high concentration of H_2O_2 causes the decay of 90 % QDs fluorescence. All measurements were recorded three times after five minutes of mixing H_2O_2 with QDs stock solutions.

The fluorescence of QDs quenched by 20 to 237 µM of H_2O_2 was plotted in Figure 3.16 (b). The linear range of H_2O_2 measurement was 20 to 237 µM with a correlation coefficient of 0.999. Limit of detection was calculated from the blank and standard deviation of the blank and intercept and slope of the calibration curve.

$$LOD = \frac{[(b + \sigma b) - c]}{S}$$

Where "b" is the blank the "σb" is the standard deviation of the blank, "S" is the slope and "c" is the intercept of the calibration curve. The results obtained were reproducible and repeatable. The calculated detection limit was 3.3 µM.

We concluded that QDs are extremely sensitive to H_2O_2 (Table 2.3). The best sensitivity, response and a board linear range were achieved for GHS capped QDs. The GHS QDs were further used to measure the H_2O_2 at low concentrations levels (4 to 300 µM) to validate that QDs can be used for the measurement of very low H_2O_2 trace and the sensing system can be designed to measure glucose of 75 µM which is the saliva glucose range. Additionally, the end point equilibrium method is easy and simple for H_2O_2 measurement.

Calibrations	**[QDs]/mg/L**	**Linear range/µM**	**Detection limit/µM**	**Slope**
1	0.110	390 – 7000	160	16283 CPS/mM
2	0.128	40 – 1107	11.8	151.1 CPS/µM
3	0.086	4 – 16	0.58	5548 CPS/µM
4	0.238	20 – 237	3.3	1939 CPS/µM

Table 3.2 Comparison of calibration obtained by using different QDs concentrations.

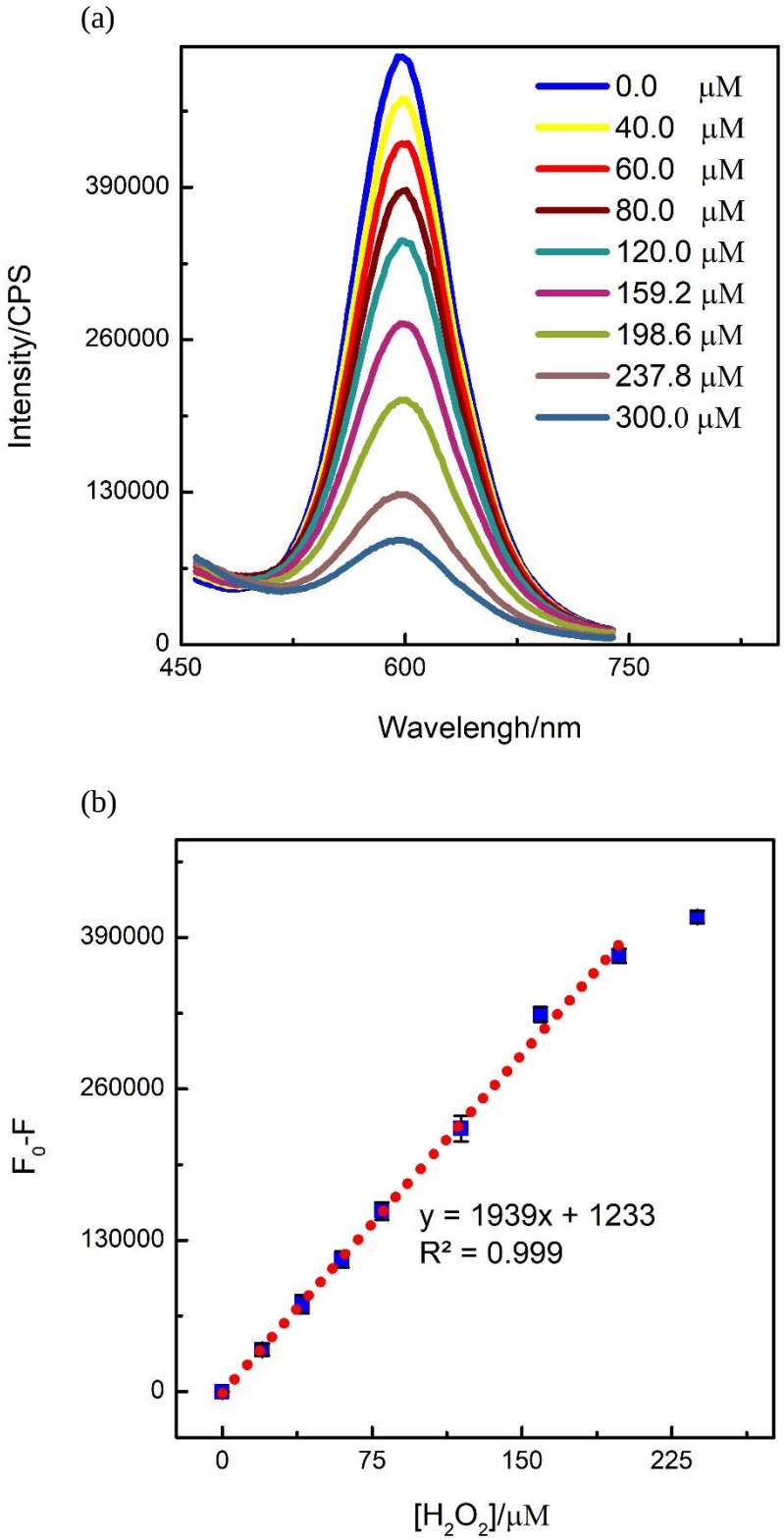

Figure 3.16 (a) Fluorescence emission of GHS capped QDs (0.238 mg/L) quenched by 40 to 300 μM H_2O_2, and (b) The corresponding calibration curve, the error bar represent the standard deviation of the three repeats.

3.3.4 Glucose sensing by GHS-QD-GOx

Glucose sensing was further performed with QDs and GOx that oxidized glucose to form hydrogen peroxide and gluconic acid. It is based on the measurement of hydrogen peroxide discussed in the previous sections. The linear range of hydrogen peroxide measurement was 20 to 350 µM with a detection limit of 3.3 µM (Figure 3.16-b). Gluconic acid can alter the pH of QDs-GOx sensing platform, to overcome this problem a buffering system was used to control the pH. The pH was real-time monitored during the experiment and negligible change in pH was observed and the quenching effect is due to the production of H_2O_2 which breaks the linkage between surface legends with CdTe nanocrystals (reaction scheme 3.4 and 3.5).

$$\text{D-Glucose} + O_2 \xrightarrow{\text{GOx}} \text{Gluconic acid} + H_2O_2 \qquad (3.4)$$

$$\text{RS-QD} + H_2O_2 \rightleftharpoons \text{RS-SR} + H_2O \qquad (3.5)$$

The glucose sensing procedure was optimized by changing the QDs and GOx concentrations. Initially, a high concentration of QDs 0.7 mg/L and GOx 2.6 unite/mL (200 µL of 1.7 mg/mL GOx stock) was used to measure glucose in millimolar range. The results are represented in Figure 3.17 and shows that the fluorescence spectra of QDs were quenched by 0.4 to 4.9 mM of glucose. The corresponding fluorescence quenched was plotted in figure 3.18. The linear range of glucose measurement was from 0.4 to 2 mM with a correlation coefficient of 0.994. A wide linear range was achieved at high QDs concentration but the response is suitable for high concentration of glucose. This setup can be used to estimate glucose level in blood but cannot be used for measuring saliva glucose.

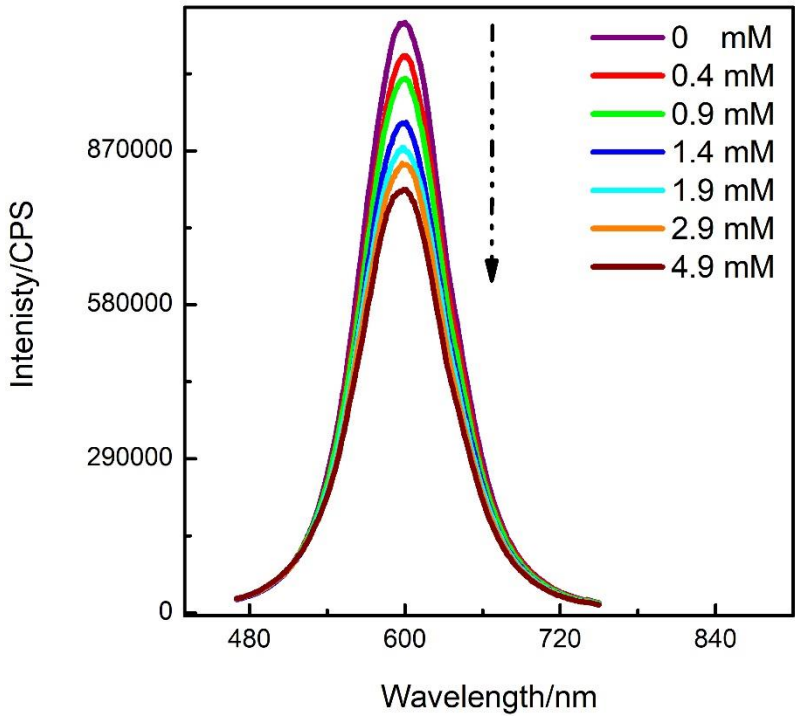

Figure 3.17 The QDs fluorescence spectra of GHS capped QDs quenched by 0.4 to 4.9 mM of glucose.

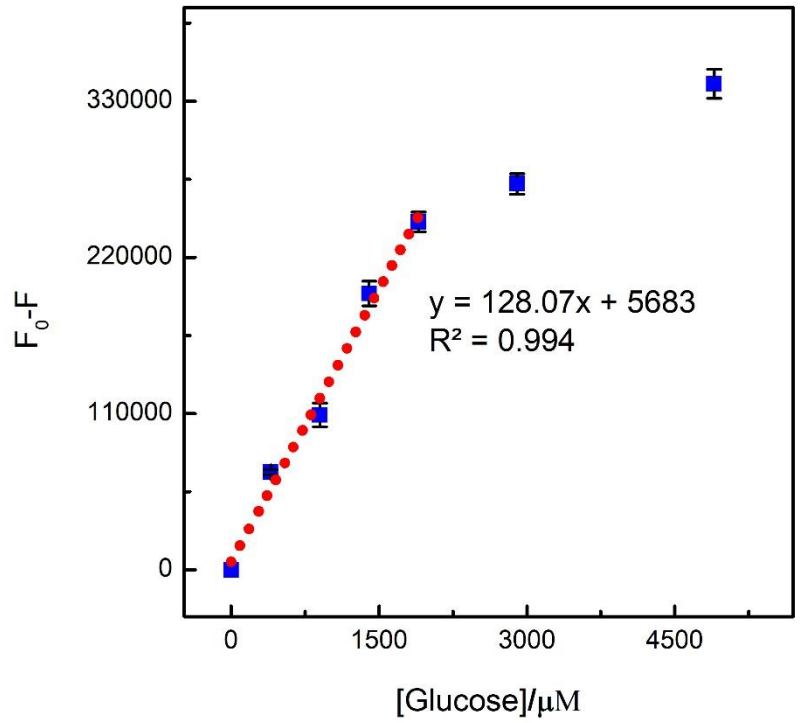

Figure 3.18 The calibration plot of GHS capped QDs fluorescence response to 400 to 5900 μM glucose. Where the error bars N = 3 are the standard deviations.

The GOx and QDs concentrations were reduced to 0.85 units/mL of QDs and 0.105 mg/L. The range of glucose used was 20 to 1708 µM, the linearity was found in the range of 20 to 100 µM with a correlation coefficient of 0.996 and the calculated detection limit was 8.2 µM (Figure 3.19).

The QDs concentration is increased to 0.162 mg/L and the GOx concentration was reduced to 0.68 units/mL to investigate the QDs and GOx concentration influence on the performance of sensors. QD (0.162 mg/L), and GOx 0.68 units/mL (40 µl of GOx stock 1.7 mg /mL) with 19 to 596 µM of glucose was used. The linear range found was 80 to 318 µM with a correlation coefficient of 0.989 and 54.6 µM detection limit was achieved (Figure 3.20).

The concentration of GOx influence the response in calibration mentioned in Figure 3.20 the response (slope) is 295 CPS/µM with 0.68 GOx units/mL, while the response in calibration mention in Figure 3.19 is 632 CPS/µM with 0.85 GOx units/mL. The adequate amount of QDs allowed the sensor performance at board linear range hence it is important to increase the QDs and GOx concentration for better response and high sensitivity.

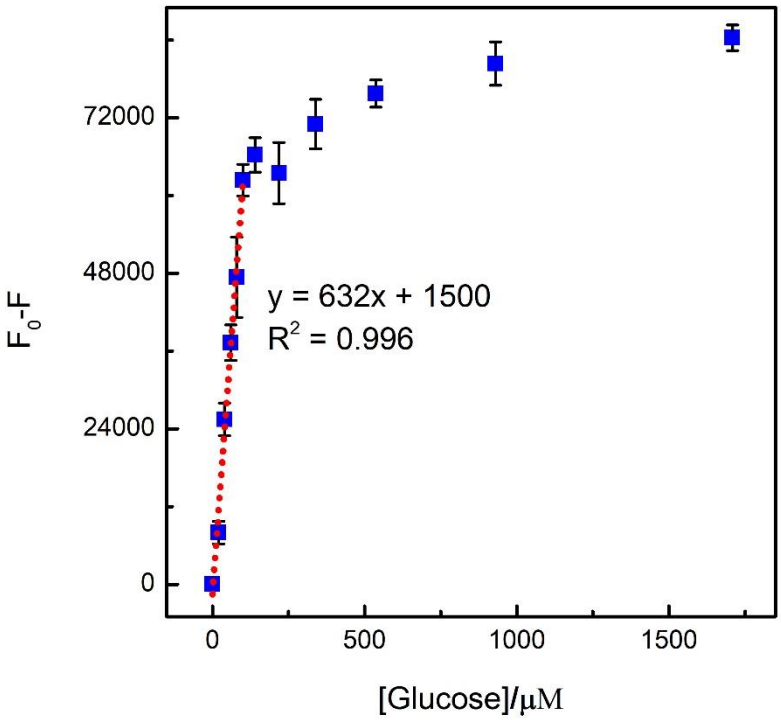

Figure 3.19 Calibration plot representing the fluorescence response of GHS capped QDs (0.105 mg/L) to 20 - 1700 µM of glucose. 0.85 units/mL of GOx was used.

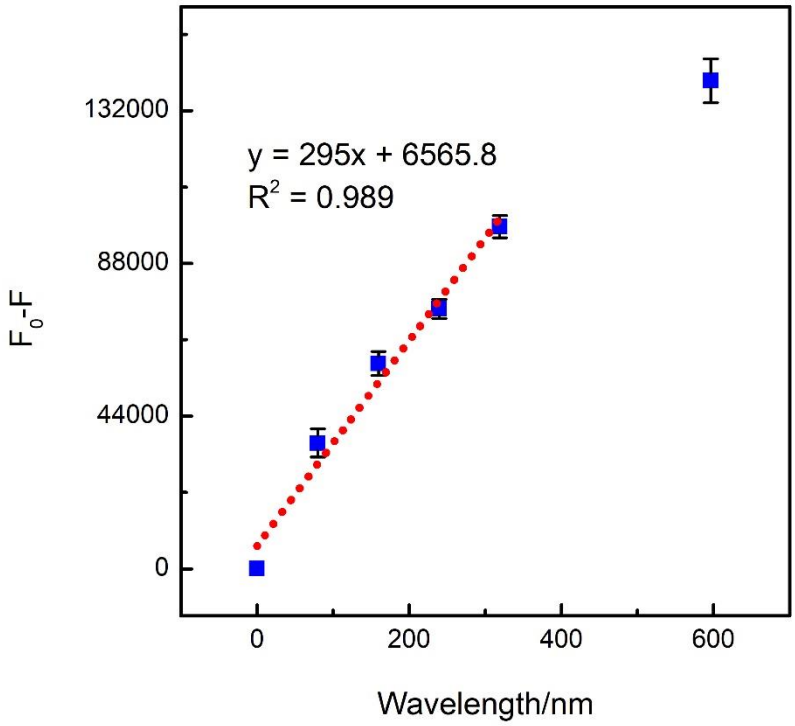

Figure 3.20 Calibration plot of the fluorescence response of GHS capped QDs (0.162 mg/L) to 80 to 596 µM of glucose in the presence of 0.68 units/mL GOx.

(a)

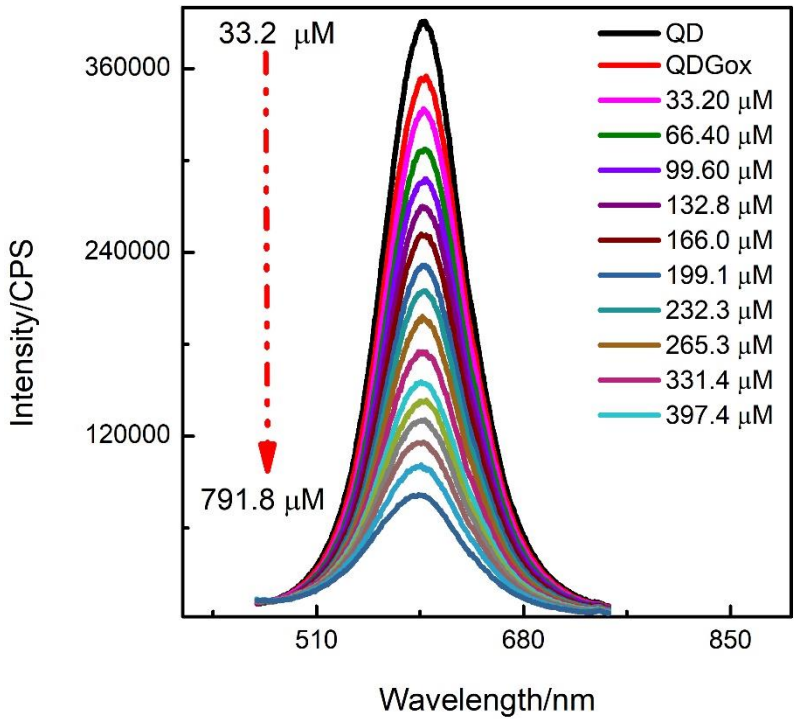

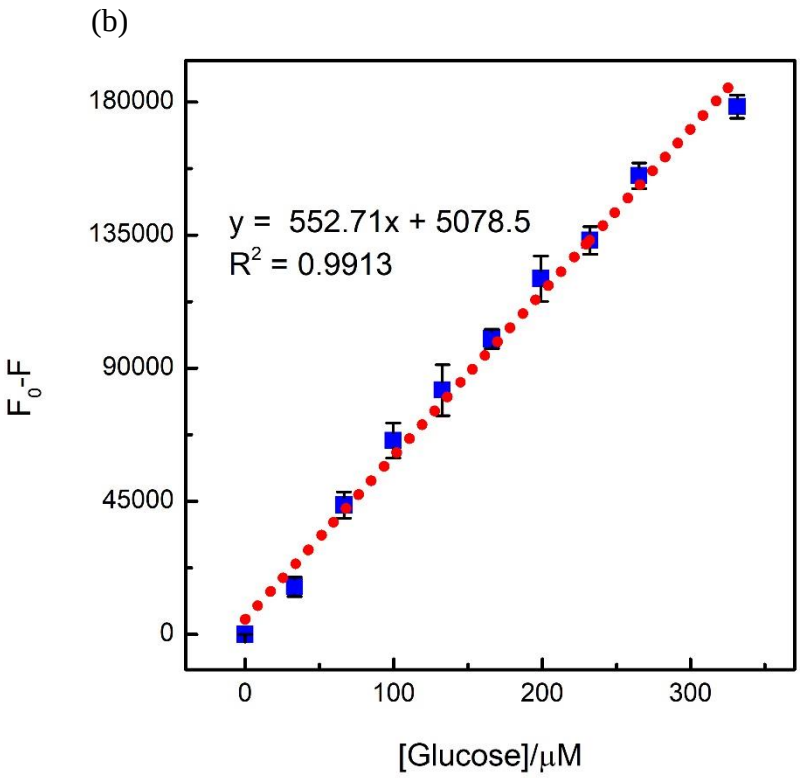

Figure 3.21 (a) Fluorescence Emission spectra of GHS capped QD, quenched by 33.3 µM to 791 µm glucose in the presence of GOx, and (b) the corresponding calibration curve, the error bar represents the standard deviation of three repeats.

As described the basic principle of the sensing techniques that QDs are degraded which because the fluorescence quenched, hence it is important that the concentration of QDs should be enough to complete the calibration in desired linear range. The optimal response of GHS-CdTe QDs toward the glucose was Figured in 3.21 (a-b). The GOx and QDs concentration used was 1.6 units/mL and of 0.33 mg/L respectively. The linearity glucose range obtained was 33 to 331 µM with the correlation coefficient of 0.991. The response of the calibration plot was 552.7 CPS/µM and the calculated LOD was 20 µM according to the equation mention above. The sensitivity and detection limit enough to quantify saliva glucose.

The range of glucose and H_2O_2 was 31 to 331 µM (Figure 3.21) and 31 to 237 µM (Figure 3.16). The result shows that glucose can be quantified using the principle of H_2O_2, sensing. In our experiments to minimum glucose concentration was used as 20 µM and the high concentration of glucose was 7000 µM. A different linear ranges was achieved at different condition. Hence the optimized condition range can be used to measured saliva glucose.

[QDs] mg/L	[GOx] units/mL	Linear range/µM	Slope	Detection Limit /µM
0.7	2.6	400 - 2000	128	123.4
0.105	0.85	20 - 100	632	8.2
0.162	0.68	80 - 318	295	54.6
0.33	1.6	33 - 331	552.7	14.5

Table 3.3 The linear range, slope of the linear range and the detection limit obtained calibrations at different conditions.

3.3.5 Saliva glucose sensing by GHS capped QDs

Unknown human saliva glucose concentration was measured from the calibration of glucose standards. Human saliva was added into the QDs-GOx solution and the quenching of fluorescence by human saliva glucose was measured.

Glucose standard solution was then added to the same solution already with human saliva. After each addition the fluorescence quenching was observed. The fluorescence quenched by glucose standard was plotted in Figure 3.22 and 3.23 for use in evaluating stimulated and non-stimulated saliva glucose concentration of volunteer A1. The calibration shows a linear response to saliva and glucose standard.

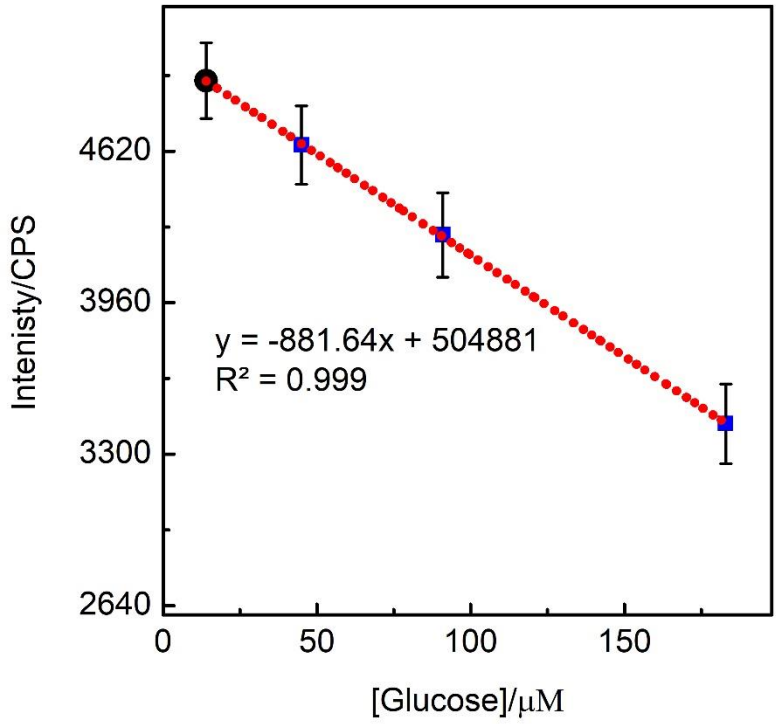

Figure 3.22 A calibration plot obtained from glucose standards for the measurement of stimulated saliva glucose using liquid phase equilibrium method, Where N = 3.

The saliva glucose was estimated from the calibration curve using the linear equation. The X (unknown saliva glucose) was determined from (y= -881.64X + 504881) for each measurement and then adjusted to the original concentration by the dilution factor. This method of saliva glucose determination was used for both stimulated and non-stimulated saliva samples, the calculated saliva glucose concentration for stimulated saliva for individual A was 82.7 $\pm$ 10.4 µM and for non-stimulated saliva was 89.4 $\pm$ 10.2 µM

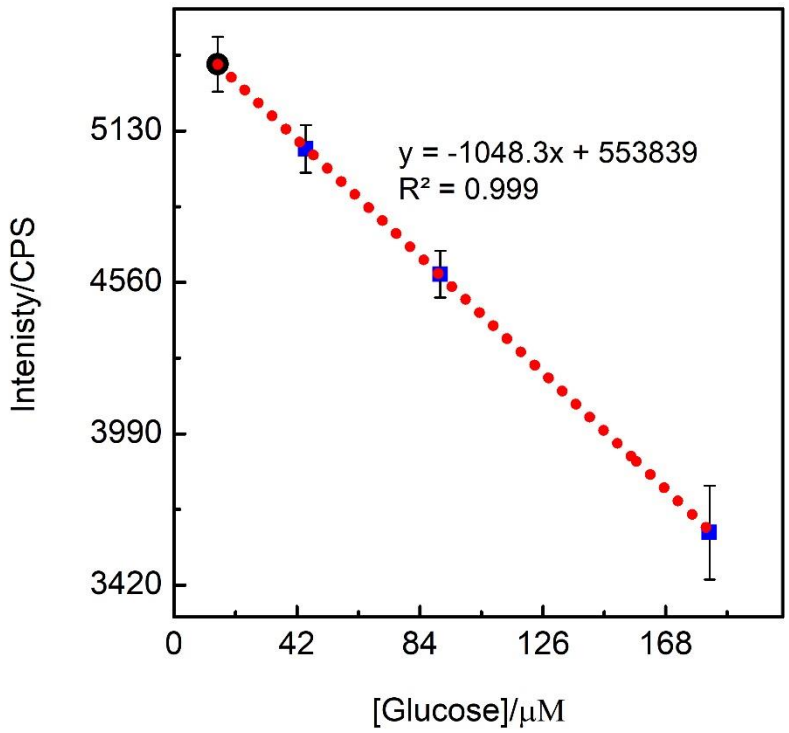

Figure 3.23 A calibration plot obtained from glucose standards for the measurement of non-stimulated saliva glucose using liquid phase equilibrium method, Where N = 3.

3.3.5 Cholesterol sensing by GHS-QD-ChOx

It is very important to maintain cholesterol levels within the normal range human body. The cholesterol level in serum should be lower than 5.18 mM for normal subjects and any serum cholesterol level higher than 6.2 mM causes serious health problems. The cholesterol level in saliva for the normal subject is 1.4 to mM, above 7.5 µM is considered a high cholesterol level (Table 1.1). Enzymatic cholesterol sensor was developed based on the cholesterol oxidation by cholesterol oxidase that released H_2O_2, which quenched the fluorescence intensity of QDs.

The performance of the sensor was evaluated at different QDs and ChOx concentrations. The QDs of 0.1 mg/L with ChOx of 0.616 units/mL were used. The average fluorescence was quenched by the addition of 5.2, 10.3, 15.3, 25.4, and 49.7 µM of cholesterol in Figure 3.2. The fluorescence response for the known cholesterol concentrations was not reliable as represented with error bars (standard deviation of the response) in a calibration plot.

The average fluorescence response with standard deviation was plotted in Figure 3.25. The linear range obtained was 5 to 16 µM with a correlation coefficient of 0.987. The standard deviation calculated was 3.2 µM. The response in calibration 3.14 is with high standard deviations.

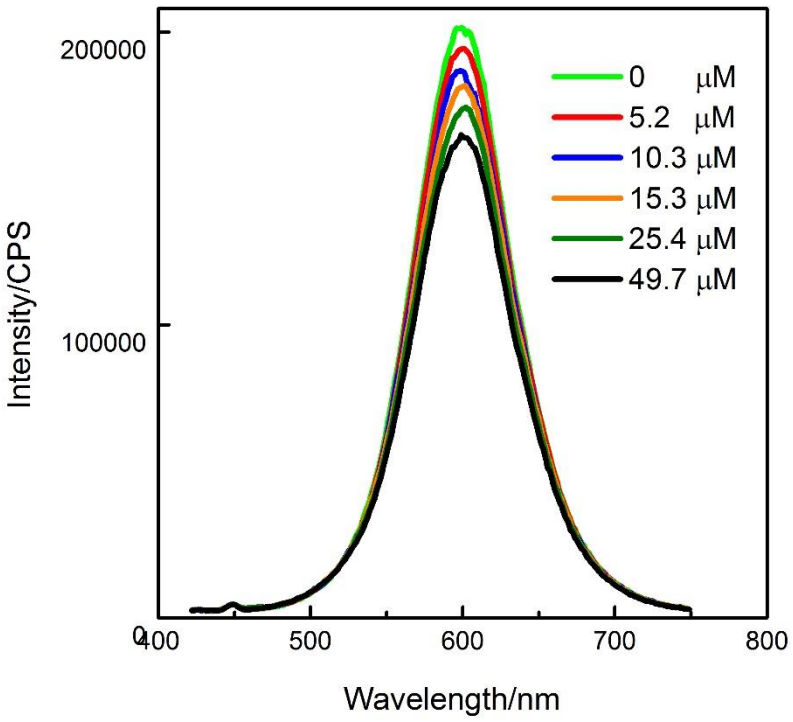

Figure 3.25 The fluorescence spectra of GHS capped QDs (0.11 mg/L), quenched by cholesterol, in the presence of 0.616 units of ChOx.

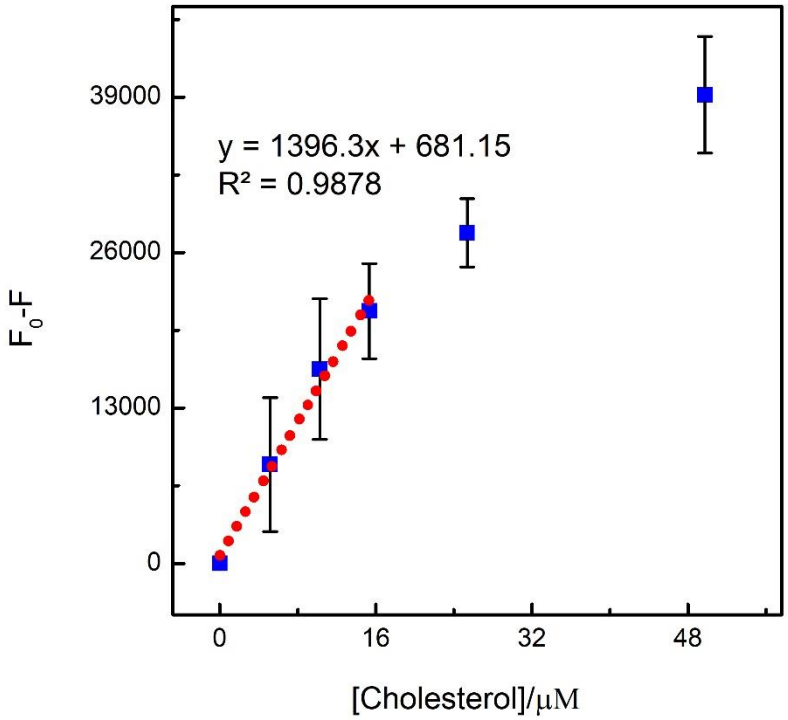

Figure 3.26 Calibration plot of the fluorescence response of GHS capped QDs to 5 – 50 µM of cholesterol. The error bars representing the standard deviation of 3 repeats.

In another calibration, ChOx 2.2 units/mL (100 µl of from stock of 11 mg/mL ChOx in the buffer pH 7.2) and QDs 0.11 mg/L was used to measured cholesterol at 1 to 45 µM range. The dilution factors and the effect of 5 µl of triton (1 % in phosphate buffer pH 7.2) in 10 ml of QDs (0.133 mg/L in phosphate buffer) were studied before the analysis and negligible fluorescence intensity change was observed on the addition of 5 µL of triton and water.

The experimental data of cholesterol sensors is shown in Figure 3.27. The fluorescence spectra gradually declining by the addition of 2.5 to 45 µM of cholesterol. The linearity was ranged from 2.5 to 26 µM with a correlation coefficient of 0.985. The range of cholesterol achieved was enough to measure the trace amount of cholesterol in blood and saliva. The sensitivity of the sensor was 1396 CPS/µM with the detection limit of 1.5 µM was achieved. Our experimental designed for cholesterol measurement was simple easy and can measure cholesterol at the range of saliva cholesterol.

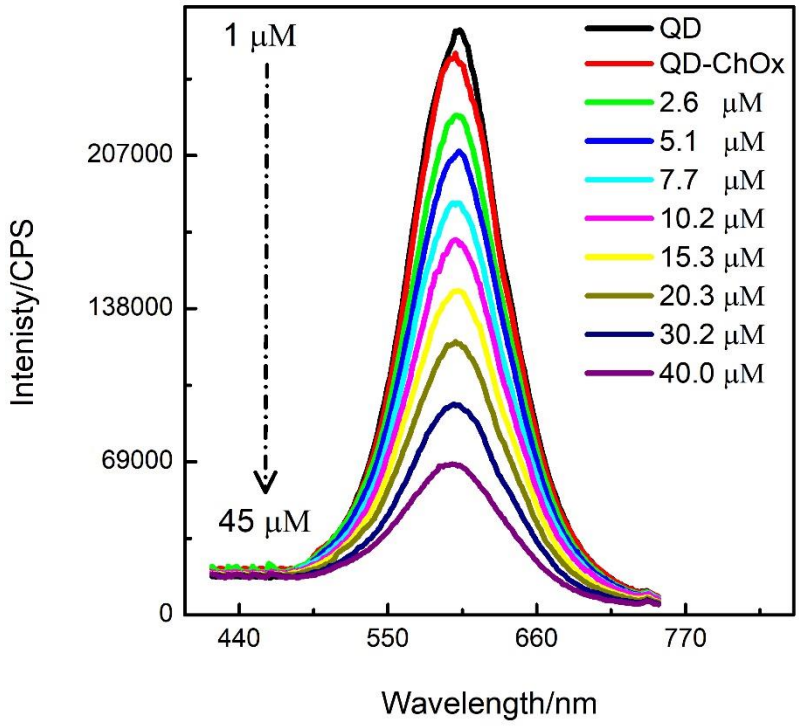

Figure 3.27 The fluorescence spectra of GHS capped QDs quenched by 1 to 45 μM of Cholesterol. The error bars representing the standard deviation of three repeats.

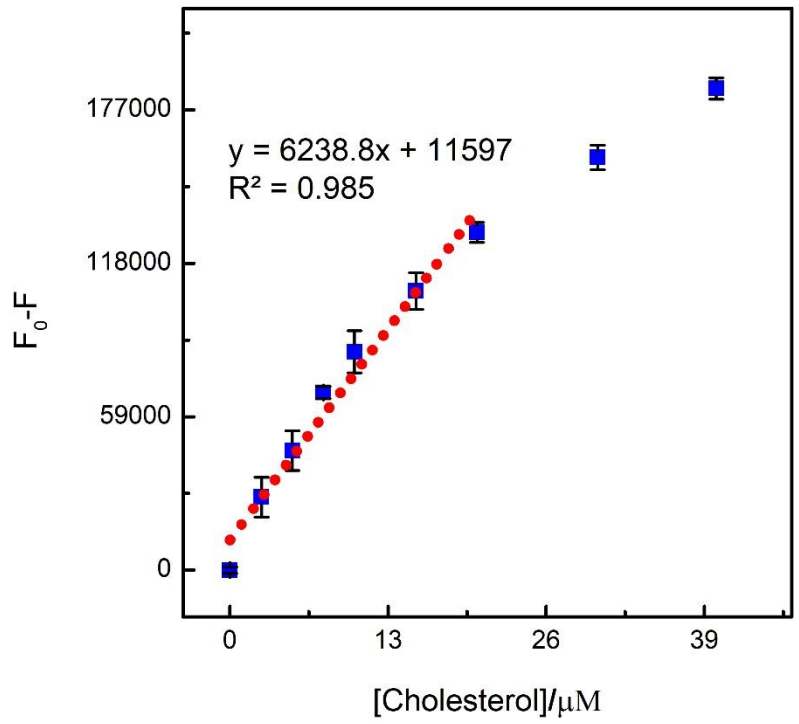

Figure 3.28 The calibration plot representing the fluorescence response of GHS capped QDs to 1 - 45 μM cholesterol, the error bars represent the standard deviation of three repeats.

Analyte	[QDs]/mg^{-L}	Linear range /µM	Detection limit/µM
H_2O_2	0.238	4 - 237	0.4
Glucose	0.33	33 - 336	8.2
Cholesterol	0.11	2.5 - 26	1.5

Table 3.4 The table concluding the QDs concentration used for H2O2 analysis, the linear range, detection limits, and limit of quantification.

3.4 Conclusion

The QDs based optical detection techniques were used for the analysis of H_2O_2, glucose, and cholesterol. Initially, the pH sensitivity of QDs was investigated, it was found that QDs are very sensitive to hence buffer was used for all analysis. The basic model was established for H_2O_2 measurement and was further extended to glucose and cholesterol measurements. The cholesterol and glucose sensors are based on enzymes, thus the measurement methods for cholesterol and glucose was investigated using an adequate amount of oxidases. H_2O_2 was measured at a different range, the limit of detection was 0.4 µM with different linear range, covering the millimolar and micromolar region. The limit of detection was 8.2 µM for glucose with the linear range of 33 to 336 µM (saliva glucose range) and 0.4 to 5 mM (blood glucose region). The linear range of cholesterol detection was from 2.5 to 26 µM with the detection limit of 1.5 µM. We concluded that GHS-capped QDs can be used for the highly sensitive measurement of saliva, tear, blood, and urine glucose.

3.5 References

(1) Gaponik, N.; Talapin, D. V.; Rogach, A. L.; Eychmüller, A.; Weller, H. Efficient Phase Transfer of Luminescent Thiol-Capped Nanocrystals: From Water to Nonpolar Organic Solvents. *Nano Letters* **2002,** *2* (8), 803.

(2) Lesnyak, V.; Gaponik, N.; Eychmuller, A. Colloidal semiconductor nanocrystals: the aqueous approach. *Chemical Society Reviews* **2013,** *42* (7), 2905.

(3) Gaponik, N. Assemblies of thiol-capped nanocrystals as building blocks for use in nanotechnology. *Journal of Materials Chemistry* **2010,** *20* (25), 5174.

(4) Gill, R.; Bahshi, L.; Freeman, R.; Willner, I. Optical Detection of Glucose and Acetylcholine Esterase Inhibitors by H_2O_2-Sensitive CdSe/ZnS Quantum Dots. *Angewandte Chemie* **2008,** *120* (9), 1700.

(5) Ford, E. S.; Li, C.; Zhao, G. Prevalence and correlates of metabolic syndrome based on a harmonious definition among adults in the US. *Journal of Diabetes* **2010,** *2* (3), 180.

(6) Veal, E. A.; Day, A. M.; Morgan, B. A. Hydrogen Peroxide Sensing and Signaling. *Molecular Cell 26* (1), 1.

(7) Wu, G.; Fang, Y.-Z.; Yang, S.; Lupton, J. R.; Turner, N. D. Glutathione Metabolism and Its Implications for Health. *The Journal of Nutrition* **2004,** *134* (3), 489.

(8) Gan, T.-T.; Zhang, Y.-J.; Zhao, N.-J.; Xiao, X.; Yin, G.-F.; Yu, S.-H.; Wang, H.-B.; Duan, J.-B.; Shi, C.-Y.; Liu, W.-Q. Hydrothermal synthetic mercaptopropionic acid stabled CdTe quantum dots as fluorescent probes for detection of Ag. *Spectrochimica Acta Part A: Molecular and Biomolecular Spectroscopy* **2012,** *99*, 62.

(9) Ruedas-Rama, M. J.; Hall, E. A. pH sensitive quantum dot? anthraquinone nanoconjugates. *Nanotechnology* **2014,** *25* (19), 195501.

(10) Medintz, I. L.; Stewart, M. H.; Trammell, S. A.; Susumu, K.; Delehanty, J. B.; Mei, B. C.; Melinger, J. S.; Blanco-Canosa, J. B.; Dawson, P. E.; Mattoussi, H. Quantum-dot/dopamine bioconjugates function as redox coupled assemblies for in vitro and intracellular pH sensing. *Nature materials* **2010,** *9* (8), 676.

(11) Tan, X.; Liu, S.; Shen, Y.; He, Y.; Liu, Y.; Yang, J. Glutathione-capped CdTe quantum dots for the determination of fleroxacin with dual-wavelength fluorescence signals. *Analytical Methods* **2014,** *6* (13), 4860.

(12) Veal, E. A.; Day, A. M.; Morgan, B. A. Hydrogen peroxide sensing and signaling. *Molecular cell* **2007,** *26* (1), 1.

(13) Li, Y.; Li, B.; Zhang, J. H_2O_2 - and pH-sensitive CdTe quantum dots as fluorescence probes for the detection of glucose. *Luminescence* **2013,** *28* (5), 667.

(14) Cao, L.; Ye, J.; Tong, L.; Tang, B. A new route to the considerable enhancement of glucose oxidase (GOx) activity: the simple assembly of a complex from CdTe quantum dots and GOx, and its glucose sensing. *Chemistry* **2008,** *14* (31), 9633.

(15) Priyam, A.; Chatterjee, A.; Bhattacharya, S. C.; Saha, A. Conformation and activity dependent interaction of glucose oxidase with CdTe quantum dots: towards developing

a nanoparticle based enzymatic assay. *Photochemical & Photobiological Sciences* **2009,** *8* (3), 362.

(16) Parani, S.; Bupesh, G.; Manikandan, E.; Pandian, K.; Oluwafemi, O. S. Facile synthesis of mercaptosuccinic acid-capped CdTe/CdS/ZnS core/double shell quantum dots with improved cell viability on different cancer cells and normal cells. *Journal of Nanoparticle Research* **2016,** *18* (11), 347.

(17) Abedinzadeh, Z.; Gardes-Albert, M.; Ferradini, C. K inetic study of the oxidation mechanism of glutathione by hydrogen peroxide in neutral aqueous medium. *Canadian journal of chemistry* **1989,** *67* (7), 1247.

(18) Guideline, I. H. T. Q2B validation of analytical procedures: methodology. *Fed. Regist* **1997,** *62*.

Chapter 4. Using the rate Constant as an Analytical Tool for the Measurement of H_2O_2, Glucose, and Cholesterol.

4.1 Introduction

The detection in analytical sciences can be classified into the equilibrium state and the transient based method[1,2]. Generally most of the sensors are developed based on measuring the concentration at equilibrium. Although the kinetic analytical approach has been identified, developed, and implemented for past century. The kinetic methods of analysis are extensively and effectively used in enzymes induce analysis especially for the determination of biomolecules. In comparison with kinetic method, equilibrium state measurement is executed in a manner such that the signal is not interrupted in any way by any type of kinetic process while for kinetic method the measuring signal is influenced by many or one transient activity. The kinetics methods are used in analysis in such way that the measuring signal is equal to the interfering species that to be examined[3]. The kinetics analytical is not well developed because of the limitation of instruments and experimental techniques, The kinetics analysis were done using the same techniques and instrumentation, which were designed for equilibrium method[1]. The recent progress in instrumentation for monitoring in the kinetics of reaction make it possible to use reaction rate, or reaction constant for measuring analytical signal with more precision and accuracy [4-10]. Transient method of analysis is recently increasing and make a new window in analytical sciences, many analytical investigation of chemical, biological species were developed using analytical method of analysis[11-13]. Contrast to equilibrium method transient analytical experimental techniques are more elastic, which could produce a reliable results with precision and high accuracy than equilibrium method [3]. The transient method offer advantages of fast analysis time, than conventional endpoint method, it is a reagent saving methods and eliminate the background signal[14]. Kinetic methods based on organic fluorophores or fluorescent nanomaterials, the fluorescent material have self-quenching properties and long-term instability in system.

The kinetic approach of analysis is extensively used for measurement of biomolecules including bilirubin, amino acid, nucleic acid, glucose uric acid, cholesterol, proteins, and other biomarkers [15-17].

QDs based H_2O_2, glucose, and cholesterol sensors had been reported before [18] , however the kinetic degradation profile of QDs for sensing application has not been studied. Here we describe new transient methods for the measurement of H_2O_2, glucose, and cholesterol and the methods were also compared with equilibrium method. GHS capped QDs has been investigated as potential fluorescent probe to detect glucose, cholesterol in previous chapter, hence in this study GHS QDs has been used to developed a new kinetic method of analysis.. H_2O_2 is the byproduct of enzymatic oxidation of glucose and cholesterol hence the developed method was also used for described analyte measurements. Fluorescence of QD is quenched by H_2O_2 which is due to the removal of QDs caps from the core. The trace of H_2O_2 reacting with QDs was correlated to the rate of fluorescence quenched. A pseudo-first orders kinetic model was established by keeping the QDs concentration very high hence the rate of fluorescence decay is due to the concentration of hydrogen peroxide used.

4.2 Experimental

4.2.1 Reagents and apparatus

D-glucose was purchased from Aladdin China. Cholesterol, Ascorbic acid, Uric acid, Cholesterol oxidase and glucose oxidase (GOx) (17300 Units/G) was from Sigma-Aldrich USA. Lactate, potassium thiocyanate (KSCN) and ammonium chloride were purchased from Sinopharm chemical Reagents. Co. Ltd, China. Sodium hydroxide, dipotassium hydrogen phosphate, dihydrogen potassium phosphate, citric acid trisodium salt dihydrate 99 %, cadmium chloride 99 %, Calcium chloride 96%, sodium chloride 99.5 %, sodium borohydride 98 %, H_2O_2 35 % in water, glutathione (GHS) and 1-propanol were obtained from Acros Organic USA. Potassium chloride and citric acid were purchased from Enox® Changshu, China. Sodium tellurium (IV) Oxide 99.5 % was purchased from Alfa Aesar-Johnson Matthey Company, Tianjin, China. All the chemicals were of analytical grade and ultra-purified water of Milli-Q system (Millipore Co., Billerica, MA, USA) were used in all analysis.

4.2.2 Instruments for analysis

FluoroMax-4 spectrophotometer (Horiba scientific USA) was used for recording fluorescence spectra; Cary 300 UV-VIS spectrophotometer (Agilent Technology USA) was used for recording UV-Visible spectra. Bio-Logic stopped-flow (SFM-3000 S01/N with MPS-70, France with MOS-250 spectrometer, France) were used for kinetics analysis.

4.2.3 H_2O_2 measurement by Pseudo first order kinetic model

A series of H_2O_2 standards with concentrations of 1.5, 3, 6, 12, and 24 mM were made up in Milli-Q water from a 0.6 M H_2O_2 stock solution. 10 µL of H_2O_2 standard was added into a 1 mL cuvette, followed by 1 mL of QDs solution (6.3 mg/L). The kinetics of fluorescence intensity at 595 nm wavelength degrade by H_2O_2 standard solution was monitored by using an excitation wavelength of 420 nm and the obtained fluorescence intensity 10 DPS was exported into excel for analysis.

4.2.4 Measuring high concentration of H_2O_2 by Kinetic model

The performance of QDs based sensor was investigated at different concentration range of H_2O_2. The kinetic model applied for H_2O_2 sensing approach consist high concentration of QDs solutions with low concentration of H_2O, so that is important to investigate the application of the sensor at high concentration of analyte. 200 µL of QD aliquots from 180.0 mg/L QDs concentration was diluted to 60 ml Sodium phosphate buffer of 10 mM, the final concentration of QD stock was 62.0 mg/L. 5, 10, 20 µl of 0.1mM of H_2O_2 was spiked into the cuvettes followed by the addition of 1 mL QD stock solution (62.0 mg/L). The kinetics of fluorescence intensity quenching was measured at 594 nm emission wavelength, using the excitation of 400 nm wavelength. The data obtained was exported and analyzed to investigate the kinetic model and measure the amount of H_2O_2.

4.2.5 Measurement of H_2O_2 (25 to 400 µM) by kinetic method

H_2O_2 standards of 2.1, 4.2, 8.4, 16.8, 33.6 mM were made in phosphate buffer pH 7.2 from a stock solution of 2.1 M H_2O_2. QDs solution of concentration 6.2 mg/L was made in 5

mM potassium phosphate buffer pH 7.2. The equilibrium temperature of the instrument was measured, which was 28 °C. All the standard solutions were kept in water bath at constant temperature of 28 °C. Briefly, H_2O_2 of 12 µL from freshly prepared standard solutions was added into 1 ml of cuvette, followed by 1 ml of QDs solution. The final concentration of H_2O_2 in the reaction mixture was 24.9, 49.8, 99.6, 199.2, 398.4 µm. The kinetics of QDs degradations were measured at 600 nm emission wavelength at the rate of 10 data points per second (DPS) with excitation of 400 nm. Each measurement of H_2O_2 concentrations were recorded three times.

4.2.6 Measurement of low H_2O_2 concentration by kinetic method

H_2O_2 standards of 0.04, 0.16, 0.307, 0.62, and 1.3 mM were made in phosphate buffer pH 7.2 from a stock solution of 32 mM H_2O_2. The QDs solution (6.2 mg/L) was made in 5 mM potassium phosphate buffer pH 7.2. Briefly, H_2O_2 of 10 µL was spiked into 1 ml cuvette, followed by 1 ml of QDs solution. The reaction mixture of QDs and H_2O_2 in spectrophotometric cuvette were mixed by gentle shaking before recording the fluorescence emission. The final concentration of H_2O_2 in a reaction mixture was 0.38, 1.5, 3.02, 6.4, and 12.7 µM. The kinetics of QDs degradations were measured at 600 nm emission wavelength at the rate of 10 data points per second (DPS) with excitation of 400 nm. All the measurements were recorded three times at room temperature of 26 °C.

4.2.7 Measurement of H_2O_2 using bio-kinetic stopped flow

Bio-Logic stopped-flow (SFM-3000 S01/N with MPS-70, France) was used to carry out the kinetics study. The instrument is equipped with four motor-driven syringes (S1, S2, S3, and S4) of 10 ml; the injection can operate independently to carry out single or double-mixing. The stopped-flow device is attached to a MOS-250 spectrometer. The flow rate for all measurements was 5 mL^{-s} was used. Temperature was maintained at 26 °C by circulating water around the syringe chamber and the observation head. H_2O_2 standard solutions of 6, 3 and 1.5 mM is used. The QDs of 92.00 mg/L was used for kinetics. Different ratios of QDs and H_2O_2

were used for analysis, the final concentration of H_2O_2 after mixing was 16, 32, 64, 256, 512, 1024 and 2096 µM.

4.2.8 Measurement of glucose by kinetic method

Glucose standards; 2.5, 5, 10, 20, 40 mM were made in phosphate buffer pH 7 from 2.5 M glucose stock solution. Glucose oxidase (GOx) solution was made by dissolving 1.3 mg of GOx in 1 ml of 50 mM phosphate buffer pH 6.8. QDs solution (6.00 mg/L) was made in 5 mM sodium phosphate buffer pH 7.2. QD-GOx conjugation was made by adding 35 ml of QD solution and 1 ml of GOx solution with continuous stirring for 20 minutes. The equilibrium temperature of the instrument was recorded, which was 28.5 °C. All the solutions were kept at constant temperature 28.5 °C. Briefly, 10 µL of glucose standard solutions was added to 1 ml cuvette followed by 1 ml of QD-GOx standard solution. The fluorescence was measured at 600 nm emission wavelength at the rate of 10 data points per second (DPS) with excitation of 400 nm.

4.2.9 Measurement of glucose in saliva by kinetic method

Measurement of artificial saliva

An artificial saliva was prepared containing 5 mM of NaCl, 1 mM of $CaCl_2$, 15 mM of KCl, 1 mM of citric acid, 5 mM of uric acid, 1 mM of ascorbic acid, 0.2 mM of lactate, 1.1 mM of Potassium thiocyanate KSCN, 4 mM of NH4Cl in water [19]

Glucose standards of 5.2, 10.4, 20.8, 41.6, mM were made in artificial saliva. The QDs solution (9.3 mg/L) was made of in 5 mM potassium phosphate buffer of pH 7.2. GOx (1.5 mg/ml) was made in 50 mM potassium phosphate buffer. QD-GOx was prepared by adding 0.6 ml of GOx solution in 30 ml of QDs solutions with continuous stirring for 20 minutes. Briefly glucose of 10 µL was pipetted into 1 ml of cuvette, followed by 1 ml of QDs-GOx solution. The kinetics of fluorescence was measured at 600 nm emission wavelengths at the rate of 10 data points per second (DPS) with excitation of 400 nm wavelengths, the slit width used was 5 and 2 nm for emission and excitation respectively.

Measurement of human saliva

8.4 mg/mL of GHS capped QDs solution was made in phosphate buffer pH 7.5. Glucose oxidase solution was made by the addition of 4 mg GOx in 1 mL of the same buffer. 500 µL of prepared GOx solution was spiked into 5 mL QDs stock solution was stirred for two minutes. The pH of the QDs-GOx solution was checked and readjusted to 7.5 by the addition of 1 mM sodium hydroxide.

50 µL of human non-stimulated saliva of volunteer subject A4 (saliva collection procedure described in chapter 5 section 5.2.10) was added into 96 well microplate, followed by the addition of 150 µL QD-GoX solution. The fluorescence response of QDs after the addition of saliva was recorded. Glucose of 2, 4, and 6 µL from 4 mM stock solution was added into the microwell of a 96-well microplatefollowed by the addition of 50 µL of saliva. 150 µL of QD-GOx solution was added in the well already contain glucose standard and saliva and the fluorescence response was recorded after each addition of standards with saliva. All the measurements were recorded at 605 nm of emission wavelength with excitation of 396 nm.

4.2.10 Measurement of cholesterol by kinetic method

Cholesterol stock was prepared by dissolving 50 mg of cholesterol in 1 ml triton-100 (density 1.067) in a 50 ml volumetric flask. The mixture was sonicated and heated at 60 ºC for one hour and finally the mixture was make up to 50 ml by 100 mm potassium phosphate buffer of 7.2. Cholesterol standard of 0.5, 1, 2, and 4 mM were made in phosphate buffer of pH 7 from glucose stock solution of 6 mM. Cholesterol Oxidase solution was stock solution was prepared by dissolving 2 mg of Cholesterol oxidase in 1 ml of 50 mM acetate buffer pH 7. QDs solution (6.00 mg/L) was made in 5 mM sodium phosphate buffer pH 7.2. QD-ChOx conjugation was made by adding 10 ml of QD solution and 0.1 ml of ChOx solution with continuous stirring for 20 minutes. The equilibrium temperature of the instrument was recorded, which was 28.0 °C. All the solutions were kept at constant temperature 28.0 °C. Briefly, 5 µL of cholesterol standard solutions was added to 300 µl cuvette followed by 200

µL of QD-ChOx standard solution. The fluorescence was measured at 600 nm emission wavelength at the rate of 10 data points per second (DPS) with excitation of 400 nm

4.2.11 Measurement of glucose by kinetic stopped flow

A kinetics measurement of glucose was carried out using the same procedure and instrumental setup. GOx of 1.5mg/mL concentration was mixed to 10 mL QDs (98.0 mg/L) with continuous stirring for 20 minutes. The final concentrations of glucose was 80, 160, 320, 640, 1280, 2560 µM. The total fluorescence was collected using the excitation of 400 nm for glucose and H_2O_2 kinetics. Each Glucose and H_2O_2 standards were measured three times and the standard deviation of average were calculated.

4.3 Results and discussions

The fluorescence quenching was a result of the reaction between glutathione capped QDs and hydrogen peroxide; in which the surface bound glutathione was oxidized. The oxidation of surface bound glutathione molecules into the corresponding disulfide re-modified the QD surface which disrupted the electron-hole recombination process to result in the observed fluorescence quenching (reaction 4.3). Therefore in this detection scheme, the QDs can be seen to function as signal transducer for the chemical reaction between the glutathione and hydrogen peroxide.

There are two important parameters in this reaction that are not well established. Firstly, the loading of glutathione on the QD surface is not determined. Secondly, the degree of surface glutathione oxidation to effect QD fluorescence quenching is not established; which infer that the stoichiometry of hydrogen peroxide and QD reaction is therefore unknown. It has been verified that the measured degradation of fluorescence intensity of glutathione capped QDs is linearly related to the H_2O_2 concentration. It is therefore possible to make use of the QDs fluorescence degradation as a mean to elucidate the consumption of H_2O_2 in the reaction mixture.

It was designed that in this detection process, very small amount (10 µL) of dilute H_2O_2 was added into a 1 mL of strong QD solution. The overall concentration of QD and thus

glutathione (bound on the surface of QD) are in large excess compared to that of the H_2O_2; hence the reaction can be regarded as a pseudo first-order reaction with respect to H_2O_2.

The kinetics of reaction is represented below in equation. GHS-capped QDs react with hydrogen peroxide and diminished the bond between the surface capping agent and nanocrystals.

$$\text{RS-QD} + H_2O_2 \rightleftharpoons \text{RS-SR} + H_2O \quad \textbf{(4.1)}$$

According to the rate law

$$Rate = k\,[GHS - QD][H_2O_2] \qquad (1)$$

Assuming pseudo first order condition by keeping the concentration of GHS-capped QDs constant hence the modified equation (1) is

$$Rate = \mathrm{K}\,[H_2O_2] \qquad (2)$$

4.3.1 Kinetic model of analysis

Initial rate methods were used to establish a relation between the rate of reaction and concentration of the analyte. A pseudo-first kinetics was applied by using the concentration of QDs in excess. The rate of change in fluorescence intensity is

$$-\frac{d[F]}{dt} = k\,\mathrm{F} = k'\,\frac{d[H_2O_2]}{dt} \qquad (3)$$

Since $-\frac{d[H_2O_2]}{dt} = k''\cdot[H_2O_2]$ (4)

Hence the experimental observed quenching rate is

$$= -\frac{d[F]}{dt} = k'\cdot k''.[H_2O_2] = k.[H_2O_2] = k\,\mathrm{F} \qquad (5)$$

Where *k*, *k*' and *k*'' is *K* are constants

Hence $kF = K.[H_2O_2]\ or\ \frac{k[H_2O_2]}{F}$ (6)

Therefore, the relationship between fluorescence intensity and H_2O_2 concentration was established.

For a first order reaction, the observed rate of fluorescence decay is:

$$-\frac{d[F]}{dt} = kF \quad (7)$$

Solving eq (7), we get: $F=F_0 \exp(-kt)$ (8)

And $\ln F = \ln F_0 - kt$ (9)

Plotting ln F *vs* t give a straight line with the slopes the observed fluorescence decay constants k.

The kinetic model was verified and the pseudo-first order rate constants were evolved by using the rate equation, the QDs fluorescence quenching induced by the initial concentration of H_2O_2 is shown in Figure 4.1. The experimental fluorescence decay acquired from a reaction using excess QDs and different initial concentration of H_2O_2 (25 to 200 µM) was plotted following the pseudo first order rate equation ($\ln F = \ln F_0 - kt$). The ln F vs t plot was linear, showing that the experimental results obey pseudo first order rate law, which was represented in Figure 4.2.

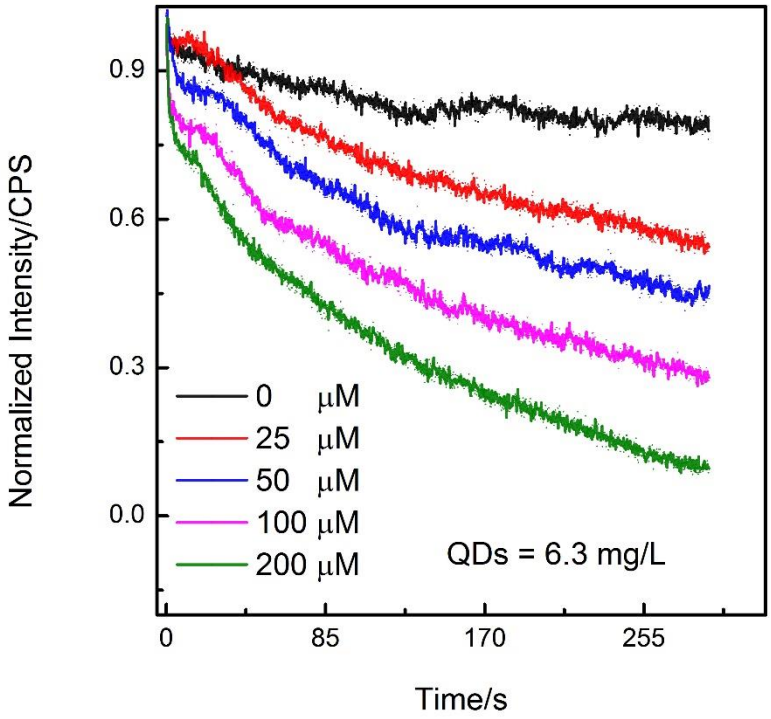

Figure 4.1The fluorescence decay profile of GHS capped QDs induced by 25 to 200 μM of H_2O_2.

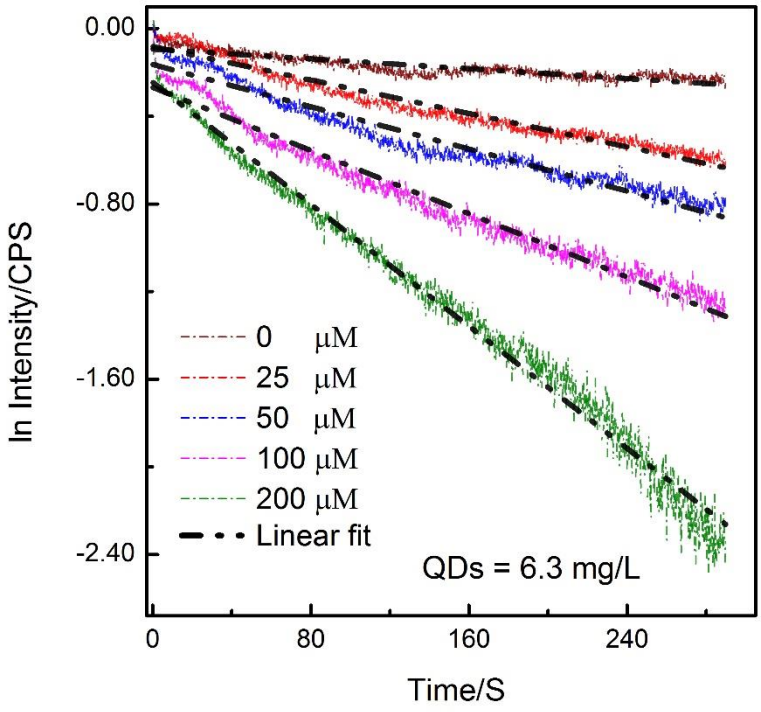

Figure 4.2 The pseudo first order decay of glutathione QDs fluorescence induced by the 25 to 200 μM H_2O_2 trace.

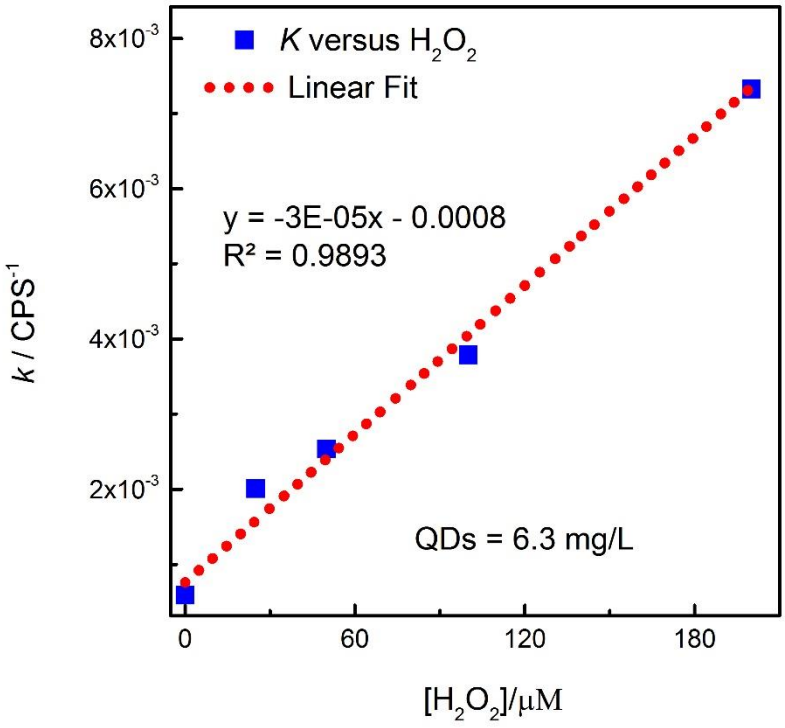

Figure 4.3 The calibration plot of H_2O_2 concentrations used in analysis versus the pseudo first-order rate constant.

Figure 4.3 presents the use of kinetic data for quantitative chemical analysis. For better comparison, *-k* shown in Table 2 were plotted against H_2O_2 concentration with base-line corrected to zero. A linear line was obtained with a slope of 3 x 10-5 S^{-1} μM^{-1}. This result suggests that kinetic data has significant analytical value and benefit. The measurement of pseudo-equilibrium data can be prone to error unless extreme care and precautions are taken for reagent mixing and data collection. Whereas the rate constant *k* is determined by using data collected within a specific time frame rather than a discrete instance of time, it is hence a more robust method of analysis. However, there are drawbacks in using kinetic method for analysis. It is necessary to control the temperature, reduce sample volume, and shorten the analysis time. The mixing of reactants and monitoring of the fluorescence signal has to be instantaneous.

4.3.2 Measurements of H_2O_2

H_2O_2 was measured according to the kinetic model established in section above and obtained data were showed in Figure 4.1 to 4.3. A constant QDs concentration react with a

range of different H_2O_2 concentrations, it was important, that the range of H_2O_2 concentrations used should not affect and change the nature of reaction hence it was important to optimized the concentration of QDs for the measurement of H_2O_2 in a specific range. Some of the features of QDs are fluorescence self-quenching at high concentration, saturation effect, aggregation, and self-trapping of QDs at low concentration, that was a challenge to optimize QDs concentration, neglecting the fact will lead to error in the analysis. Three separate calibrations for the measurements of H_2O_2 at mille molar (0.5 to 2mM), the micromolar (25 to 400 µM), and nanomolar range was achieved (300 to 16000 nM). The process was optimized by repeating and reproducing the results, by different experimental techniques.

H_2O_2 was analyzed initially in millimolar range to understand the QDs concentration effect on the higher concentration of hydrogen peroxide. This details will lead us and will make it feasible to analyze H_2O_2 in 25 to 500 micromolar range (glucose target level was 60 µM). One stock solution (0.1 M) of the H_2O_2 with different volume was used, the resultant concentrations were 0.497, 0.995, and 1.99 mM. The concentration of QDs were 62 mg/L, which was 10 times high than the concentration of QDs used to established the pseudo first order kinetic model for H2O2 analysis (25 to 200 µM).

The fluorescence spectra (average of three repeats) were presented in Figure 4.4 which gives different reaction rates. The spectra were plotted accordingly to the pseudo first order kinetic model (Figure 4.5) and the initial rates' constants were calculated and were plotted against the concentrations of hydrogen peroxide. A results was a linear plot with R^2 value of 0.9854 in Figure 4.6.

The linear plot of rate constant versus the H_2O_2 concentration indicated that the results follow pseudo first order rate law. The linear range was 0.49 to 1.9 mM with correlation coefficient of 0.0987. The detection limit was 0.48 mM. The kinetic of QDs fluorescence quenched was faster and with greater sensitivity. The sensitivity of the calibration plot achieved was with 0.018 CPS^{-1}/mM of H_2O_2. The estimated time for the measurement of 0.5 to 2 mM range of H_2O_2 was 1 S.

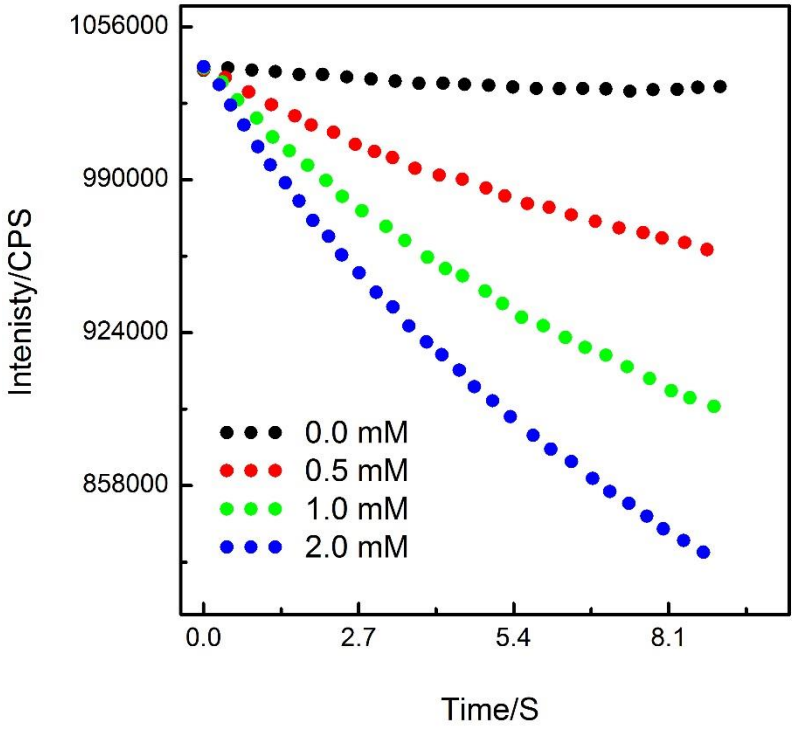

Figure 4.4 The kinetics of QDs fluorescence quenching induced by 0.49 to 1.99 of mM H_2O_2.

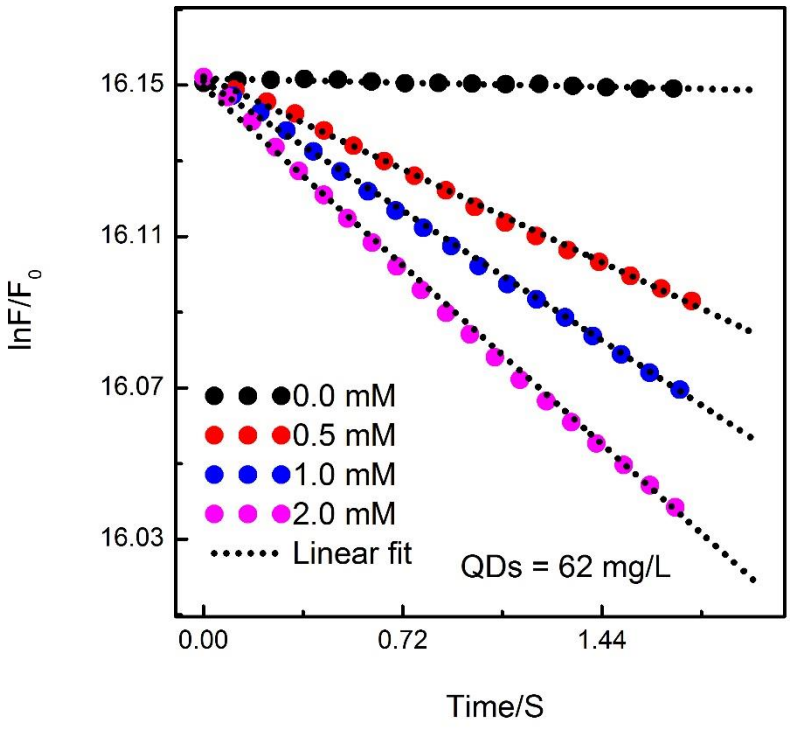

Figure 4.5 Pseudo first order kinetics of GHS-capped QDs fluorescence induced by H_2O_2. (Where n = 3).

[H_2O_2]/mM	0.497	0.995	1.99
***k* CPS-S^{-1}**	0.0001	0.0003	0.00051

Table 4.1 The corresponding rates constant of 0.497 to 1.99 mM of H_2O_2.

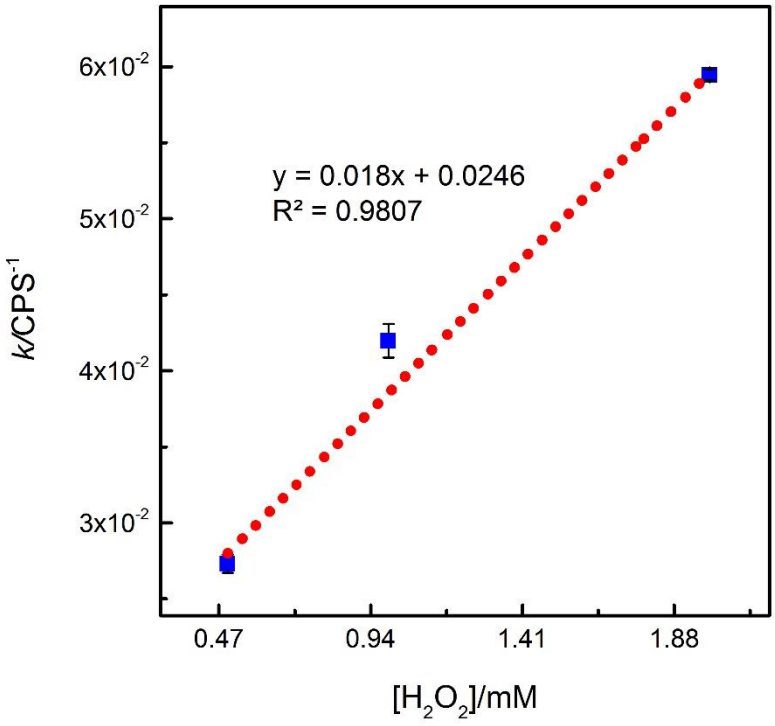

Figure 4.6 Calibration plot of pseudo first order rate constants versus H_2O_2. (The error bar indicates the standard deviation of three repeats).

Another calibration for the measurements of H_2O_2 was achieved at the range of 24.9 to 398.4 µM with the QDs concentration of 6.2 mg/L. The kinetics of fluorescence decay induced by 24.9 to 398.4 µM of H_2O_2 was repeated three time and the average data obtained was plotted in Figure 4.7 according to the kinetic model of analysis. The steady line of fluorescence response in Figure 4.7 is of QDs stock with 10 µL of phosphate buffer pH 7.2. This indicates that the fluorescence of QDs by the addition of 10 µL of buffer is stable up to 300 seconds. Once the appropriate QDs concentration was made and the fluorescence is stable the kinetics analyses were performed.

In Figure 4.7 shows that the fluorescence intensity is diminishing by a series of 24.9, 49.8, 99.6, 199.2, and 398.4 µM of H_2O_2. The fixed time initial rates were used to evaluate the

pseudo first order rats constants. The minimum time required for the analysis was 0.8 seconds but to get more reliable and precise results we used 3 seconds for the evaluation of initial rates. The average rate constants of three repeats were evaluated H_2O_2 concentration in micro molar range shows below in table 4.2.

It was observed that the pseudo first order rates were linearly related to the concentration of hydrogen peroxide used in the calibration showed in Figure 4.8. Three consecutive calibrations were made and the linear range of H_2O_2 measurement was form 24.9 to 398.4 µM with correlation coefficient of 0.995. The linear plots of rates constants vu the concentration of H_2O_2 also confirming that the experimental results following the pseudo first order rate law.

[H_2O_2]/µM	24.9	49.8	99.6	199.2	398.4
***k* CPS-S^{-1}**	0.0109	0.0147	0.0217	0.0313	0.0462

Table 4.2 The pseudo first order rates constant induced H_2O_2 in micro molar range.

Limit of detection was calculated from the blank and standard deviation of the blank and slope of the calibration curve.

$$LOD = \frac{[(b + \sigma b) - c]}{S}$$

Where "b" is the blank the "σb" is the standard deviation of the blank, "S" is the slope and "c" is the intercept of the calibration curve. Hence the calculated limit of detection was 12.5 µM.

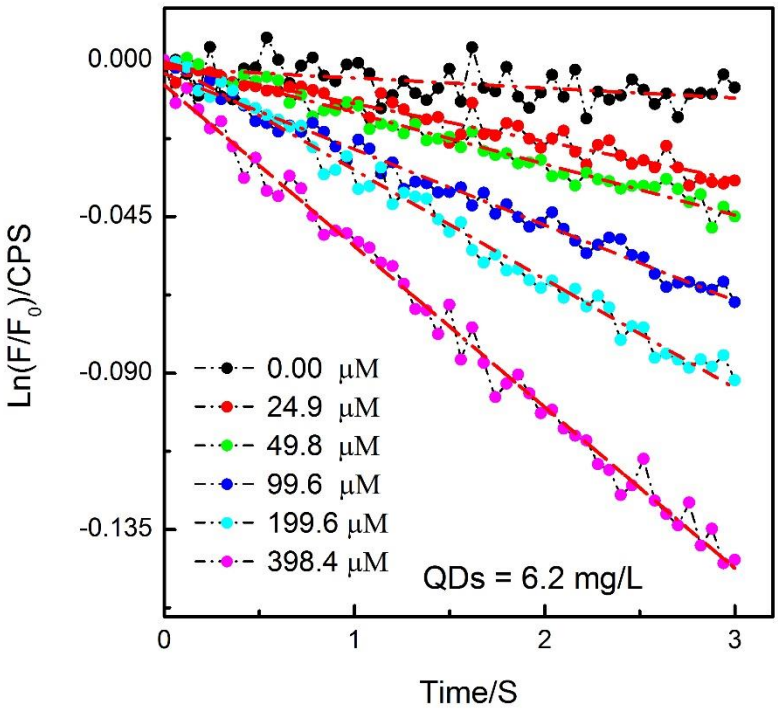

Figure 4.7 Pseudo first order kinetics of GHS-capped QDs fluorescence induced by 24.9, 49.8, 99.6, 199.2, 398.4 µM of H_2O_2. (n=3).

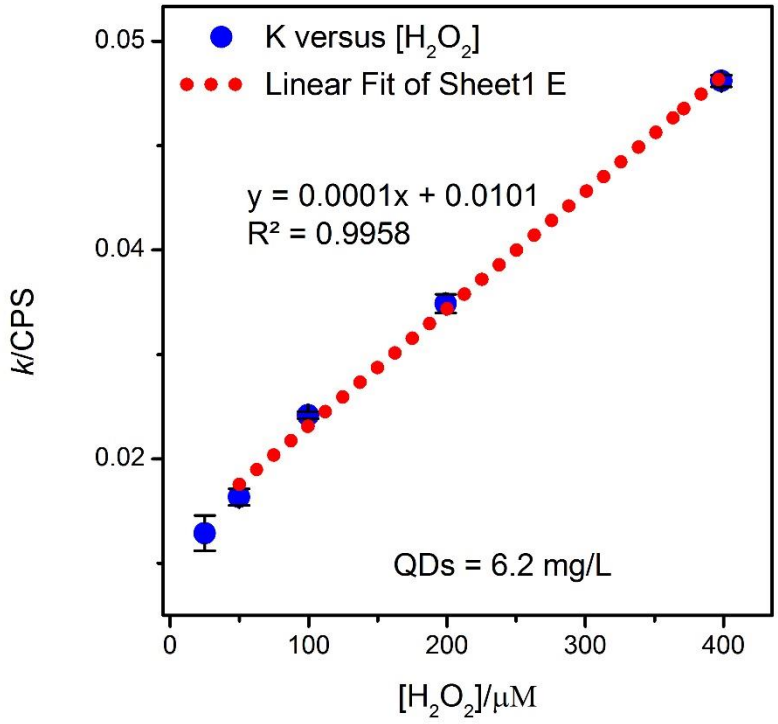

Figure 4.8 Calibration plot of initial rate constants (k) versus 24.9, 49.8, 99.6, 199.2, and 396.4 µM H_2O_2. (The error bar indicates the standard deviation of three repeats).

The QDs fluorescence responded to a very low range of H_2O_2 concentration (0.25 to 13 µM) and the concentration of QDs were kept constant to 6.2 mg/L. The procedure mention above for 24 to 398 µM hydrogen peroxide measurement was used to measure the low concentrations of hydrogen peroxide. The rates of QDs fluorescence quenched obtained were comparatively lower than obtained in previous calibrations using higher concentrations of H_2O_2. We conclude that the rates depend on H_2O_2 concentrations but as the rates subdue the sensitivity decrease. Figure 4.9 show the identical fluorescence decays profile induced by 0.38 to 12.6 µM of hydrogen peroxide. The [ln F] vs [t] were linear which indicate that the experimental condition obeys the rate of pseudo-order reaction kinetics.

The average pseudo first order rates constant was evaluated which were induced by 0.38 to 12.6 µM of H_2O_2 and shown in table below (Table 3.4).

[H_2O_2]/µM	0.38	1.5	3.08	6.08	12.6
***k* CPS-S^{-1}**	0.0001	0.0003	0.00051	0.0008	0.0019

Table 4.3 The pseudo first order rate constant induced H_2O_2 in micro molar range.

The rates constants versus concentrations of H_2O_2 were plotted in Figure 4.10. The linear relationship was from 0.37 to 13 µM with correlation coefficient of 0.998. The slope and the standard deviation of the blank were used to calculate the detection limit. The calculated limit of detection was 0.2 µM. We assuming that kinetic method of analysis is sensitive enough to be used for H2O2 detection in nanomolar range i.e. 200 nM detection limit.

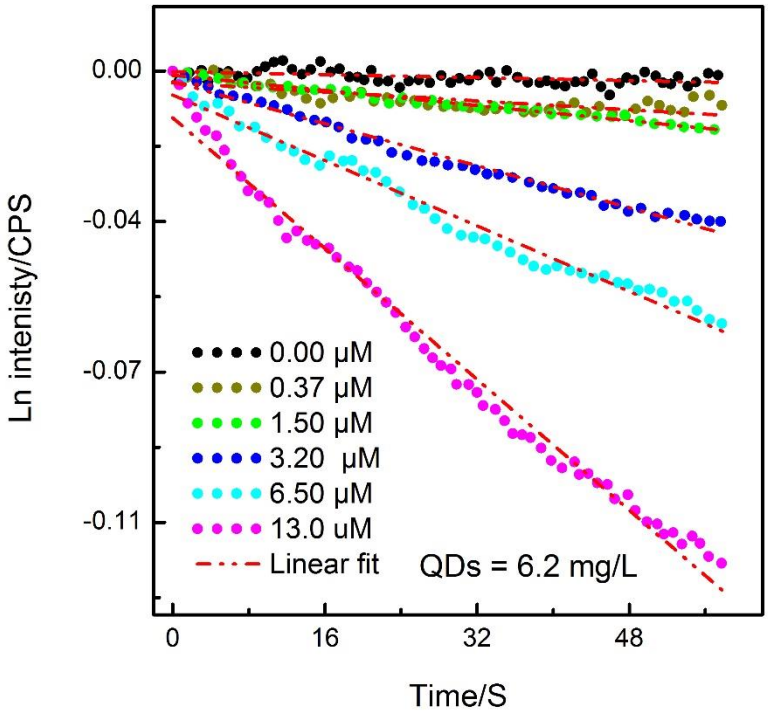

Figure 4.9 Pseudo first order kinetics of GHS- QDs fluorescence by 0.37 to 13 µM of H_2O_2.

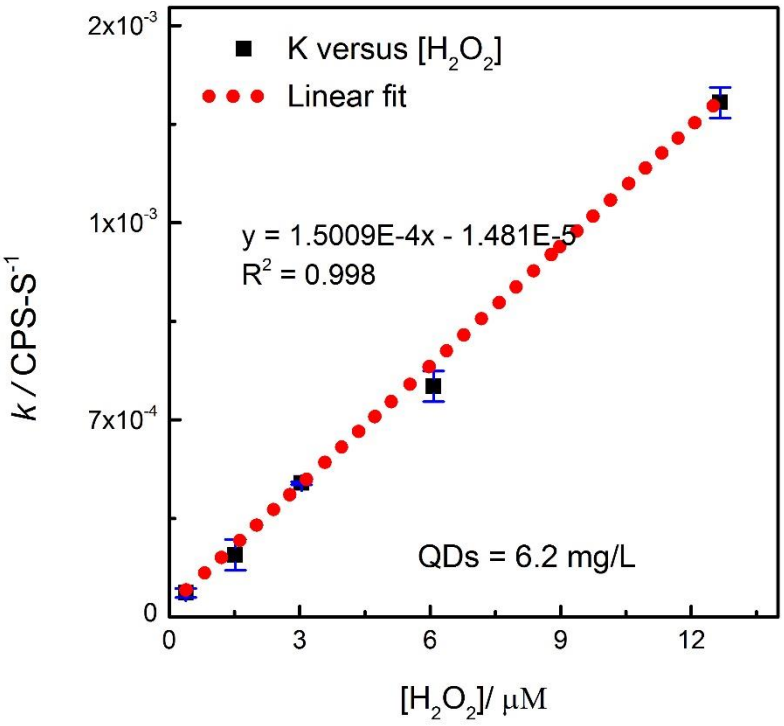

Figure 4.10 Calibration plot of rate constants (k) versus 0.38 to 12.7 µM H_2O_2. (The error bar indicates the standard deviation of three repeats).

Three different linear calibrations (0.3 to 12.6, 24 to 396, and 497 to 1990 µM) was obtained by adjusting the QDs concentration (0.0062, 0.0062, and 0.062 respectfully for 0.3 to 12.6, 24 to 396, and 497 to 1990 µM) to pseudo first order, all the analysis preform was consistent and repeatable. We conclude that the method is reliable and could be used for the quantification of H_2O_2 and the other biological species that produce hydrogen peroxide in the presence of oxidase i.e. glucose, and cholesterol. The sensitivity of the methods is very high as compare to the analytical equilibrium methods. The reaction kinetics of QDs and $H_2O_2$was undetermined, thus the analysis based on the equilibrium of reaction significantly brings errors.

4.3.3 Measurements of H_2O_2 by kinetic stopped-flow

We established a kinetic model for the analysis of hydrogen peroxide, glucose, and cholesterol using a spectrometer designed for the equilibrium analysis. The essential stage of this analysis is to verify and validate all the results obtained from the manual kinetic analysis. Kinetic stopped the flow is an automatic instrument and designed for the kinetics analysis. The most important steps in validating and verifying an analytical process are to confirm the accuracy, precision, repeatability, detection limit, quantitation Limit, and a linearity range.

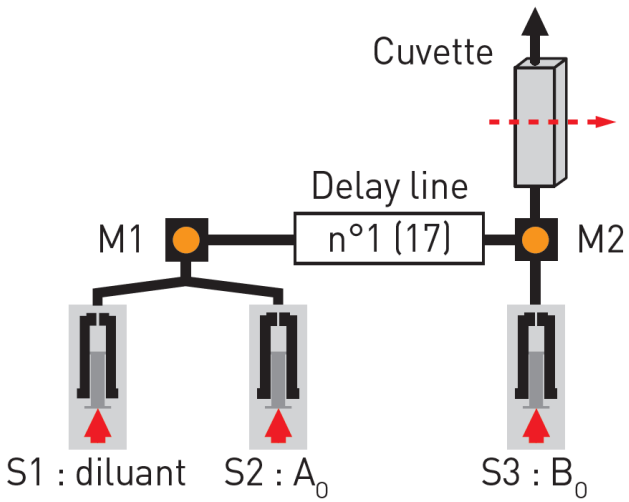

Figure 4.11 A schematic representation of the mixing of QDs with analytes in kinetic stopped flow [20]

A standard model Bio-Logic stopped-flow consists of SFM-3000 S01/N with MPS-70, and MOS-250 spectrometer. SFM is designed for the concentration of An at each shot while

keeping B unchanged. The total numbers of syringes are 3 in SFM, a schematic representation of kinetics equipment used in this work is shown in Figure 4.11. S1 and S2 are the first mixers are used to set the concentration of A by mixing A with diluent. Then A is mixed with B in the M2 and the reaction is monitor through spectrophotometer. The dead time is same for each concentration and every individual step. MOS-250 is single grating manual monochromatic spectrometer with Xe (Hg) or Xe high-intensity light source is used for excitation. The MOS is connected to the stopped-flow cuvette through optical fiber cable. The temperature for each experiment was kept constant by circulating water from a constant temperature 26C° ±0.1 C° water bath. The fluorescence signal was recorded by MPS-70.

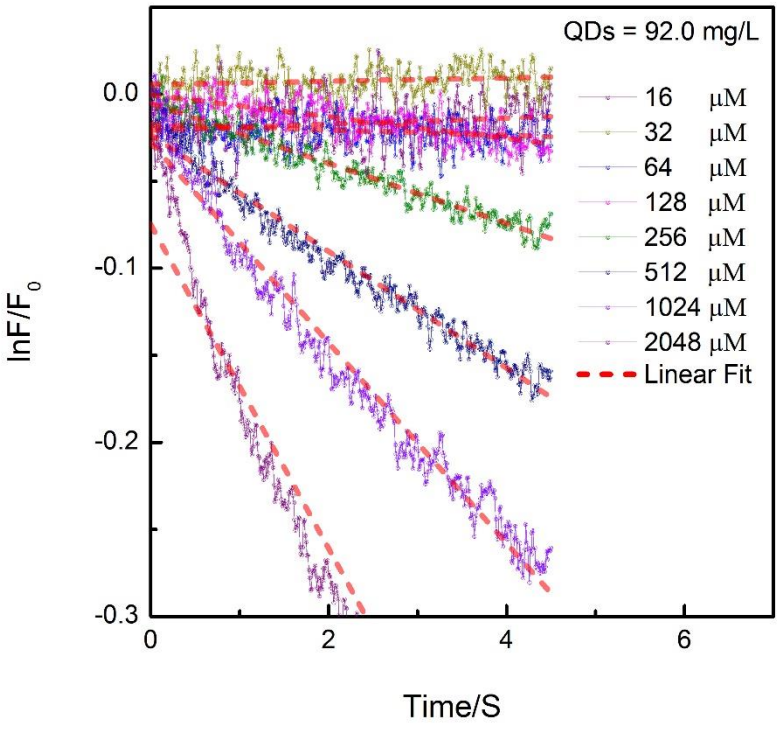

Figure 4.12 Pseudo first order kinetics of GHS-capped QDs fluorescence induced by 16, 32, 2074 µM of H_2O_2 using the kinetic stopped flow.

H_2O_2 were measured at the range of 80 to 2540 µM. H_2O_2 standard solution was used for all analysis, the amount of total volume for analysis was kept constant (700 µL) for each measurement. The change in fluorescence intensity with respect to time is fitted according to pseudo first order equation (Figure 4.12). The rate constants for each concentration of H_2O_2

and glucose were evaluated from the slope of $\ln F/F_0$ versus time plot. The rates constant evaluated for H_2O_2 for 16 to 2018 µM of H_2O_2 concentrations is shown in Table 4.4 below.

$[H_2O_2]$/µM	16	32	64	128	256	512	1024	2018
***k* CPS-S^{-1}**	0.0005	0.00052	0.0014	0.005	0.018	0.0375	0.0673	0.12

Table 4.4 The pseudo first order rate constant induced H_2O_2 in micro molar range.

The calibration yield of H_2O_2 concentration versus the rates constants was linear, it is confirming that the overall reaction is pseudo first order. The linear range of measurement was from 32 to 2018 µM with the slope of 6E-05 CPS-S^{-1}. The detection limit of 14.9 µM was achieve, which was calculated from the standard deviation of the blank, slope and intercept.

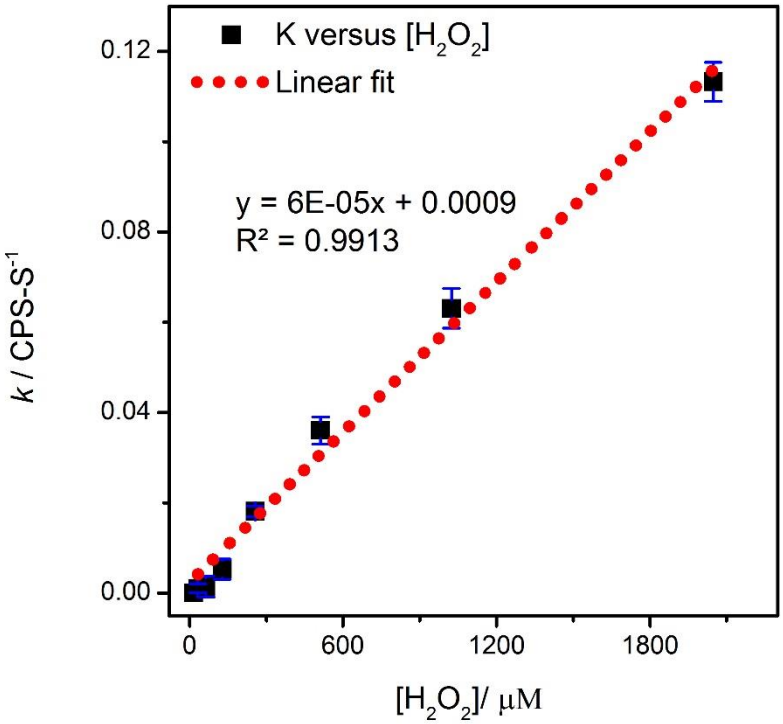

Figure 4.13 A calibration plot of Initial rates constant (3 Sec) versus 16, 32, 64, 128, 256, 512, 1024, 2074 µM H_2O_2.

Calibration	[QD]/mg/mL	Linear range/µM	Detection Limit/µM
1 Figure (4.3)	6.3	25 – 200	17.60
2 Figure (4.6)	62.0	497 - 1990	480
3 Figure (4.8)	6.2	24.9 – 398.4	12.5
4 Figure (4.10)	6.2	0.37 – 13	0.2
5 Figure (4.13)	92.0	16 – 1024	14.9

Table 4.5 The linear range and detection limits obtained from different calibrations using QDs concentration accordingly to pseudo first order kinetic model conditions.

The experimental results concluded in Table 4.5 shows that kinetic model for analysis is an effective tool for the determination of hydrogen peroxide at different ranges. The QDs concentrations used for the analysis of hydrogen peroxide at different level is mention above. It was clear that the concentration ratio of analysts and QDs were important to peruse the pseudo first order kinetic model, hence measuring the high H_2O_2 concentration need a high QDs concentrations i.e. 62 and 92 mg/mL was used to measure the H_2O_2 concentration at mill molar range and 6.2 mg/mL of QDs were utilized for the low concentration of H_2O_2 (0.37 to 400 µM). We assume that kinetic model is competitive and sensitive enough to analyzed H_2O_2 with low concentrations i.e. 320 nM (detection Limit of low H_2O_2 measurement). The results yield from different experiments for H_2O_2 measurement lead us to use the same setup for the measurement of glucose and cholesterol.

4.3.4 Measurements of glucose

On the successive completion of H_2O_2 analysis using the kinetic model, we applied the kinetic model for the measurement of glucose at saliva glucose range. The concentration of glucose in human saliva is reported to be 70 + 10 µM, hence the target range selected was 10 to 200 µM. The usual glucose fluorescent sensor has a limitation of saturation in case of using low concentration of fluorophore or measurement before the completion of reactions. The data showed in Figure 4.1 for H_2O_2 indicate that 24 to 200 µM of H_2O_2 reaction with QDs of 6.3 mg/mL continue tell 6 minutes. The measurement of glucose is based on enzymes catalyzed reaction that produce H_2O_2 hence the amount of glucose oxidized produced equal amount of

H_2O_2 that change the reaction rates. The reaction rates of H_2O_2 produced during the GOx catalyzed reaction with QDs and H_2O_2 with QDs was expected to be different. Therefore the kinetic analysis using the initial rates (within the first half-life) is an affective parameter for the determination of glucose and cholesterol.

The kinetic of QDs fluorescence was initiated by the addition of 10 µL of glucose trace of in 1 ml of QDs stock solutions (containing 6.2 mg/mL of QDs and 6.75 units/mL of GOx). The reaction rats (slope) produced by the addition of different concentrations of glucose were shown in Figure 4.14. It is shown that the reaction rates of range of glucose concentrations (25 to 200 µM) with constant QDs concentrations (6.3 mg/L) are different. Hence it is shown that the rates were induced by one species which was glucose. The [ln F] versus t plot yield a straight line shows that the data comply the pseudo first order kinetics. The ln plots for each glucose concentrations were linear which are shown in Figure 4.15.

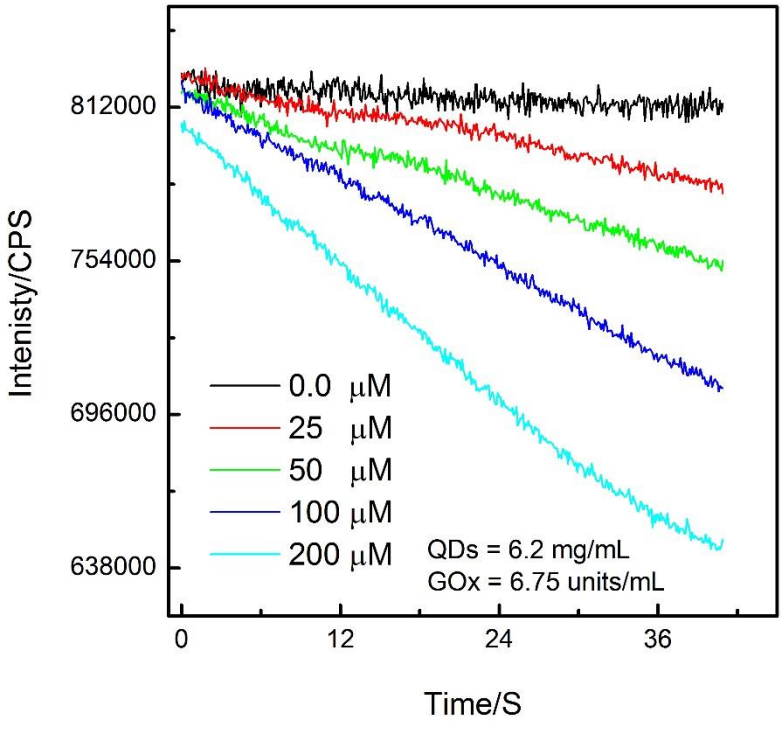

Figure 4.14 The fluorescence decay profile of QDs induced by H_2O_2 produced from the enzymatic oxidation of different glucose concentrations.

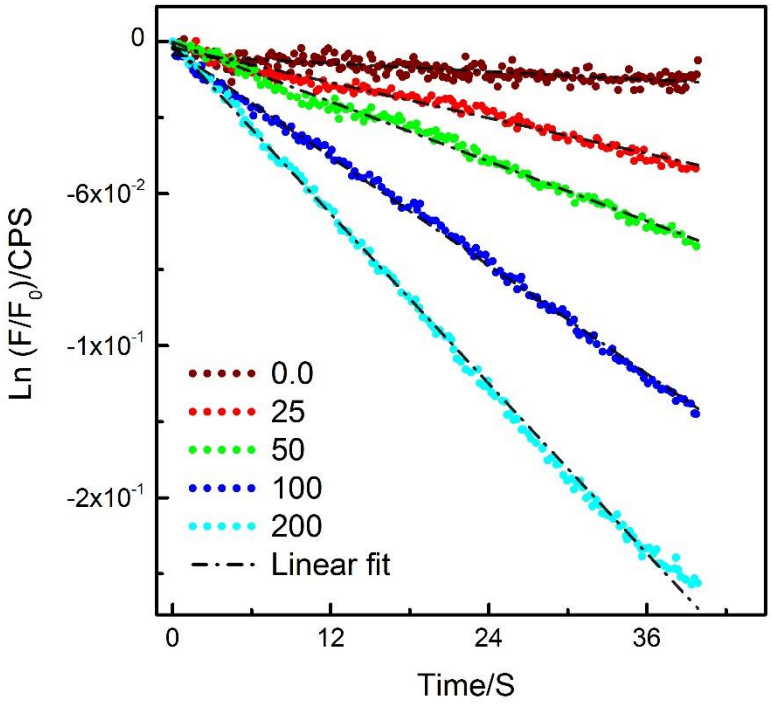

Figure 4.15 the ln plot of the fluorescence decay of QDs induced by H_2O_2 produced from the enzymatic oxidation of different glucose concentrations.

The rate constants *k* was calculated from the ln [F] plot of the QDs fluorescence quenched by the series of glucose concentrations which were presented in Table 4.6. The relationships of the pseudo first order rates constant versus the concentrations of glucose were presented in Figure 4.16 in a calibrations plot. The linear calibration was yield for 25 to 200 µM of glucose concentration. The calibrations confirmed that the change in rates of reaction was linearly related to the glucose concentrations which authenticating the kinetic model established.

[Glucose]/µM	25	50	100	200
***k* CPS-S^{-1}**	0.0005	0.00052	0.0014	0.005

Table 4.6 The pseudo first order rate constant induced glucose in micro molar range.

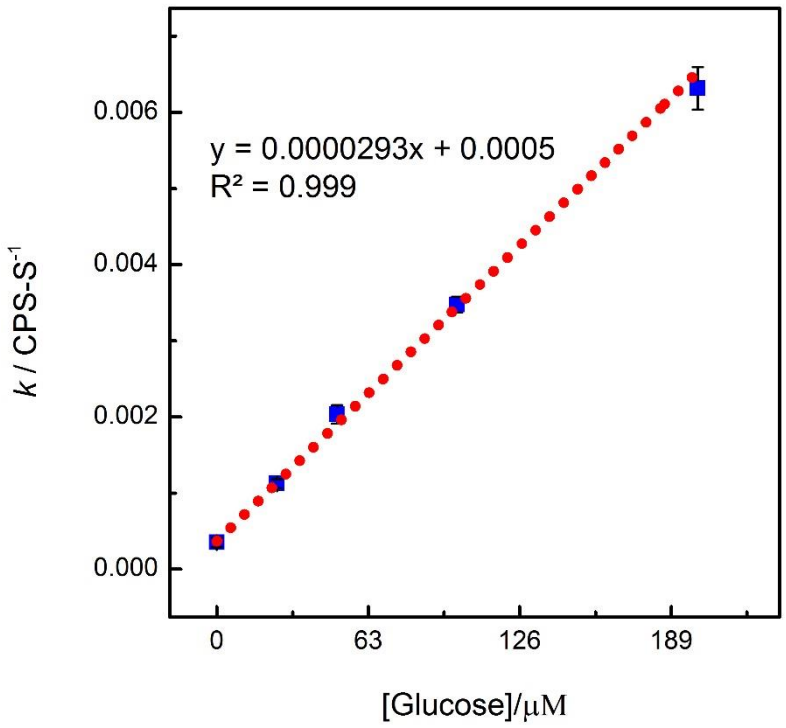

Figure 4.16 A calibration plot of the rates constants and glucose of 25 to 200 μM.

Another calibration was performed with changing the concentration of QDs to 7.4 mg/mL and reducing the concentration of GOx to 2.75 units/mL. The fluorescence degradation profile was observed which were plotted accordingly to the kinetic model in Figure 4.17. The initial pseudo first order rates constant were evaluated from the plot by using the fixed time methods (0 to 5 seconds). The pseudo first order rates constants were linearly related to the amount of glucose used to diminish QDs fluorescence. The calculated rates constants are presented below in Table 4.7.

[Glucose]/μM	8.6	24.5	49.5	99.2	198.4
***k* CPS-S^{-1}**	0.00063	0.001	0.0023	0.00387	0.0064

Table 4.7 The pseudo first order rates constants versus the concentrations of glucose.

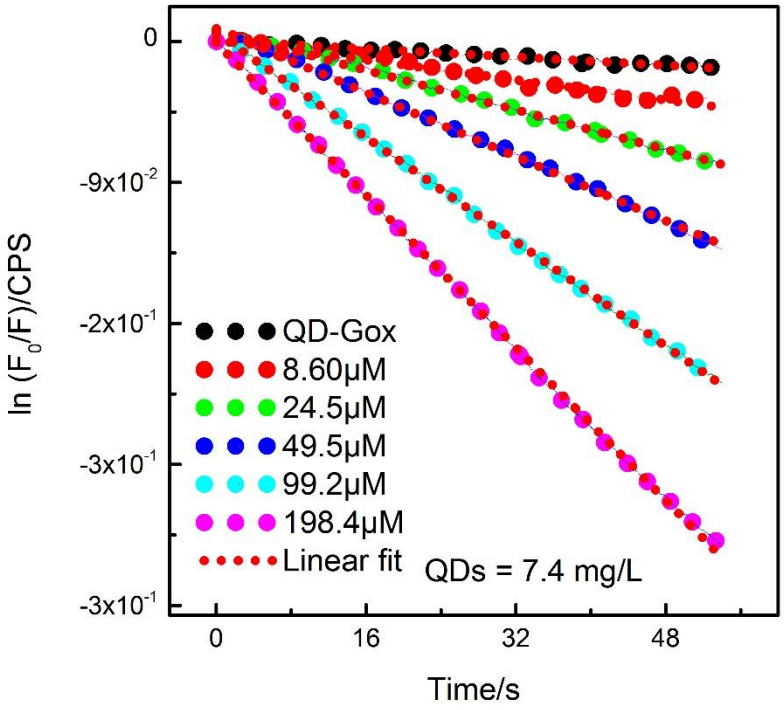

Figure 4.17 The pseudo first order decay of QDs fluorescence versus time for 8.6 to 198.4 μM glucose.

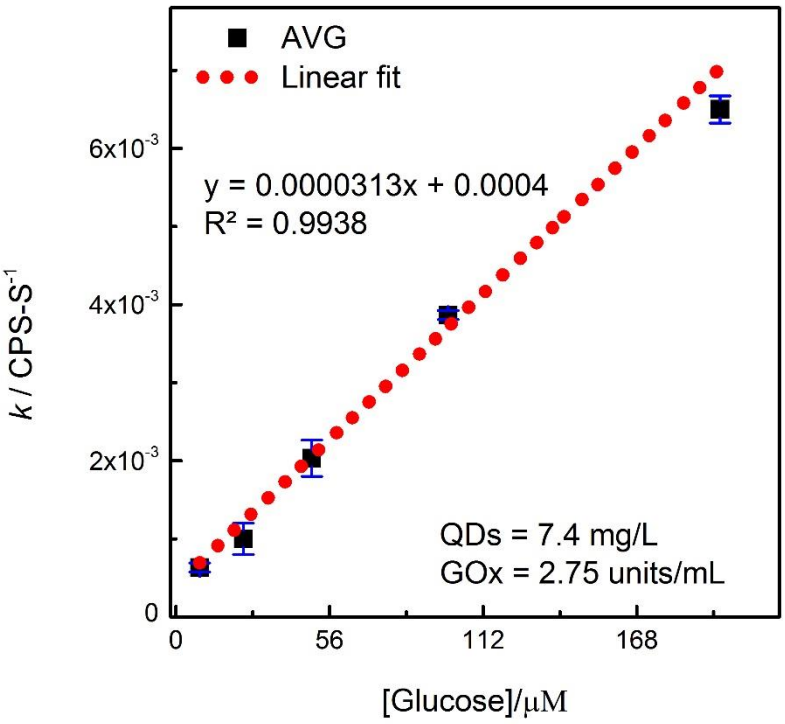

Figure 4.18 The calibration plot of rate constants calculated in figure 4.17 versus the glucose concentrations.

The rates constants were plotted against the concentration of glucose to yield a linear plot, verifying that the kinetics of fluorescence quenching obey pseudo first order rate law. The detection limit calculated 2.0 µM of glucose.

The two calibrations carried out with different QDs and Enzymes concentrations confirm that the reaction is induced by the amount of glucose neither by GOX or QDs. The slope obtained from the first calibration was 0.0000293 and 0.0000313 CPS-S^{-1}/µM of glucose. The change in slope of the calibration was negligible. The detection limit was 9.4 and 2.0 respectively for first and second calibration. The change in QDs concentration has no significant effect on the rate of reactions as well the enzymes concentration has no effect on reaction rats, that is mean that the amount of enzymes and QDs are sufficient to assume a pseudo first order reaction.

Calibration	[QD] (mg/mL)	[GOx] (units/mL)	Linear range (µM)	Slope	Detection limits (µM)
1 Figure 4.16	6.2	6.75	25 to 200	0.0000293	9.4
2 Figure 4.18	7.4	2.75	8 – 198	0.0000313	2.0

Table 4.8 The performance of the glucose response at different QDs and GOx concentrations.

Compared with other glucose measurements methods, this kinetic method of analysis of glucose has the advantages of low detection limit, highly sensitivity, and fast analysis time. Saliva glucose is measurement is a challenge in a scientific community that could overcome lots of obstacles in painful blood sampling and continuous glucose monitoring. The concentration reported for the saliva glucose is from 70 to 100 µM, which is extremely low but using this technique the detection limit is 2.0 µM, which is in the range of saliva glucose.

4.3.5 Measurements of glucose in saliva

Measurement in artificial saliva

The challenges in salivary glucose analysis are the interferences of the saliva constituent with glucose, which affected the measuring signal of glucose. Glucose concentrations in normal subjects are 70 to 130 µM in saliva and 8 to 200 µM in tears[21], the detection limit of glucose in our developed QD-GOx model is 11.3 µM which is lower than the glucose level in tear and saliva.

The interferences study was performed by making glucose standards solutions in artificial saliva [19]. An artificial saliva was prepared containing 5 mM of NaCl, 1 mM of $CaCl_2$, 15 mM of KCl, 1 mM of citric acid, 5 mM of uric acid, 1 mM of ascorbic acid, 0.2 mM of lactate, 1.1 mM of Potassium thiocyanate KSCN, 4 mM of NH_4Cl, NaH_2PO_4 (0.124 g) and urea (1 g) and 10 g l−1 of sodium carboxymethyl cellulose (CMC) in 1 dm3 water [22-24].

NaCl	CaCl	KCl	Citric acid	Uric acid	Ascorbic acid	Lactate	KSCN	NH_4Cl	NaH_2PO_4	Urea	CMS
5 mM	1 mM	15 mM	1 mM	5 mM	1mM	0.2 mM	1.1 mM	4 mM	0.124 g	1 g	10 g

Table 4.9 The formulation of Artificial saliva prepared in phosp hate buffer of buffer.

Figure 4.19 shows the gradual increase in the rate of reaction with an increase in glucose concentrations. Hence the applying the kinetic model for pseudo first order decay of fluorescence the data comply the model. The pseudo first order rates constant was evaluated from the log plot of the fluorescence decay versus time at fix initial time 0 to 5 S. The evaluated initial rates constants are tabulated in Table 4.10 below.

[A. Saliva Glucose]/µM	51.5	102.9	205.9	411.8
***k* CPS-S^{-1}**	0.00086	0.00308	0.00817	0.01637

Table 4.10 Representing the pseudo first orders rates constants and the concentration of glucose in artificial saliva.

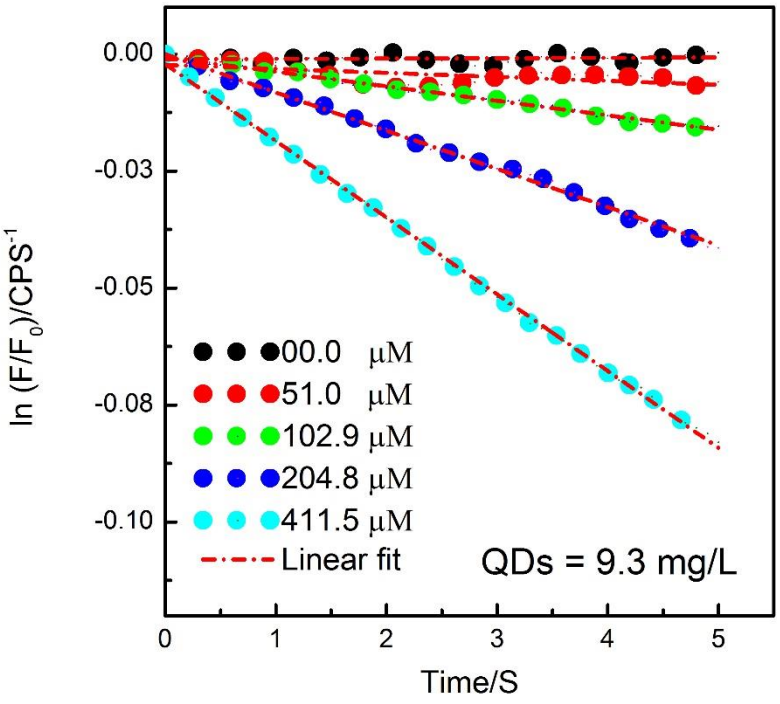

Figure 4.19 Pseudo first order kinetics decay of glutathione-capped QDs fluorescence by the addition of 51.4 to 411.8 µM of glucose in artificial saliva.

The rates constants were plotted against the concentration of glucose yield a linear plot that shows the validity and performance of the sensor in artificial saliva interferences and shows that the pseudo-first order reaction is valid (Figure 4.20). The linear range was 50 to 403 µM. The calibration shown in Figure 4.20 has a slope of 4E-05 CPS-S^{-1} /µM of glucose, which is sensitive enough to be used for glucose analysis.

The calculated detection limit was 26.6 µM while the detection limit calculated for glucose analysis in phosphate buffer was 8.1 µM.

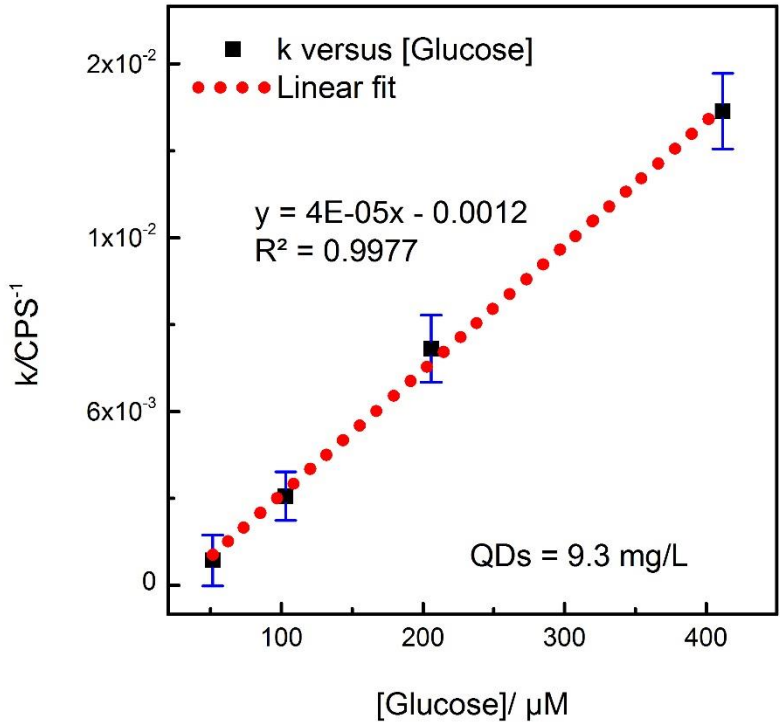

Figure 4.20 Initial rates (15 Sec) of pseudo-order kinetics of glutathione-capped QDs fluorescence quenched by 51.4, 102.9, 205.9, 411.8 µM glucose concentrations. Where N = 3.

Measurement of human saliva

Human saliva contain a number of interfering species, including electrolytes, enzymes and protein and glucose, cholesterol, and triglyceride. The measurement of single anaylate i.e. glucose in human saliva was performed by kinetic model of analysis. Glucose oxidase has specificity to glucose, upon oxidation it produced hydrogen peroxide that was measured in salivary interference. The background signal of human saliva in Figure 4.21 shows, that saliva glucose produced hydrogen peroxide which quenches the QDs fluorescence.

The fluorescence response of saliva glucose and glucose standard was with different reaction rates. The [ln] vs [t] plot was linear as showed in Figure 4.21. The rates constants of non-stimulated human saliva glucose and glucose standards was -0.0002, -0.0003, -0.00055, -0.0008 CPS-S^{-1} respectively. The rate constants of standard glucose were plotted against the glucose standard and a linear calibration was obtained (Figure 4.22). The unknown human

saliva glucose was from the linear equation of glucose standards (y = -7E-06X - 4E-05, R^2 = 1) and was adjusted to the original concertation by dilution factor 4. The estimated glucose level for non-stimulated saliva of a subject A4 was 96.3 µM.

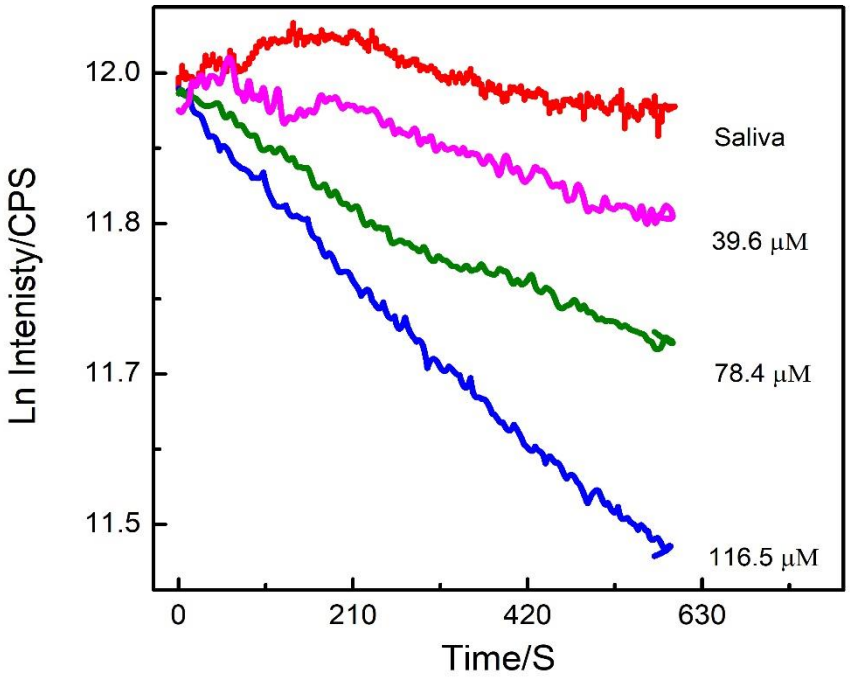

Figure 4.21 Pseudo first order kinetics of GHS-QDs fluorescence quenching by human saliva and human saliva with 39.6, 78.4, 116.5 µM of glucose.

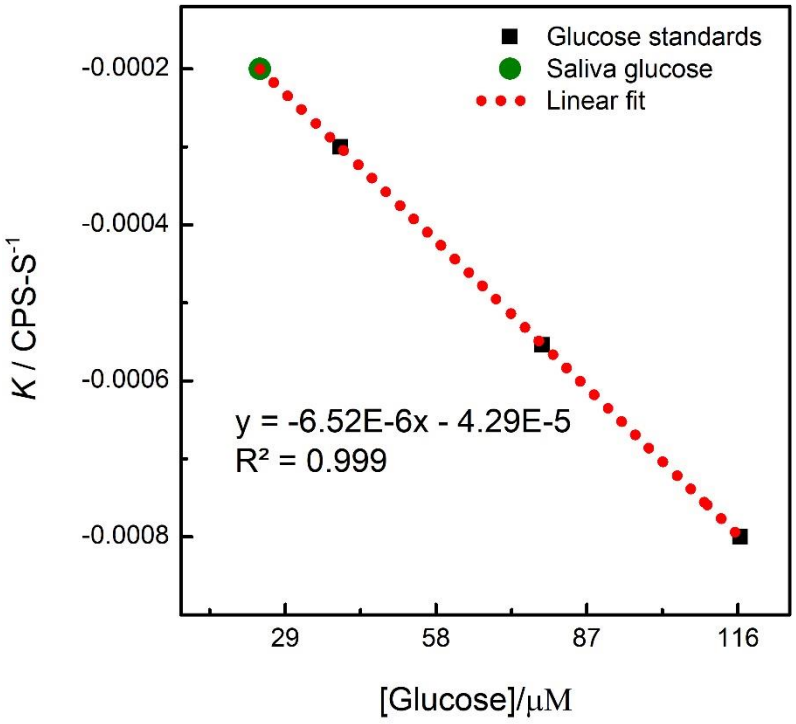

Figure 4.22 A calibration plot of rate constant (*k*) versus glucose standard (black square) for the measurement of unknown saliva glucose (green circle).

4.3.6 Measurements of glucose by kinetic stopped-flow

The kinetic model for glucose analysis was confirmed and validate via bio kinetic stopped flow. The bio kinetic is an instrument specialized for the reaction kinetic measurements. The details operations and working principles was shows in Figure optical properties of materials 4.11. The details kinetic profile was investigated with a wide range glucose and constant QDs concentration (92 mg/mL).

The average (N =4) raw data was analyzed accordingly to the kinetic model shown in Figure 4.23. The log plots of the fluorescence quenched versus time were linear. The rates constants were evaluated for 80 to 2560 μM of glucose which were tabulated in Table 4.11 below.

[Glucose]/μM	80	160	640	1280	2560
***k* CPS-S^{-1}**	0.00098	0.0016	0.003	0.006	0.0133

Table 4.11 the pseudo order rates constant produced by glucose concentration using Kinetic stopped flow.

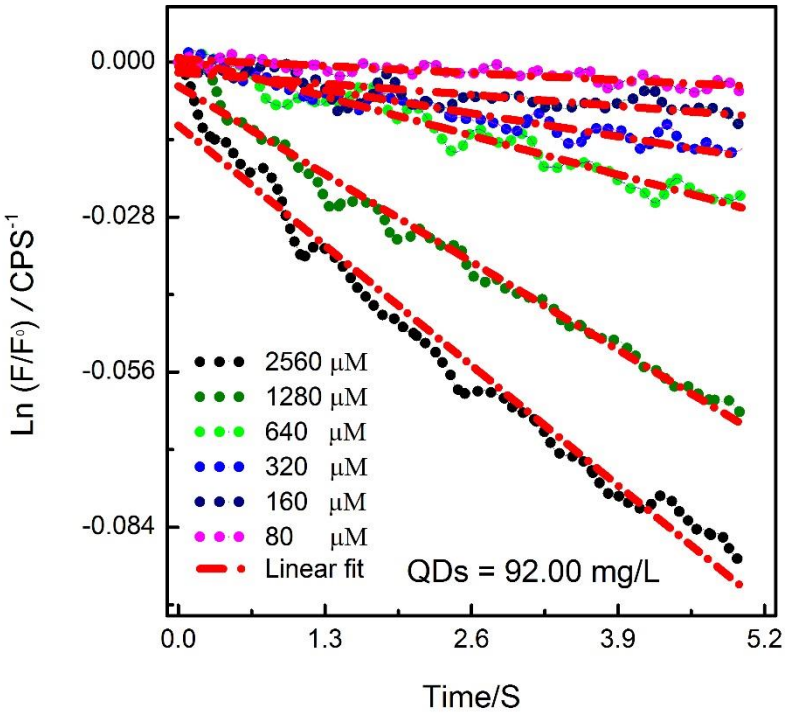

Figure 4.23 the log plot of the QDs fluorescence quenched versus time by the addition of various concentration of glucose.

A calibration plot of glucose concentrations versus the rates constants was linear shown in Figure 4.24. The initial rates constants for glucose and hydrogen peroxide was evaluated by fixed time methods (0 to 3 seconds for hydrogen peroxide and 0 to 5 seconds for glucose). The calibration plot of glucose and hydrogen peroxide was compared shows that the linear range of H_2O_2 detection was 16 to 2018 while for glucose it was 80 to 2560 µM.

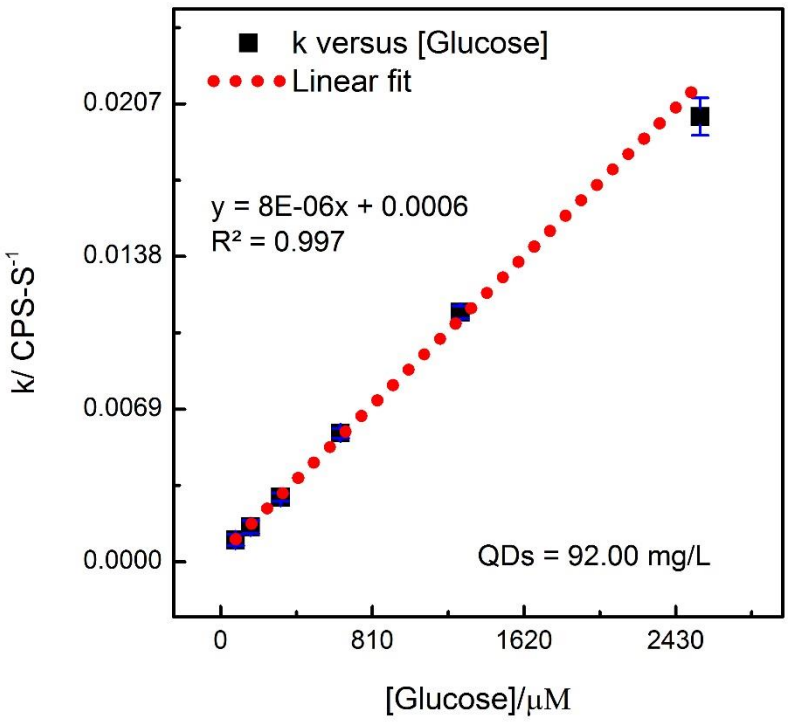

Figure 4.24 Calibration Plot of 80 µM to 2580 µM range of Glucose versus the rates constants, where N= 4.

4.3.7 Measurements of cholesterol by kinetic method

The kinetic model established for H_2O_2, glucose. The experimental conditions were used for the cholesterol determination by reaction kinetics of QDs fluorescence quenching by the various concentration of cholesterol. The concentration range of cholesterol was 17.4 to 136.8 µM and the QD concentration was 6.00 mg/L. The ChOx concentration in QDs solution was 0.4 units/mL.

The obtained results are shown in Figure 4.25. Each concentration of cholesterol induced the kinetic of fluorescence quenched were repeated thrice. The Raw data were plotted according to the kinetic model established for H_2O_2, which is presented in Figure 4.26. The linearity of the log plot of fluorescence quenched shows that the kinetic model was valid for cholesterol measurements. Furthermore the rates constant produced by 17 to 136 µM of cholesterol were evaluated from the data shown in Figure 4.26 using fixed time (0 to 5 S) initial rates methods and tabulated in below Table 4.12.

[Cholesterol]/µM	17.2	34.4	68.97	136.6
***k* CPS-S^{-1}**	0.0013	0.00263	0.00448	0.0068

Table 4.12 The pseudo first order rates constants produced by respective cholesterol concentrations.

A linear plot was yield when pseudo first order rates constants were plotted against the cholesterol concentrations. A linear range for the quantification of cholesterol was 17 to 137 µM. The slope of the calibration plot was 0.0000452 CPS-S^{-1}/µM of cholesterol with correlation coefficient of 0.976. The detection limit was calculated from the linear range of the calibration plot, which was 3.46 µM.

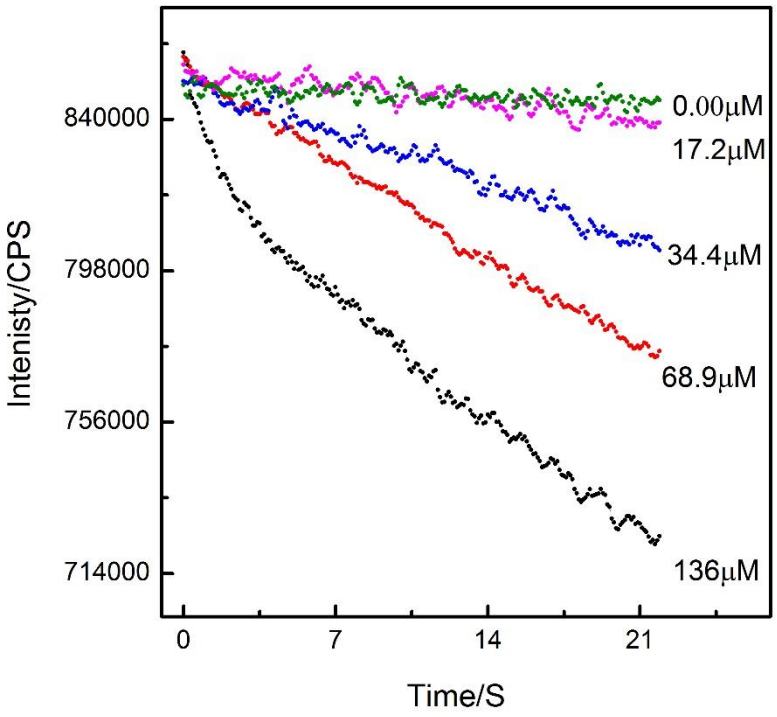

Figure 4.25 The kinetics of fluorescence quenched by 17.2 to 136 µM of cholesterol oxidase concentrations.

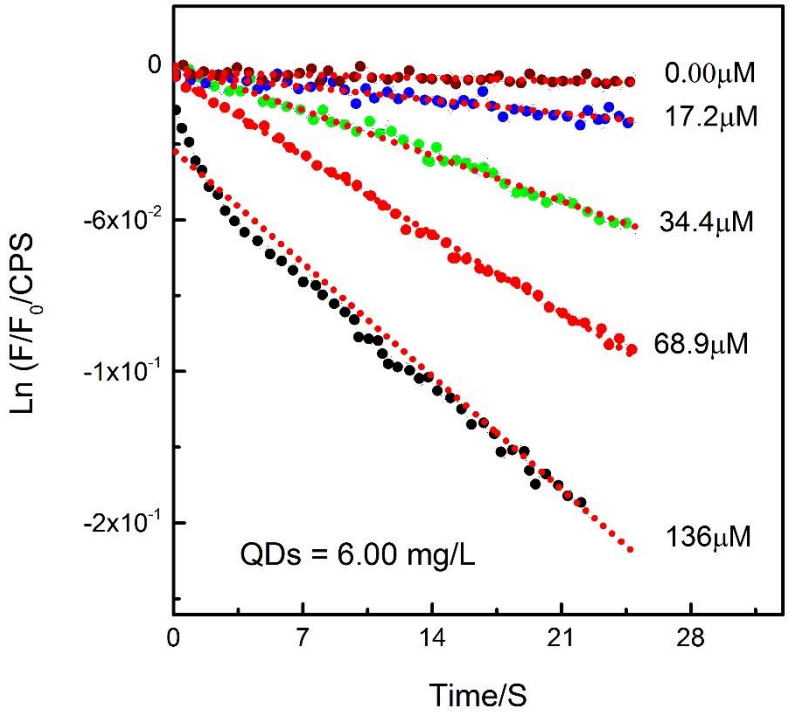

Figure 4.26 The pseudo first order kinetics of QDs fluorescence quenched by the addition of 17.2 to 136 μM of cholesterol in QDs-ChOx solutions.

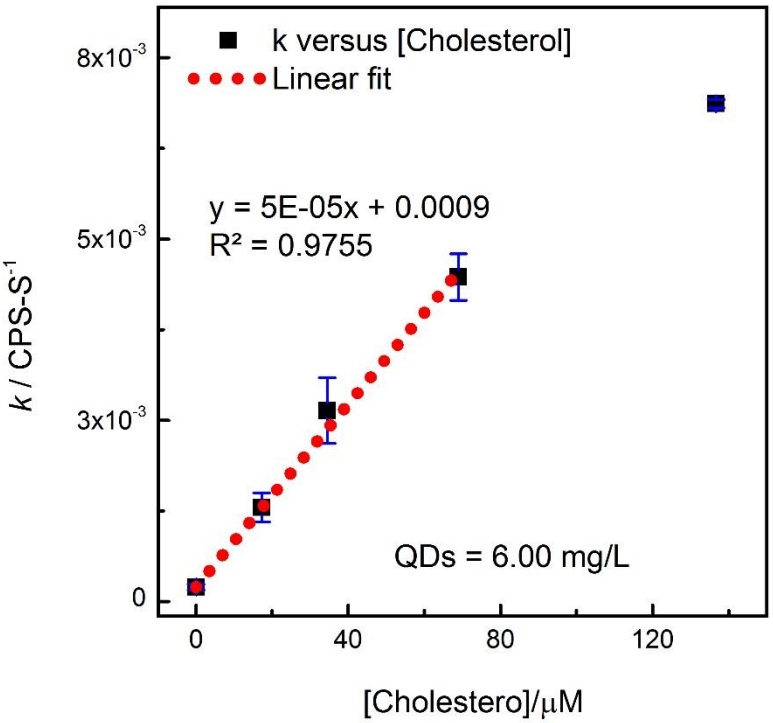

Figure 4.27 A calibration plot of initial rates constants produced by 17.4, 34.4, 68.9, 136.7 μM cholesterol concentrations. Where N = 3.

The comparison of H_2O_2, glucose, and cholesterol measurement by rates constant method were presented in table 4.13. The slope of H_2O_2 calibrations was higher than glucose and cholesterol. The detection limit for H_2O_2 was 0.2 µM which indicating that the rate constant method is highly sensitive and can be effectively used. The detection limit and the range of detection for glucose was 2.0 and 8 to 200 µM. The range of glucose measurement covers the salivary glucose, which is 75 µM.

The stopped flow methods verify the rate constant method of analysis and the detection limit for H_2O_2 and glucose was 14.9 to and 75.6 µM. The linear range was 32 to 2048 (slope of 0.00006) and 80 to 2560 (slope of 0.00001) respectively for hydrogen peroxide and glucose. The change of slope H_2O_2 and glucose calibration using stop flow indicating that the reaction between QDs and H_2O_2 is faster than glucose which oxidized to H_2O_2 and then react with QDs.

The range of cholesterol measured (17 to 136 µM) by rate constant methods were comparable to H_2O_2 and glucose. The slope of cholesterol calibration was 0.00005, which was higher than glucose calibration in phosphate buffer i.e 0.00003.

Analyte	**Instrument**	**Sensetivity/CPS-S^{-1}-µM^{-1}**	**R^2**	**Linear Range/µM**	**Detection Limit/ µM**
H_2O_2	FluoroMax	0.00010	0.9851	0.37 - 396	0.2
	Stopped flow	0.00006	0.9912	32 - 2048	14.9
Glucose	FluoroMax	0.00003	0.9908	8 - 200	2.0
	Stopped flow	0.00001	0.9968	80 - 2560	75.6
Cholesterol	FluoroMax	0.00005	0.9755	17.2 - 136.7	3.46

Table 4.13 Summary of the kinetic methods of analysis for H2O2, glucose, and cholesterol with different detection techniques.

Our methods based using rates constant for the analysis has valued for fast analysis time, greater sensitivity, and accuracy. The obtained results from the rates constant methods of analysis were compared with end point equilibrium methods. The results obtained from equilibrium methods in chapter 3 and this chapter was tabulated in Table below. The detection

limit for H_2O_2 measure using the kinetic method was 0.32 µM while it was 8.1 using equilibrium method. The glucose results were comparable to the equilibrium method the detection limit using end point and kinetic methods was 20 and 8.1 µM respectively. The range of cholesterol measurement by end point and kinetic method was different. The linear range by using kinetic method was 17 to 136 µM while it was 1 to 45 µM for equilibrium method.

Analyte	**Method**	**Linear range/µM**	**Detection limit/µM**	**Analysis time**
H_2O_2	Equilibrium	4 to 237	0.4	10 mins
	Kinetic	0.37 to 396	0.2	0-3 Sec
Glucose	Equilibrium	33 to 300	8.2	10 mins
	Kinetic	8 to 200	2.0	0-5 Sec
Cholesterol	Equilibrium	2.5 to 45	1.5	10 mins
	Kinetic	17- 136	3.46	0-20 Sec

Table 4.14 Summary of the kinetic methods of analysis for H2O2, glucose and cholesterol with different detection techniques.

4.4 Conclusion

In summary we concluded that the kinetic methods of analysis are feasible for the detection of H_2O_2, glucose and cholesterol by QDs as an optical transducer. The methods have high accuracy, repeatability, reproducibility as well the analysis results are comparable with the results obtained from the equilibrium method. The kinetic methods of analysis is fast, easy, simple and cheap, the analysis need low amount of sample usually in microliter.

4.5 References

(1) Pardue, H. L. A comprehensive classification of kinetic methods of analysis used in clinical chemistry. *Clinical chemistry* **1977,** *23* (12), 2189.

(2) Radić, N.; Kukoc-Modun, L. *Kinetic Methods of Analysis with Potentiometric and Spectrophotometric Detectors-Our Laboratory Experiences*; INTECH Open Access Publisher, 2012.

(3) Pardue, H. L. Unified view of kinetic-based analytical methods with emphasis on ruggedness. A review. *Analyst* **1996,** *121* (4), 385.

(4) Zheng, X.; Bi, C.; Li, Z.; Podariu, M.; Hage, D. S. Analytical methods for kinetic studies of biological interactions: a review. *Journal of pharmaceutical and biomedical analysis* **2015,** *113*, 163.

(5) Foley, D. A.; Wang, J.; Maranzano, B.; Zell, M. T.; Marquez, B. L.; Xiang, Y.; Reid, G. L. Online NMR and HPLC as a reaction monitoring platform for pharmaceutical process development. *Analytical chemistry* **2013,** *85* (19), 8928.

(6) Christianson, M. D.; Tan, E. H.; Landis, C. R. Stopped-Flow NMR: Determining the Kinetics of [rac-(C2H4 (1-indenyl) 2) ZrMe][MeB (C6F5) 3]-Catalyzed Polymerization of 1-Hexene by Direct Observation. *Journal of the American Chemical Society* **2010,** *132* (33), 11461.

(7) Srisa-Art, M.; Dyson, E. C.; deMello, A. J.; Edel, J. B. Monitoring of real-time streptavidin− biotin binding kinetics using droplet microfluidics. *Analytical chemistry* **2008,** *80* (18), 7063.

(8) Han, Z.; Li, W.; Huang, Y.; Zheng, B. Measuring rapid enzymatic kinetics by electrochemical method in droplet-based microfluidic devices with pneumatic valves. *Analytical chemistry* **2009,** *81* (14), 5840.

(9) Trojanowicz, M.; Kołacińska, K. Recent advances in flow injection analysis. *Analyst* **2016,** *141* (7), 2085.

(10) Nacapricha, D.; Sastranurak, P.; Mantim, T.; Amornthammarong, N.; Uraisin, K.; Boonpanaid, C.; Chuyprasartwattana, C.; Wilairat, P. Cross injection analysis: Concept and operation for simultaneous injection of sample and reagents in flow analysis. *Talanta* **2013,** *110*, 89.

(11) Crouch, S. R.; Scheeline, A.; Kirkor, E. S. Kinetic determinations and some kinetic aspects of analytical chemistry. *Analytical chemistry* **2000,** *72* (12), 53.

(12) Prigodich, R. V. A Stopped-Flow Kinetics Experiment for the Physical Chemistry Laboratory Using Noncorrosive Reagents. *Journal of Chemical Education* **2014,** *91* (12), 2200.

(13) Wang, R.-Y.; Ji, M.-N.; Wang, R.; Shi, J. Stopped-flow kinetic fluorimetric studies of the interaction of Ru (II) complex with DNA and its analytical application. *Spectrochimica Acta Part A: Molecular and Biomolecular Spectroscopy* **2008,** *71* (3), 1042.

(14) Wang, R.-Y.; Gao, X.; Lu, Y.-T. A surfactant enhanced stopped-flow kinetic fluorimetric method for the determination of trace DNA. *Analytica chimica acta* **2005,** *538* (1), 151.

(15) Oguz, O.; Inal, B. B.; Emre, T.; Ozcan, O.; Altunoglu, E.; Oguz, G.; Topkaya, C.; Guvenen, G. Is automated kinetic measurement superior to end-point for advanced oxidation protein product? *Clinical Laboratory* **2014,** *60* (6), 925.

(16) Selmeci, L.; Seres, L.; Soós, P.; Székely, M.; Acsády, G. Kinetic assay for the determination of the oxidative stress biomarker, advanced oxidation protein products (AOPP) in the human blood plasma. *Acta Physiologica Hungarica* **2008,** *95* (2), 209.

(17) Leroux, A. E.; Haanstra, J. R.; Bakker, B. M.; Krauth-Siegel, R. L. Dissecting the catalytic mechanism of trypanosoma brucei trypanothione synthetase by kinetic analysis and computational modeling. *Journal of Biological Chemistry* **2013,** *288* (33), 23751.

(18) Yuan, J.; Guo, W.; Yin, J.; Wang, E. Glutathione-capped CdTe quantum dots for the sensitive detection of glucose. *Talanta* **2009,** *77* (5), 1858.

(19) Claver, J. B.; Mirón, M. V.; Capitán-Vallvey, L. Disposable electrochemiluminescent biosensor for lactate determination in saliva. *Analyst* **2009,** *134* (7), 1423.

(20) Biologic; 1 ed.; Biologic: http:www.bio-logic.info, 2016; Vol. 2016.

(21) Liu, C.; Sheng, Y.; Sun, Y.; Feng, J.; Wang, S.; Zhang, J.; Xu, J.; Jiang, D. A glucose oxidase-coupled DNAzyme sensor for glucose detection in tears and saliva. *Biosens Bioelectron* **2015,** *70* (0), 455.

(22) Brozek, R.; Rogalewicz, R.; Koczorowski, R.; Voelkel, A. The influence of denture cleansers on the release of organic compounds from soft lining materials. *Journal of Environmental Monitoring* **2008,** *10* (6), 770.

(23) Gal, J.-Y.; Fovet, Y.; Adib-Yadzi, M. About a synthetic saliva for in vitro studies. *Talanta* **2001,** *53* (6), 1103.

(24) Oh, D. J.; Lee, J. Y.; Kim, Y. K.; Kho, H. S. Effects of carboxymethylcellulose (CMC)-based artificial saliva in patients with xerostomia. *International Journal of Oral and Maxillofacial Surgery* **2008,** *37* (11), 1027.

Chapter 5. Development of Optical Solid-sate sensor Based on Fluorescent QDs

5.1 Introduction

Based on the results obtained from liquid phase measurements this chapter describes the attempt to fabricate and characterized solid state sensors based on QDs and a polymer composite. Nafion and PVA were used as matrixes to encapsulate QDs and fabricate solid state sensor. Solid state sensors are practical and implementable in portable devices. The portable glucose sensors are easy to use and can improve health care of the patient suffering from diabetes and heart disease [1]. The advancement in fluorescence and optical sensing technology have had minimized the size of the instrumentation[2]. Tremendous developments have been done recently to develop, solid-state devices and sensors with a high degree of stability, sensitivity, and selectivity, for a blood or urine glucose measurement[3] but the glucose sensor that detect glucose in saliva is not available yet.

Various strategies were adopted to fabricate solid state fluorescence-based glucose sensors. Strategies included, fabrication techniques, materials development, and substrates selection. To date the formulations of most solid state glucose sensors were composed of fluorescence active materials, polymer composites[4], sol–gel[5], silica gel[6], gelatin membrane[7], Polyacrylamide gel[8], cellulose paper[9], polyacrylamide[10], silicone membrane[11] polystyrene[12] ormosil [13] hydrogel [14] hypan [15] and montmorillonite clay [16]. The development of a solid state sensor with required sensitivity and selectivity to precisely measure the glucose level in saliva and tears is challenging. To overcome all these issues, it was useful to look back at the materials, and fabrication techniques for the fabrication of solid state sensor.

Fabrication materials	**Rang/mM**	**Ref**
Hexokinase enzymes entrapped in sol gel,	1-120	[6]
Glucose oxidase immobilized on polyacrylamide with fluorescence	2-11	[17]

Decacyclene in silicone membrane with glucose oxidase immobilization in nylone membrane	5 -8	[11]
GOx entrapped in a gelatin membrane;	2.5-20	[10]
porphyrins and their metal derivatives	---	[18]
Swim bladder membrane with glucose oxidase immobilization.	3 – 10	[19]
immobilized glucose oxidase on bamboo inner shell membrane	0.058-0.5	[20]
Glucose oxidase immobilization with sol–gels and (3-glycidoxypropyl-trimethoxysilane (GPTMS) as a fluorophore in micro-plates	0.2 - 2	[21]
silica sol-gel encapsulated glucose oxidase	0.1 - 5	[13]
Quantum dots and glucose oxidase nanocomposite film	2 - 18	[22]
Glucose Oxidase Modified by PVA-Pyrene	0.25 to 3.0	[23]

Table. 5.1 Fluorescence based solid state glucose sensors and glucose measuring range of the sensors.

In this work, we used an emerging fluorescence nanomaterials within polymer matrix for solid optical film fabrications. QDs reactivity with chemicals species is intrinsic. QDs are not passive to a chemicals moieties, they might react with the QDs which lead to denaturing the QDs-caps linkage that causes etching of capping agents or charge transfer occur which traps and alter the fluorescence signal[24].

The stability of QDs can be achieved by the appropriate capping agents [25], core/shell structure[26], encapsulation of nanocrystals in microcrystals[27] encapsulation in polymeric matrix[28] and silica-polymer double encapsulation[29]. The encapsulation of QDs in ionic macro crystals and polymeric matrix is simple and of low-cost [30-33]. The prolonged stability of QDs fluorescence in composites polymer materials attends a great interest in optoelectronic devices, and sensing applications[34,35].

5.1.1 Strategy for QDs Entrapment in a polymers matrix

The area of QD-polymer matrix is increasing due to the unique feature of composite polymer materials with QDs. The summarized study on functionalization of QDs with polymers can be grouped into chemical entrapment and physical entrapment. The chemical entrapment is further

grouped into direct functionalization during the synthesis of QDs[36] and functionalization of quantum dots after synthesis by functionalizing of the surface capping agent. The polymer could be used as a capping agents that stabilize QD during synthesis with desired size and size distributions[37-42]. The strategy of direct functionalization of QDs or the surface ligand of QD with polymers has been used by many researchers and highly luminescent polymer-QDs composites were obtained and applied in various areas of research. QDs were also directly modified by polymers or macromolecules were grown on the surface of QDs[43-45].

Second classes of QDs-Polymer entrapments were made by simple mixing of QDs with selected polymer or polymers combinations. This physical entrapments were done after the synthesis of QDs and polymer separately. The entrapments of QDs with polymers were completed using layer by layer assembly or mixing appropriate polymers and QDs formulations[47-50]. In this study, we developed a simple mixing techniques by using appropriate amount of QDs with a suitable polymer compositions. The physical entrapment approach has the advantages of reliability, reproducibility, and uniform nanocrystals distribution with high quantum yield.

5.1.2 Nafion-PVA membrane

Nafion structure consists of polytetrafluoroethylene, shown in Figure 5.1. Nafion has unique membrane forming properties, which have been used for many applications. In nafion membrane cation freely move along the polymeric network but it does not allowed to conduct electrons[52,53]. This nature of nafion is suitable for fabricating QDs-nafion-membrane s[54,55]. The main features of nafion membrane are the chemical and thermal stability, resist against any chemical attacks[56].

The membrane structure of nafion with PVA and QDs was reported to be highly permeable to water molecules, which could facilitate the activation of dry membrane with water or buffer. PVA has outstanding adhesive membrane forming properties. PVA films are elastic with high strengthens and protect the embedded materials from the outer environment. Additionally, PVA is also thermally and mechanical stable at a wide range of temperature [57,58].

The composite polymer membrane of nafion and PVA has been used for many applications. Nafion/PVA hybrid structure is used to enhance the membrane properties for respective applications[59-62]. PVA-nafion could form suitable, biocompatible composite with QDs for biosensing application. The details study on characterization and the performance of sensors were performed in this work. The solid state sensor was optimized by controlling thickness of the membrane, oxidase, and QDs concentration.

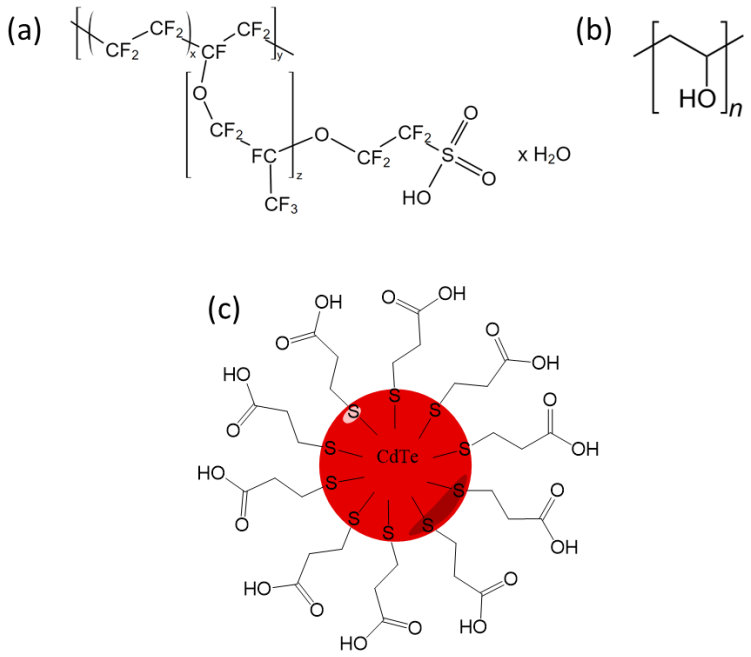

Figure 5.1. The chemical structure of nafion and polyvinyl alcohol (PVA) and CdTe QDs.

5.2. Experimental

5.2.1 Materials and instruments

MPA and GHS capped CdTe quantum dots were synthesized (referred to chapter 2). D-glucose was purchased from Aladdin Industrial Corporation, China. Nafion, Poly (vinyl alcohol) 87 to 90 % hydrolyzed, glucose oxidase (GOx) (17300 units/G) was from Sigma Aldrich, USA. Sodium hydroxide, dipotassium hydrogen phosphate, dihydrogen potassium phosphate, citric acid trisodium salt dihydrate 99 %, sodium chloride 99.5 %, and H_2O_2 35 % in water, were obtained from Across Organic, USA. PVA with an average MW of 50000 was used with nafion

(tetrafluoroethylene-perfl uoro-3, 6-dioxa-4-methyl-7-octene-sulfonic acid copolymer). The ultra-purified water of milli-Q system (Millipore Co., Billerica, MA, USA) was used in all analysis. All the chemicals were of analytical grade.

FluoroMax-4 spectrophotometer (Horiba scientific USA) was used for recording fluorescence spectra; Cary 300 UV-VIS spectrophotometer (Agilent Technology USA) was used for recording UV-Visible spectra. The atomic force microscope (AFM) from Bruker Multimode 8 with nasoscope V controller was used in a tapping mode to the studied surface morphology of glucose sensor. All the measurements were done at ambient environment.

5.2.2 Fabrication techniques

Various fabrication techniques have been used for the developments of various optoelectronic devices. The solution based coating techniques are based on zone coating, dip-coating, drop casting, and zone casting. The drop casting techniques are the one widely used in the fabrication of optoelectronic devices [63]. The major advantage of drop casting methodology is to simplify the fabrication process without the use of any sophisticated instrumentations. The major problems of fabricating the optical membrane are controlling the surface area, and thickness of the film. The surface area coverage and the thickness of the surface could be controlled by optimizing the droplet volume during fabrication[64].

It is quit challenging to optimize the drop casting fabrication method, which including the evaporation time and temperature. These factors subsequently influence the stability of enzymes, QDs, and polymers. Morphology and thickness of the solid state sensors can be improved to achieved high performance sensors by controlling the fabrication process [65,66].

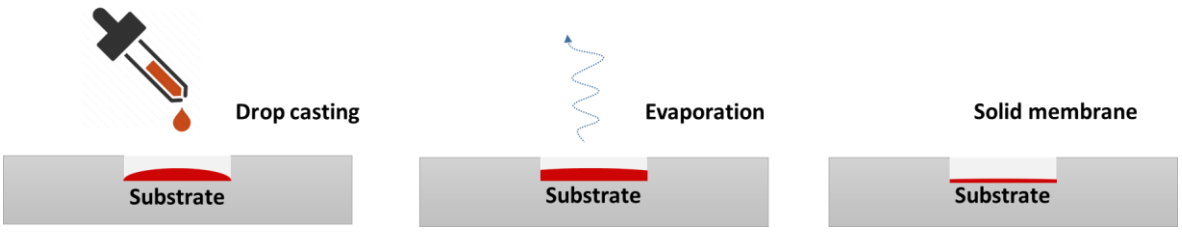

Figure 5.2 The dropt casting techniques used for the fabrication of solid state H_2O_2, glucose and cholesterol sensor.

5.2.3 Fabrications of solid state H_2O_2 sensor

The membranes were fabricated by 1% PVA and 0.05 % nafion and with QDs. 0.5 ml of PVA (1 %) and 0.5 ml of nafion (0.05 %) were mixed in 10 ml bottle and stirrer at room temperature for 15 minutes. The mixing ratio of PVA-nafion was 20:1. 30 µL of QDs (1.78 mg/mL) was added into 1 mL the PVA-nafion solution already made and was stirrer continuously for 5 minutes. The mixture was sonicated for 30 seconds. After mixing and sonication, a uniform nafion-PVA and QDs solution was obtained, which were immediately used to fabricate the sensor. The sensors were fabricated on 96-well plates. 20µL of PVA-nafion-QDs membrane was spiked in 96 well-plates or PET sheet and were dried in open air at room temperature overnight.

5.2.4 H_2O_2 measurement

Two different strategies were used to measure the H_2O_2. The first method series of sensors A1, A2, A3…… was selected and the H_2O_2 standards of 1.6, 16, 32, 64, 128, 256, 512, 1024, 2048, 3200 µM were spiked in each sensor well respectively. The second method was comprised of titration of H_2O_2 standards in a single well with simultaneously monitoring the fluorescence signal after each addition.

Method 1; The H_2O_2 standards of 1.6, 16, 32, 64, 128, 256, 512, 1024, 2048, 3200 µM were prepared from the 20 mM stock solutions. Initially, the sensors were pre-hydrated by 40 µL of buffer and kept it for 2 minutes. The fluorescence spectra of all blank sensors were recorded using the excitation of 400 nm with a slit of 5 nm. The H_2O_2 was measured by adding 10 µL of the standards solutions in the activated sensors. The final concentration of H_2O_2 standards after the addition into activated sensor (already contained 30 µL of buffer) was 0.4, 4, 8, 16, 32, 128, 256, 512, and 800 µM. The fluorescence spectra were recorded immediately after the addition of H_2O_2 standards. All the measurements were done four times and the average data was calculated with standard deviations using excel.

Method 2; The H_2O_2 stock of 640 µM was used for the whole calibration. The sensors were activated by 100 µL of buffer and kept at 25 $^{\circ}$C for 10 minutes. The fluorescence

change during the hydration of a sensor was observed. When the fluorescence signal became stable the measurements was started. Gradually1, 2, 4, 6, 8, 12, 16, 24 µL H_2O_2 stock of (640 µM) was added and after each addition the fluorescence emission at 586 nm with a slit of 5 nm was recorded for 600 seconds. The final concentration of H_2O_2 in activated sensors was 6.2, 12.5, 25.0, 50.1, 75.3, 100.4 µM after the addition of 1, 2, 4, 6, 8, 12, 16, 24 µL H_2O_2 stock of (640 µM). All the measurement was performed thrice and the average and standard deviation of three repeats was calculated. The H_2O_2 measurements were repeated by increasing the sensors activation times from 10 to 30 minutes. The H_2O_2 stock of 2560 µm was used. The fluorescence of sensors was measured before and after the addition of H_2O_2. The H_2O_2 added from 2560 µM stock was 2, 4, 6, 8, 10, 12, 16, 18, and 20 µL. The final concentration was 50.1, 100, 150.6, 200.8, 250.8, 301.2, 351.4 µM. All the measurements were repeated three times and the average and standard deviation was calculated of three repeats.

5.2.5 Real-time monitoring of fluorescence quenching

The reaction kinetics of QDs-membrane fluorescence quenching by H_2O_2 was measured. The sensor was fabricated. The nafion PVA was 1.5 and 0.25 % respectively was used. The QDs concentrations used was 40 µL from the stock solution of 8.2 mg/mL. The fabricated sensor was dried at 60 ^{0}C in the oven. The kinetics of fluorescence quenching was measured by the instantaneous addition of H_2O_2 standard. The sensor was pre-hydrate 1.2 hours before analysis with 120 µL of waters. The sensors were kept at a constant temperature in dark microMax (Horiba spectrometer accessories for well plate). The H_2O_2 standard solutions were 1500, 4900, 7900, and 11200, µM were made from 2 mM H_2O_2 stock solution. The shutter of the fluorimeter was kept on with the addition of H_2O_2 standards. The H_2O_2 standard was spiked into microplate and the fluorescence was immediately recorded at excitation and emission of 420 and 593 nm respectively. The slit width of 2 nm was used for both emission and excitation. The procedure was repeated for each H_2O_2 standard solution. After the addition of stander, the final concentration of H_2O_2 calculated was 25, 80, 130, and 185 µM. The data was further analyzed in excel.

5.2.6 Fabrication of glucose sensor

Preparation of bioactive solution for glucose sensor fabrication

Glucose sensing membrane was fabricated using the same techniques mention in previous section. The mixing ratio of PVA and nafion was changed hence the thickness of membrane was increased. The polymers composite was made of 0.5 ml of nafion (0.2 %) and 0.5 % of PVA (4%). The final concentration of nafion and PVA was 0.1 and nafion was 2 % respectively. The mixture was stirred for 10 minutes at room temperature. Once the polymer solution is completely homogeneous and clear QDs of 40 µL from a stock of 1.87 mg/mL was added. Glucose oxidase stock solution was made by dissolving 2 mg of a solid GOx in 1.5 mL water. Furthermore 50 µL of GOx solution (2 mg/1.5 mL) was added to the QDs and polymer solution. The solution was stirrer at room temperature for 15 minutes followed by sonication for 20 seconds.

Fabrication procedure

The Polystyrene made 96 well plates were used for the fabrication. The plates were washed with milli-Q water followed by sonication in water for one minute. The 96 well plates were dried at 60 $^{\circ}$C in the oven. The polystyrene substrate was kept in ozone cleaner for 2 minutes to make the well surface hydrophilic. The drop-casting methods were used for the fabrication of membrane. The formulation solution (PVA 2 % 0.1 % Nafion) 25 µL was added to each well. The membrane was kept at room temperature for 5 hours. After drying the membrane was observed under an optical microscope and UV lamp. The sensor were stored in the fridge at 4 ^{o}C for further analysis.

5.2.7 Optimization of solid state sensor

The membrane was optimize by using different concentration of glucose oxidase. The sensor was fabricated from 2 % of nafion and 1 % of PVA solutions. The nafion-PVA solution was made of 0.5 ml of nafion (2 %) and 0.5 ml of PVA (1%). The final concentration of nafion and PVA was 1.0 % and 0.5 % respectively. The solution was mixed and stirrer for 10 minutes and 40 µL of QDs solution (1.87 mg/mL) was added. The 1 mL of polymers-QDs solution was

made separately in 10 mL bottles following the above procedure and 50, 40 and 20 µL of GOx (2 mg/mL) was spiked in each bottle respectively. Three solutions consist of equal amount of QDs, PVA and nafion but with 50, 40 and 20 µL of GOx.

The above mention fabrication procedure was used. 25 µL of active solution containing QDs PVA, nafion and GOx were spiked in 96 well plats flowed b drying procedure at 45 ^{o}C for three hours. The fabricated sensor was kept in fridge at 4 ^{o}C before analysis.

5.2.8 Glucose measurement

1. The glucose measurement was performed by using glucose standard solutions of 640, 1250, 2560 µM. Initially, the sensor was activated by 5 mM phosphate buffer of pH 7.4 at 25 ^{o}C for one hour. Aliquots of 1, 2, 4, 6, 8, 12 µL from 640 µM, 4 µL from 1250 µM and 4 from 2560 µM glucose standard solutions were added in the sensor. After each addition of glucose into the activated membrane, the fluorescence was monitor using for 6 minutes. The procedure was repeated thrice and the average of the data was obtained with standard deviation.
2. The membrane fabricated for GOx optimization was used to calibrate 6.2 to 366 µM of glucose hence the optimal glucose oxidase concentration can be evaluated. The glucose standard solution of 320, 640, 1280, 2560, 5120 µM was used for analysis. The membrane was activated by 100 µL phosphate buffer (5 mM) of pH 7.4. The analysis was performed by the addition 2 µL glucose standard into the activated membrane. The final concentration of glucose in the activated membrane after the addition of glucose standard was 6.2, 18.6, 42.7, 90.1, 183.2, and 366 µM. The fluorescence change was monitor continuously for 600 seconds. The excitation and emission used were 400 and 586 nm respectively with a slit width of 5 nm.
3. The performance of glucose sensors (0.25 %, 1.5% Nafion, 50µL of QDs 50 µL of GOx from 1.7mg/ml) was studied. The fabricated sensors were activated by 5 mM phosphate buffer of pH 7.4 for one hour. The calibration methods for all sensors were kept constant. Glucose standards of 500, 800, 1400, 2600, 5000 µM were prepared from a stock of 20 mM glucose. The measurements were performed by adding 1 or 2 µL of standard solution

into the sensor. The final concentration of glucose was 9.8, 25.2, 51.6, 99.8, 190.7, 369.2 µm. The fluorescence change after each addition of glucose was a monitor for 600 seconds. The excitation and emission wavelength used was 400 and 586 nm wavelength respectively with a slit of 5 nm.

5.2.9 Glucose measurement in artificial saliva

An artificial saliva was prepared containing 5 mM of NaCl, 1 mM of $CaCl_2$, 15 mM of KCl, 1 mM of citric acid, 5 mM of uric acid, 1 mM of ascorbic acid, 0.2 mM of lactate, 1.1 mM of Potassium thiocyanate KSCN, 4 mM of NH_4Cl in water [67]. The measurements of artificial saliva glucose were performed on optimized glucose sensing membrane. Glucose standards of 500, 800, 1400, 2600, 5000 µM in artificial saliva was prepared from a stock of 20 mM glucose. The sensor was activated by 5 mM phosphate buffer of pH 7.4 for one hour before calibration. The measurements were performed by adding 1 or 2 µL of standard solution into the sensor. The final concentration of artificial saliva glucose was 9.8, 25.2, 51.6, 99.8, 190.7, 369.2 µm. The fluorescence change after each addition of glucose in artificial saliva was a monitor for 600 seconds. The excitation and emission wavelength used was 400 and 586 nm wavelength respectively with a slit of 5 nm.

5.2.10 Procedure of Human saliva collection

The saliva was collected from five subjects of age 25-34 years. The donor was trained on saliva collection and a donor information sheet for saliva collection was signed by donors.

- There was no intake of any drugs/medicines by the subjects.
- There was no any infective Hepatitis B or Hepatitis C and HIV, musculoskeletal or co-morbid oral disease or recent operation of the donors.
- The individuals were non-smokers with excellent oral health.
- The individual abstained from drinking, oral hygiene procedures, and eating at least 2 h prior to the collection.
- The subjects not to cough up mucus during saliva collection, it was the goal is to collect saliva passively.
- All the doners washed mouth with clean water prior to saliva collection.

- During saliva collection, the doner was set comfortably and bend their head down to assemble saliva in the mouth.
- The first lots of saliva expectoration were discarded to avoid any food partials and other contaminants that interfere with analysis.
- A second lot of saliva was expectorated into sterile cleaned tubes and place the tube on ice while collecting more saliva.
- The total average volume of saliva collected was 5 ml.
- A stimulated saliva sample was collected during collection the mouth cleaning and all the basic and initial procedure was kept constant.
- Where the subjects were asked to chew a cotton for 2 min, cotton was kept in sterile test-tube, while collection the test tube was placed in an ice bath.
- The saliva was extracted from the salivary cotton by centrifugation and filtration. The saliva was centrifuge two times at 4000 RPM followed by filtration.
- No, any stimulants were used in saliva collecting procedure.
- The collected saliva was stored in the fridge at 37 ^{o}C and used for analysis when needed.
- The pH of saliva stimulated and non-stimulated saliva was recorded.

Subject	**Method**	**Volume/mL**	**pH**
A1	Non-stimulated	10	7.51
	Stimulated	5.2	7.45
A 2	Non-stimulated	4.5	7.50
	Stimulated	4.2	7.52
A3	Non-stimulated	5	7.50
A4	Non-stimulated	3	7.43
A5	Non-stimulated	5	7.44

Table 5.2 The table showing the collected stimulated and non-stimulated saliva from a normal subject.

5.2.11 Glucose Measurement in human saliva

The human stimulated and non-stimulated saliva was measured for two individuals A1 and A2. A pH 7.48 phosphate buffer was used throughout the experiment.

1.8 mL of nafion (5 %) was added into a 10 mL vial containing 1.2 mL of 10 mM sodium phosphate buffer. 0.1 % PVA stocked solution was also made in the same phosphate buffer. 0.5 mL of PVA and 0.5 mL nafion polymers were mixed by gentle shaking until polymers were mixed completely. The oxidase solution was made by the addition of 2 mg of GOx in 1 mL of phosphate buffer.

The Enzyme and polymers formulation was made by the addition of 50 µL of already prepared GOx solution to 1 mL of nafion-PVA solution. The final addition of QDs was made by the addition of 25 µL of 18.3 mg/mL QDs into GOx polymers solution. The solution was kept stirring for 2-5 minutes followed by sonication for 2 minutes. The pH of the formulation for sensor fabrication was checked to be 7.48.

30 mM Glucose stock solution was made by the addition 0.54 g of glucose in 100 mL of phosphate buffer. Glucose standard solutions were made by the addition of 1.2, 0.6, 0.3 µL of 30 mM stock into 12 mL test tubes, which was made up to 5 mL by phosphate buffer. The concentration of glucose standards were 1800, 3600, and 7200 µM.

Saliva glucose measurement

The sensor was activated /hydrated for one hour by 100 µL of phosphate buffer prior to the calibration and the fluorescence spectra were recorded.

Prior to the addition of saliva into the hydrated sensor, the pH of the saliva was adjusted to pH 7.5 by addition of 0.1 M sodium hydroxide or HCl. Once the sensor was hydrated 30 µL of human saliva was added and the fluorescence emission was recorded at 605 nm wavelength for 5 minutes. Once the fluorescence response of saliva glucose was measured 3, 2, and 2 µL of glucose standard of 1800, 3600, 7200 µM respectively was added and the fluorescence response for each addition was recorded. The final concentration of glucose in the sensor was 40, 93.9, 199 µM. Stimulated and non-stimulated saliva was separately measured and all the measurements were repeated four times.

5.2.12 Validation by Gas Chromatography

Purification of saliva sample

Human saliva was collected according to the protocol mention above. Proteins in saliva were removed by precipitation method. 300 µL of 0.3 N barium hydroxide and 300 µL of 0.3 N zinc sulfate were added to 5 mL saliva sample in a glass vial. The precipitated protein was removed by centrifugation and the supernatant was collected in a glass vial for further derivatization.

Derivatization

10 mL of 5 mM glucose stock solution and 3 mL each of stimulated and non-stimulated saliva from volunteers A1 and A2 were freeze-dried using freeze dryer. The freeze-dried saliva purified samples and glucose stock were used for further derivatization. Derivatization was proceeded by the addition of 300 µL methoxyamine hydrochloride (0.18 M in pyridine) at 75 ^{o}C. The reaction proceeded for one hour. Acetic anhydride of 300 µL was added and reacted at 50 ^{o}C for one hour. The glucose derivatives were collected by evaporating the acetic acid and pyridine using rotary evaporator at 50 ^{o}C. The derivatized glucose stock and saliva glucose sample were dissolved in ethyl acetate to make standard and sample for GC-MS and GC-FID analysis.

GC/MS setup

The glucose derivative chromatogram was identified and confirmed by GC-MS 7890A-5975C (Agilent, USA) system. The injection volume was one microliter with a split ratio of 10:1 and 30 m × 0.25 mm i.d. fused silica capillary column with a chemically bonded 0.25 µm DB-5 MS capillary column (J&W Scientific Inc., USA) was used. Helium (99.9%) flow rate of 1.0 mL min^{-1} was kept constant. The column temperature was kept at 80 °C for 2 min and gradually at the rate of 10 °C min^{-1} to 300 °C. The oven temperature was 280 °C.

GC/FID setup

An Agilent gas chromatographic system 7820A (Agilent Technologies, California, USA) with a flame ionization detector (FID) and an automated liquid sampler (ALS) was used for the

analysis of glucose deravatives in saliva. The oven temperature was kept at 280. The initial temperature used was 60 ^{o}C which was ramped at 10 ^{o}C/min to 300 ^{o}C.

5.2.13 Interference study of glucose sensor

The 4 mM stock solution of glucose, Uric acid, ascorbic acid and 115 mg/mL of stock solution of albumin was made in 10 mM of phosphate buffer at pH 7.4. The sensor was pre-hydrate by the addition of 120 uL of 10 mM phosphate buffer pH 7.4 prior one hour at constant temperature before analysis. The measurement was done by the addition of 3 µL of glucose into the pre-hydrate sensor wells with gentle mixing followed by the measurement. Likewise the measurement for 3 µL uric acid, 3 µL ascorbic acid and 3 µL cysteine and 1.5 µL of albumin was done separately. The fluorescence emission at 591 nm was recorded excited by 400 nm with slit width of 5 nm for both excitation and emission. The measurement was repeated three time for each interfering species.

5.2.14 Stability of glucose sensor

The stability of a glucose sensor was measured using optimized glucose sensors. The optimized sensor was kept in the fridge (4 ^{o}C) in a dark and the performance was checked at after each 7 days. The calibration procedure used for each stability testing remained constant. The standard solution of 500, 800, 1400, 2600, 5000, 10000 µM was made by adding 0.25, 0.4, 0.7, 1.3, 2.5, 5 ml of 20 mM of stock glucose solution in a test tube, which was makeup by milli-Q water to 10 ml. The solid state sensing membrane was activated by 5 mM phosphate buffer of pH 7.4 at 25 ^{o}C for one hour prior to the analysis. Once the membrane was activated the analysis was immediately started by adding the glucose standard solution. The final concentration of glucose in activated sensors was 24.3, 51.2, 100.3, 192.9, 374.7 µM. The fluorescence emission spectra of the QDs were a monitor at 586 nm wavelength consistently after 8 minutes of time after the addition of each addition of glucose. The experimental conditions for all calibrations were kept constant. Each measurement was performed at seven days of interval.

5.2.15 Cholesterol sensor fabrications

Preparation of bioactive solution for cholesterol sensor fabrication

The glucose sensing membrane was modefied to cholesterol sensing membrane by changing the enzyme. The mixing ratio of PVA and nafion was changed and the concentration of both polymers was adjusted. The polymer composite was made by mixing 0.48 mL of nafion (3 %) and 0.48 % of PVA (0.25 %). The mixture was stirred for 10 minutes at room temperature. Once the polymers solution are completely homogeneous, QDs of 40 µL from a stock of 0.125 mg/mL was added. Cholesterol oxidase solution was prepared from the stock solution by dissolving 2 mg of ChOx in 1 mL of 50 mM acetate buffer pH 7. The cholesterol oxidase (100 µL from a stock, contained 4 units) was added to the QDs-polymer formulated solution. The solution was again starrier at room temperature for 15 minutes followed by 20 seconds sonication. The membrane solution was analyzed by optical microscope and UV lamp to confirm the dissolution of all QDs in a polymeric matrix.

Fabrication of cholesterol sensor

The fabrication procedure remained the same, with slight modifications. The membrane solution was fabricated on polystyrene 96 well plates followed by drying procedure at 45 ºC. The drop-casting techniques was used in cholesterol fabrication. 30 µL of the membrane active solution was drop-cast in 96 well plates and dried at 45 C for 4 hours. After drying the membrane was observed under an optical microscope and UV_{365nm} lamp. The biologically active membrane was stored in the fridge at 4 ºC for further analysis.

5.2.16 Cholesterol measurement

Cholesterol stock was prepared by dissolving 96 mg of cholesterol in 1 ml triton-100 (density 1.067) in a 50 mL volumetric flask. The mixture was sonicated and heated at 60 ºC for one hour and finally the mixture was make up to 50 mL by 100 mM potassium phosphate buffer of 7.2. Cholesterol standards was made in phosphate buffer of pH 7 from cholesterol stock solution of 4.9 mM. The analysis was performed after the activation of the solid membrane by 100 µL of phosphate buffer of pH 7.4. The final concentration of cholesterol in the activated membrane was 9.9, 19.7, 38.9, 76.7, 150.7 µM. The cholesterol standard solutions were added to the membrane and the fluorescence was monitor at 586 nm after each addition.

5.2.17 Characterization of membrane

The surface of QDs was characterized by AFM and the fluorescence emission spectra were analyzed by fluorescence spectrometer. The AFM (atomic force microscopy) surface characterization was performed in tapping mode.

5.3 Results and discussion

5.3.1 Characterization of membrane

The optical properties are an important indicator of QDs. A selection of suitable composite materials for the solid sensor fabrication is the key to develop a sensitive sensor because the surface capping agent sensitivity to chemical species. The selected materials should not alter or diminish QDs fluorescence.

Nafion and PVA polymer composite were suitable materials that did not affect the optical feature of QDs. The fluorescence characterization of the solid membrane (PVA-Nafion-QDs-GOx) and liquid QDs were shown in Figure 5.3. The fluorescence of QDs in the polymeric composite was redshifted in comparison with liquid MPA QDs. The red-shifting the fluorescence spectra shows that the surface passivation of QD nanocrystal by polymers, which make QDs stable in polymers membrane. It was observed that QDs in polymer membrane was outstanding platforms which were used for the further experimentations.

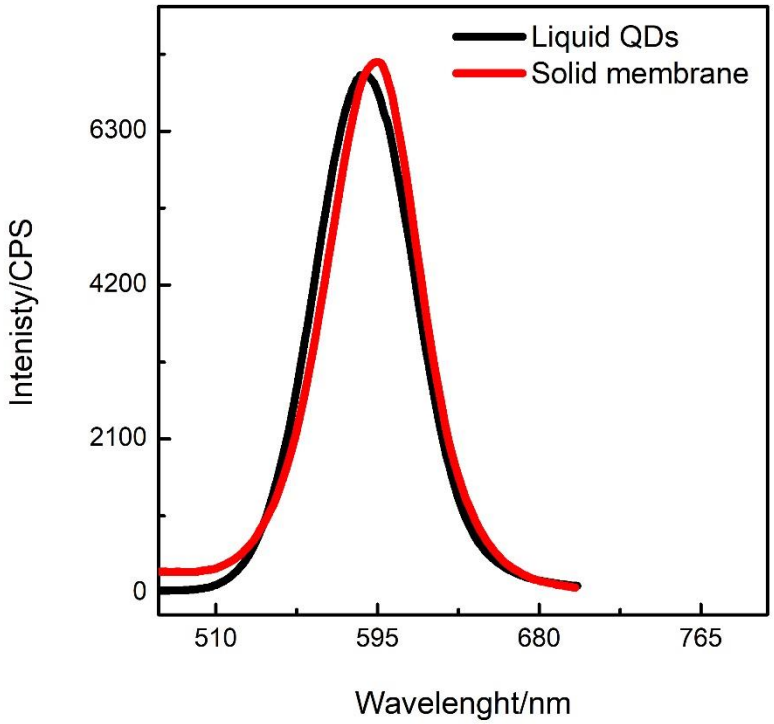

Figure 5.3 The fluorescence spectra QDs in solution phase and QDs encapsulated in a solid membrane of polymer composite.

Surface roughness is an important feature of the solid membrane that could affect the performance of the sensor. It is also contributes to membrane fouling thus a uniform and smooth membrane surface is a key to designing a reliable optical sensor. In Figure 6.3 (b, c) the solid membrane surface is analyzed by AFM which is smooth and uniform. The roughness 8.5 nm was of 4 μm × 4 μm area. The film of PVA-Nafion (without-QDs) was also characterized with an optical microscope which shows the transparency and no aggregation of the polymer were found. The development of sensors was categorized in three different phases, initially, the sensor was optimized for H_2O_2 measurement followed by glucose, and cholesterol.

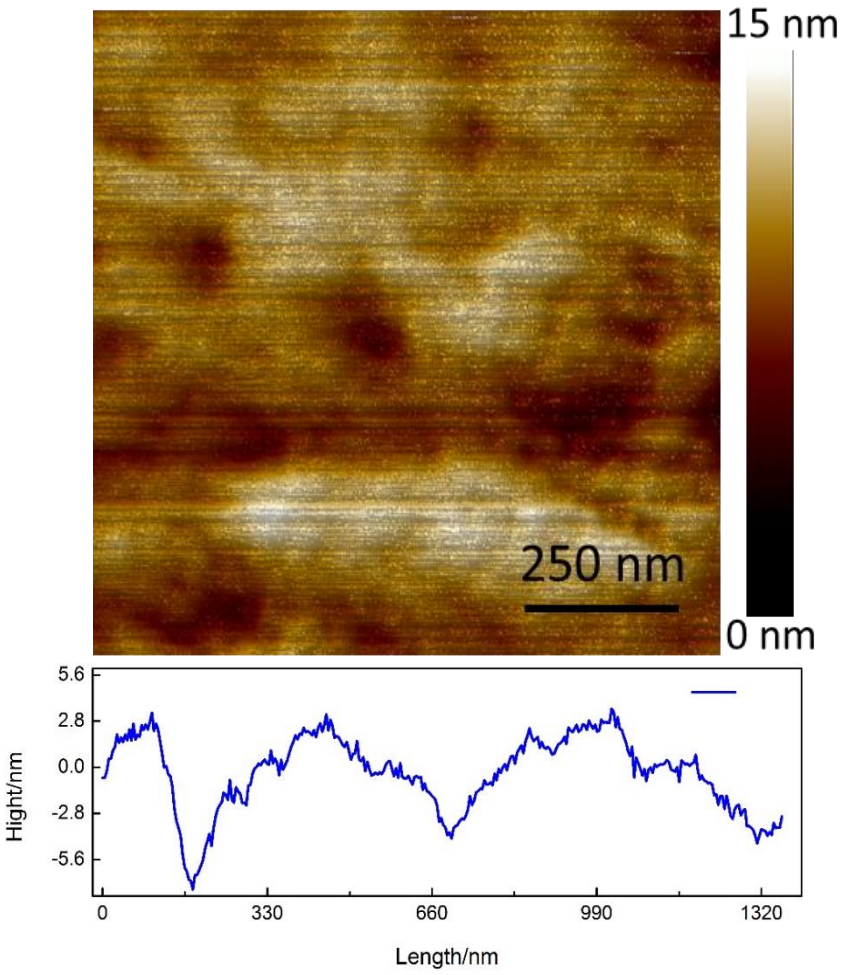

Figure 5.4 Surface morphology of solid membrane surface by atomic force microscopy.

5.3.2 Hydrogen peroxide sensor

Thiol QDs ae highly sensitive to oxidative species, any oxidative species in a surrounding environment alter QDs structure. The long term storage of thiol QDs in water were observed to be denaturing and aggregate due to oxidation in the respective solvent or surrounding environment. Hence recently the polymer encapsulation of QDs has been increase to improve the stability of materials additionally the polymers have solid film forming properties[68]. In this work, thiol-capped QDs had been encapsulated with nafion and PVA polymers which improve the structural and fluorescence stability of QDs. The H_2O_2 sensor is based on the reduction of QDs fluorescence signal by the trace of H_2O_2 hence the encapsulated

QDs with higher fluorescence stability response to only the amount of H_2O_2 diffused into the solid membrane.

Simple method of sensors fabrication was used, as mention below in Figure 5.5. The whole processes were consist of four steps. First step toward sensor development was to optimize formulation. Initially enzyme-less solution were made to optimize the performance of sensor using H_2O_2. Once the solutions were optimized the GOx and ChOX enzymes containing solutions were used to fabricate glucose and cholesterol sensor and optimized with respective oxidase concentrations. Adjusting appropriate ratio of the nafion, PVA, GOx or ChOx and QDs are important to develop the optical sensor with high performance and with higher sensitivity.

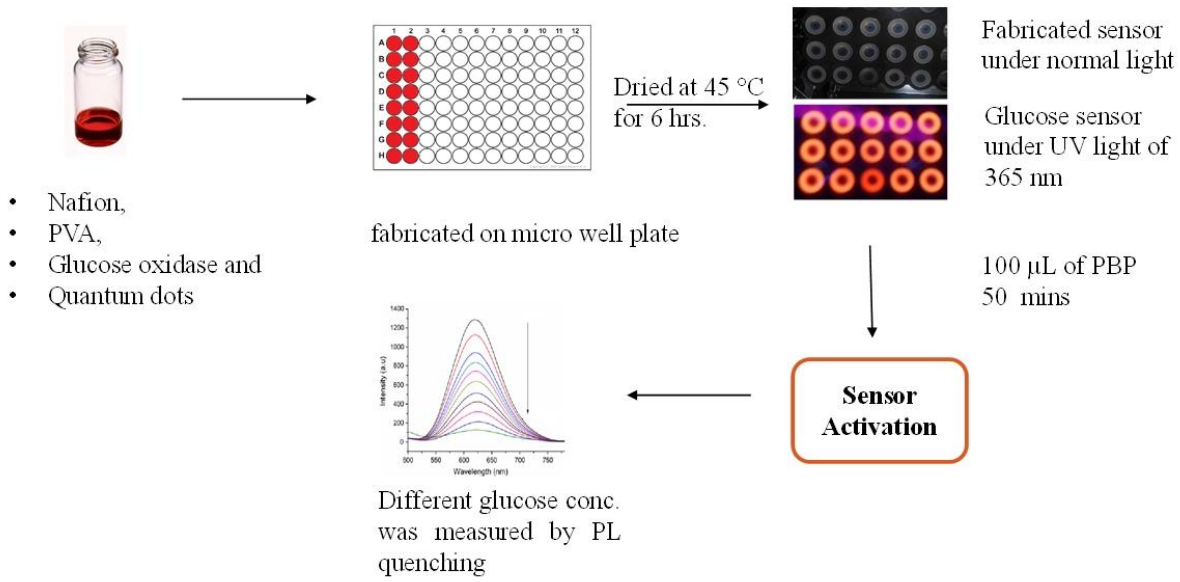

Figure 5.5. The optimaization process of the QDs-polymeric membrane. (a) Preparation of the active membrane solutions. (b) Fabrication of the solid state sensor (c) Drying procedures (d) solid membrane activation (e) calibration with H_2O_2, glucose or with cholesterol.

Next step was to fabricate the sensor in microplate well followed by drying procedure. 10 to 15 µL was added in 96-well plates. All the sensors were kept in oven at 45 ^oC for 6 hours. After drying procedure the sensor was stored in dark at 4 ^oC in fridge.

The third step was to activate the solid sensing membrane by hydration using phosphate buffer of pH 7.2. Different hydration time and different volume of phosphate buffer were used to get an appropriate conditions. At the last once the sensor was fully activate the calibration was immediately performed.

H_2O_2 response of the solid state sensor fabricated from 0.5 % PVA and 0.025 % nafion was achieved at different conditions. The membrane was characterized and the strength was physically and visually inspected before used. While optimizing the sensor various calibrations were performed with the different experimental condition and membrane structures.

Initially, the H_2O_2 calibration was performed without the activation of the solid membrane. The fluorescence emission spectra after the addition of 4 to 800 µM of H_2O_2 are presented in Figure 5.6. The response shows the gradual reduction of the fluorescence as the H_2O_2 concentration increase. This shows that the QDs are completely stabilized within the polymeric matrix that prevents QDs aggregations which causes the fluorescence bleaching.

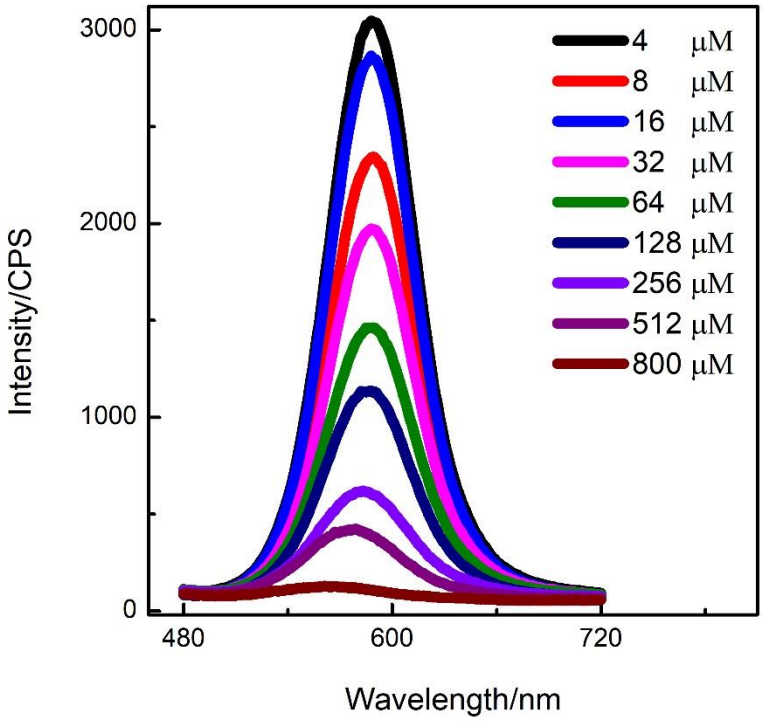

Figure 5.6 A fluorescence emission spectra of the solid state glucose sensor (0.5 % PVA, 0.025 % nafion 20 µL of QDs from 1.87 mg/mL stock) activated by 30 µL of buffer and with the 4 to 800 µM of H_2O_2.

The fluorescence quenched by H_2O_2 was plotted in Figure 5.7 and linear range obtained was from 4 to 32 µM with correlation coefficient of 0.993. The measurements suffered from an extensive standard deviation. The fluorescence response with standard deviation for blank, 0.4, 4, 8, and 16 was 17244 $\pm$ 1599, 744416 $\pm$ 64322, 786036 $\pm$ 30939, and 886680 $\pm$ 91392 CPS respectively. Consequently, it was important to change the concentration range of H_2O_2.

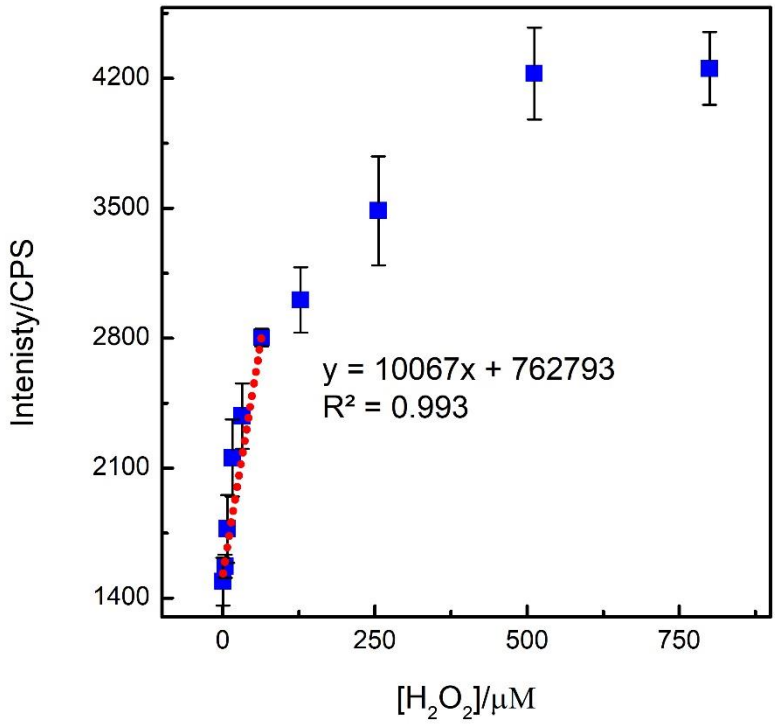

Figure 5.7 The fluorescence response of the solid state sensor to 0.4 to 800 µM H_2O_2.

In Figure 5.8 the fluorescence of QDs was quenched by 6 to 100 µM of H_2O_2. The sensor was fabricated from the 0.05 % nafion, 1 % PVA solution. In this calibration the sensor was activated by 100 µL of phosphate buffer of pH 7.4 for 10 minutes.

The fluorescence response was monitor for 300 seconds and was calibrated with corresponding H_2O_2 concentrations. The calibration plot reveals that H_2O_2 can be measured within the narrow range (1 to 100 µM), and sensitivity and performance of the sensor can be elevated by increasing the sensor activation time to 10 minutes as well increasing the volume of buffer i.e. to 100 µM used for hydrating the sensor. The linear range of 6.2 to 100 µM was established with the detection limit of 2.8 µM using the formula (LOD = [(B+3*STDB)-C]/m).

While comparing the calibration presented in Figure 5.7 and 5.9, it was clear that activation of sensor for 10 minutes and with 100 µL of phosphate buffer the linear range and the sensitivity can be improved. The response of the sensor calibrated in Figure 5.8 is with high standard deviation hence to measure the accurate level of saliva glucose it is important to optimize the activation time to allow sensor to be fully hydrated as well to adjust volume of buffer used for hydration.

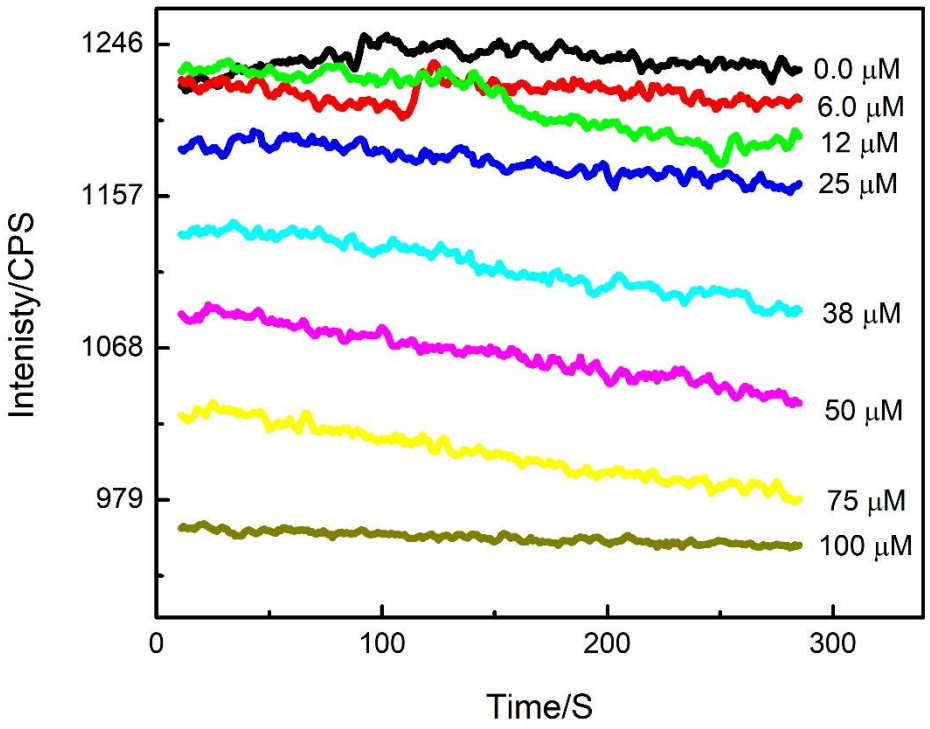

Figure 5.8 The fluorescence response of solid state sensor to 6 to 100 µM of H_2O_2. The sensor was activated by 102 µL of buffer pH 7.4 for 10 minutes.

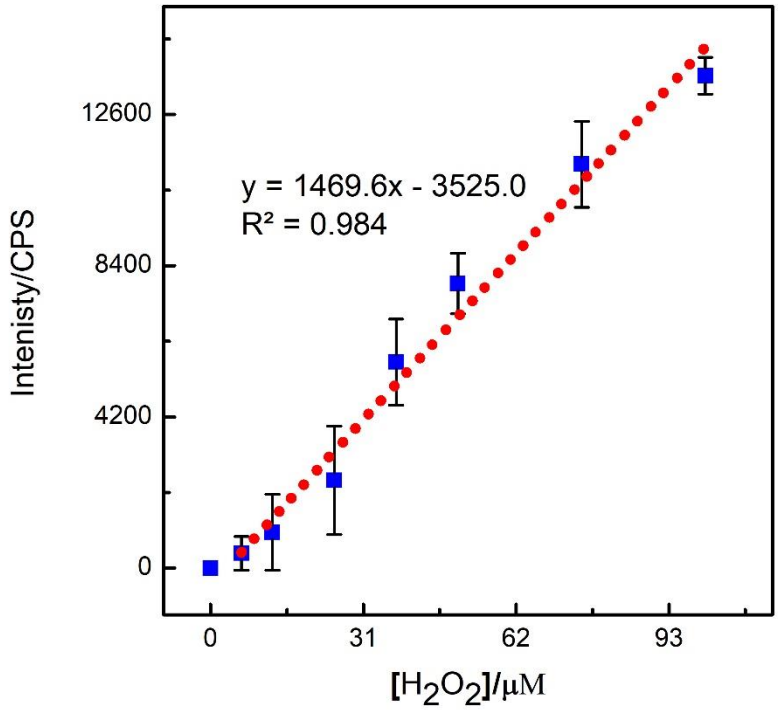

Figure 5.9 The corresponding calibration plot of the fluorescence response presented in Figure 5.10 for 6 to 100 µM of H_2O_2, Where the N = 4.

Nafion is stable upon hydration, but the morphology and structure can be change upon hydration hence the mechanical properties and thickness of the membrane also transformed. It has been reported[71-74] by various research groups that the morphological, mechanical, and electro-chemical properties change upon hydration of nafion membrane.

PVA morphology, structure, mechanical properties are also reported to change upon activations [75,76]. The nafion-PVA composite that hosting QDs with physical or chemical linking is certainly mutable upon hydration. Therefore the morphological, structural, and electrochemical changes upon hydration affect the optical feature of embedded QDs within the composite. The sensor response predicted to be robust once all other factor been inert. To achieve a robust and highly reliable fluorescence signal the sensor needed to goes through further optimization procedures.

Hydration of PVA and nafion efficiently changed the nature and properties of the membrane. The resultant hydration profile of the sensor comprised of 0.05 % nafion 1 PVA

and QDs was presented in figure 5.10. The data shows that the rate of fluorescence is increased on hydration. The total time consumed to achieve a stable fluorescence was 30 minutes.

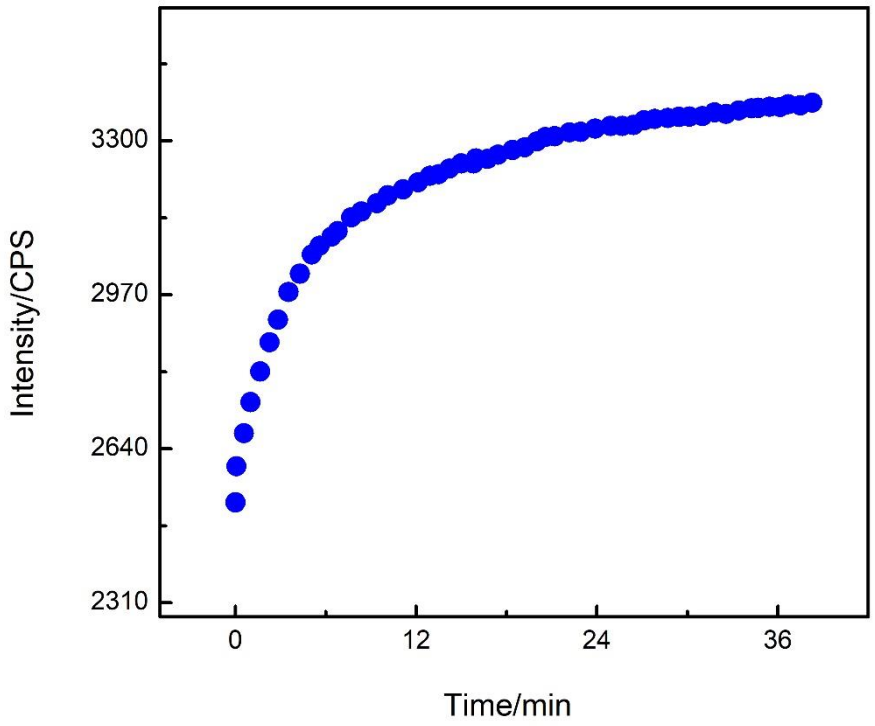

Figure 5.10 The fluorescence response of the sensor on hydration 100 µM of phosphate buffer.

Hydration profile (sensor activation) of the solid state sensor was presented in Figure 5.10. Upon the addition of buffer to the solid sensor the fluorescence started to be increasing for 30 minutes and after 30 minutes, it was stable enough to be use for analysis. Fluorescence response on hydration shows that increasing the activation time of membrane, sensitivity, and linearity of the sensors can be enhanced, hence the solid membrane activation time was further increased to 30 minutes. The concentration of QDs was slightly increased in the medium to allow the use of a greater concentration of hydrogen peroxide during calibration.

The data from the modified condition of sensor were presented in Figure 5.11 shows that the average fluorescence response of four calibrations was quenched by 50 to 451 µM of H_2O_2.

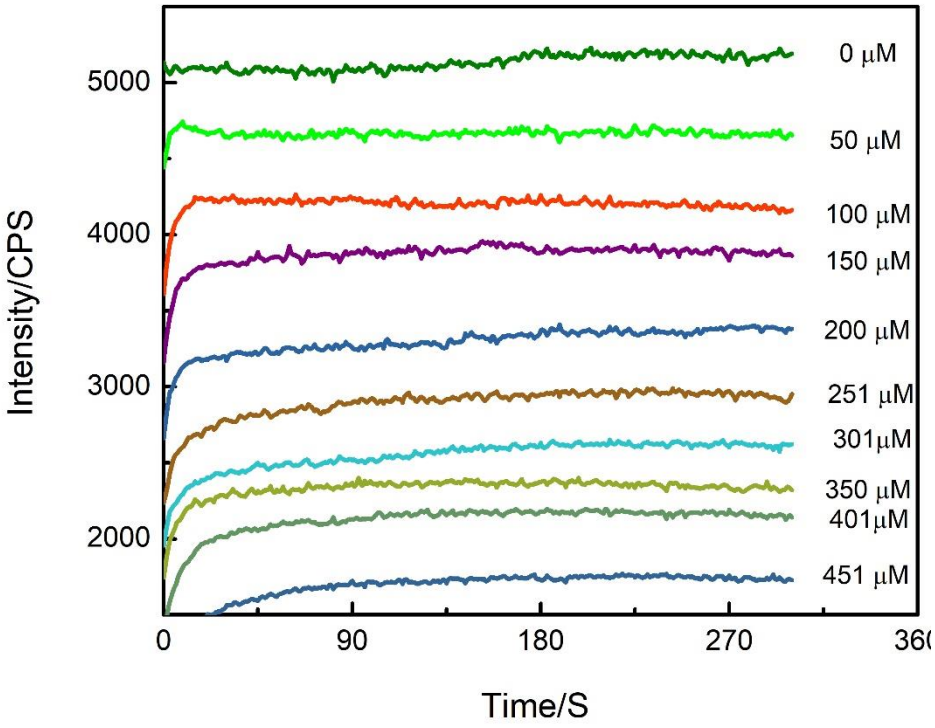

Figure 5.11 The fluorescence response of solid state sensor (0.5 % PVA, 0.025 % nafion 20 µL of QDs from 1.87 mg/mL stock) to H_2O_2.

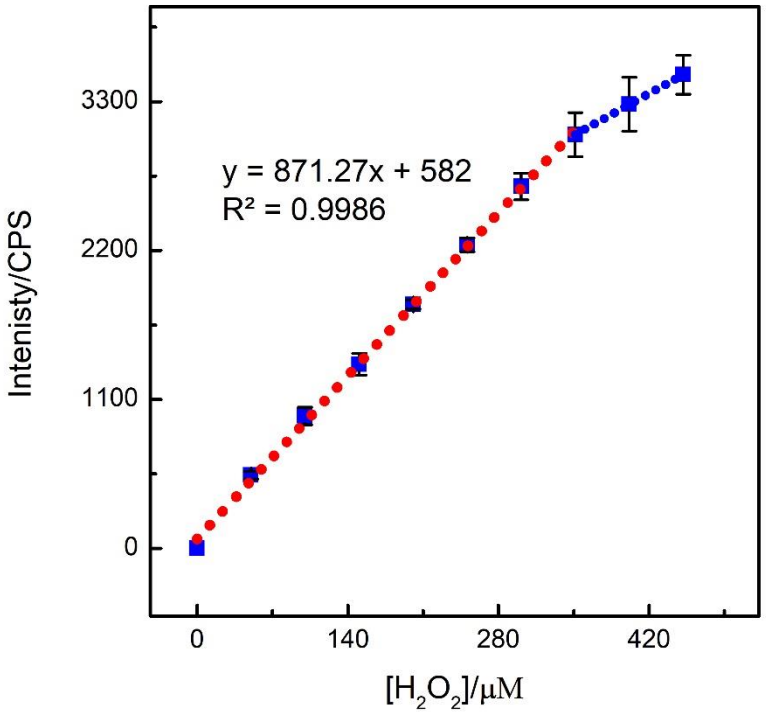

Figure 5.12 The Calibration plot fluorescence response of the sensor activated by 102 µL of water for 30 minutes and quenched by 6 to 451 µM of H_2O_2. Where N = 4.

Results obtained in the third calibration with prolonging activation time and greater QDs concentrations are shown in Figure 5.12. The extended linear range was 50 to 350 µM with the detection limit of 10 µM. The obtained linear range was suitable for H_2O_2 measurement and appropriate to modified it for further glucose sensor development.

In this work, we developed a drop casting techniques for the fabrication of solid membrane to detect H_2O_2 in micromolar range. The fabrication process was further optimized and controlled. The important to use this technique was the improving the performance of solid state sensor.

5.3.3 Reaction kinetics of QDs fluorescence quenching

Kinetic method for analysis and determination of H_2O_2, glucose and cholesterol has been proven in the previous chapter. In this study we used QDs in a solid membrane which is composed of polymers as a fluorescence agent. Kinetic of QDs fluorescence quenched in solid membrane by H_2O_2 was investigated. The reaction kinetic studies allow us to determine the nature and stoichiometry of reaction, which could increase sensitivity, and performance of the sensor.

The fluorescence solid membrane of QDs with polymers is different in nature. The polymer changes the diffusion and permeability of quencher hydrogen peroxide in the membrane, thus the rate of fluorescence quenching of QDs is predicted to be slower and naturally pseudo first order.

Reaction rates of the corresponding H_2O_2 concentrations were presented in Figure 5.13. The reaction kinetics induced by 25, 80, 130, and 185 µM of H_2O_2 was having different reactions rates. The reaction rates were calculated from the slope of the data presented in Figure 5.13 and tabulated below.

[H_2O_2]/µM	25	80	130	185
Rates CPS/S	992.6	2190.7	2914.3	3799.8

Table 5.2 The rate of reaction and the concentration of H_2O_2 used.

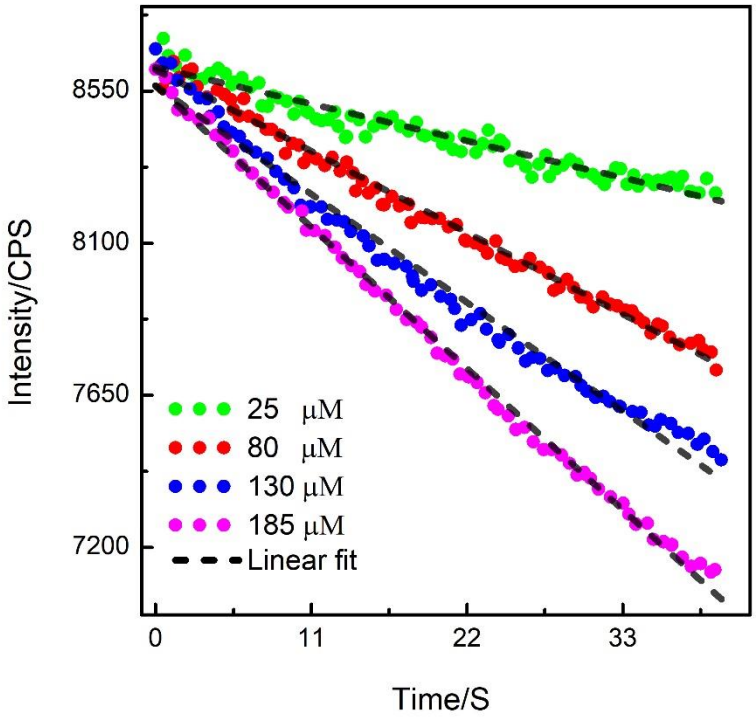

Figure 5.13 The kinetics of the solid state fluorescence based sensor to H_2O_2.

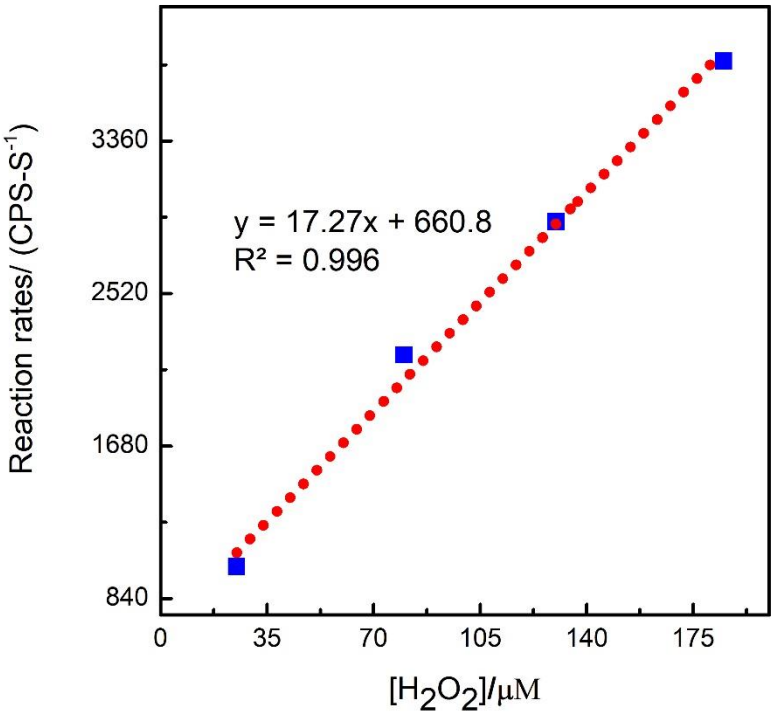

Figure 5.14 The calibration plot of reaction rates versus the concentrations of H_2O_2 used.

The calibrations plot is shown in Figure 5.14 shown, the linear range of 25 to 185 µM of H_2O_2 was achieved with correlation coefficient is 0.998. The detection limit calculated for this calibration plot was 23.21 µM. This was confirmed that entrapped nanocrystals in the polymeric matrix were successfully used for kinetic based determinations of H_2O_2. The kinetic method is fast and reagent saving and a powerful alternative to equilibrium methods. This kind of methods relevance to the measurement of the same reaction for biological molecules.

The obtained results for the hydrogen peroxide measurements show that the QDs in polymer membrane increase the performance and the sensitivity under optimized conditions. Hence the detection limits for the hydrogen peroxide was 0.93 µM and the range of hydrogen peroxide measurement was 0.4 to 451 µM. The range of hydrogen peroxide covers the range of saliva glucose i.e 75 µM. The kinetic method of analysis was also validated by using the solid state sensor.

5.3.4 Glucose measurements

In previous chapters glucose has been measured in solution phases using equilibrium methods and rate constant methods. Hence the glucose solid state sensor was fabricated to improve the stability and performance of the sensor as well increase the sensitivity. The glucose sensing membrane consists of QDs, nafion, and PVA polymers with the glucose oxidase. The membrane designed primarily to stabilized QDs and enzymes in polymer matrix to enhance the sensitivity and performance of solid state sensor. PVA is highly biocompatible and used for stabilizing GOx. The immobilization of GOx in PVA membrane is a known technique and has been used before for the development of solid state sensor. The polymers composition for membrane construction was started from 2:0.1 ratio of PVA and nafion.

Initially the sensor was fabricated with 1 to 0.05 ratio of PVA and nafion with 40 µL of GOx (1 mg/0.1mL). The sensor was dried at 45 ºC for six hour in oven and immediately used for analysis. The sensor was activated by the addition of 100 µL of 5 mM phosphate buffer for one hours. Once a stable fluoresce response for blank was achieved the calibration were started.

The average fluorescence responses of four repeats were shown in Figure 5.15. The resultant fluorescence response was the function of the glucose concentration used (6 to 109 µM) for analysis.

In Figure 5.16 shows the response of membrane to 6 to 109 µM of glucose. As the calibration plot signifying that the linear range of glucose measurement is 6 to 109 µM with a correlation coefficient of 0.9797 and the detection limit of 1 µM was achieved.

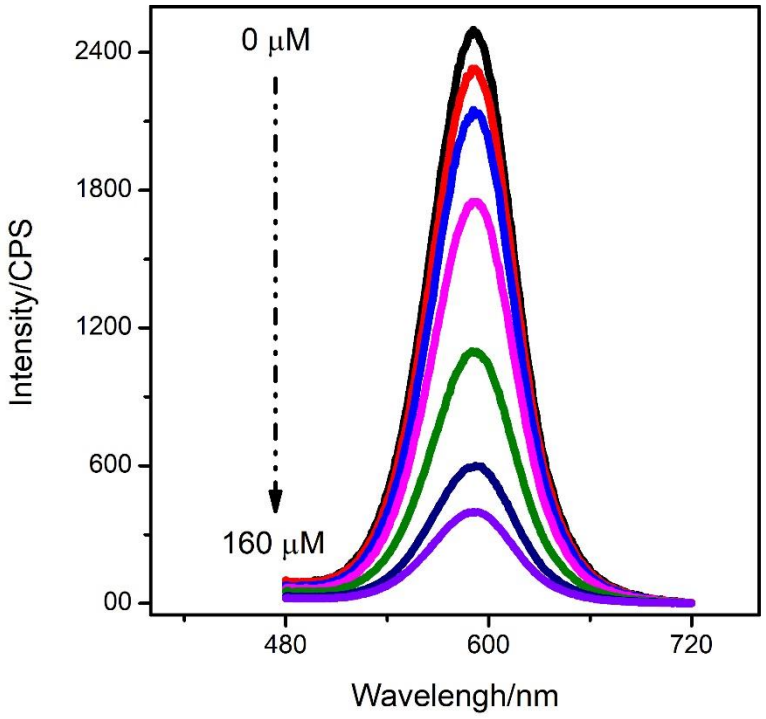

Figure 5.15 the fluorescence spectra of the QDs in polymer membrane (PVA and nafion ratio of 1.0: 0.05) quenched due to the addition of 6 to 109 µM of glucose.

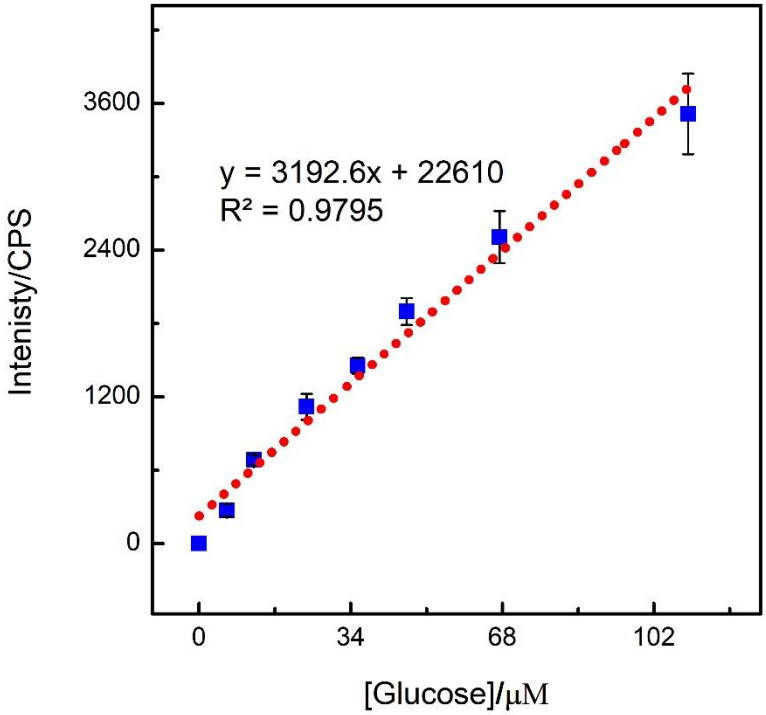

Figure 5.16 The performance of glucose sensing membrane with PVA and nafion composition of 1.0: 0.05.

The nature of the glucose sensing membrane was change due to the use of enzymes. Hence enzymes might affect the hydration. The hydration profile of the sensor was directly related to the fluorescence intensity increase. Upon absorption of water the membrane swell up and thickness was increased.

The hydration of membrane with 0.25 % of PVA with 1.5 % of nafion is presented in Figure 5.7. The fluorescence increases 30 % in 60 minutes after addition of buffer. A stable fluorescence was achieved after 55 minutes. In comparison with enzyme-less membrane used for hydrogen peroxide measurement the glucose sensing membrane need more time to fully hydrate. The difference of hydration time was because of the use of different ratio of polymers.

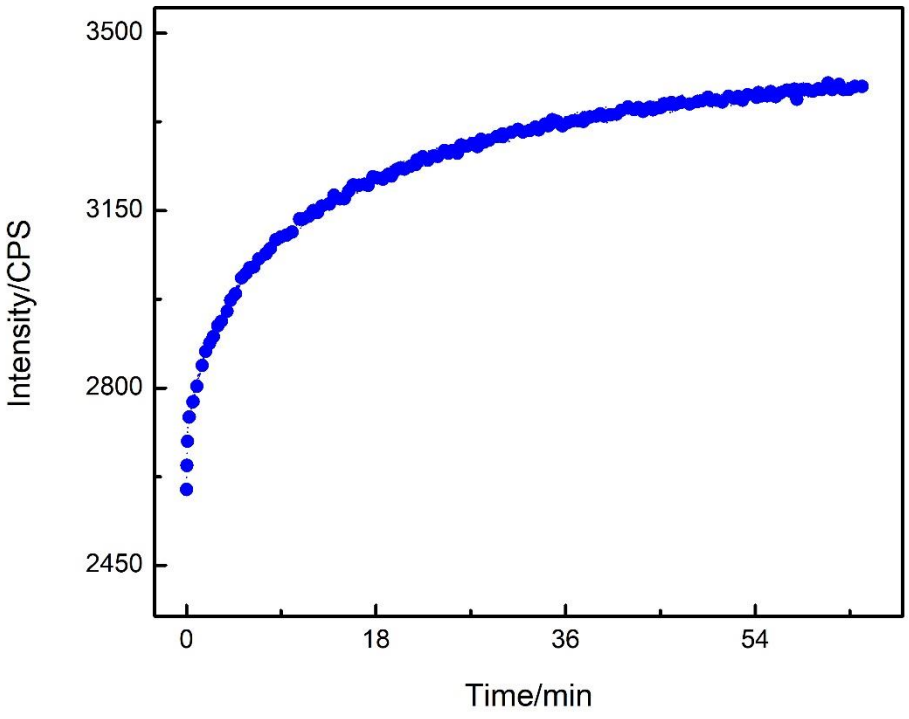

Figure 5.17 The fluorescence response of the sensor upon hydration by 100 µL of phosphate buffer pH 7.4.

Different concentration of oxidase was used to verify the oxidase function and investigate the optimal oxidase amount for glucose sensing. In Figure 5.18 it was verified that the GOx concentration was the function of the slope of calibration plot. The slope of the calibration oriented from the use of 10, 20, and 40 µL (2 mg/0.1mL) of glucose oxidase was 4.99, 1.91, and 0.477 CPS/µM.

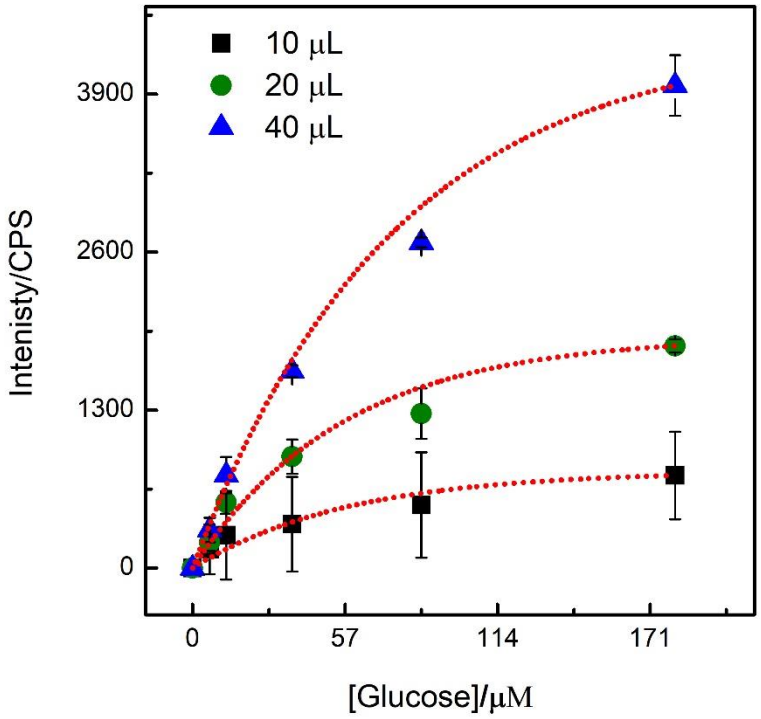

Figure 5.18 A calibration plots obtained from 10, 20 40 µL of glucose oxidase concentrations (2/mL GOx in water). The polymer composition was 1% PVA and 0.05% nafion.

The inappropriate concentration of nafion and PVA causes to disruption membrane and inducing error in fluorescence single which affects the sensitivity and accuracy of the sensor. Hence the polymer composition was important to optimize to improve the performance of sensor.

The sensor was optimized by changing the ratio of polymers compositions, showed in Figure 5.19. The different ratios of PVA and nafion were used to fabricate a stable membrane. The appropriate ratio of the polymers composite enhances the optical stability with improves sensitivity. Polymers composition redirects, strengthens and water permeability of the membrane hence changing the nafion-PVA ratios yield different membrane and the glucose response to the membrane was different. The ratio of PVA also changed the mechanical properties, and the thickness of the membrane.

The initial polymer composition was consist of 1% PVA with 0.05 % nafion. The high PVA ratio increases the permeability of the membrane that increasing the glucose diffusion in the membrane. The fluorescence quenching of QDs is increased that cause a limited range of

glucose detections. The concentration of nafion is increased and the PVA amount was decreased shown in Figure 5.19 the membrane with 0.25 % PVA and 1 % nafion. The linear range obtained with this ratio was wide enough to be used for saliva glucose analysis. The linear range obtained with 2% PVA and 0.1 % nafion concentration was 6 to 109 % and with 0.25 % PVA and 1%, nafion is 9 to 190 µM. The data shows that increasing nafion, linearity of glucose measurement was increased.

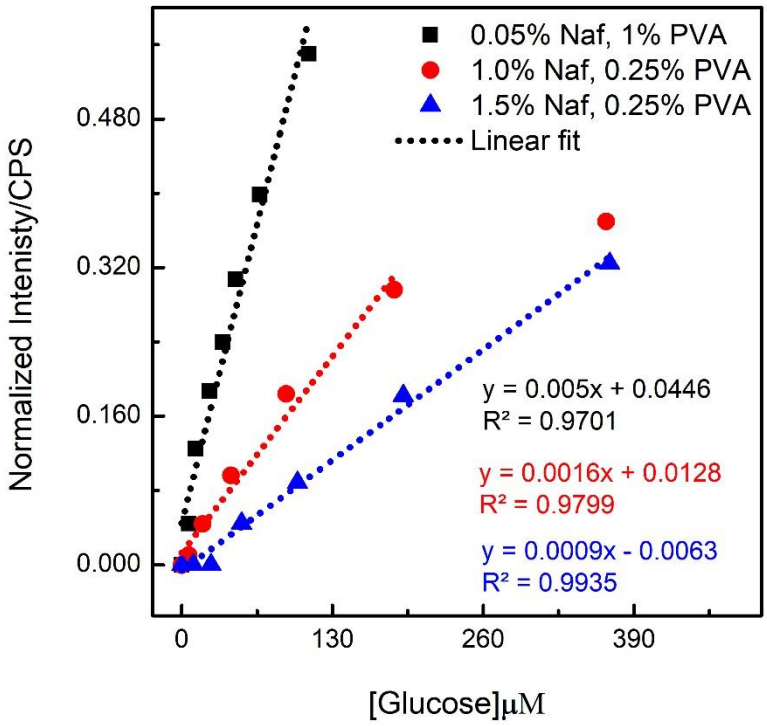

Figure 5.19 Optimization of the polymers nafion and PVA ratios in solid state glucose sensor, which yield different linear ranges.

Further increases in nafion concentrations to 1.5% and PVA with 0.25 % a linear range of 9 to 340 µM was achieved with correlation coefficient of 0.992 and the detection limit of 4.8 µM. The sensitivity and the linear range of quantification were significantly improved. The wide linear range of quantification allowed the sensor to detect glucose at concentration ranges. The developed sensor with optimal polymers composition was used to repeat results with different fluorimeter and the responses was comparable. Thus the optimized sensors were expected to detect human saliva but before introducing human saliva glucose measurement

resolution, interference and measurements was performed in artifecial saliva, which helpd us to understand the nature and the performance of the sensor.

NO	PVA %	Nafion %	Linear range/µM	Detection limit/µM
1	2	0.1	6 – 109	1.0
2	0.25	1.0	9 – 190	3.2
3	0.25	1.5	9 – 340	4.8

Table 5.3 The polymer ratio used for the measurement of glucose, with linear range and detection limit.

Glucose oxidase concentration in a sensor with 1 % PVA and 0.0.5% nafion formulation was optimized as shown in Figure 5.18 above but the optimized polymer formulation ratio was found to be 1 to 1.5 % nafion and 0.25 % of PVA. Changing the polymer ratio will influence on the stability and performance of sensor by affecting stability and the activity of enzymes within the sensor. Hence we repeated GOx optimization for the sensor with polymer formulation of 1 % nafion and 0.25 PVA. The plot obtained in Figure 5.20 shows that the activity of different GOx ratios. The different slopes were obtained for the 50, 40, and 20 µL oxidase concentrations. The slope of the calibration curve was 0.0019, 0.0011, and 0.0004 CPS/µM respectively for 50, 40, and 20 µL of GOx from 2mg/mL of stock.

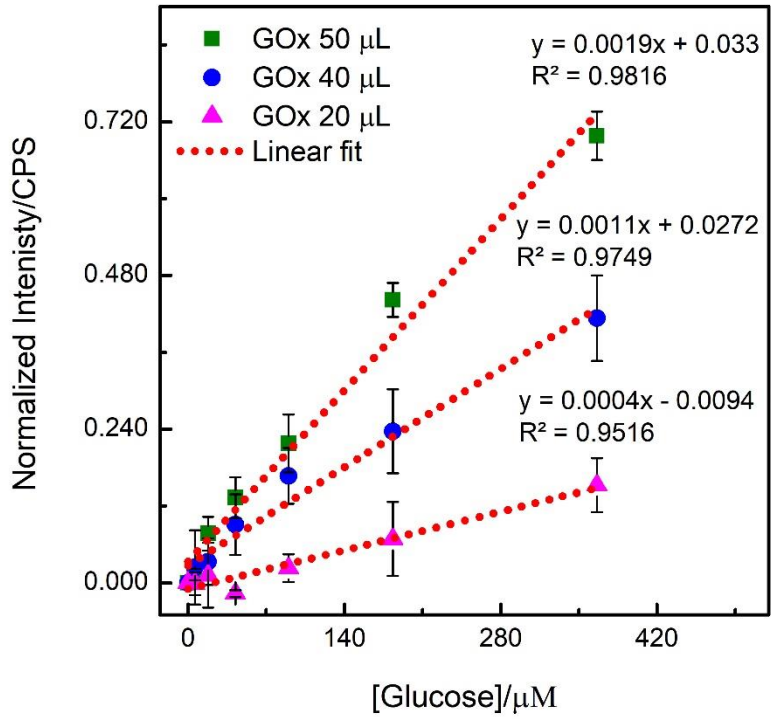

Figure 5.20 The calibration plots of solid state sensor (0.25 % PVA and 1 % nafion) with different GOx ratios

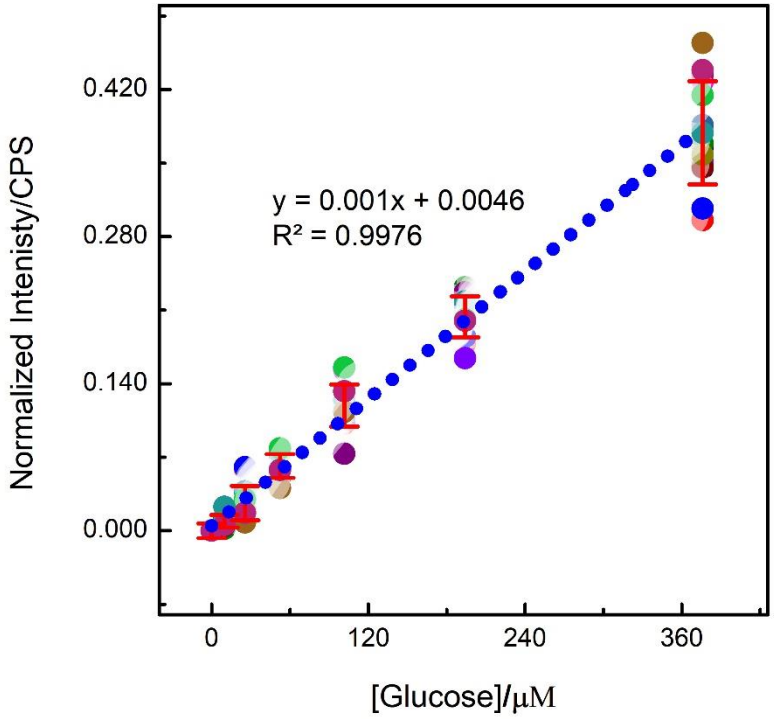

Figure 5.21 The fluorescence response of optimized solid state glucose sensor where N = 16.

We determined the accuracy of glucose sensing membrane that can detect small amount of glucose. The least amount of glucose detected precisely by the sensors was 9 µM (Figure 5.21). The range of glucose which was consistently and precisely measured was 9 to 375 µM. The data for the resolution was collected from sixteen control calibrations. The resolution study led us to use the developed sensors for interferences analysis.

In this section the optimization of glucose sensor was completed. The optimized formulation was 1.5 % of nafion, 0.25 % of PVA, 50 µL of GOx from 2 mg/mL stock. The optimized sensor was with high sensitivity and high performance, the glucose measurement range was suitable to be using the sensor for salivary glucose analysis.

5.3.5 Measurement of glucose in saliva

The performance of solid state sensor was initially investigated in artificial saliva prior to glucose analysis in human saliva. An artificial saliva was made according to the reported methods[67]. The artificial saliva was consist of 5 mM of NaCl, 1 mM of $CaCl_2$, 15 mM of KCl, 1 mM of citric acid, 5 mM of uric acid, 1 mM of ascorbic acid, 0.2 mM of lactate, 1.1 mM of Potassium thiocyanate KSCN, and 4 mM of NH_4Cl. The solid state sensor of 1.5 % nafion and 0.25 % PVA was fabricated and used for the measurement of glucose in artificial saliva.

All the standard glucose was made in artificial saliva. The concentration range of glucose in artificial saliva was 9.9 to 376.0 µM. Interfering compounds might be disturbing the balanced polymeric matrix, QDs, or glucose oxidase. A calibration was performed using glucose standard in artificial saliva the fluorescence response of glucose in artificial saliva is presented in Figure 5.22. The linear range of glucose measured was from 9 to 376 µM with correlation coefficient of 0.997. The detection limit in artificial saliva was 4.8 µM.

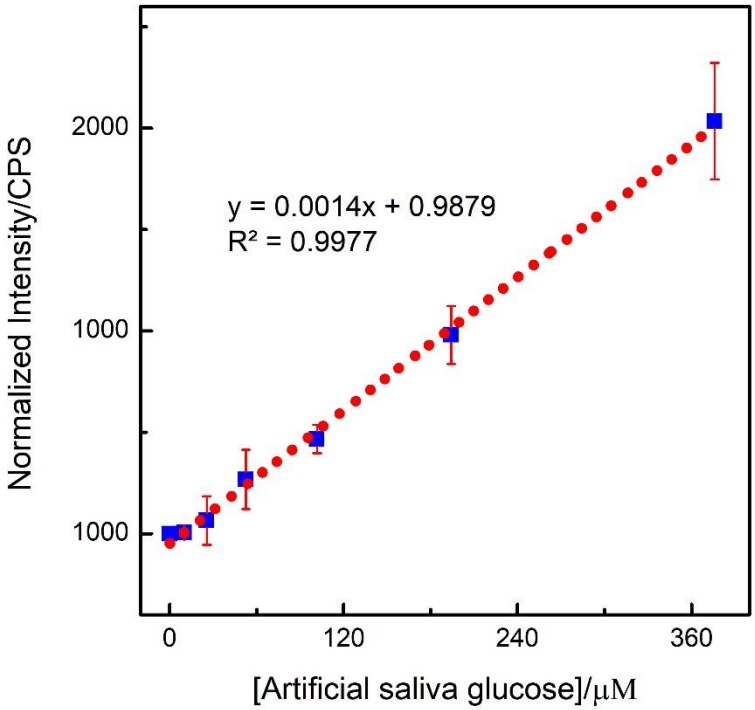

Figure 5.22 A calibration plot of the fluorescence response of glucose in artificial saliva.

Saliva is a body fluid and has a number of molecules present. It can be easily collect on non-invasive method. Human saliva was collected from six healthy individuals and was used to detect the concentration of glucose. The chemical composition of saliva is fluctuating in response to physiological status, stressors, and stimuli, according to one report the number of compounds present in human saliva is 853. The chemical nature of saliva is also dependent on the health condition of an individual[77]. Saliva body fluid is rich of proteins and other compounds that make it viscous fluid that might interfere with the fluorescence detection. The real saliva composed of highly viscous proteins that interrupt the fluorescence signal response or binding of proteins with GOx non-specifically that inhibit the oxidation of glucose.

Detection of glucose in saliva for a normal subject X

The fluorescence of the blank (buffer), and the fluorescence response of the solid state sensor to 31.8 % diluted saliva glucose of unknown concentration were shown Figure 5.23. The data presented shows that the fluorescence is significantly quenched on the addition of

glucose standard and saliva. The average of fluorescence was calculated from 10 points and was calibrated in below in figure 5.24.

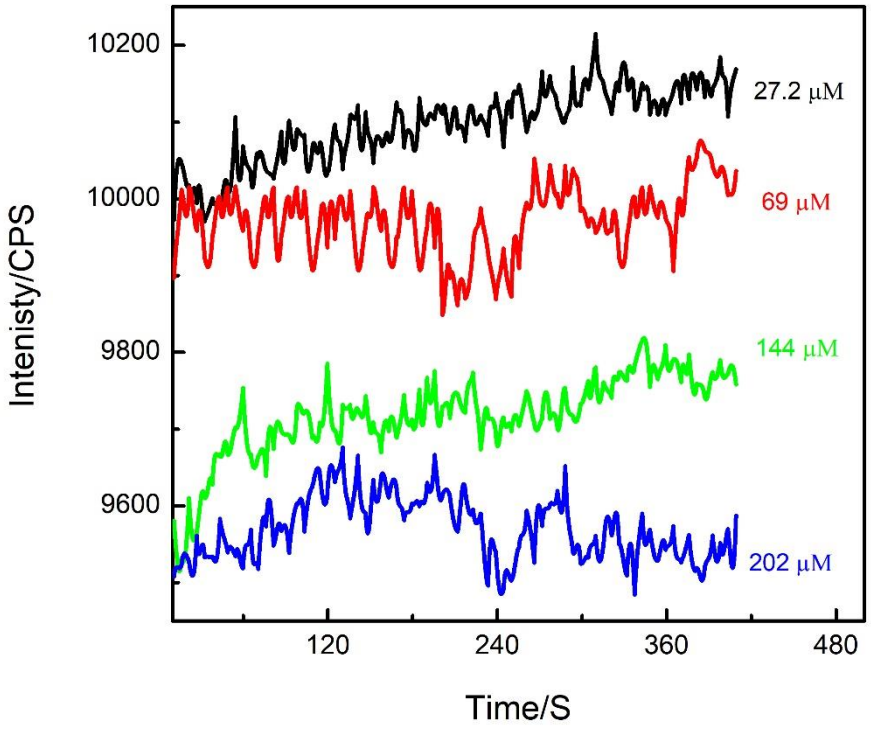

Figure 5.23 The fluorescence response of the blank, (5mM phosphate buffer of pH 7.4 mm), human saliva, (unknown concentrations) and 69, 114, 202 µM of glucose. (Emission at 593 nm and excited at 400 nm)

The unknown saliva glucose concentration was determined from the calibration curve obtained from the standard glucose solutions. The sensor was activated by 75 µL of 5 mM phosphate buffer for one hour. After hydration 35, µL of saliva was added into the sensor followed by the addition of 69, 114 and 202 µM of glucose. The fluorescence change was monitor after each addition of saliva or glucose standard solutions. The resultant fluorescence change was plotted against the concentrations of glucose. The unknown saliva glucose was determined from the linear equation obtained from the calibration curve. The X (unknown saliva glucose) was calculated from the slope and intercept in the linear plot and adjusted by dilution factor to the original concentration. The calculated glucose concentration for subject X (nondiabetic) was 86.9 with standard deviation of 6.9 µM.

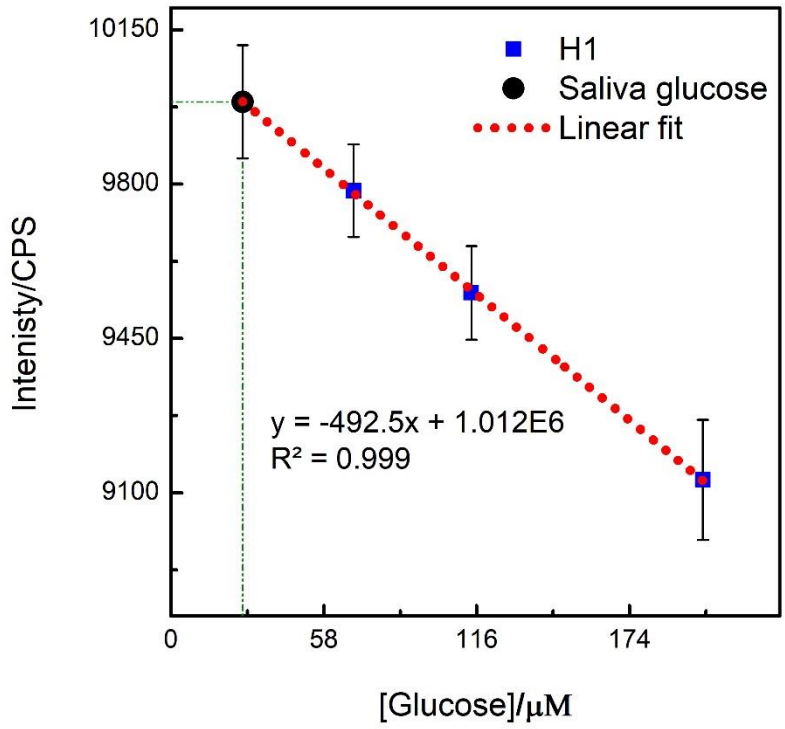

Figure 5.24 A calibration plot of 69, 114, 202 µM of glucose and the fitting value of unknown saliva glucose.

Detection of glucose in saliva for a normal subject X1 & X2

The glucose determination of two health individual X1 and X2 saliva was repeated. The 35 µL of saliva glucose was added into the activated sensor using 80 µL of phosphate buffer. The dilution factor of unknown saliva glucose was 3.28 which were equal to the total volume in a sensor. Total volume of 115 divided by 35 µL of saliva added in is equal to 3.28. The fluorescence quenched by X1 and X2 was fitted in calibration curve. The saliva glucose X1 and X2 was calculated from the calibration curve was 22 and 18.2 µM which were adjusted to the original concentration by dilution factor of 3.28. The calculated glucose was 72.9 and 61.2 µM respectively for X1 and X2 normal subjects.

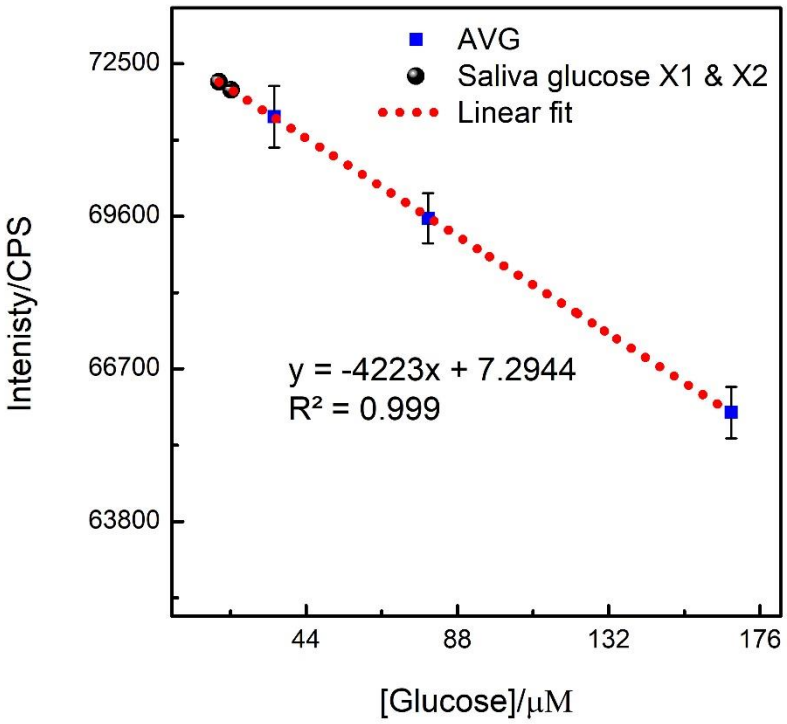

Figure 5.25 Glucose measurement in human saliva individual X1 and X2 by calibration curve of standard glucose concentrations.

Detection of Stimulated and non-stimulated Saliva Glucose

The unknown saliva glucose was determined from the calibration curve obtained from the addition of standard glucose concentrations. All the analysis was performed at pH control conditions and the pH of the solution was checked and adjusted at each stage. The solid state sensors fabricated in 96 well plate was activated by 10 mM phosphate buffer of pH 7.48 for one hour. The pH of the buffer remained at 7.48 after the complete hydration of the sensor. 30 µL human stimulated saliva from subject A1, was adjusted to pH 7.48 and added to the sensing cuvette, hence there was no pH interference on the sensor response after the addition of saliva.

The fluorescence response was recorded after saliva addition. The standard glucose was added and the fluorescence was recorded each time. The unknown saliva glucose (x) was determined from the linear equation (y = -548.4 x + 762136) shown in Figure 5.23. The determined unknown saliva glucose concentration was adjusted by the dilution factor to the

original concentration, which was 74.18 µM with a standard deviation of 9.09 for four repeats. Which is non-fasting glucose level for a healthy individual (A1).

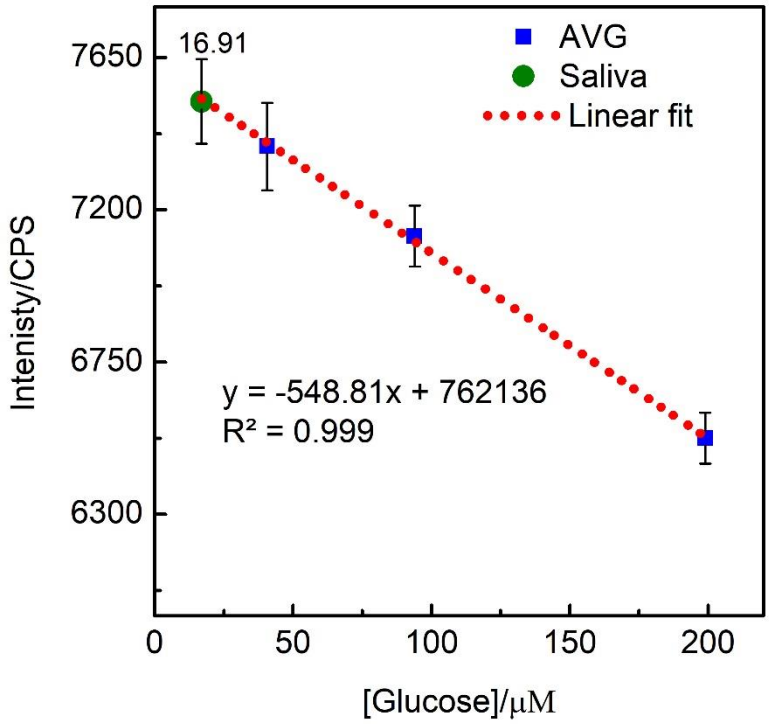

Figure 5.23. Calibration of glucose standard, and fitting the unknown saliva glucose value in calibration curve (A1 stimulated saliva), where N = 4.

The glucose concentration of non-stimulated saliva was also determined using the same protocol. The saliva glucose was estimated from the linear equation (y = -607.17x + 721900) was 79.02 µM with a standard deviation of 13.1 µM.

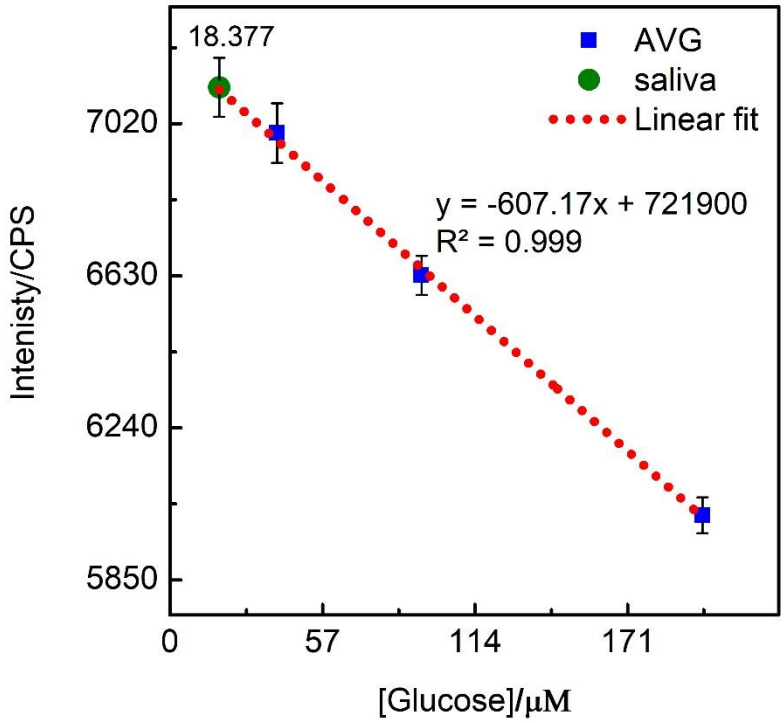

Figure 5.24. The fluorescence response of glucose standard and glucose in saliva (non-stimulated) of normal subject A1. Where N = 4.

Detection of glucose in diabetic non-stimulated saliva X3

The glucose in saliva for a diabetic individual was measured using the same method mention above. The sensor was activated by 99 µL of buffer one hour before use. Saliva of 31 µL was added to the activated sensor. The dilution factor of the unknown saliva glucose was equal to 130/31 = 4.3. The fluorescence response of the sensor for the unknown saliva glucose was determined from linear equation (y = -0.092x + 105.33) of calibration curve from standard glucoses. The slope of the calibration was 0.0009 CPS/µM with correlation coefficient of 0.998. The glucose concertation measured according to the calibration curve was 39.9 µM, which was multiplied to the dilution factor of 4.3 hence the amount of glucose in non-stimulated diabetes saliva was 167.4 with standard deviation of 18 µM.

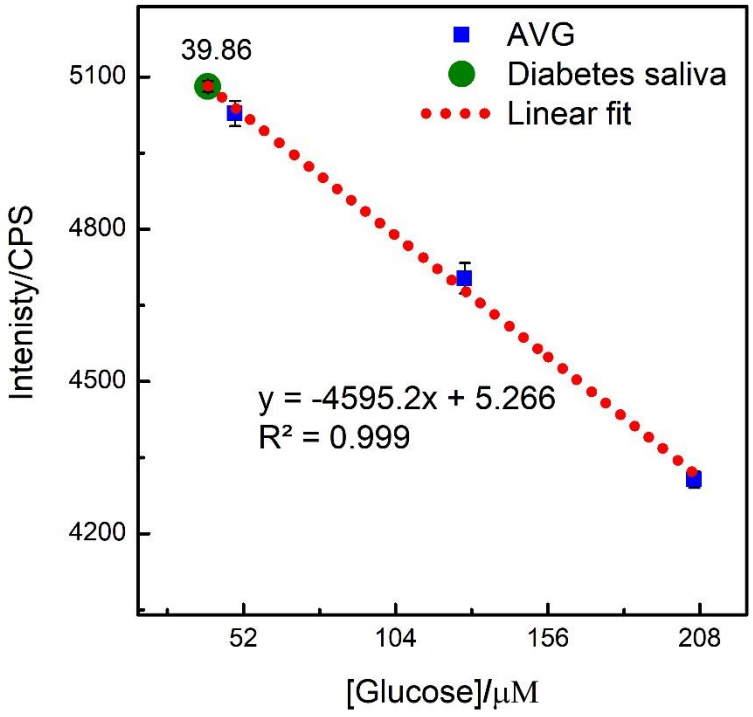

Figure 5.28 Human saliva glucose measurement of unknown concentration in diabetes individual.

Measurement of glucose in human saliva was performed for two healthy individual stimulated and non-stimulated saliva and one diabetes with non-stimulated saliva. Hence it was proven that glucose can be estimated using the developed solid state optical sensor.

3.5.6 Validation by Gas Chromatography

Analytical method validation is required to demonstrate the developed solid-state sensor is reliable. The most widely used analytical techniques are chromatographic methods (GC/ECD and HPLC/UV) and mass spectrometric method GC/MS LC/MS.The developed solid-state sensor results were validated and verified by gas chromatography. GC is an effective method for the determination of biological molecules and metabolite. Glucose has been analyzed by many research group and the detection limit estimated was 100 nM. In this method, we derivatized saliva glucose for the analysis. The derivatized glucose was measured by GC. The glucose standard was used to provide a calibration plot which was then used to determine the unknown saliva glucose.

GC analysis of carbohydrate must be derivatized into volatile molecules that can enhance the sensitivity of GC to measured glucose. Different derivatization techniques have been used for the measurement of glucose in biological samples. The derivatization method included esterification, silylation, trifluoroacetylation, and methoxymation combined with acetylation. In this work, we used methoximation and acetylation method to derivatized glucose into Penta-*O*-acetyl-D-glucose methyloxime. The derivatization is a two-step reaction, the first step involved the methoximation followed by acetylation, and the reaction scheme is below (5.1).

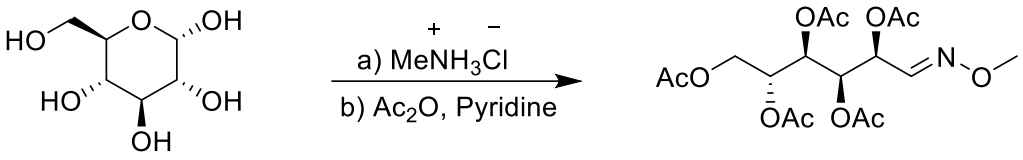

Reaction Scheme 5.1 The deravetaiztion of glucose by methoxylamine hydrochloride $MeONH_2$.HCl and acetic anhydride.

The effective derivatization of glucose has been confirmed by the GC-MS. The chromatogram shown in Figure 5.29 shows two peaks which belong to two isomers of Penta-*O*-acetyl-D-glucose methyloxime. The corresponding peaks was confirmed to belong to Penta-*O*-acetyl-D-glucose methyloxime, m/z= 419, which is the expected mass of the glucose derivatives Figure 5.30.

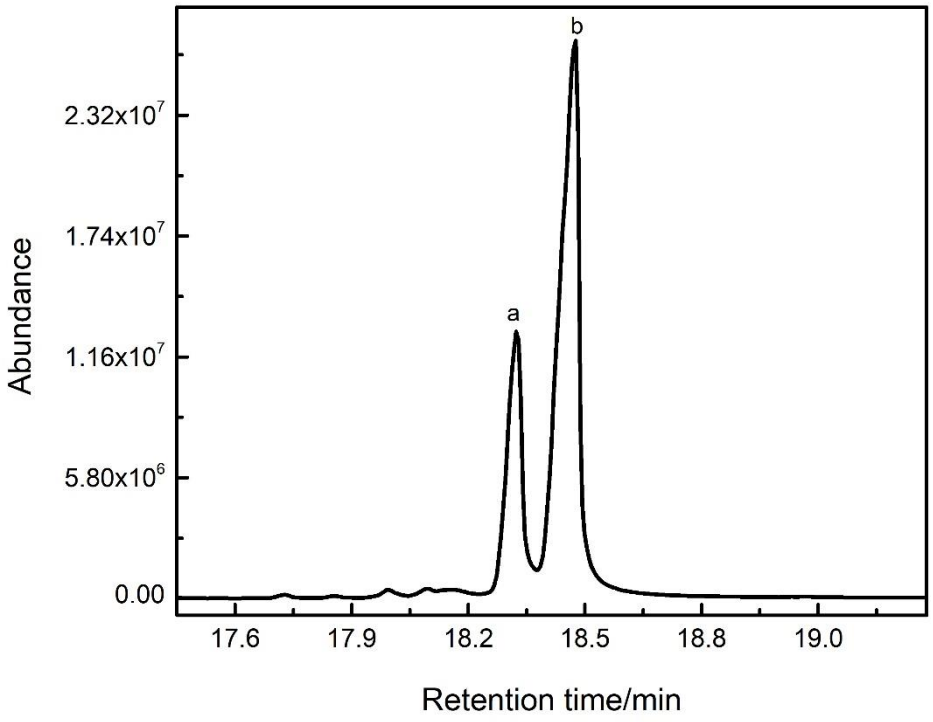

Figure 5.29 The gas chromatogram of derivatised glucose, two p eaks belong to the isomers of Penta-*O*-acetyl-D-glucose methyloxime.

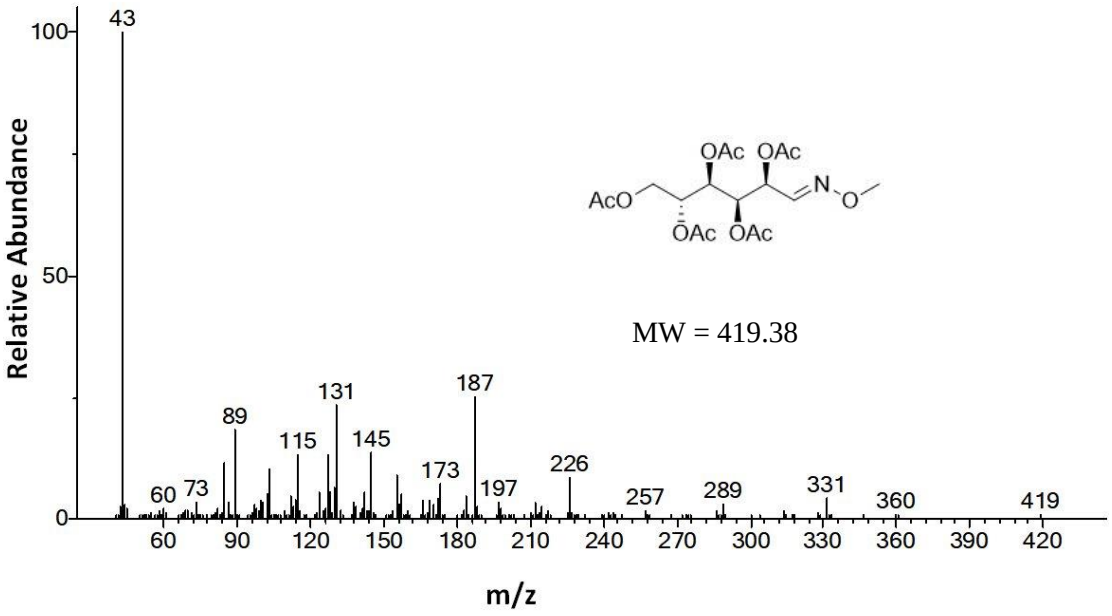

Figure 5.30 The MS spectra of the corresponding peaks (a and b) showed in Figure 5.29 (m/z = 419)

The fragmentation during of Penta-*O*-acetyl-D-glucose methyloxime is categorized by aldo-MOA (methyloxime) and keto-MOA (methyloxime). The collected MS spectrum shows the fragmentation of the glucose derivatives leads to loss different groups of the main backbone. The m/z = 60 belongs to the acetic acid formed due to fragmentation of glucose derivatives or formed during the reaction. The m/z = 131 belong to the fragment of ethyl acetate-MOA and m/z 187 hexyl acetate MOA. The electron ionization m/z at 289 shows the fragment hydroxyimino hexyl triacetate. The m/z = 360 belong to tetra acetyl hexyl MOA.

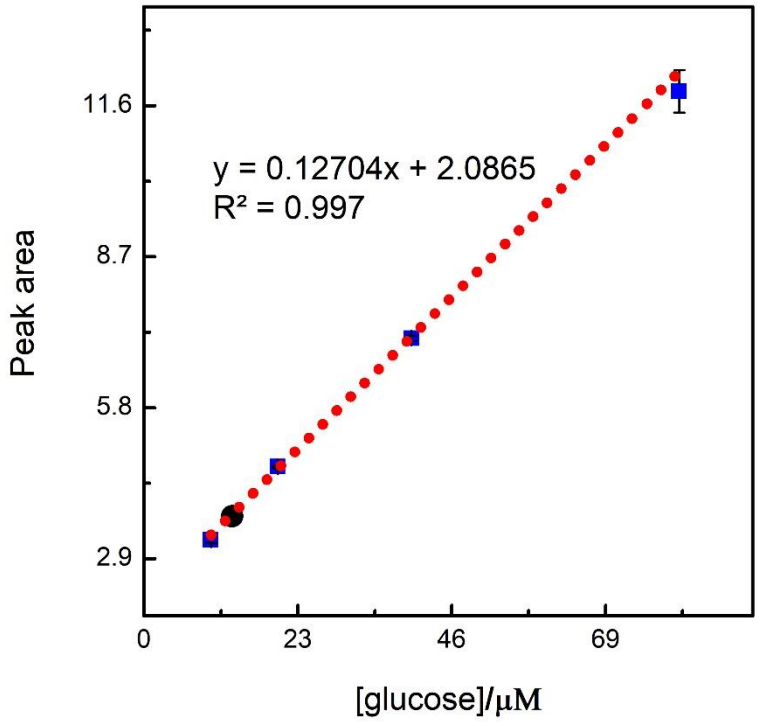

Figure 5.31 The calibration plot of glucose derivatives obtained from GC data for the standard solutions. The unknown glucose concentration in the stimulated saliva for the normal subject A1 was determined and shown in black solid circle.

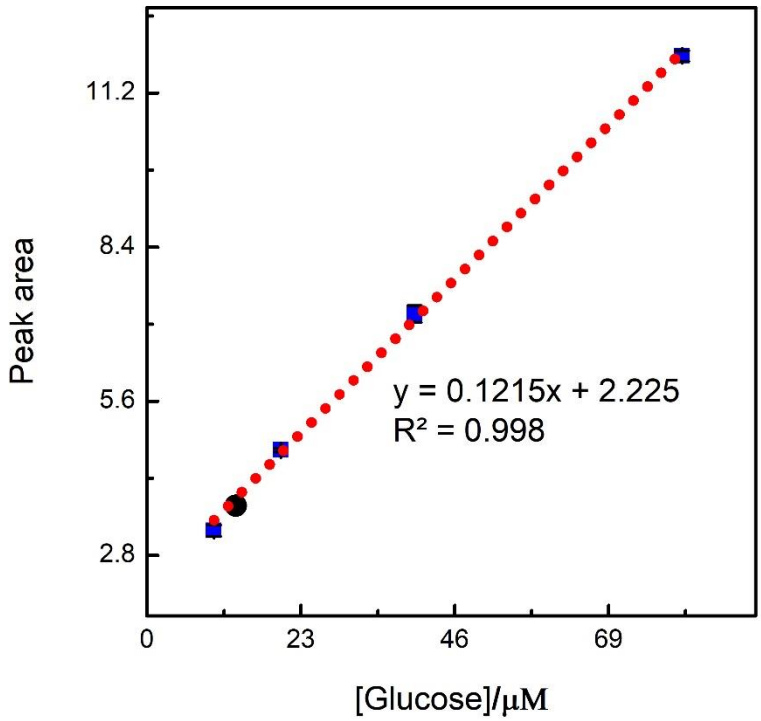

Figure 5.32 The calibration plot of glucose derivatives obtained from GC data for the standard solutions. The unknown glucose concentration in the non-stimulated saliva for the normal subject A1 was determined and shown in black solid circle.

The unknown saliva glucose derivatives concertation was determined from the calibration plot of glucose standard solution from the linear equation. The determined concentration for both stimulated and non-stimulated saliva glucose concentration was then adjusted according to the dilution factors 4.3. The measured glucose concertation for normal subject A1 with stimulated and non-stimulated saliva was 84.4 $\pm$ 1.5 and 91.5 $\pm$ 9.6 respectively.

The method was compared to liquid phase method. In liquid phase QDs and GOx by simply mixed and human saliva was added, followed by the addition of glucose standard. The fluorescence signal was recorded after each addition. The obtained results are shown in the table below in Table 5.4.

Subject	Stimulated (S)/ Non-stimulated (N)	Proposed Solid state Sensor (µM)	Proposed Sensor in liquid phase (µM)	GC-FID (µM)
A1	S	74.2 ± 9.0	82.7 ± 10.4	84.4 ± 1.5
	N	79.0 ± 13.1	89.4 ± 10.2	91.5 ± 9.6
A2	S	83.7 ± 11.0	73.0 ± 6.5	77.2 ± 1.3
	N	87.7 ± 9.9	81.8 ± 9.2	87.9 ± 1.7

Table 5.4 The solid state optical sensor, liquid phase optical sensor response, and GC results for stimulated and non-stimulated saliva glucose.

Overall the non-stimulated saliva glucose concentrations are higher than those in the stimulated saliva in all analytical method used. The GC results show higher glucose concentrations than solid-state and liquid phase sensor. The obtained results were comparable, which justified that optical sensor based on QDs are good candidates for the development of biosensors.

5.3.7 Interference study of glucose sensor

The developed glucose sensor was practically applicable for the measurement glucose in human and artificial saliva and glucose in buffer. The interference study was preform using different interfering agents. The interfering agent used was uric acid, ascorbic acid, albumin, and cysteine. The concentration of all interfering agent used were to 100 µM and effects of all interfering agents were studied separately. The measurement methods were kept constant which was used for glucose analysis in above section for glucose analysis in buffer. The sensors were activated by 100 µL of phosphate buffer for one hour followed by the addition of interfering agents. The experiment was repeated thrice for each interfering agent and the average of fluorescence response were monitor for 440 S.

The obtained results were presented in Figure 5.33 shows that the fluorescence response of 100 µM interfering agents and the fluorescence response of 100 µM of glucose. The data shows that, the sensor was highly responsive to glucose while negligible fluorescence changes were recorded for all other interfering agents. The fluorescence responses of all interfering

agents and glucose for last 100 seconds are shown in Figure 2.33 below, which indicating that the fluorescence was stable.

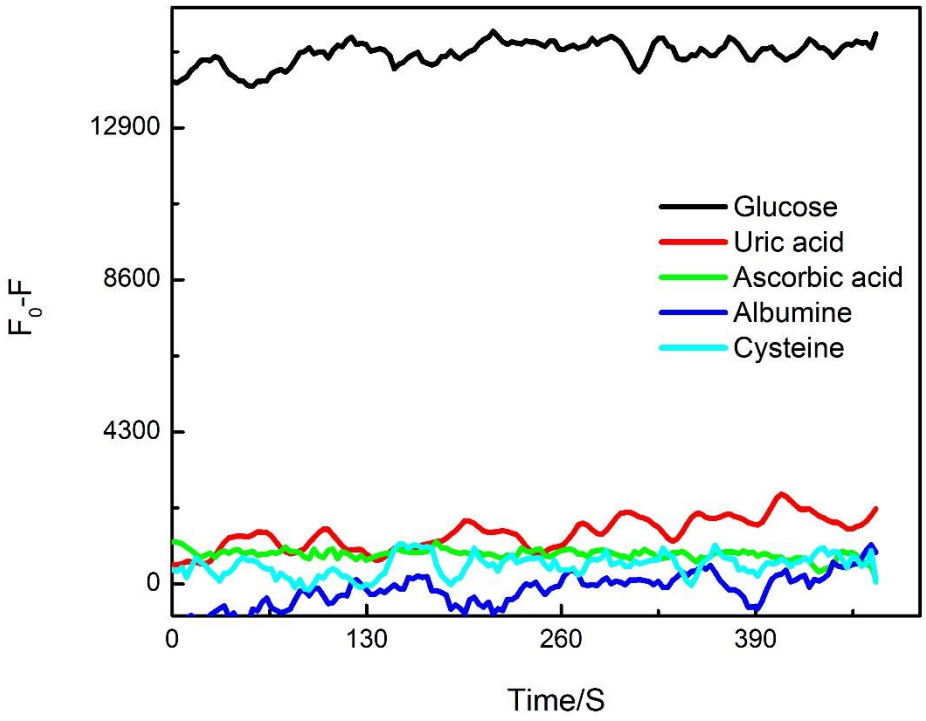

Figure 5.33 The fluorescence response of the solid state glucose sensor to 100 µM glucose, 100 µM Uric acid, 100 µM Ascorbic acid, 1.5 mg/mL of bovine albumins, and 100 µM of cysteine.

The fluorescence response of glucose and other interfering agent was presented in Figure below 5.34. The total fluorescence quenched by 100 µM of glucose was 148578 $\pm$ 8510. While the fluorescence quenched by uric acid, ascorbic acid, and cysteine were 21092 $\pm$ 4046, 389 $\pm$ 254, 561 $\pm$ 450 respectively. The albumin protein slightly enhances the fluorescence to 1420 $\pm$ 421 CPS. The uric acid slightly quench the fluorescence intensity but collective the quenching or fluorescence enhancing effect of interfering agent are negligible in comparison to 100 µM glucose. The resultant data shows that fabricated sensor were with highly selective and sensitivity toward glucose.

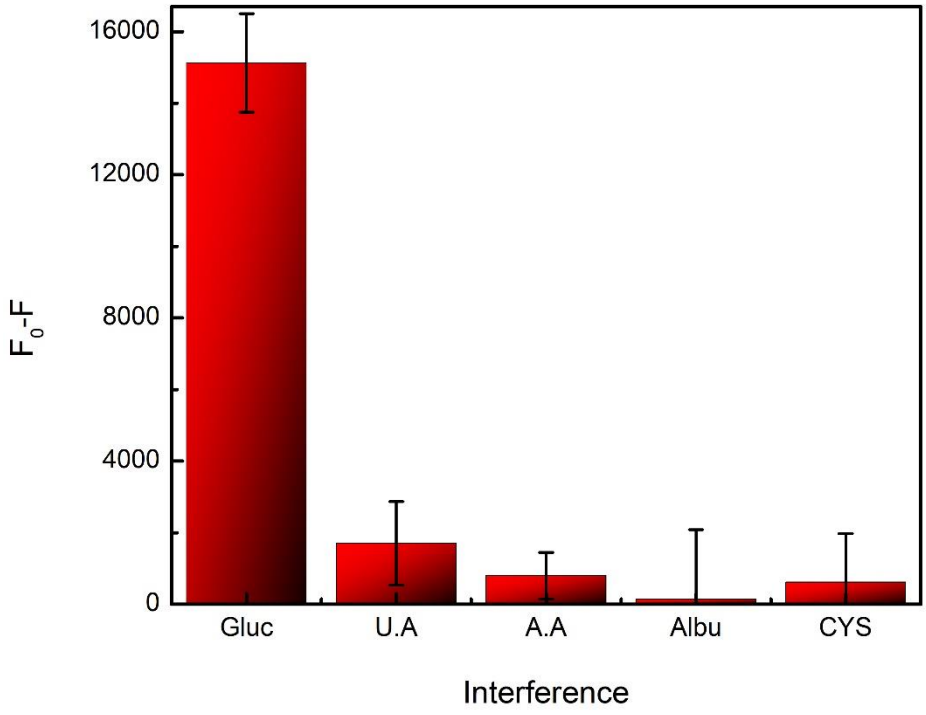

Figure 5.34 Interferences study of solid state glucose sensor with uric acid (U.A) ascorbic acid (A.A) albumin (Alb) and cysteine (CYS).

5.3.8 Stability of glucose sensor

The stability of glucose sensor is important for the practical application. The stability profile of glucose sensor fabricated from QD and polymer composite was studied for 85 days. The storage condition of the sensor was 4 ^{o}C in dark. The calibration was done after each 6 days. The experimental, fabrication procedures, and the storage conditions for all sensors were kept constant. The calibration of glucose sensor obtained from the first day, 35th day and 70th day is shown in Figure 5.35. The slope acquired at 1st, 35th, and 70th day was 0.178, 0.151, and 0.1 respectively. It is shown that glucose sensor was stable for long period of time and can be stored for 35 days in fridge at 4 ^{o}C. After 35 days the 19 % loss of the stability while after 70 days the loss was 43 % loss in stability was recorded.

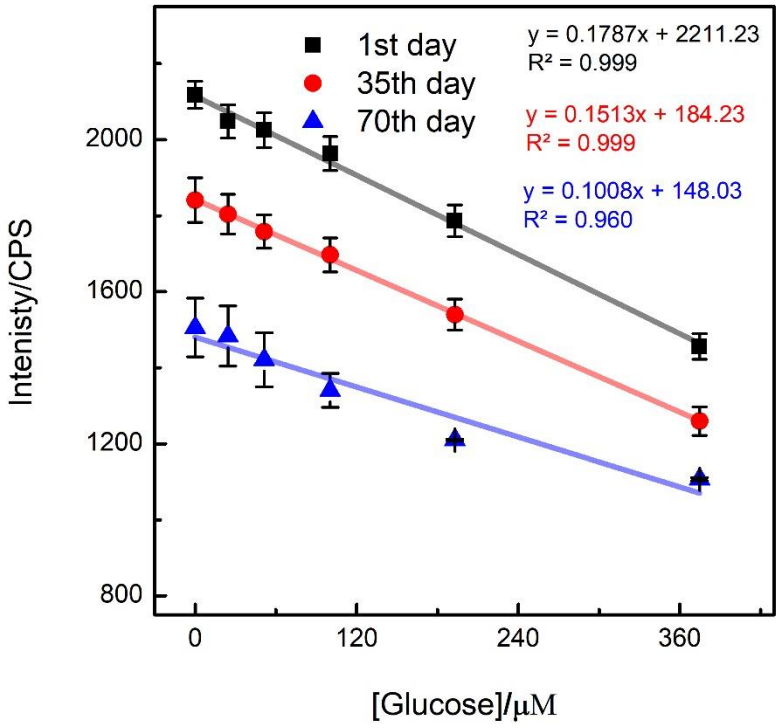

Figure 5.35 The glucose sensors calibrated at 1st day, 30th day and 70th day.

Slopes of the calibrations curve at different intervals during stability analysis of the sensor were plotted against the total time used for the stability study. The obtained Figure 5.36 is presented and showing that the sensor was losing sensitivity gradually within the initial four weeks calibrations, the sensor was stable enough to be used for analysis but afterword a greater loss of sensitivity and hence the performance was reported to be not reliable. In the first four weeks the loss of sensitivity was 18 % which gradually increased to 47 %. The loss of sensitivity was also linearly related to the time period of 63 says.

The stability profile of glucose sensor indicating that the developed glucose sensor was stable for 30 days. The stability of sensors indicating that the materials used and the formulation used for the fabrication of solid state sensor have an outstanding performance.

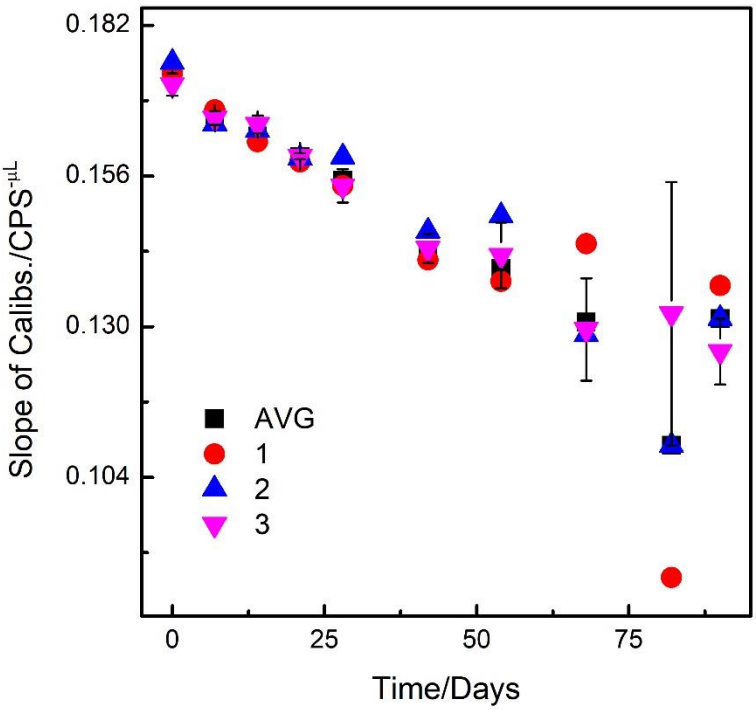

Figure 5.36 The stability profile of the glucose sensor, the slope of the calibration curve achieved at different 6 days intervals versus the total stability period.

5.3.8 Cholesterol measurements

The optical enzymatic cholesterol sensors are few due to the structural features and the solubility of cholesterol in aqueous media. Cholesterol sensing solid state sensor was fabricated using the same techniques reported above for glucose measurements. The ratio of nafion, PVA and QDs were kept constant. The thickness and the dimension of the sensor were also kept unchanged. Glucose oxidase was replaced by cholesterol oxidase that catalyzed the reaction of cholesterol oxidase which releases H_2O_2. The both glucose and cholesterol sensors were based on enzyme oxidase. The fabrication techniques were simple, by changing the single enzyme, the detection strategy was changed from one to another analyte.

The results obtained using solid state cholesterol sensor for the detection of cholesterol is shown in Figure 5.37 and 5.38. The fluorescence spectra in Figure 5.36 were presented for the activated sensor by 120 µL of phosphate buffer after one hours and the resultant fluorescence quenched by the addition of 9.9 to 439 µM of cholesterol.

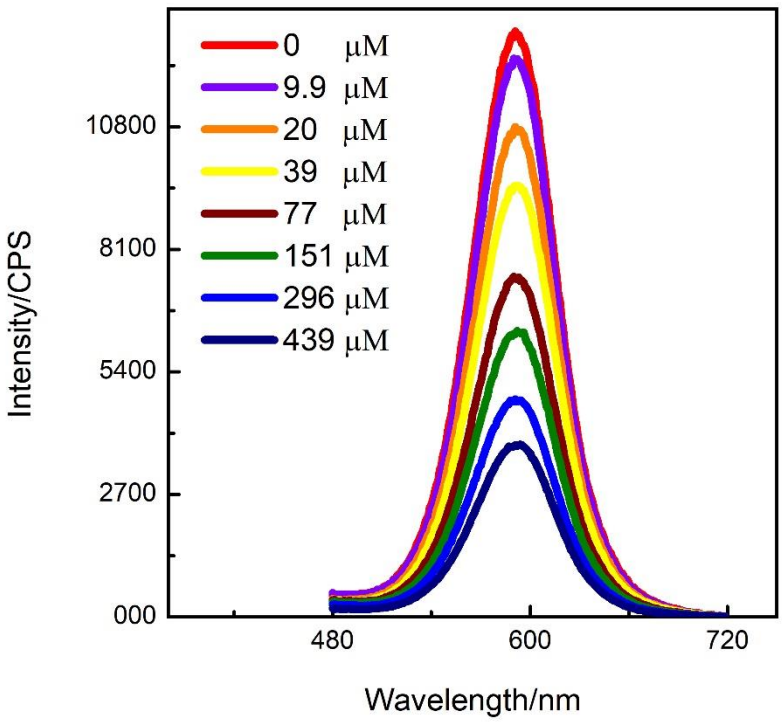

Figure 5.37 The fluorescence emission spectra of cholesterol sensor quenched by the addition of cholesterol. (N= 3).

The fluorescence response of the cholesterol sensor was plotted against the cholesterol concentrations used 9.9 to 439 µM. The linearity was from 9.9 to 150 µM with correlation coefficient of 0.987. The detection limit was calculated from the standard deviation of the blank and the slope of the linear range which was 5.4 µM. The cholesterol concentration was measured a low range and the sensor interference was also studied in details.

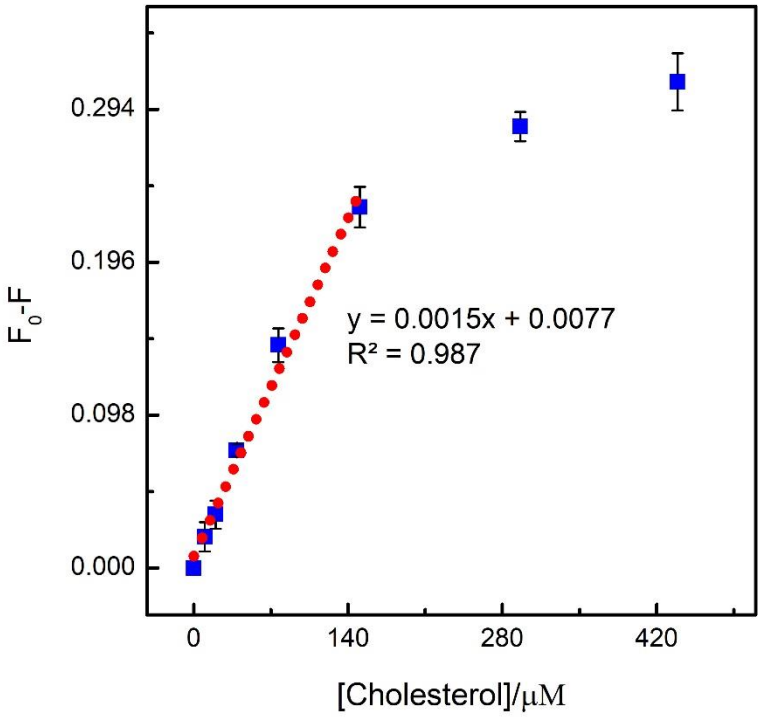

Figure 5.38 The response of cholesterol sensor by the addition of 9 to 400 μM of cholesterol.

5.3.9 Interference study of cholesterol sensor

The common interfering compound for the cholesterol sensor is cysteine, uric acid, ascorbic acid, albumin, and glucose. The cholesterol sensor interference studies were preform using a selected species; uric acid, glucose, ascorbic acid, albumin, and cysteine. The intrusion in the fluorescence intensity of the solid state sensor caused by all interfering agent were measure individually.

The methods of analysis were kept constant as mention in a section above for cholesterol measurements as well the concentration of all interfering agents and cholesterol were also kept constant (100 μM for all except albumin which were 1.5 mg/mL), hence it was possible to compare the total interference caused by individual interfering agent. The cholesterol sensor was pre-hydrated by phosphate buffer one hour prior to the analysis and the aliquot of interfering agent was added followed by the measurement of fluorescence response to the respective interfering agent.

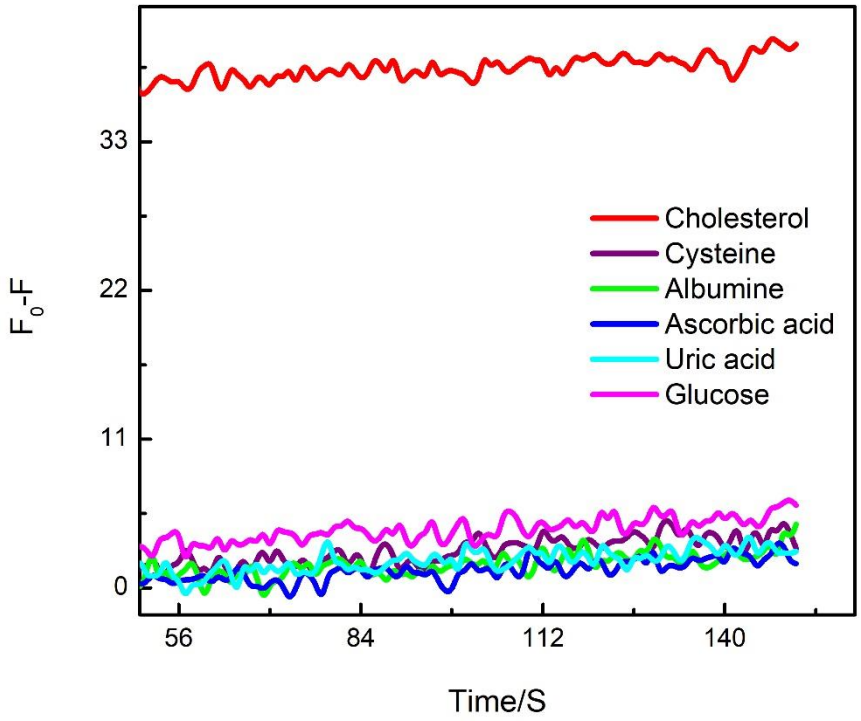

Figure 5.39 The fluorescence response of 100 µM cholesterol, all other interfering agents (100 µM except albumin 1.5 mg/mL).

The fluorescence response of 100 µM cholesterol and cysteine, glucose, uric acid, ascorbic acid and 1.5 mg/mL of albumin is presented in Figure 2.39. The results shows that 100 µM of cholesterol significantly quenched the fluoresce intensity of QDs within membrane. The albumin slightly enhancing the fluorescence whiles the other interfering agents quenching the fluorescence.

The fluorescence responses of all species were compared in bar chat represented in Figure 5.40. The total fluorescence quenched by 100 µM of cholesterol was 20 % while other has negligible effect. The response was 1.0 %, 1.5 %, 0.6 %, -1.1% (increase in fluorescence), and 0.6 % for glucose, uric acid, ascorbic acid, albumin, and cysteine respectively.

The interference study confirms that the sensor has specificity to cholesterol and detecting cholesterol at low level hence the develop sensor could be used for cholesterol measurements.

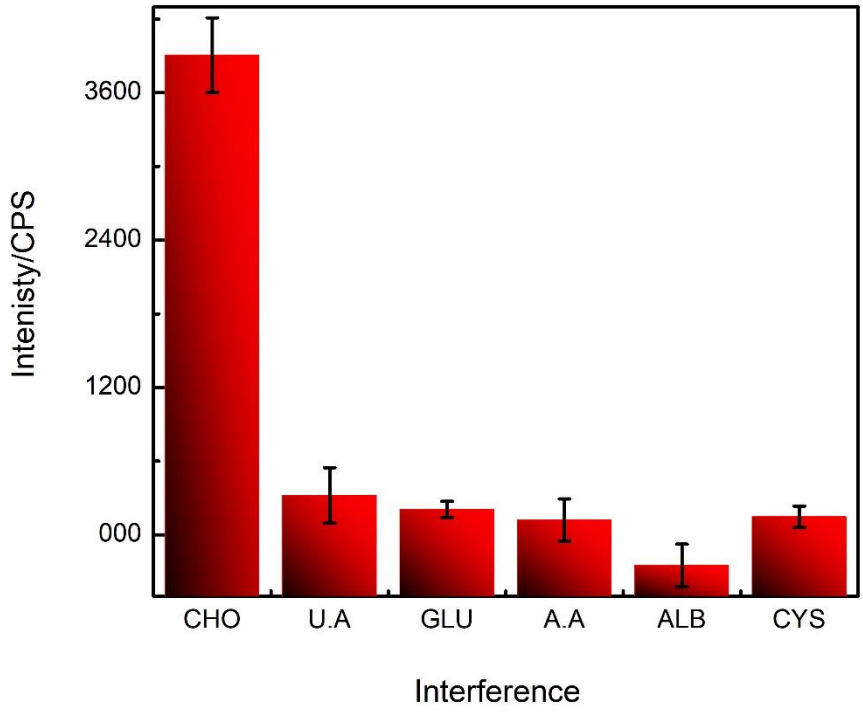

Figure 5.40 The bar chat of interferences study of cholesterol sensor by uric acid (U.A), glucose (GLU), ascorbic acid (A.A) albumin (Alb) and cysteine (CYS).

5.4 Conclusion

In this study, the QDs were used to develop reliable sensors that can detect saliva glucose and detect low cholesterol concentrations. The QDs embedded in a polymeric matrix that stabilized QDs environment interference and increasing the performance optical signal. The encapsulated QDs had a high optical response to H_2O_2, glucose, and cholesterol. The polymers composition was optimized for all the species to be measured. The developed sensors based on QD encapsulation in polymers provide a new platform for optical analysis with greater sensitivity and selectivity. The sensor was used to detect glucose in human saliva, which was 94.2, 72.2, 62.2 for normal subject, and 141.04 for diabetes. The developed sensors are with high stability and resist to interference and could be applicable for hospital applications.

5.5 References

(1) Wilson, D. M.; Hoyt, S.; Janata, J.; Booksh, K.; Obando, L. Chemical sensors for portable, handheld field instruments. *IEEE Sensors Journal* **2001,** *1* (4), 256.

(2) Taib, M. N.; Narayanaswamy, R. Solid-state instruments for optical fibre chemical sensors. A review. *Analyst* **1995,** *120* (6), 1617.

(3) Kenry; Yeo, J. C.; Lim, C. T. Emerging flexible and wearable physical sensing platforms for healthcare and biomedical applications. *Microsystems & Nanoengineering* **2016,** *2*, 16043.

(4) Shukla, S. K.; Demir, M. M.; Govender, P. P.; Tiwari, A.; Shukla, S. K. Optical fibre based non-enzymatic glucose sensing over Cu2+-doped polyaniline hybrid matrix. *Sensors and Actuators B: Chemical* **2017,** *242*, 522.

(5) Portaccio, M.; Lepore, M.; Della Ventura, B.; Stoilova, O.; Manolova, N.; Rashkov, I.; Mita, D. G. Fiber-optic glucose biosensor based on glucose oxidase immobilised in a silica gel matrix. *Journal of Sol-Gel Science and Technology* **2009,** *50* (3), 437.

(6) Hussain, F.; Birch, D. J. S.; Pickup, J. C. Glucose sensing based on the intrinsic fluorescence of sol-gel immobilized yeast hexokinase. *Analytical Biochemistry* **2005,** *339* (1), 137.

(7) Sierra, J. F.; Galbán, J.; Castillo, J. R. Determination of Glucose in Blood Based on the Intrinsic Fluorescence of Glucose Oxidase. *Analytical Chemistry* **1997,** *69* (8), 1471.

(8) Sanz, V.; de Marcos, S.; Galbán, J. Direct glucose determination in blood using a reagentless optical biosensor. *Biosensors and Bioelectronics* **2007,** *22* (12), 2876.

(9) Im, S. H.; Kim, K. R.; Park, Y. M.; Yoon, J. H.; Hong, J. W.; Yoon, H. C. An animal cell culture monitoring system using a smartphone-mountable paper-based analytical device. *Sensors and Actuators B: Chemical* **2016,** *229*, 166.

(10) Sanz, V.; Galban, J.; de Marcos, S.; Castillo, J. R. Fluorometric sensors based on chemically modified enzymes: Glucose determination in drinks. *Talanta* **2003,** *60* (2–3), 415.

(11) Trettnak, W.; Leiner, M. J. P.; Wolfbeis, O. S. Optical sensors. Part 34. Fibre optic glucose biosensor with an oxygen optrode as the transducer. *Analyst* **1988,** *113* (10), 1519.

(12) Papkovsky, D. B.; Ovchinnikov, A. N.; Ogurtsov, V. I.; Ponomarev, G. V.; Korpela, T. Biosensors on the basis of luminescent oxygen sensor: the use of microporous light-scattering support materials. *Sensors and Actuators B: Chemical* **1998,** *51* (1–3), 137.

(13) Chang, G.; Tatsu, Y.; Goto, T.; Imaishi, H.; Morigaki, K. Glucose concentration determination based on silica sol–gel encapsulated glucose oxidase optical biosensor arrays. *Talanta* **2010,** *83* (1), 61.

(14) Brown, J. Q.; McShane, M. J. Modeling of spherical fluorescent glucose microsensor systems: Design of enzymatic smart tattoos. *Biosensors and Bioelectronics* **2006,** *21* (9), 1760.

(15) Wolfbeis, O. S.; Schäferling, M.; Dürkop, A. Reversible Optical Sensor Membrane for Hydrogen Peroxide Using an Immobilized Fluorescent Probe, and its Application to a Glucose Biosensor. *Microchimica Acta* **2003,** *143* (4), 221.

(16) Chih, T.; Jao, H.-J.; Wang, C. M. Glucose sensing based on an effective conversion of O2 and H2O2 into superoxide anion radical with clay minerals. *Journal of Electroanalytical Chemistry* **2005,** *581* (2), 159.

(17) De Luca, P.; Lepore, M.; Portaccio, M.; Esposito, R.; Rossi, S.; Bencivenga, U.; Mita, D. Glucose Determination by Means of Steady-state and Time-course UV Fluorescence in Free or Immobilized Glucose Oxidase. *Sensors* **2007,** *7* (11), 2612.

(18) Papkovsky, D. B. Luminescent porphyrins as probes for optical (bio)sensors. *Sensors and Actuators B: Chemical* **1993,** *11* (1), 293.

(19) Zhou, Z.; Qiao, L.; Zhang, P.; Xiao, D.; Choi, M. M. F. An optical glucose biosensor based on glucose oxidase immobilized on a swim bladder membrane. *Analytical and Bioanalytical Chemistry* **2005,** *383* (4), 673.

(20) Yang, X.; Zhou, Z.; Xiao, D.; Choi, M. M. F. A fluorescent glucose biosensor based on immobilized glucose oxidase on bamboo inner shell membrane. *Biosensors and Bioelectronics* **2006,** *21* (8), 1613.

(21) Duong, H. D.; Rhee, J. I. Preparation and characterization of sensing membranes for the detection of glucose, lactate and tyramine in microtiter plates. *Talanta* **2007,** *72* (4), 1275.

(22) Li, X.; Zhou, Y.; Zheng, Z.; Yue, X.; Dai, Z.; Liu, S.; Tang, Z. Glucose Biosensor Based on Nanocomposite Films of CdTe Quantum Dots and Glucose Oxidase. *Langmuir* **2009,** *25* (11), 6580.

(23) Odaci, D.; Gacal, B. N.; Gacal, B.; Timur, S.; Yagci, Y. Fluorescence Sensing of Glucose Using Glucose Oxidase Modified by PVA-Pyrene Prepared via "Click" Chemistry. *Biomacromolecules* **2009,** *10* (10), 2928.

(24) Moreels, I.; Justo, Y.; De Geyter, B.; Haustraete, K.; Martins, J. C.; Hens, Z. Size-tunable, bright, and stable PbS quantum dots: a surface chemistry study. *Acs Nano* **2011,** *5* (3), 2004.

(25) Green, M. The nature of quantum dot capping ligands. *Journal of Materials Chemistry* **2010,** *20* (28), 5797.

(26) Ji, B.; Giovanelli, E.; Habert, B.; Spinicelli, P.; Nasilowski, M.; Xu, X.; Lequeux, N.; Hugonin, J.-P.; Marquier, F.; Greffet, J.-J. Non-blinking quantum dot with a plasmonic nanoshell resonator. *Nature nanotechnology* **2015,** *10* (2), 170.

(27) Müller, M.; Kaiser, M.; Stachowski, G. M.; Resch-Genger, U.; Gaponik, N.; Eychmüller, A. Photoluminescence Quantum Yield and Matrix-Induced Luminescence Enhancement of Colloidal Quantum Dots Embedded in Ionic Crystals. *Chemistry of Materials* **2014,** *26* (10), 3231.

(28) Dubertret, B.; Skourides, P.; Norris, D. J.; Noireaux, V.; Brivanlou, A. H.; Libchaber, A. In Vivo Imaging of Quantum Dots Encapsulated in Phospholipid Micelles. *Science* **2002,** *298* (5599), 1759.

(29) Hu, X.; Gao, X. Silica− Polymer Dual Layer-Encapsulated Quantum Dots with Remarkable Stability. *ACS nano* **2010,** *4* (10), 6080.

(30) Talapin, D. V.; Poznyak, S. K.; Gaponik, N. P.; Rogach, A. L.; Eychmüller, A. Synthesis of surface-modified colloidal semiconductor nanocrystals and study of photoinduced charge separation and transport in nanocrystal-polymer composites. *Physica E: Low-dimensional Systems and Nanostructures* **2002,** *14* (1–2), 237.

(31) Gaponik, N.; Rogach, A. L. Thiol-capped CdTe nanocrystals: progress and perspectives of the related research fields. *Physical Chemistry Chemical Physics* **2010,** *12* (31), 8685.

(32) Lee, J.; Sundar, V. C.; Heine, J. R.; Bawendi, M. G.; Jensen, K. F. Full color emission from II–VI semiconductor quantum dot–polymer composites. *Advanced Materials* **2000,** *12* (15), 1102.

(33) Zhang, H.; Cui, Z.; Wang, Y.; Zhang, K.; Ji, X.; Lü, C.; Yang, B.; Gao, M. From Water-Soluble CdTe Nanocrystals to Fluorescent Nanocrystal–Polymer Transparent Composites Using Polymerizable Surfactants. *Advanced Materials* **2003,** *15* (10), 777.

(34) Demir, H. V.; Nizamoglu, S.; Erdem, T.; Mutlugun, E.; Gaponik, N.; Eychmüller, A. Quantum dot integrated LEDs using photonic and excitonic color conversion. *Nano Today* **2011,** *6* (6), 632.

(35) Otto, T.; Müller, M.; Mundra, P.; Lesnyak, V.; Demir, H. V.; Gaponik, N.; Eychmüller, A. Colloidal Nanocrystals Embedded in Macrocrystals: Robustness, Photostability, and Color Purity. *Nano Letters* **2012,** *12* (10), 5348.

(36) Luccardini, C.; Tribet, C.; Vial, F.; Marchi-Artzner, V.; Dahan, M. Size, Charge, and Interactions with Giant Lipid Vesicles of Quantum Dots Coated with an Amphiphilic Macromolecule. *Langmuir* **2006,** *22* (5), 2304.

(37) Gao, X.; Cui, Y.; Levenson, R. M.; Chung, L. W. K.; Nie, S. In vivo cancer targeting and imaging with semiconductor quantum dots. *Nat Biotech* **2004,** *22* (8), 969.

(38) Liu, J.; Chen, H.; Lin, Z.; Lin, J.-M. Preparation of Surface Imprinting Polymer Capped Mn-Doped ZnS Quantum Dots and Their Application for Chemiluminescence Detection of 4-Nitrophenol in Tap Water. *Analytical Chemistry* **2010,** *82* (17), 7380.

(39) Boulmedais, F.; Bauchat, P.; Brienne, M. J.; Arnal, I.; Artzner, F.; Gacoin, T.; Dahan, M.; Marchi-Artzner, V. Water-Soluble Pegylated Quantum Dots: From a Composite Hexagonal Phase to Isolated Micelles. *Langmuir* **2006,** *22* (23), 9797.

(40) Guo, L.; Yang, S.; Yang, C.; Yu, P.; Wang, J.; Ge, W.; Wong, G. K. L. Highly monodisperse polymer-capped ZnO nanoparticles: Preparation and optical properties. *Applied Physics Letters* **2000,** *76* (20), 2901.

(41) Pellegrino, T.; Manna, L.; Kudera, S.; Liedl, T.; Koktysh, D.; Rogach, A. L.; Keller, S.; Rädler, J.; Natile, G.; Parak, W. J. Hydrophobic nanocrystals coated with an amphiphilic polymer shell: a general route to water soluble nanocrystals. *Nano letters* **2004,** *4* (4), 703.

(42) Mancini, M. C.; Kairdolf, B. A.; Smith, A. M.; Nie, S. Oxidative Quenching and Degradation of Polymer-Encapsulated Quantum Dots: New Insights into the Long-

Term Fate and Toxicity of Nanocrystals in Vivo. *Journal of the American Chemical Society* **2008,** *130* (33), 10836.

(43) Milliron, D. J.; Alivisatos, A. P.; Pitois, C.; Edder, C.; Fréchet, J. M. J. Electroactive Surfactant Designed to Mediate Electron Transfer Between CdSe Nanocrystals and Organic Semiconductors. *Advanced Materials* **2003,** *15* (1), 58.

(44) Skaff, H.; Emrick, T. The use of 4-substituted pyridines to afford amphiphilic, pegylated cadmium selenide nanoparticles. *Chemical Communications* **2003**, DOI:10.1039/B208718A 10.1039/B208718A(1), 52.

(45) Mitchell, G. P.; Mirkin, C. A.; Letsinger, R. L. Programmed Assembly of DNA Functionalized Quantum Dots. *Journal of the American Chemical Society* **1999,** *121* (35), 8122.

(46) Empedocles, S. A.; Bawendi, M. G. Quantum-confined stark effect in single CdSe nanocrystallite quantum dots. *Science* **1997,** *278* (5346), 2114.

(47) da S. Pinto, T.; Alves, L. A.; de Azevedo Cardozo, G.; Munhoz, V. H. O.; Verly, R. M.; Pereira, F. V.; de Mesquita, J. P. Layer-by-layer self-assembly for carbon dots/chitosan-based multilayer: Morphology, thickness and molecular interactions. *Materials Chemistry and Physics* **2017,** *186*, 81.

(48) Yang, G.; Shen, P.; Tan, K.; Xia, Y. Quantum dots and polymer hybrid composites: new insights into fluorescence switch and turn-on anion sensing. *Microchimica Acta* **2014,** *181* (5), 607.

(49) Bae, W. K.; Kwak, J.; Lim, J.; Lee, D.; Nam, M. K.; Char, K.; Lee, C.; Lee, S. Multicolored Light-Emitting Diodes Based on All-Quantum-Dot Multilayer Films Using Layer-by-Layer Assembly Method. *Nano Letters* **2010,** *10* (7), 2368.

(50) Constantine, C. A.; Gattás-Asfura, K. M.; Mello, S. V.; Crespo, G.; Rastogi, V.; Cheng, T.-C.; DeFrank, J. J.; Leblanc, R. M. Layer-by-Layer Biosensor Assembly Incorporating Functionalized Quantum Dots. *Langmuir* **2003,** *19* (23), 9863.

(51) Tomczak, N.; Jańczewski, D.; Han, M.; Vancso, G. J. Designer polymer–quantum dot architectures. *Progress in Polymer Science* **2009,** *34* (5), 393.

(52) Mauritz, K. A.; Moore, R. B. State of understanding of Nafion. *Chemical reviews* **2004,** *104* (10), 4535.

(53) Zawodzinski, T. A.; Derouin, C.; Radzinski, S.; Sherman, R. J.; Smith, V. T.; Springer, T. E.; Gottesfeld, S. Water uptake by and transport through Nafion® 117 membranes. *Journal of the electrochemical society* **1993,** *140* (4), 1041.

(54) Frasco, M. F.; Chaniotakis, N. Semiconductor quantum dots in chemical sensors and biosensors. *Sensors (Basel)* **2009,** *9* (9), 7266.

(55) Frigerio, C.; Ribeiro, D. S.; Rodrigues, S. S.; Abreu, V. L.; Barbosa, J. A.; Prior, J. A.; Marques, K. L.; Santos, J. L. Application of quantum dots as analytical tools in automated chemical analysis: a review. *Anal Chim Acta* **2012,** *735*, 9.

(56) Samms, S.; Wasmus, S.; Savinell, R. Thermal stability of Nafion® in simulated fuel cell environments. *Journal of the Electrochemical Society* **1996,** *143* (5), 1498.

(57) Hallensleben, M. L.; Fuss, R.; Mummy, F. Polyvinyl compounds, others. *Ullmann's Encyclopedia of Industrial Chemistry* **2000**.

(58) Grassie, N.; Melville, H. Proceedings of the Royal Society of London A: Mathematical, Physical and Engineering Sciences, 1949; p 1.

(59) Shao, Z.-G.; Wang, X.; Hsing, I. M. Composite Nafion/polyvinyl alcohol membranes for the direct methanol fuel cell. *Journal of Membrane Science* **2002,** *210* (1), 147.

(60) Mollá, S.; Compañ, V. Performance of composite Nafion/PVA membranes for direct methanol fuel cells. *Journal of Power Sources* **2011,** *196* (5), 2699.

(61) Mollá, S.; Compañ, V.; Gimenez, E.; Blazquez, A.; Urdanpilleta, I. Novel ultrathin composite membranes of Nafion/PVA for PEMFCs. *International Journal of Hydrogen Energy* **2011,** *36* (16), 9886.

(62) DeLuca, N. W.; Elabd, Y. A. Nafion®/poly(vinyl alcohol) blends: Effect of composition and annealing temperature on transport properties. *Journal of Membrane Science* **2006,** *282* (1–2), 217.

(63) Liu, Y.; Zhao, X.; Cai, B.; Pei, T.; Tong, Y.; Tang, Q.; Liu, Y. Controllable fabrication of oriented micro/nanowire arrays of dibenzo-tetrathiafulvalene by a multiple drop-casting method. *Nanoscale* **2014,** *6* (3), 1323.

(64) Park, J.; Lee, S.; Lee, H. H. High-mobility polymer thin-film transistors fabricated by solvent-assisted drop-casting. *Organic Electronics* **2006,** *7* (5), 256.

(65) Bussetti, G.; Trabattoni, S.; Uttiya, S.; Sassella, A.; Riva, M.; Picone, A.; Brambilla, A.; Duò, L.; Ciccacci, F.; Finazzi, M. Controlling drop-casting deposition of 2D Pt-octaethyl porphyrin layers on graphite. *Synthetic Metals* **2014,** *195*, 201.

(66) Zhu, X.; Zhu, L.; Chen, H.; Yang, L.; Zhang, W. Micro-ball lens structure fabrication based on drop on demand printing the liquid mold. *Applied Surface Science* **2016,** *361*, 80.

(67) Claver, J. B.; Mirón, M. V.; Capitán-Vallvey, L. Disposable electrochemiluminescent biosensor for lactate determination in saliva. *Analyst* **2009,** *134* (7), 1423.

(68) Li, Y.; Fang, X.; Wang, Y.; Ma, B.; Sun, J. Highly Transparent and Water-Enabled Healable Antifogging and Frost-Resisting Films Based on Poly(vinyl alcohol)–Nafion Complexes. *Chemistry of Materials* **2016,** *28* (19), 6975.

(69) Vishnyakov, A.; Neimark, A. V. Self-assembly in nafion membranes upon hydration: Water mobility and adsorption isotherms. *The Journal of Physical Chemistry B* **2014,** *118* (38), 11353.

(70) Vishnyakov, A.; Neimark, A. V. Molecular Simulation Study of Nafion Membrane Solvation in Water and Methanol. *The Journal of Physical Chemistry B* **2000,** *104* (18), 4471.

(71) Doyle, M.; Rajendran, G. In *Handbook of Fuel Cells*; John Wiley & Sons, Ltd, **2010**, 41, (1) 54.

(72) Kwon, O.; Park, S.; Kim, J. G.; Son, B.; Lee, D.-H. Morphological characterization of sulfonated graphene and Nafion composite membrane by dynamic mode atomic force microscopy. *International Journal of Energy Research* **2015,** *39* (12), 1698.

(73) Mecheri, B.; Felice, V.; D'Epifanio, A.; Tavares, A. C.; Licoccia, S. Composite Polymer Electrolytes for Fuel Cell Applications: Filler-Induced Effect on Water Sorption and Transport Properties. *ChemPhysChem* **2013,** *14* (16), 3814.

(74) Sutor, A. K.; Huguet, P.; Morin, A.; Gebel, G.; Le, T. S.; Deabate, S. Influence of Compressive Stress on the Water Content of Perfluorosulphonated Membranes: A μ-Raman Study. *Fuel Cells* **2012,** *12* (2), 162.

(75) Quintero, S. M. M.; Ponce F, R. V.; Cremona, M.; Triques, A. L. C.; d'Almeida, A. R.; Braga, A. M. B. Swelling and morphological properties of poly(vinyl alcohol) (PVA) and poly(acrylic acid) (PAA) hydrogels in solution with high salt concentration. *Polymer* **2010,** *51* (4), 953.

(76) Shin, J.; Kim, J.-C.; Chang, J.-H. Flexible clay hybrid films with various poly(vinyl alcohol) contents: Thermal properties, morphology, optical transparency, and gas permeability. *Macromolecular Research* **2013,** *21* (12), 1349.

(77) Dame, Z. T.; Aziat, F.; Mandal, R.; Krishnamurthy, R.; Bouatra, S.; Borzouie, S.; Guo, A. C.; Sajed, T.; Deng, L.; Lin, H.et al. The human saliva metabolome. *Metabolomics* **2015,** *11* (6), 1864.

(78) Wu, H.; Lu, L.; Zhang, Y.; Sun, Z.; Qian, L. A facile method to prepare porous graphene with tunable structure as electrode materials for immobilization of glucose oxidase. *Colloids and Surfaces A: Physicochemical and Engineering Aspects* **2016,** *502*, 26.

(79) Ren, G.; Xu, X.; Liu, Q.; Cheng, J.; Yuan, X.; Wu, L.; Wan, Y. Electrospun poly(vinyl alcohol)/glucose oxidase biocomposite membranes for biosensor applications. *Reactive and Functional Polymers* **2006,** *66* (12), 1559.

Chapter 6. The development of QDs based sensors; concluding remarks

6.1 Objectives and approach

The determination and monitoring of glucose are important analytical tasks for the researchers. Developing a sensitive and selective sensor for the monitoring of glucose in saliva or tear could help practitioners and hospital to use saliva as a glucose indicator instead of blood. The blood glucose concentration is high enough to be adequate for monitoring but it is quite challenging to use blood for continues non-invasive monitoring of glucose, especially continuous blood sampling from the patient under intensive care and suffering from diabetics may cause metabolic syndromes severe[1,2].

A great importance is attached to replace this painful sampling procedure and using saliva is the best alternative, as it can be used as a biomarker for the analysis of glucose[3] but due to the presence of very low concentration of glucose, it has been challenging for the scientific community. The average range of blood glucose in a common sample is 4 to 5.9 mM but for glucose in saliva this value is quite lower, about 0.070 mM, which is almost 2% as compared to blood [4]. Therefore highly sensitive and selective of the sensor are required to detect glucose in saliva.

The objective of this work was to develop a high-performance and sensitive sensor with improved selectivity that can measure glucose at very low concentration range as well as detect glucose in saliva. To achieve this objective fluorescence technique was adopted and Quantum Dots (QDs) were used as fluorescence prob. The design of the study was to synthesis and characterization biocompatible QDs, selection of QDs with high performance and high fluorescence stability for enzymatic glucose sensing. The sensor stability at physiological pH and the calibration with hydrogen peroxide in a liquid phase was an initial objective. The aqueous phase calibration was performed for H_2O_2, glucose cholesterol which helped to design

the solid-state sensor. The ultimate goal was to design and fabricate a solid-state sensor that is robust, sensitive, and selective enough to detect glucose at low concentration range.

6.2 The brief summary of the results

The chapter first reviews the existing glucose, cholesterol sensors, and methods and materials used for detections. The gaps and the limitation of the existing sensors, was discus and concluded to be used QDs with excellent optical properties and the highly sensitive fluorescence detection techniques can potentially increase the performance of the glucose and cholesterol sensor.

Chapter two consists of QDs synthesis and characterizations of selective and biocompatible thiol capped QDs. Chapter three work explain the pH sensitivity of QDs at different ranges and selection of the most sensitive QDs to hydrogen peroxide. GHS capped QDs was selected which have sensitivity of 4243.9 CPS/µM in the linear range of 100 to 1200 µM with detection limit of 49.9 µM, hence the GHS capped QDs was used for further sensor developments.

Chapter 4 centered and explains the kinetic aspect of the H_2O_2, glucose, and cholesterol measurements. The pseudo-first order kinetic model was established and validated. The rates constants were used as a tool that can be used to measure the hydrogen peroxide, glucose, and cholesterol concentrations. The kinetic method of analysis was also validated by bio-kinetic stopped flow.

Chapter 5 describing the development and optimization of solid state hydrogen peroxide, glucose, and cholesterol sensor. The QDs were encapsulated in polymer membrane which extremely sensitive to hydrogen peroxide, glucose. The solid state sensor was optimized at different GOx, QDs, and polymer ratios for the optimum range of glucose analysis i.e. 5 to 300 µM. The sensor was used to detect glucose in artificial saliva and human saliva for normal and diabetic subjects. The developed sensor was further used to measured cholesterol.

6.3 QDs preparations characterizations and selection.

The highly fluorescent water soluble, and stable CdTe with different thiol capped (CYS, GHS, MPA, and MSA) were synthesized and characterized. We revolved that MPA and GHS QDs are easy and fast in synthesis. GHS capped allow us to select a wide range of emission spectra (514 to 612 nm) and GHS capped QDs are the smalllist QDs than MPA, MSA and CYS.

Appropriate QDs for the glucose and cholesterol sensing application was selected. Initially the pH sensitivity of QDs was investigated at different pH ranges. It was concluded that QDs are highly sensitive to pH change, hence the buffer of physiological pH was used for all analysis. The sensitivity of selected thiol capped QDs for H_2O_2 was determined and highly selective QDs were GHS and MPA capped. The sensitivity of GHS and MPA QDs were 4243.9 2624.2 CPS/µM respectively. The linear range was 100 to 1200 and 100 with detection limit of 49.9 µM for GHS capped QDs and 100 to 750 µM with detection limit of 55.07 µM for MPA capped QDs.

6.3 Summary of liquid phase measurements

The QDs responses to H_2O_2, glucose and cholesterol were investigated in an aqueous phase by two different methods; equilibrium (end point) and kinetic method. Initially an equilibrium method was used and optimized for H_2O_2, glucose, and cholesterol measurements. The linear range of measurement for H_2O_2, glucose and cholesterol was 4 to 237, 33 to 336, and 205 to 26 µM respectively. The detection limits achieved was 0.4, 8.2, and 1.5 µM respectively for H_2O_2, glucose, and cholesterol. Using this model the glucose concentrations detected was nine times lower the glucose in saliva for a normal subjects.

6.4 Development of kinetic method of analysis for biomarkers

The role of kinetic methods in analytical science is under-utilized, the kinetics approach was generally utilized for a narrow and small fraction of informations[5]. The kinetic methods of analysis in the liquid phase as well as solid phase were presented and justified that the role of kinetics measurement method is greater than generally understood. The methods allowed to use rate of reactions and the rate constant, for the determination and measurement of hydrogen

peroxide, glucose, and cholesterol. The comparison between kinetic and equilibrium methods with the presented experimental data argue that kinetic analytical methods is a potential candidate for clinical chemist along with sensor development and it represents a larger fraction of analytical science than generally recognized.

The kinetic method was designed and then the model was experimentally verified. The pseudo-first order kinetic model was established between the measuring analyte and QDs, hence the model was verified and proved experimentally. The comparative results originated obtained from the kinetic analytical and equilibrium method are presented in table 7.1 below.

Analyte	**Method**	**Linear range/μM**	**Detection limit/μM**	**Analysis time**
H_2O_2	Equilibrium	4 to 237	0.4	10 mins
	Kinetic	0.37 to 396	0.2	0-3 Sec
Glucose	Equilibrium	33 to 300	8.2	10 mins
	Kinetic	8 to 200	2.0	0-5 Sec
Cholesterol	Equilibrium	2.5 to 45	1.5	10 mins
	Kinetic	17- 136	3.46	0-20 Sec

Table 6.1 Comparative account of measurement based on the kinetics of reaction and equilibrium method.

The kinetic methods are criticized for lacking the reliability in comparison to some common equilibrium methods. Although with advancement and sophistication in analytical instruments, kinetic method of analysis is allowed. Most of the kinetic analytical measurements were done using the instrumentation used for equilibrium methods. The advantages of kinetic methods include, fast analysis time and simple in operations. The kinetic profile of glucose and QDs illustrated that, the reaction is slower and needs more time to reach equilibrium hence the kinetic approach is more accurate and fast for measuring these kinds of reactions.

6.5 The polymer encapsulation of QDs for saliva glucose analysis

Biocompatible surface sensitive QDs tend to optically detect H_2O_2 which are final species produced in enzymatic oxidation of a wide range of biological molecules. The thiol-capped QDs are surface sensitive to oxidation and can detect H_2O_2 in addition to all other biological species produced by H_2O_2 oxidation. Surface capped glutathione and mercaptopropionic acid

CdTe nanocrystals were also explored for sensitivity, selection, and high accurate measurement of H_2O_2, glucose, and cholesterol.

In this study, thiol-capped QDs were used as an example of water-soluble QDs to develop reliable sensors that can detect glucose in saliva as well as detect low cholesterol concentrations. The QDs embedded in a polymeric matrix stabilized the QDs environment interference and increased its optical signal performance. The encapsulated QDs had a high optical response to H_2O_2, glucose, and cholesterol. The polymers formulation was optimized for measuring all the species. The polymers formulation of nafion and PVA were hosting QDs, which were not only providing stability but protecting QDs, binding them in polymers functionality via a surface linkage or directly to the core of nanocrystals. The developed sensors based on QD encapsulation in polymers provide a new platform for optical analysis with greater sensitivity and selectivity. The linear range of glucose analysis was from 6 to 340 µM with detection limit of 1.0 µM. The sensor was used to detect human saliva and was validated. The developed sensors are with high stability and resist interference and therefore, can be used in hospital applications. The developed sensor for glucose was modified by changing enzyme for the measurement of cholesterol. The linear range was 9 to 150 µM with detection limit of 13.5 µM.

6.6 Summary

This project was aimed to develop a non-invasive QDs based sensors for the detection of glucose, which is the main marker for the development of metabolic syndrome. A brief method was presented including, preparation of biocompatible and water-soluble QDs, its characterization, and screening through optical properties, pH sensitivity response, and stability of fluorescence at physiological range along with sensitivity for hydrogen peroxide. These properties were used to screen QDs with different capping agents for the measurement of glucose and cholesterol at physiological pH. Among those QDs, CYS capped QDs lost almost all the optical properties at physiological pH and MSA QDs are not sensitive enough to measure H_2O_2 at a low and wide detection ranges. The MPA and GHS capped CdTe QDs were selected for the sensor development which were highly sensitive to H_2O_2.

The liquid phase sensors were developed using the equilibrium and kinetic method, the two methods were also compared. The solution phase equilibrium methods were highly sensitive at low quantification range for glucose (linear range was 33 to 300 µM with a detection limit of 8.2 µM) and cholesterol (linear range of 2.5 to 45 µM with a detection limit of 1.5 µM).

The pseudo-first order kinetic model was presented for hydrogen peroxide, glucose, and cholesterol analysis. The pseudo first order conditions were established for analysis of H_2O_2, glucose and cholesterol. The sensitivity and performance of the kinetic-based sensor were comparable to equilibrium method. The linear range was 0.37 to 396, 8 to 200, and 17 to 136 µM respectively for hydrogen peroxide, glucose, and cholesterol and detection limit was 0.2, 2.0, 3.46 µM respectively for hydrogen peroxide, glucose, and cholesterol. The glucose level in artificial saliva was at the range of 50 to 396 µM. The kinetic method was fast and sensitive enough to measure low glucose level.

The solid state sensor was developed using polymer nafion and PVA along with the QDs and enzymes. The QDs embedded in a polymeric matrix that stabilized QDs environment and increasing the performance optical signal. The polymers nafion and PVA membrane hosting QDs, and not only provide stability but protecting QDs. The developed sensors based on QD encapsulation in polymers provide a new platform for optical analysis with greater sensitivity and selectivity.

The polymers along with QDs and enzymes formulation were optimized to measure glucose at lower range. The detection limit for H_2O_2 and glucose was 1.0 µM. The linear range of glucose estimation was from 6 to 400 µM which is sufficient to measured saliva and tear glucose level. The optimized sensor was used to measure human saliva glucose level for normal and diabetes. The developed sensors are with high stability and resist to interference and could be applicable for hospital applications. The cholesterol was fabricated by replacing GOx by ChOx and keeping all other formulation constants. The linear range was 9.9 to 150 µM with detection limit of 4.5 µM.

6.7 References

(1) Sadikot, S.; Hermans, M. Here we go again … The metabolic syndrome revisited! *Diabetes & Metabolic Syndrome: Clinical Research & Reviews* **2010,** *4* (2), 111.

(2) Abikshyeet, P.; Ramesh, V.; Oza, N. Glucose estimation in the salivary secretion of diabetes mellitus patients. *Diabetes Metab Syndr Obes* **2012,** *5*, 149.

(3) Jurysta, C.; Bulur, N.; Oguzhan, B.; Satman, I.; Yilmaz, T. M.; Malaisse, W. J.; Sener, A. Salivary glucose concentration and excretion in normal and diabetic subjects. *J Biomed Biotechnol* **2009,** *2009*, 430426.

(4) Vasconcelos, A. C. U.; Soares, M. S. M.; Almeida, P. C.; Soares, T. C. Comparative study of the concentration of salivary and blood glucose in type 2 diabetic patients. *Journal of oral science* **2010,** *52* (2), 293.

(5) Pardue, H. L. A comprehensive classification of kinetic methods of analysis used in clinical chemistry. *Clinical chemistry* **1977,** *23* (12), 2189.

(6) Chen, H.; Gai, H.; Yeung, E. S. Inhibition of photobleaching and blue shift in quantum dots. *Chem Commun (Camb)* **2009**, DOI:10.1039/b819356h 10.1039/b819356h(13), 1676.

(7) Zhang, Y. Time-dependent photoluminescence blue shift of the quantum dots in living cells: Effect of oxidation by singlet oxygen. *J. Am. Chem. Soc.* **2006,** *128*, 13396.

Appendix

1. Ahmad I, Zhang H, and Lau K. The Reaction Kinetics of Glutathione-Capped Quantum Dots for the Detection of Hydrogen Peroxide. Austin J Biosens & Bioelectron. 2015; 1(2): 1010.
2. Ahmad I, Zhang H, and Lau K. Ultrasensitive quantum dot based biosensor using kinetic model for analysis. 4th Nano Today Conference 6-9 December 2015 Dubai.